NASA TECHNICAL MEMORANDUM

NASA TM X-72670

COPY NO.

NASA TM X-72670

(NASA-TM-X-72670) LONGITUDINAL AERODYNAMICS OF A LOW-WING LIFT-FAN TRANSPORT INCLUDING HOVER CHARACTERISTICS IN AND OUT OF GROUND EFFECT (NASA) 155 p HC $6.25 CSCL 01A

N75-21248

G3/02 Unclas 18667

LONGITUDINAL AERODYNAMICS OF A LOW-WING LIFT-FAN TRANSPORT INCLUDING HOVER CHARACTERISTICS IN AND OUT OF GROUND EFFECT

Danny R. Hoad
Langley Directorate, U.S. Army Air Mobility R&D Laboratory
and
Garl L. Gentry, Jr.
Langley Research Center
Hampton, Va. 23665

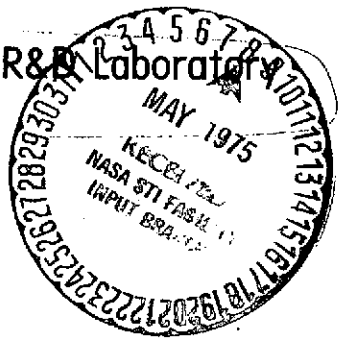

NATIONAL AERONAUTICS AND SPACE ADMINISTRATION
LANGLEY RESEARCH CENTER, HAMPTON, VIRGINIA 23665

1. Report No.	2. Government Accession No.	3. Recipient's Catalog No.
TM X-72670		

4. Title and Subtitle	5. Report Date
LONGITUDINAL AERODYNAMICS OF A LOW-WING LIFT-FAN TRANSPORT INCLUDING HOVER CHARACTERISTICS IN AND OUT OF GROUND EFFECT	April 1975
	6. Performing Organization Code
7. Author(s)	8. Performing Organization Report No.
Danny R. Hoad and Garl L. Gentry, Jr.	
9. Performing Organization Name and Address	10. Work Unit No.
Langley Directorate, U.S. Army Air Mobility R&D Lab. and Langley Research Center Hampton, VA 23665	505-10-31-02
	11. Contract or Grant No.
	13. Type of Report and Period Covered
12. Sponsoring Agency Name and Address	Technical Memorandum
National Aeronautics and Space Administration Washington, D.C. 20546	14. Sponsoring Agency Code

15. Supplementary Notes

16. Abstract

A wind-tunnel investigation has been conducted in the Langley V/STOL tunnel to determine the longitudinal aerodynamic characteristics of a six-fan, tip-driven (remote) lift-fan VTOL transport throughout transition. The large midspan lift-fan pods and cruise fans were also removed to determine their influence on the stability and control of the configuration. Data were also obtained in the hovering mode for ranges of model height above ground. The data are presented without analysis or discussion.

17. Key Words (Suggested by Author(s)) (STAR category underlined)	18. Distribution Statement
Remote lift-fan VTOL aerodynamics Ground effect Low wing	Unclassified - Unlimited Star Category 01

19. Security Classif. (of this report)	20. Security Classif. (of this page)	21. No. of Pages	22. Price*
Unclassified	Unclassified	152	$6.25

*Available from { The National Technical Information Service, Springfield, VA 22151
NASA STIF, P.O. Box 8757, Baltimore/Washington International Airport, MD 21240

LONGITUDINAL AERODYNAMICS OF A LOW-WING LIFT-FAN TRANSPORT INCLUDING HOVER CHARACTERISTICS IN AND OUT OF GROUND EFFECT

Danny R. Hoad
Langley Directorate, U.S. Army Air Mobility R&D Laboratory

and

Garl L. Gentry, Jr.
Langley Research Center
Hampton, Virginia

SUMMARY

A wind-tunnel investigation has been conducted on the effects of ground proximity on the longitudinal forces and moments of a tip-driven (remote) lift-fan VTOL transport. Longitudinal aerodynamic data were obtained at various fan-exit deflection angles simulating aircraft configurations through transition. Data were also obtained to determine the effects on the aerodynamics and stability of the lift-fan pods and large lift-cruise fans. The data are presented without analysis or discussion.

INTRODUCTION

A viable VTOL transport using tip-driven lift fans providing vertical thrust is of considerable interest for future application. The design of VTOL aircraft requires a detailed knowledge of the propulsion-induced effects, in and out of ground effect, in hover and in transition flight. Considerable research has been expended to date (refs. 1 to 4). Large-scale wind-tunnel investigations of several different configurations have been made at the NASA Ames Research Center to determine static aerodynamic and stability and control charactersitics (refs. 5 to 9). Small-scale wind-tunnel investigations of two different configurations have been

conducted at the NASA Langley Research Center, including free-flight model tests (refs. 10 to 13). Flight tests have been conducted on a VTOL jet transport (ref. 14) and a tip-driven lift-fan aircraft (ref. 15).

Preliminary design work has been undertaken by several organizations for a lift-fan VTOL transport. Hawker-Siddeley has conducted a preliminary design study on a 16-fan VTOL transport (ref. 16), McDonnell Douglas Corporation on a 6-fan VTOL transport (ref. 17), and Dornier GMBH on a 12-fan VTOL transport (ref. 18). NASA Ames Research Center has sponsored a series of conceptual design studies (refs. 19 to 22). For the present investigation, NASA Langley Research Center chose the configuration in reference 22 to provide basic longitudinal aerodynamic characteristics of a representative configuration.

The configuration is a low-wing, tip-driven lift-fan VTOL transport. Two lift fans were enclosed in each pod located approximately midspan on each wing and two lift-cruise fans were located on the aft portion of the fuselage. A turbojet engine is used to drive each tip-turbine fan.

The investigation was conducted in the Langley V/STOL tunnel. The 8.6-percent scale model was tested in hover at various heights above the ground board; it was also tested through a range of angles of attack at simulated speeds from hover through transition at two power conditions. The data from the investigation have been corrected for wall effects (ref. 23).

SYMBOLS

The aerodynamic data in this report are referred to the stability-axis system. (See fig. 1.) All of the moment data are referred to a moment center located on the fuselage reference line at the 32.7-percent point of the mean geometric chord, the center of thrust in the hover condition. (See figs. 2 and 3.) The physical quantities in this paper are given in the International System of Units (SI).

A_j fan-exit area (0.078 m^2 total for six fans)

b wing span, m

c local wing chord, m

$\bar{c}$ mean geometric chord, m

c_h local chord, horizontal stabilizer, m

c_v local chord, vertical stabilizer, m

C_D drag coefficient, $\frac{D}{q_\infty S}$

C_L lift coefficient, $\frac{L}{q_\infty S}$

C_m pitching-moment coefficient, $\frac{M_Y}{q_\infty S\bar{c}}$

C_μ fan-thrust coefficient, $\frac{T}{q_\infty S}$

D drag, N

D_e effective fan-exit area (0.314 m), $\sqrt{\frac{4A_j}{\pi}}$

h height, orthogonally, from ground plane to moment reference center of model, m

i_t horizontal-tail incidence angle (positive direction, trailing edge down), deg

L lift, N

M_X rolling moment, m-N

M_Y pitching moment, m-N

M_Z yawing moment, m-N

p_a ambient pressure, N/m^2

$p_{t,e}$ exit local total pressure, N/m^2

q_∞ free-stream dynamic pressure, N/m^2 (lbf/ft^2)

S wing area, m^2

T static thrust, N

V_e effective velocity ratio, $\sqrt{\frac{q_\infty}{\frac{T}{2A_j}}}$

V_j fan-exit velocity, m/sec

V_∞ free-stream velocity, m/sec

$\dot{w}_p$	fan-primary mass flow, kg/sec
$\dot{w}_s$	fan-inlet mass flow, kg/sec
x	chordwise station measured from airfoil nose, m
Y	side force, N
z_ℓ	lower-surface distance perpendicular to chord of airfoil, m
z_u	upper-surface distance perpendicular to chord of airfoil, m
α	angle of attack, deg
β	angle of sideslip, deg
δ_e	elevator deflection (positive direction, trailing edge down), deg
δ_f	wing trailing-edge flap deflection (positive direction, trailing edge down), deg
δ_L	lift-fan louver deflection angle, deg
$\delta_{L,J}$	lift-fan exit-flow deflection angle, deg
δ_{LC}	lift-cruise fan-exit deflection angle, deg

$\delta_{LC,J}$	lift-cruise fan-exit-flow deflection angle, deg
ρ_j	fluid density, fan-exit flow, kg/m^3
ρ_∞	fluid density, free-stream flow, kg/m^3
ϕ	angle of roll, deg

NOTATIONS

B.L.	bunt line, distance along Y-axis, m
$\mathbb{C}_L$	centerline
Dia.	diameter, m
Fus. Ref.	fuselage reference line, W. L. 0.218 m
H-tail	horizontal tail
rpm	revolutions per minute
Sta.	station
W. L.	water line, distance along Z-axis, m

MODEL AND APPARATUS

The model used in this investigation was a 8.6-percent-scale model of the tip-driven (remote) lift-fan VTOL transport described in reference 22. A three-view drawing of the base model used for model geometric references is presented in figure 2, and a three-view drawing of the VTOL transport model is presented in figure 3. The ordinates for the wing are presented in Table I at four spanwise locations. A photograph of the model installed in the Langley V/STOL tunnel is presented in figure 4.

The 30-percent-chord, translating wing flaps were single slotted. The flap slot was 1-percent local wing chord when deflected at 40° from the wing reference chord. Cross-sectional views of the flap and wing are presented in figure 5. The 30-percent-chord, simple-hinged ailerons (fig. 2) had a deflection range of $\pm 25°$ in 5° increments.

The geometric characteristics of the horizontal tail are presented in figure 6. (See Table II for ordinates.) It was pivoted about the 60.5-percent root chord with an incidence range of $\pm 180°$ in 2.5° increments. The 25-percent-chord, simple-hinged elevator had a deflection angle range of $\pm 15°$ in 5° increments. Ordinates for the vertical tail are presented in Table III. The 28-percent-chord, simple-hinged rudder had a deflection angle range of $\pm 25°$ in 5° increments.

Six tip-turbine fan engine simulators similar to the one shown in figure 7 were used to represent the four lift-fans mounted in pods on the wing, and the two lift-cruise fans mounted on the fuselage. Each fan simulator was instrumented with: (1) a magnetic fan-speed indicator; (2) bearing temperature measurement devices; (3) 20 total pressure probes in the exit; and (4) tip and hub static pressure taps in the exit. Each fan required an oil mist system for bearing lubrication.

A pod was located on each wing at the 52.8-percent semispan. In each pod, two lift-fans were mounted with vertical fan axes (see fig. 8). These fans were mounted forward of the moment reference center to provide a thrust balance in hover with the aft lift-cruise fans. The transition

from takeoff to wingborne flight or wingborne flight to landing was accomplished by deflecting a set of louvers, from the fan axis, in the exit of the lift fans on a schedule with deflection of the lift-cruise fan exits as shown in the sketch below:

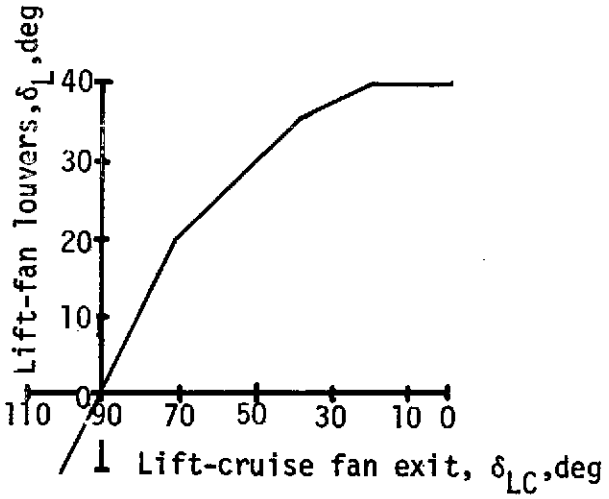

The louver deflections tested were -5° for landing, 0° for hover, +7.5° for takeoff, +20° for speed in the middle of transition, +40° for the high-speed end of transition, and closed (+90°) for wingborne flight. (See fig. 9.)

The lift-cruise fans are located with axis horizontal on the aft portion of the fuselage. (See fig. 3.) Transition flight was simulated by deflecting the lift-cruise fan exit, from the fan axis, in a lobster-tail fashion on a schedule with the lift-fan louvers. The deflected lift-cruise fan exits were 94° for landing (fig. 10(a)), 90° for hover (fig. 10(b)), 82° for takeoff (fig. 10(c)), 70° for mid-transition (fig. 10(d)), and 0° for end of transition (fig. 10(e)). The 0° deflection of the lift-cruise fans was also used with lift fan inlets and exits closed for wingborne flight.

The lift-fan pods and lift-cruise fans were separately removeable such that a component breakdown could be performed to determine their effect on the aerodynamics and stability of the configuration.

The model was mounted in the Langley V/STOL tunnel on a sting-supported six-component strain-gage balance for measurement of the total forces and moments.

TEST AND CORRECTIONS

The free-stream dynamic pressure for the investigation varied from 0 to 2681 N/m^2 (56 lbf/ft^2). The Reynolds number (based on wing $\bar{c}$ and free-stream velocity) ranged from 0 to 1.376×10^6. The data presented in this report have been corrected for wind-tunnel wall effects using reference 23.

Calibrations were made to determine the individual thrust and the individual primary mass-flow and fan-inlet mass flow of each fan simulator for each deflection angle. The data were obtained at zero air-speed and reflect static fan parameters only. Figure 11 presents the thrust as a function of fan speed and as a function of exit-pressure ratio for a typical lift fan and a typical lift-cruise fan for each deflection angle. The primary mass flow and fan inlet mass flow for a typical lift fan and a typical lift-cruise fan at each deflection angle are presented in figure 12. The fan-exhaust deflection angles for a typical lift fan and a typical lift-cruise fan at each deflection angle are presented in figure 13. The flow deflection for the 40° lift-fan louver was approximately 20°; therefore, it was used for the simulation of the 20° deflection lift-fan configuration. As a result, the flow deflection of 40° required for the end-of-transition configuration was not available for the present investigation.

Thrust coefficient and effective velocity ratio presented in this report were determined from the static-thrust calibration as a function of rpm (using the total of the individually measured thrusts) from the following equation:

$$C_\mu = \frac{T}{q_\infty S}$$

$$V_e = \sqrt{\frac{\rho_\infty V_\infty^2}{\rho_j V_j^2}} = \sqrt{\frac{q_\infty}{\frac{T}{2A_j}}}$$

The relationship between C_μ and V_e is presented in figure 14.

Ground-effect data were obtained during hovering at zero wind velocity for several angles of attack and two roll angles. The wind-tunnel walls were removed for all hovering tests to reduce circulation induced by them. The height of the model above the floor was measured orthogonally from the floor to the moment reference center of the model. Three configurations were tested in ground effect at zero wind speed: (1) Landing configuration, $\delta_L = -5°$, $\delta_{LC} = 94°$; (2) Takeoff configuration, $\delta_L = 7.5°$, $\delta_{LC} = 82°$; and (3) Hover configuration, $\delta_L = 0°$, $\delta_{LC} = 90°$. The longitudinal aerodynamic characteristics of the model were obtained such that the free-stream dynamic pressure over the model at a particular deflection configuration matched that proposed for that airplane configuration in reference 22. The effective velocity ratio proposed in that reference was simulated by two set velocity ratios in the wind tunnel, one slightly lower and one slightly higher than that in reference 22. Data were obtained through a range of angles of attack from approximately -6° to 20°. Data were obtained for each configuration at various tail incidence, and various elevator deflections for selected configurations.

PRESENTATION OF RESULTS

In order to hasten the availability of these data on this remote lift-fan transport, the data are being presented without analysis or discussion.

The ground-effect data at zero wind speed are presented in ratios of lift and drag to thrust and pitching moment and rolling moment to the product of the thrust and effect diameter of the operating fans. These

parameters are presented at various thrust settings as a function of the ratio of height above the floor to the effective diameter of the operating fans.

The longitudinal aerodynamic data for configurations: δ_L = -5° and δ_{LC} = 94°; δ_L = 0° and δ_{LC} = 90°; and δ_L = 7.5° and δ_{LC} = 82° are are presented as ratios of lift and drag to thrust and pitching moment to the product of the effective diameter of the operating fans. The data for δ_L closed and δ_{LC} = 0° are presented as lift, drag, and pitching-moment coefficients. The data for configurations denoted δ_L = 40° and δ_{LC} = 70° are presented in both formats.

Results of the investigation are presented in the following figures:

Langley Research Center,
National Aeronautics and Space Administration
March 19, 1975

REFERENCES

1. Gentry, Garl L.; and Margason, Richard J.: Jet-Induced Lift Losses on VTOL Configurations Hovering In and Out of Ground Effect. NASA TN D-3166, 1966

2. Margason, Richard J.: The Path of a Jet Directed at Large Angles to a Subsonic Free Stream. NASA TN D-4919, 1968

3. Carter, Arthur W.: Effects of Jet-Exhaust Location on the Longitudinal Aerodynamic Characteristics of a Jet V/STOL Model. NASA TN D-5333, 1969

4. Margason, Richard J.: Review of Propulsion-Induced Effects on Aerodynamics of Jet/STOL Aircraft. NASA TN D-5617, 1970

5. Kirk, Jerry V.; Hickey, David H.; and Hall, Leo P.: Aerodynamic Characteristics of a Full-Scale Fan-In-Wing Model Including Results in Ground Effect with Nose-Fan Pitch Control. NASA TN D-2368, 1964

6. Kirk, Jerry V.; Hodder, Brent K.; and Hall, Leo P.: Large-Scale Wind-Tunnel Investigation of a V/STOL Transport Model with Wing-Mounted Lift Fans and Fuselage-Mounted Lift-Cruise Engines for Propulsion. NASA TN D-4233, 1967

7. Hall, Leo P.; and Kirk, Jerry V.: Large-Scale Wind-Tunnel Investigation of a V/STOL Transport Model with Podded Lift Fans Forward and Aft of a Low Mounted Wing. NASA TM X-62102, 1971

8. Dickinson, Stanley O.; Hall, Leo P.; and Hodder, Brent K.: Aerodynamic Characteristics of a Large-Scale V/STOL Transport Model with Tandem Lift Fans Mounted at Mid-Semispan of the Wing. NASA TN D-6234, 1971

9. Kirk, Jerry V.; Dickinson, Stanley O.; Hall, Leo P.; and Coffman, Mary G.: Aerodynamic Characteristics of a Large Scale Lift Fan Transport Model with Podded Fans Forward and Lift Cruise Fans Mounted Over the Wing. NASA TM-X 62151, 1972

10. Newsom, William A., Jr.; and Moore, Frederick L.: Wind-Tunnel Investigation of a V/STOL Transport Model with Six Wing-Mounted Lift Fans. NASA TN D-5695, 1970

11. Newsom, William A., Jr.: Wind-Tunnel Investigation of a V/STOL Transport Model with Four Pod-Mounted Lift Fans. NASA TN D-5942, 1970

12. Newsom, William A., Jr.; and Grafton, Sue B.: Flight Investigation of a V/STOL Transport Model with Four Pod-Mounted Lift Fans. NASA TN D-6129, 1971

13. Newsom, William A., Jr.; and Grafton, Sue B.: Flight Investigation of a V/STOL Transport Model Having Six Wing-Mounted Lift Fans. NASA TN D-6198, 1971

14. Holzhauser, Curt A.; Morello, Samuel A.; Innis, Robert C.; and Patton, James M., Jr.: A Flight Evaluation of a VTOL Jet Transport Under Visual and Simulated Instrument Conditions. NASA TN D-6754, 1972

15. Anon.: XV-5A Lift Fan Flight Research Aircraft. Phase I Flight Test Results. Vol I. (AD-639231), Vol. II (AD-639232), and Vol. III (AD-639233). G.E. Rep. 166, March 1966

16. Szlenkier, T. K.: Latest Civil V/STOL Aircraft Projects of Hawker Siddeley Aviation. NASA TT F-14619, 1972

17. Anon.: Near Term V/STOL Lift Fan Research Transport Update. Vol. I - Technical Data. McDonnell Aircraft Corp. Rep. MDC A1602, July 1972. (Also available as NASA CR-114537.)

18. Anon.: Considerations Regarding the Design of the V/STOL Project Dornier DO 231. Luftfahrtechnik Raumfahrttechnik, vol. 16, Jan. 1970, pp. 15-20

19. Eldridge, W. M.; Ferrell, J. A.; McKee, J. W.; Wayne, J. F., Jr.; and Zabinsky, J. M.: Conceptual Design Studies of Candidate V/STOL Lift Fan Commercial Short Haul Transport for 1980-85 V/STOL Lift Fan Study. NASA CR-2183, 1973

20. Knight, Ronald G.; Powell, William V., Jr.; and Prizlow, Jerome A.: Conceptual Design Study of a V/STOL Lift Fan Commercial Short Haul Transport. NASA CR-2185, 1973

21. Anon.: Conceptual Design Studies of a V/STOL Civil Lift Fan Transport Including Effect of Size and Fan Pressure Ratio. NASA CR-2426, 1974

22. Anon.: Study of Near-Term V/STOL Lift-Fan Research Transport. North American Rockwell Rep. NA-72-444, vol. 1, 1971

23. Heyson, Harry H.: Linearized Theory of Wind-Tunnel Jet-Boundary Corrections and Ground Effect for VTOL-STOL Aircraft. NASA TR R-124, 1962

TABLE I - WING AIRFOIL ORDINATES

Spanwise Location: Root
c: 43.688 cm

x/c	z_u/c	z_ℓ/c
0	.0496	.0465
.005	.0597	.0345
.010	.0648	.0287
.015	.0686	.0242
.020	.0719	.0205
.025	.0746	.0172
.035	.0792	.0117
.050	.0842	.0048
.075	.0895	-.0042
.100	.0925	-.0113
.125	.0937	-.0173
.150	.0941	-.0224
.200	.0931	-.0305
.250	.0911	-.0366
.300	.0884	-.0406
.350	.0845	-.0427
.400	.0801	-.0436
.450	.0752	-.0436
.500	.0701	-.0428
.550	.0647	-.0414
.600	.0589	-.0394
.650	.0528	-.0371
.700	.0462	-.0343
.750	.0384	-.0311
.800	.0303	-.0271
.850	.0221	-.0222
.900	.0140	-.0166
.950	.0058	-.0102
1.000	-.0024	-.0028

Spanwise Location: 17.26 cm
c: 38.52 cm

x/c	z_u/c	z_ℓ/c
0	.0495	.0471
.0071	.0604	.0348
.0127	.0647	.0302
.0184	.0682	.0267
.0241	.0711	.0238
.0297	.0737	.0213
.0354	.0760	.0191
.0468	.0799	.0152
.0694	.0857	.0092
.0978	.0908	.0035
.1262	.0943	-.0010
.1545	.0967	-.0045
.2112	.0990	-.0099
.2679	.0991	-.0139
.3246	.0975	-.0165
.3813	.0946	-.0177
.4381	.0906	-.0177
.4948	.0858	-.0166
.5515	.0801	-.0148
.6082	.0736	-.0122
.6649	.0662	-.0089
.7216	.0580	-.0050
.7783	.0495	-.0003
.8350	.0417	.0050
.8917	.0347	.0105
.9484	.0283	.0163
1.000	.0224	.0219

Spanwise Location: 31.67 cm
c: 34.20 cm

x/c	z_u/c	z_ℓ/c
0	.0493	.0477
.0034	.0552	.0418
.0097	.0604	.0381
.0161	.0641	.0360
.0225	.0673	.0345
.0289	.0700	.0332
.0353	.0724	.0321
.0417	.0746	.0312
.0481	.0767	.0303
.0545	.0786	.0296
.0608	.0803	.0288
.0736	.0834	.0274
.1055	.0896	.0243
.1375	.0943	.0214
.1694	.0978	.0188
.2014	.1004	.0165
.2652	.1037	.0128
.3291	.1048	.0105
.3930	.1043	.0098
.4568	.1019	.0105
.5207	.0980	.0124
.5846	.0931	.0155
.6484	.0871	.0197
.7123	.0803	.0247
.7762	.0733	.0299
.8400	.0663	.0352
.9039	.0593	.0404
.9678	.0523	.0457
1.0000	.0487	.0483

Spanwise Location: 84.54 cm
c: 18.37 cm

x/c	z_u/c	z_ℓ/c
0	.2195	.2136
.0066	.2315	.1986
.0185	.2395	.1922
.0304	.2446	.1931
.0423	.2487	.1938
.0542	.2520	.1942
.0661	.2550	.1945
.0780	.2577	.1946
.0899	.2602	.1947
.1017	.2624	.1947
.1255	.2664	.1947
.1493	.2699	.1947
.1733	.2729	.1947
.1969	.2755	.1947
.2444	.2797	.1950
.3039	.2833	.1958
.3634	.2854	.1973
.4228	.2859	.1994
.4823	.2851	.2023
.5417	.2834	.2059
.6012	.2809	.2103
.6606	.2775	.2156
.7201	.2734	.2216
.7796	.2691	.2279
.8390	.2645	.2342
.8985	.2598	.2405
.9579	.2550	.2468
1.000	.2546	.2512

TABLE II - HORIZONTAL TAIL AIRFOIL ORDINATES

x/c	z_u/c	z_ℓ/c
0	0	0
.0050	.0073	-.0073
.0075	.0088	-.0088
.0125	.0111	-.0111
.0250	.0152	-.0152
.0500	.0210	-.0210
.0750	.0253	-.0253
.1000	.0288	-.0288
.1500	.0342	-.0342
.2000	.0384	-.0384
.2500	.0414	-.0414
.3000	.0434	-.0434
.3500	.0446	-.0446
.4000	.0450	-.0450
.4500	.0442	-.0442
.5000	.0424	-.0424
.5500	.0398	-.0398
.6000	.0366	-.0366
.6500	.0328	-.0328
.7000	.0286	-.0286
.7500	.0240	-.0240
.8000	.0193	-.0193
.8500	.0145	-.0145
.9000	.0097	-.0097
.9500	.0050	-.0050
1.0000	.0002	-.0002

TABLE III. - VERTICAL TAIL AIRFOIL ORDINATES

Location: W.L. 24.68 cm
c: 39.97 cm

x/c	z_u/c	z_ℓ/c
0	0	0
.0050	.0085	-.0085
.0075	.0102	-.0102
.0125	.0129	-.0129
.0250	.0178	-.0178
.0500	.0245	-.0245
.0750	.0295	-.0295
.1000	.0336	-.0336
.1500	.0400	-.0400
.2000	.0447	-.0447
.2500	.0482	-.0482
.3000	.0507	-.0507
.3500	.0521	-.0521
.4000	.0525	-.0525
.4500	.0515	-.0515
.5000	.0494	-.0494
.5500	.0464	-.0464
.6000	.0427	-.0427
.6500	.0383	-.0383
.7000	.0334	-.0334
.7500	.0280	-.0280
.8000	.0225	-.0225
.8500	.0169	-.0169
.9000	.0114	-.0114
.9500	.0058	-.0058
1.0000	.0002	-.0002

Location: W.L. 57.01 cm
c: 26.00 cm

x/c	z_u/c	z_ℓ/c
0	0	0
.0050	.0073	-.0073
.0075	.0088	-.0088
.0125	.0111	-.0111
.0250	.0152	-.0152
.0500	.0210	-.0210
.0750	.0253	-.0253
.1000	.0288	-.0288
.1500	.0342	-.0342
.2000	.0384	-.0384
.2500	.0414	-.0414
.3000	.0434	-.0434
.3500	.0446	-.0446
.4000	.0450	-.0450
.4500	.0442	-.0442
.5000	.0424	-.0424
.5500	.0398	-.0398
.6000	.0366	-.0366
.6500	.0328	-.0328
.7000	.0286	-.0286
.7500	.0240	-.0240
.8000	.0193	-.0193
.8500	.0145	-.0145
.9000	.0097	-.0097
.9500	.0050	-.0050
1.0000	.0002	-.0002

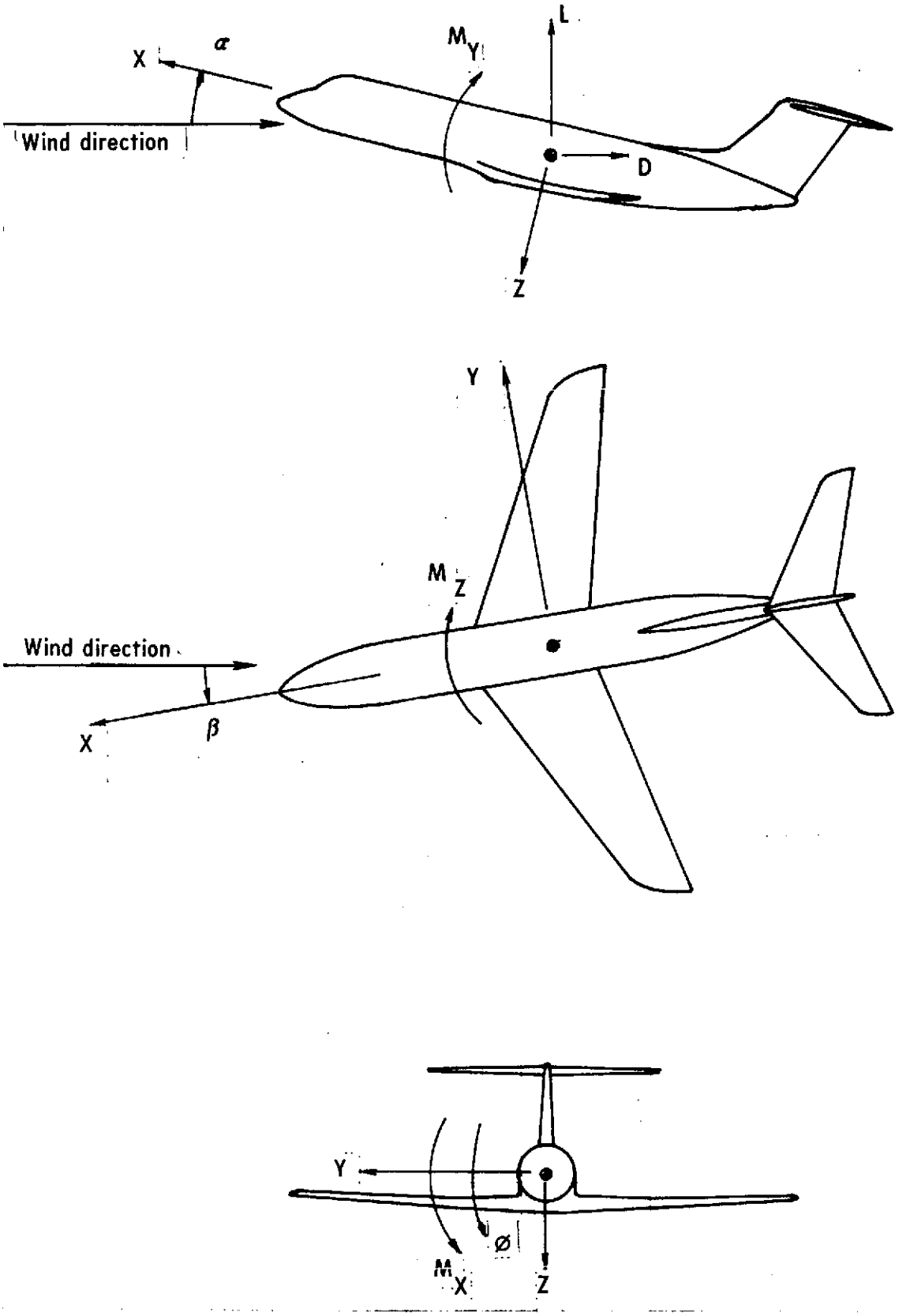

Figure 1. - Axis system used in presentation of data.
Arrows indicate positive direction of forces and moments.

Wing:		
Area, sq. m	0.5452	
Mean geometric chord, m	0.3217	
Span, m	1.8087	
Aspect ratio	6.0	
Incidence at root, wing reference plane-to-fuselage reference plane, (pos.-leading-edge up), deg	1.5	
Dihedral at wing reference plane, (pos.-wing-tip up), deg	3.0	
Horizontal Tail:		
Airfoil section	NACA 64A009	Mod.
Area, sq. m	0.1392	
Mean geometric chord, m	0.1758	
Span, m	0.8388	
Aspect ratio	5.05	
Vertical Tail:		
Airfoil section-W.L. 24.68	NACA 64A0105	Mod.
Airfoil section-W.L. 57.01	NACA 64A009	Mod.
Area, sq. m	0.1067	
Mean geometric chord, m	0.3349	
Span, m	0.3233	
Aspect ratio	0.98	

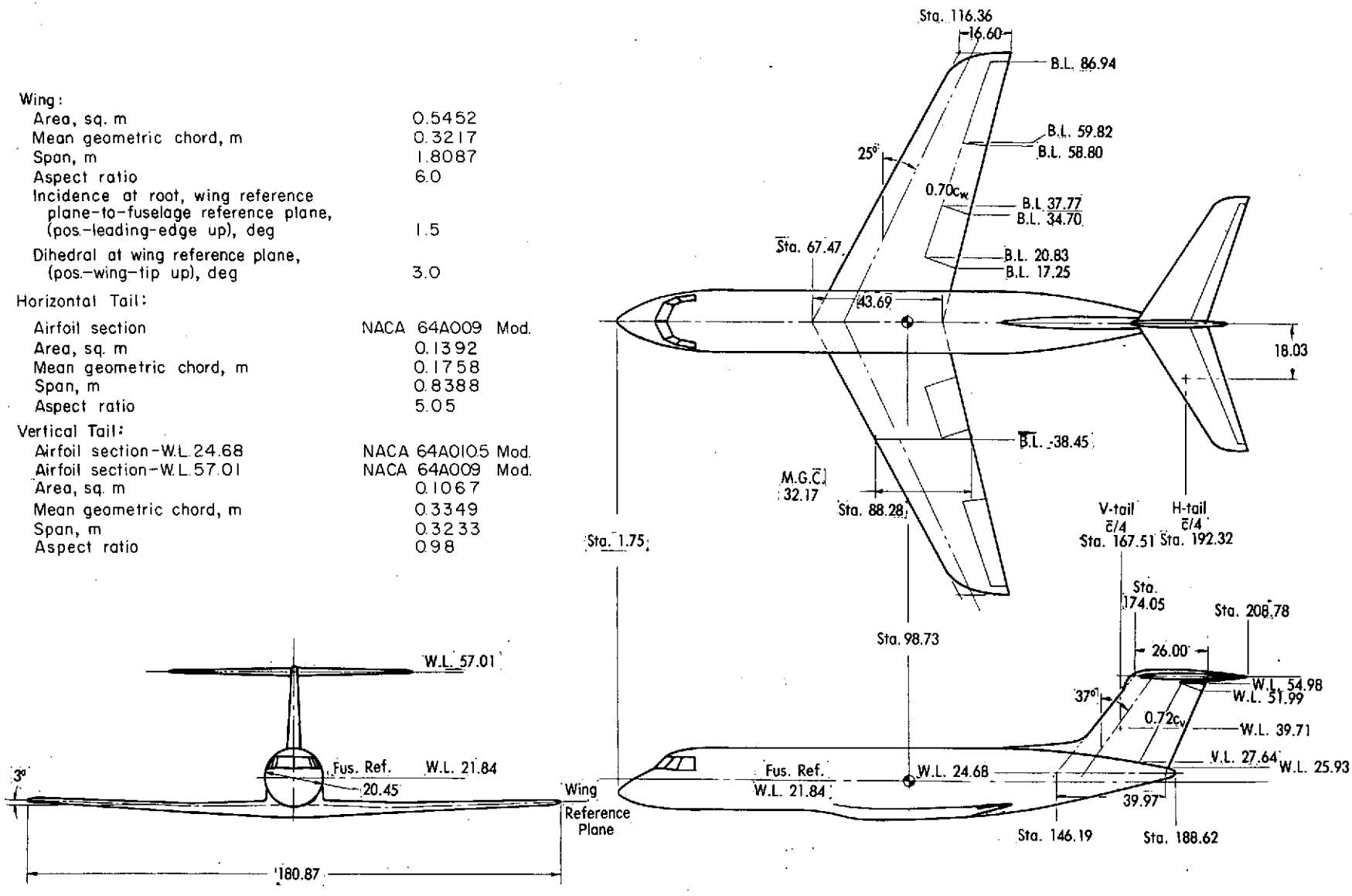

Figure 2. - Dimensional characteristics of the base model. Dimensions are in centimeters unless otherwise noted.

Wing:		
Area, sq. m	0.5452	
Mean geometric chord, m	0.3217	
Span, m	1.8087	
Aspect ratio	6.0	
Incidence at root, wing reference plane-to-fuselage reference plane, (pos.-leading-edge up), deg	1.5	
Dihedral at wing reference plane, (pos.-wing-tip up), deg	3.0	
Horizontal Tail:		
Airfoil section	NACA 64A009	Mod.
Area, sq. m	0.1392	
Mean geometric chord, m	0.1758	
Span, m	0.8388	
Aspect ratio	5.05	
Vertical Tail:		
Airfoil section-W.L. 24.68	NACA 64A010.5	Mod.
Airfoil section-W.L. 57.01	NACA 64A009	Mod.
Area, sq. m	0.1067	
Mean geometric chord, m	0.3349	
Span, m	0.3233	
Aspect ratio	0.98	

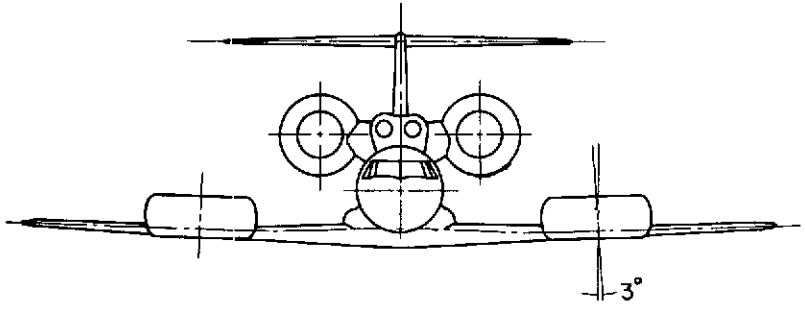

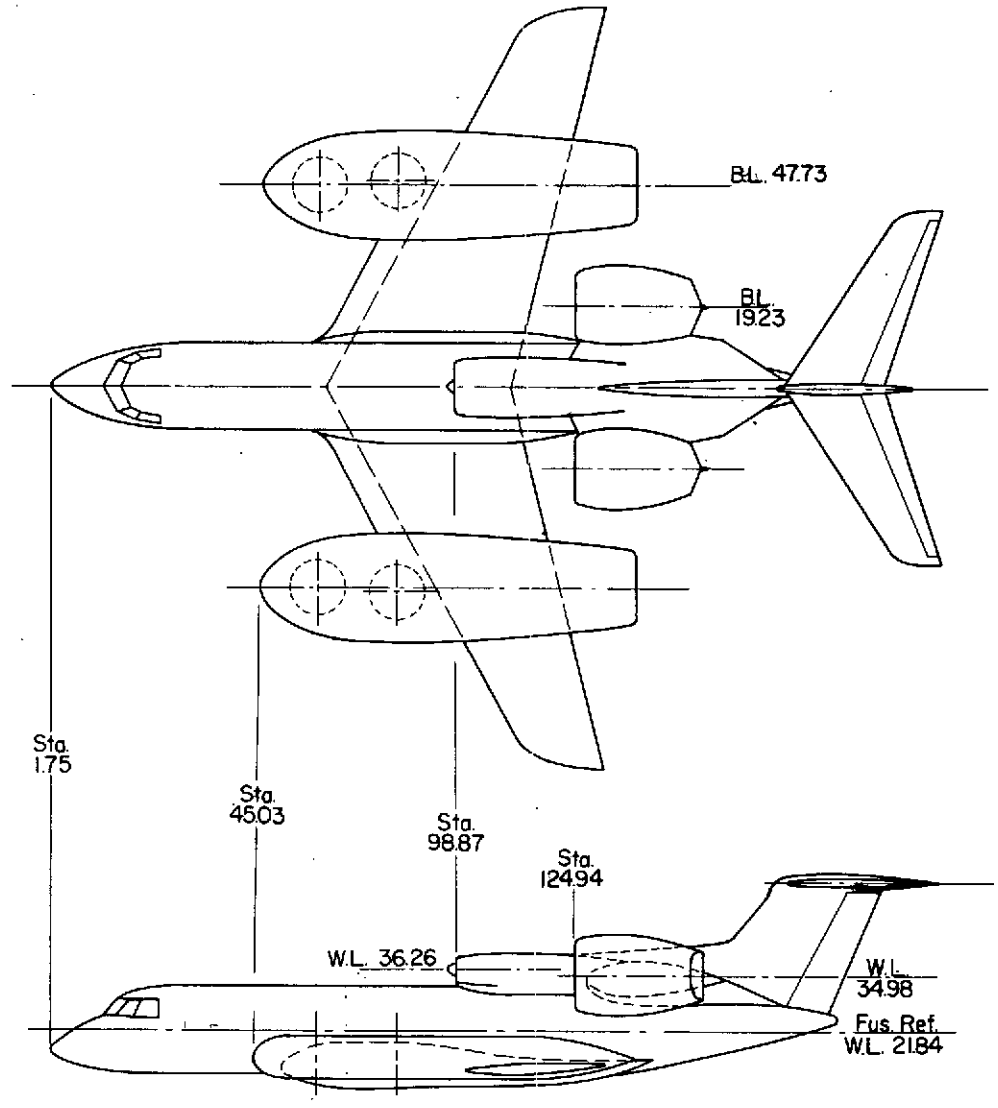

Figure 3. - Dimensional characteristics of the low-wing VTOL transport model. Dimensions are in centimeters unless otherwise noted.

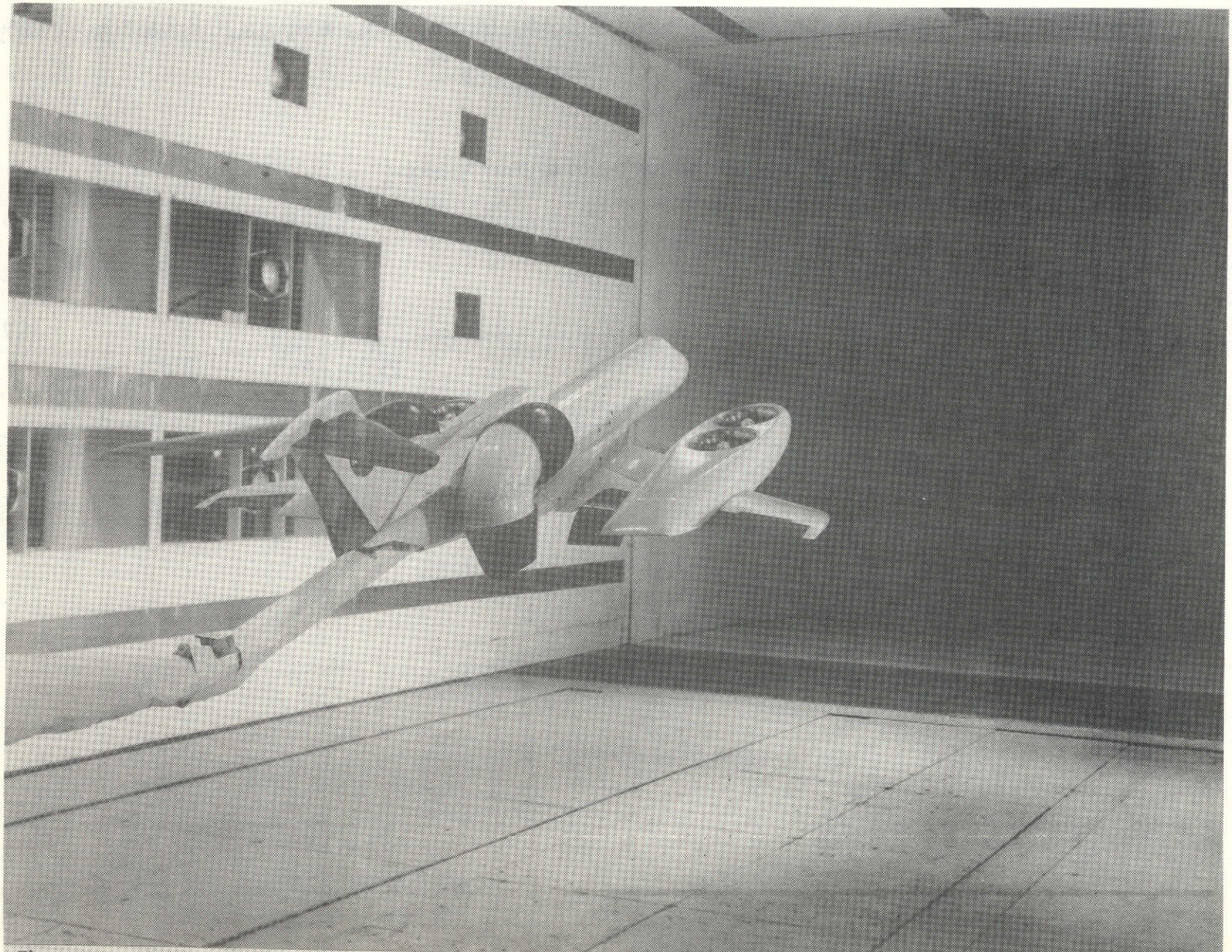

Figure 4. - Three-quarter rear view of the low-wing VTOL transport mounted in the Langley V/STOL tunnel.

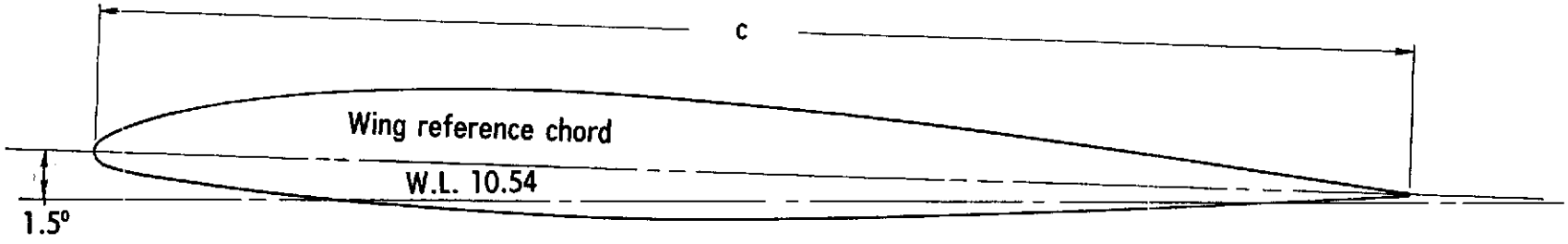

Cruise configuration

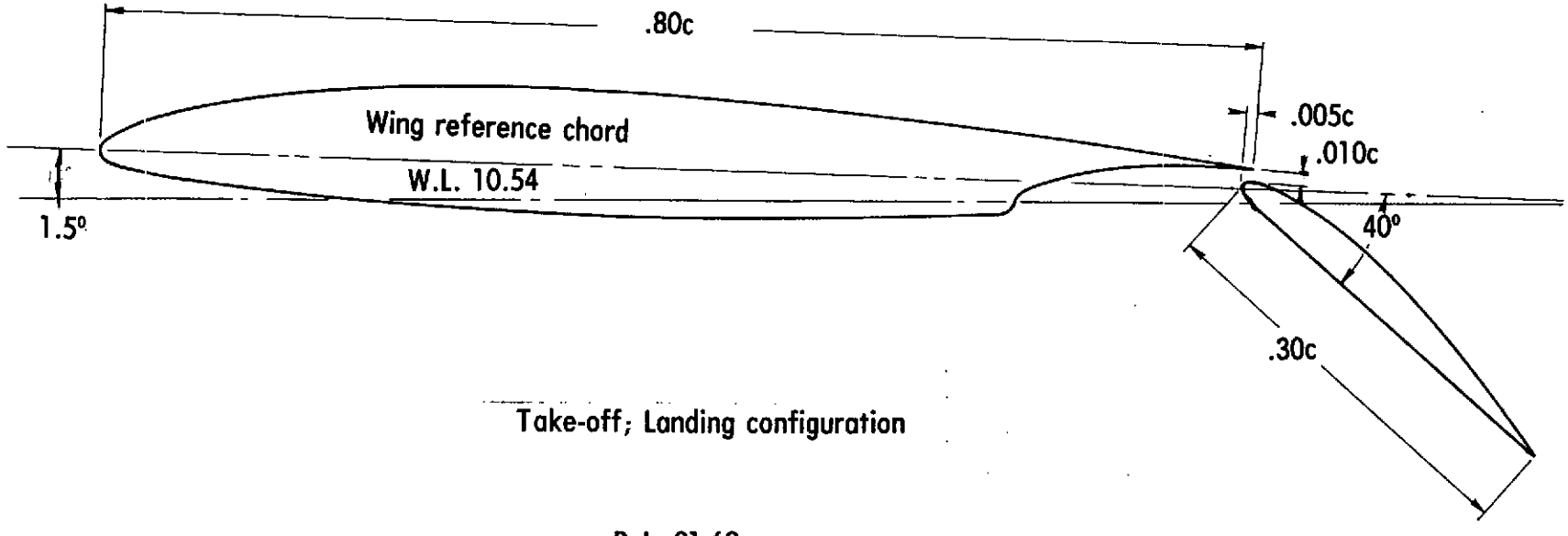

Take-off; Landing configuration

B. L. 31.62 cm

Figure 5. - Wing details in the cruise and takeoff and landing configurations. Dimensions are given in fraction of local chord.

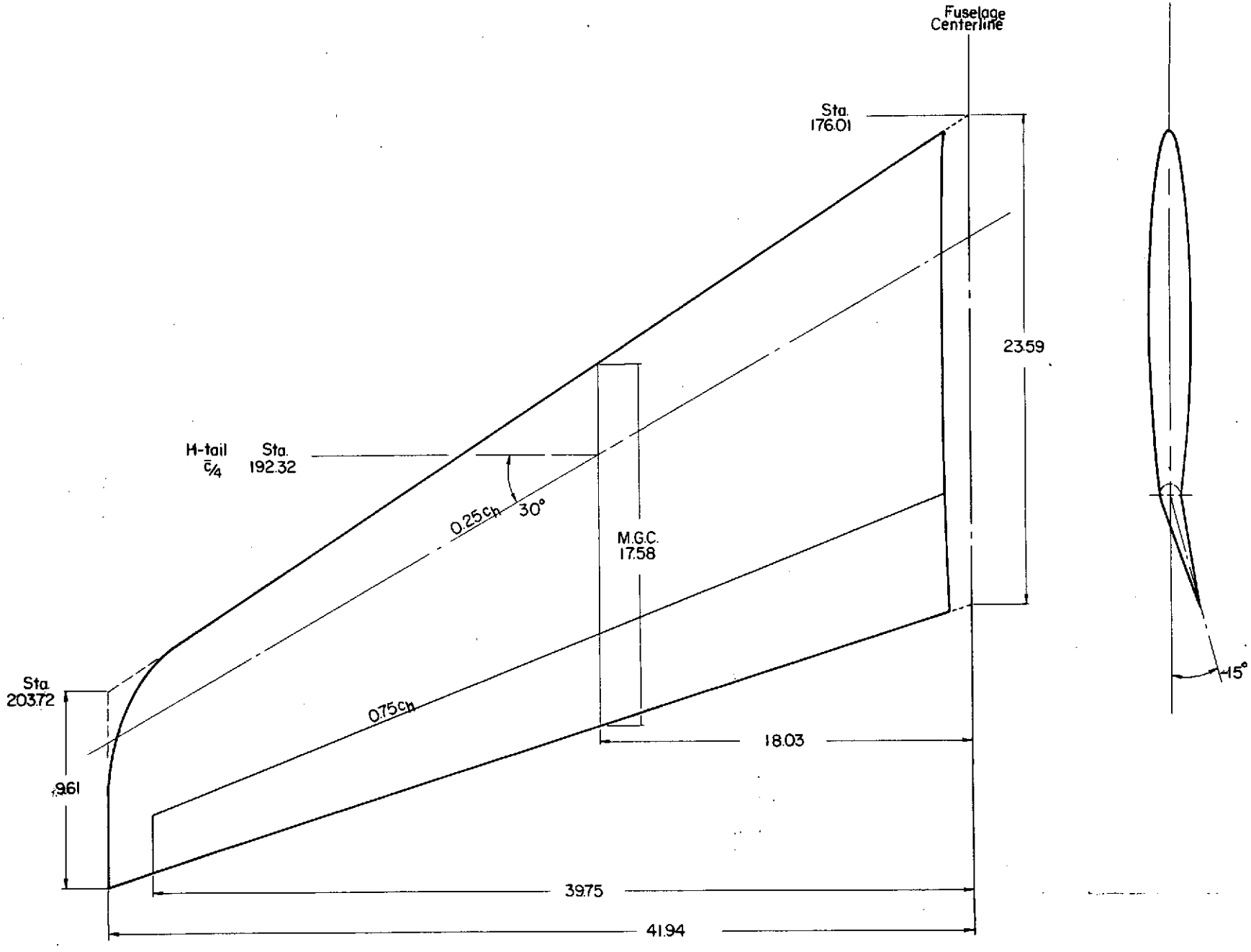

Figure 6. - Details of the horizontal tail used in the wind-tunnel investigation. Dimensions are in centimeters or fraction of local chord.

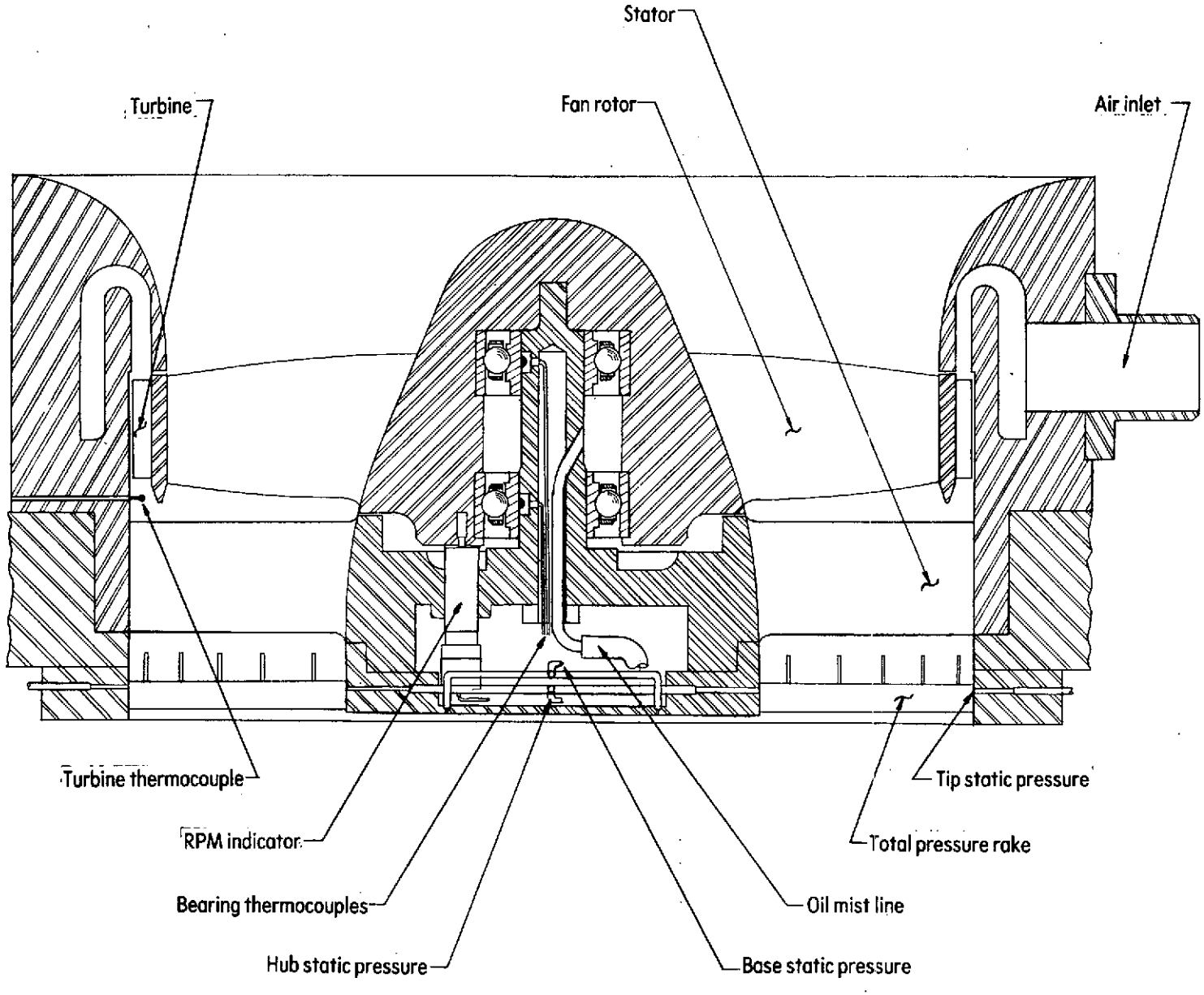

Figure 7. - Details of basic fan assembly with instrumentation.

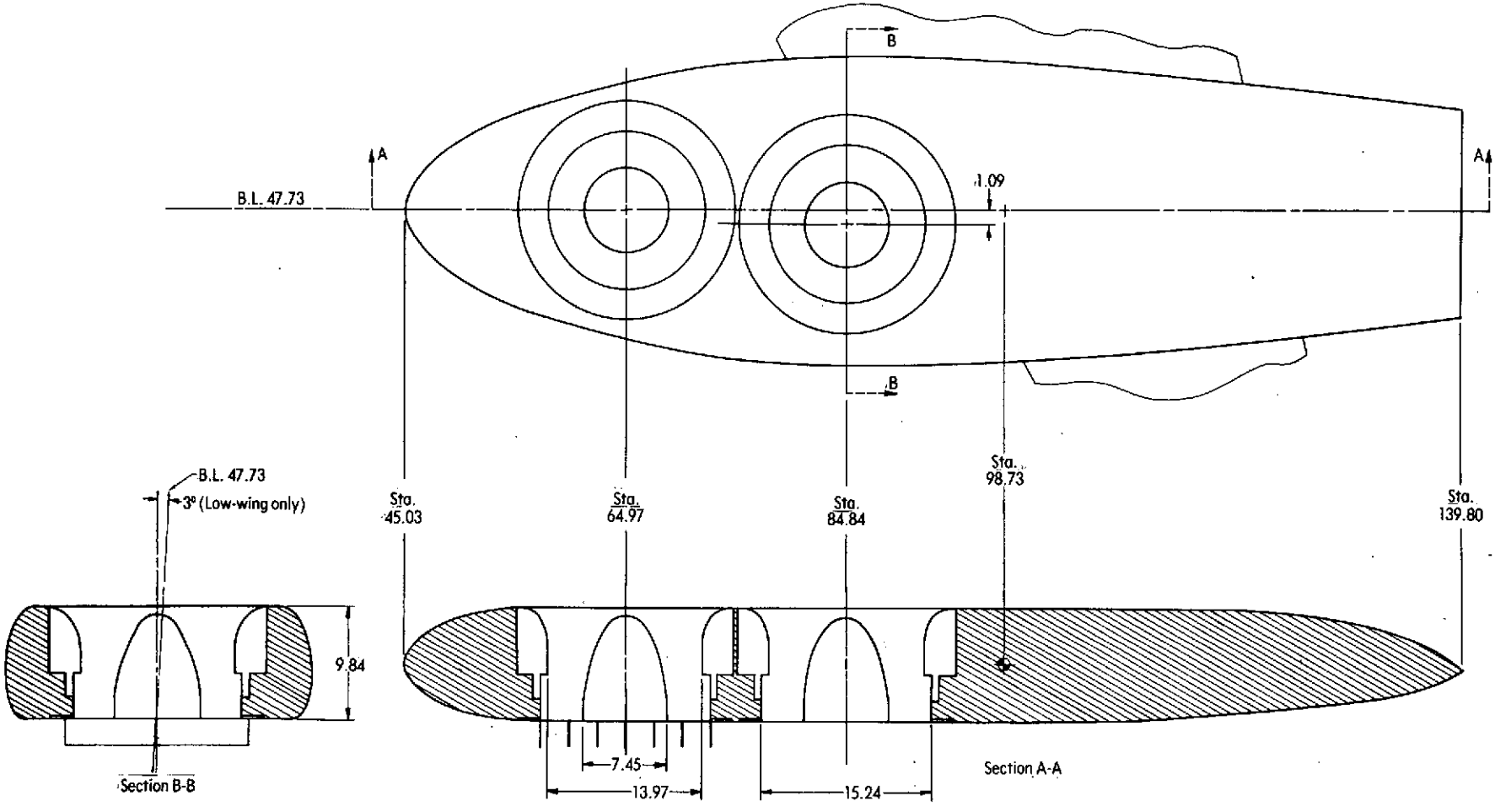

Figure 8. - Details of lift-fan pod and fan location. Dimensions are in centimeters.

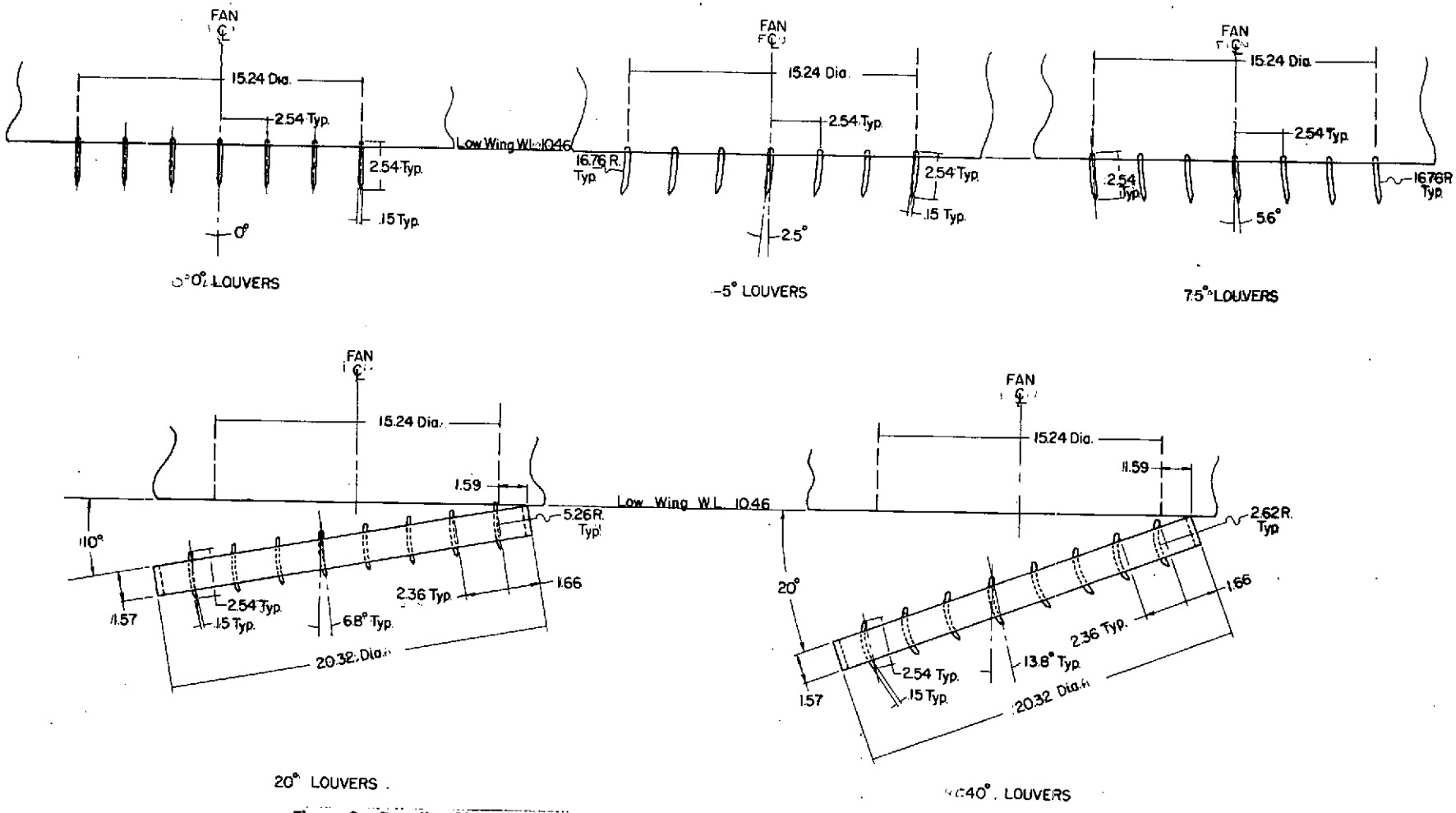

Figure 9. - Details of louver assemblies on each lift-fan exit. Dimensions are in centimeters.

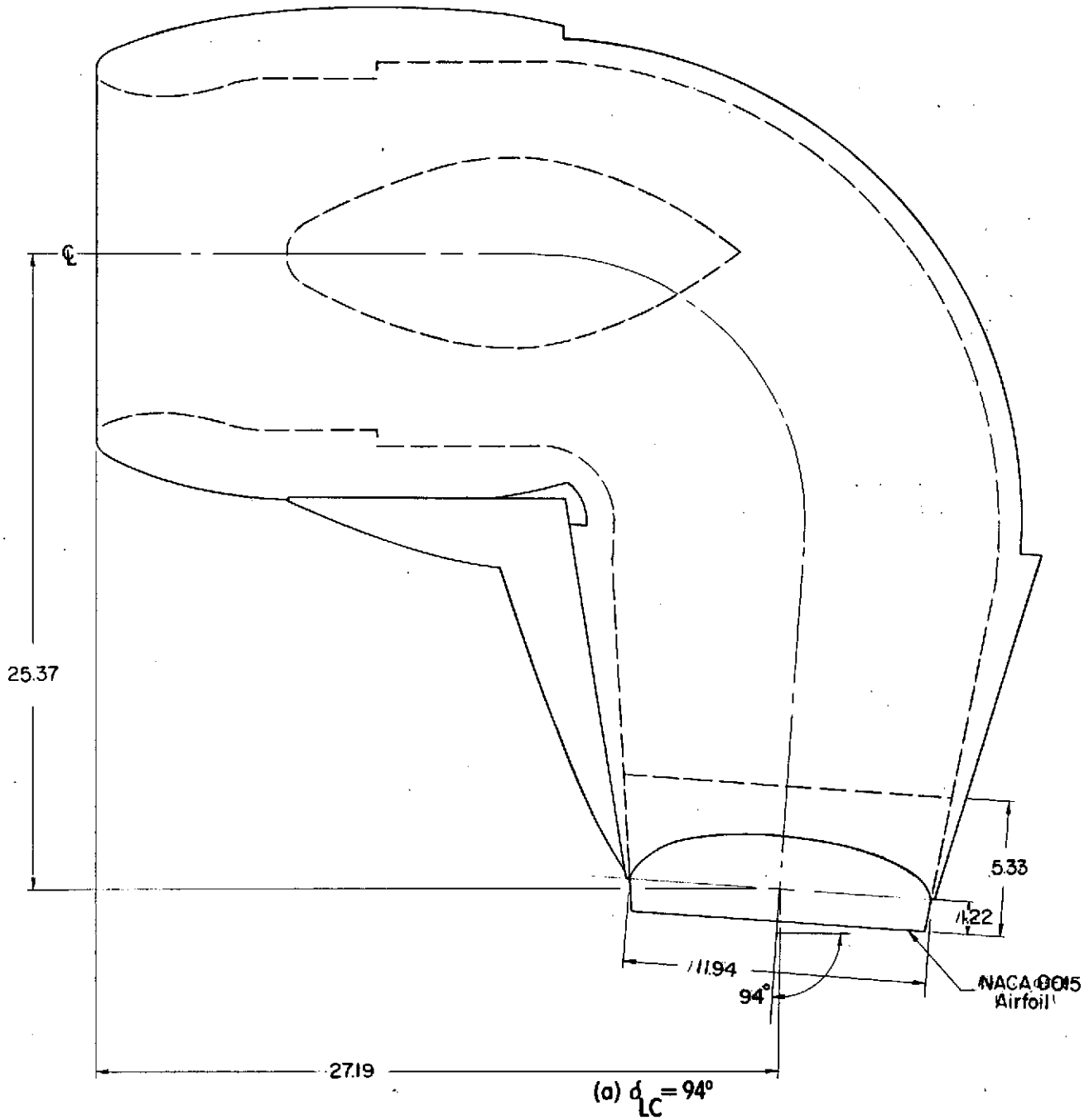

(a) $\delta_{LC} = 94°$

Figure 10. - Details of lift-cruise deflector assemblies. Dimensions are in centimeters.

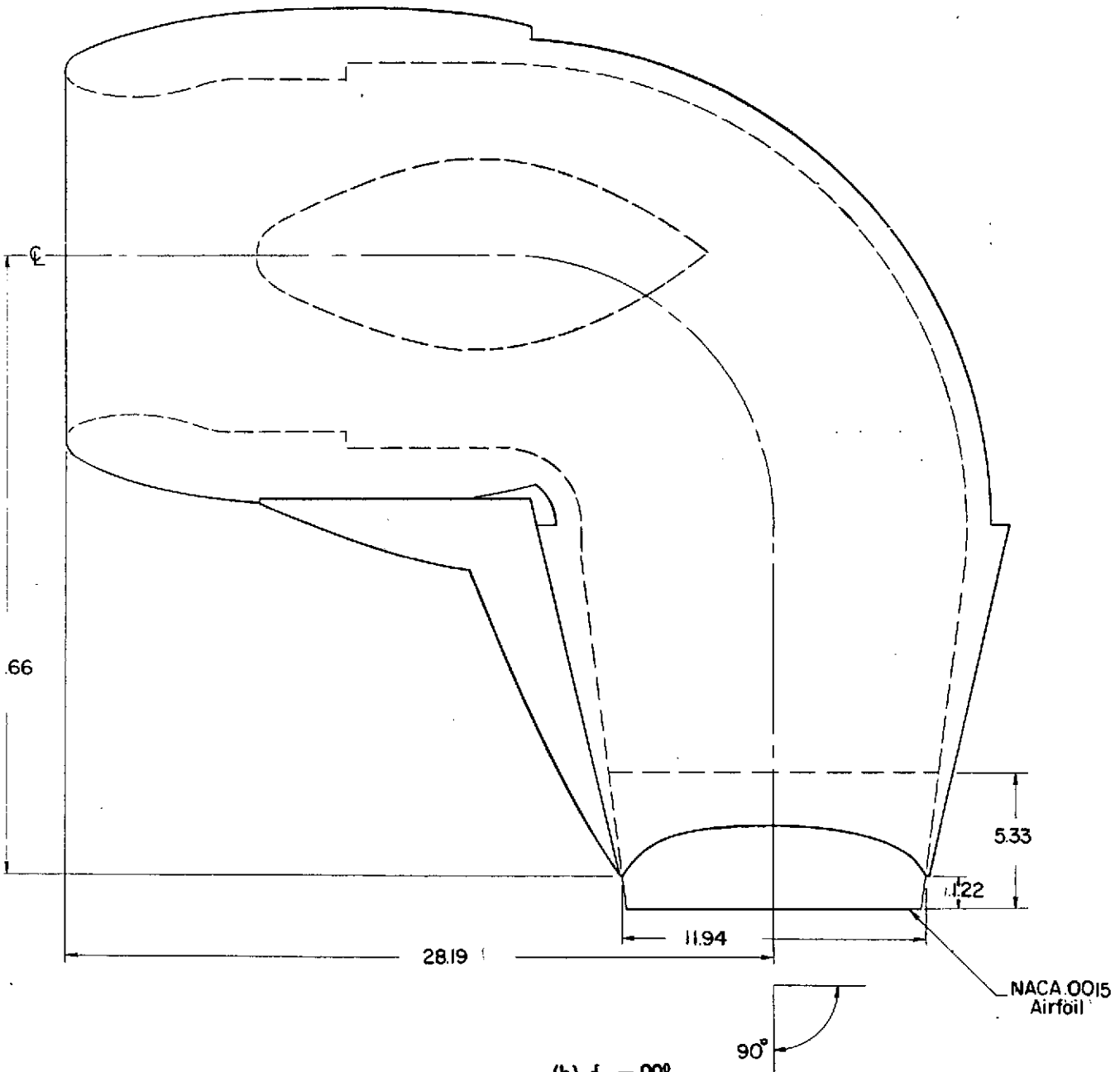

(b) $\delta_{LC} = 90°$

Figure 10. - Continued.

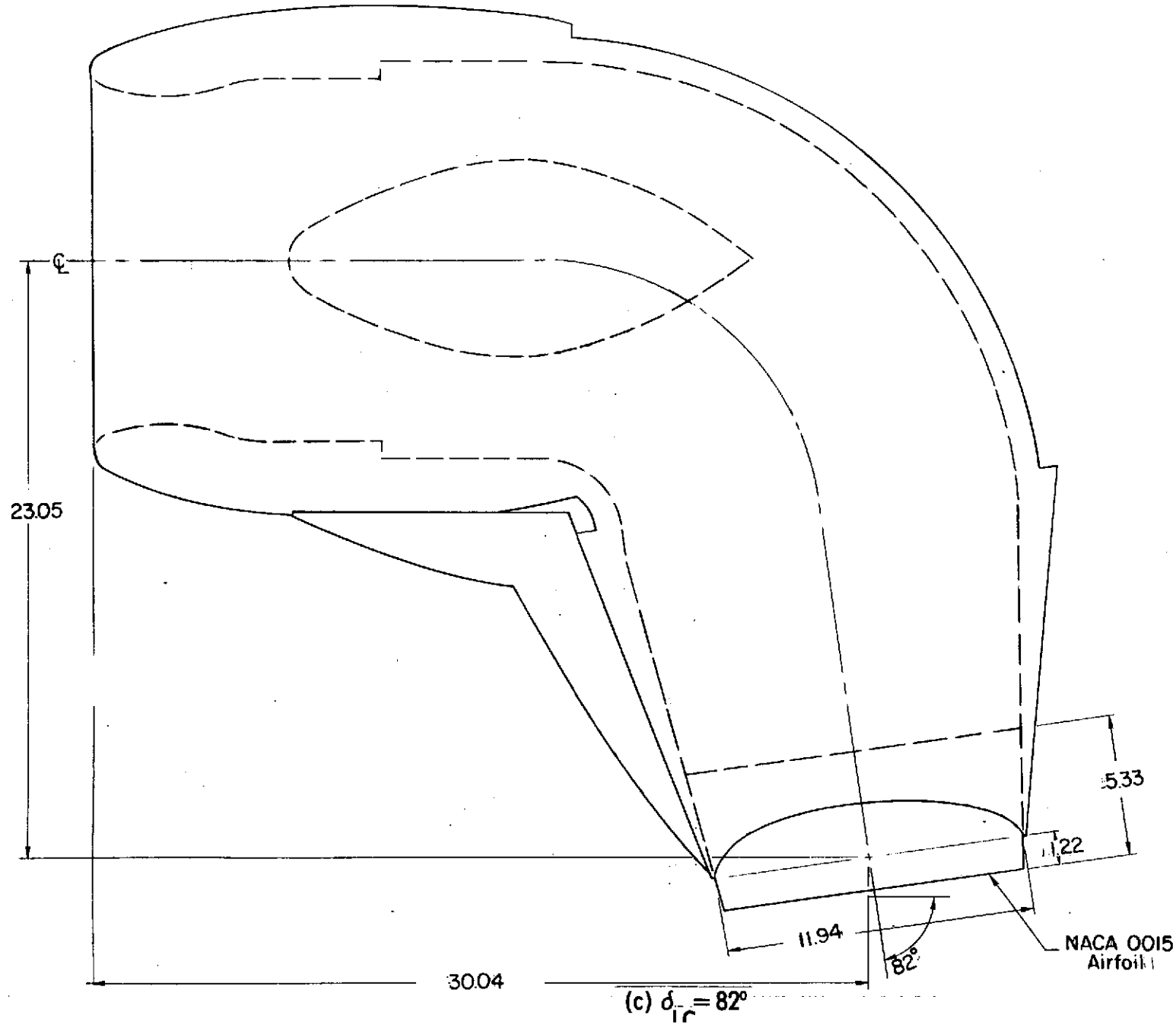

(c) $\delta_{lc} = 82°$

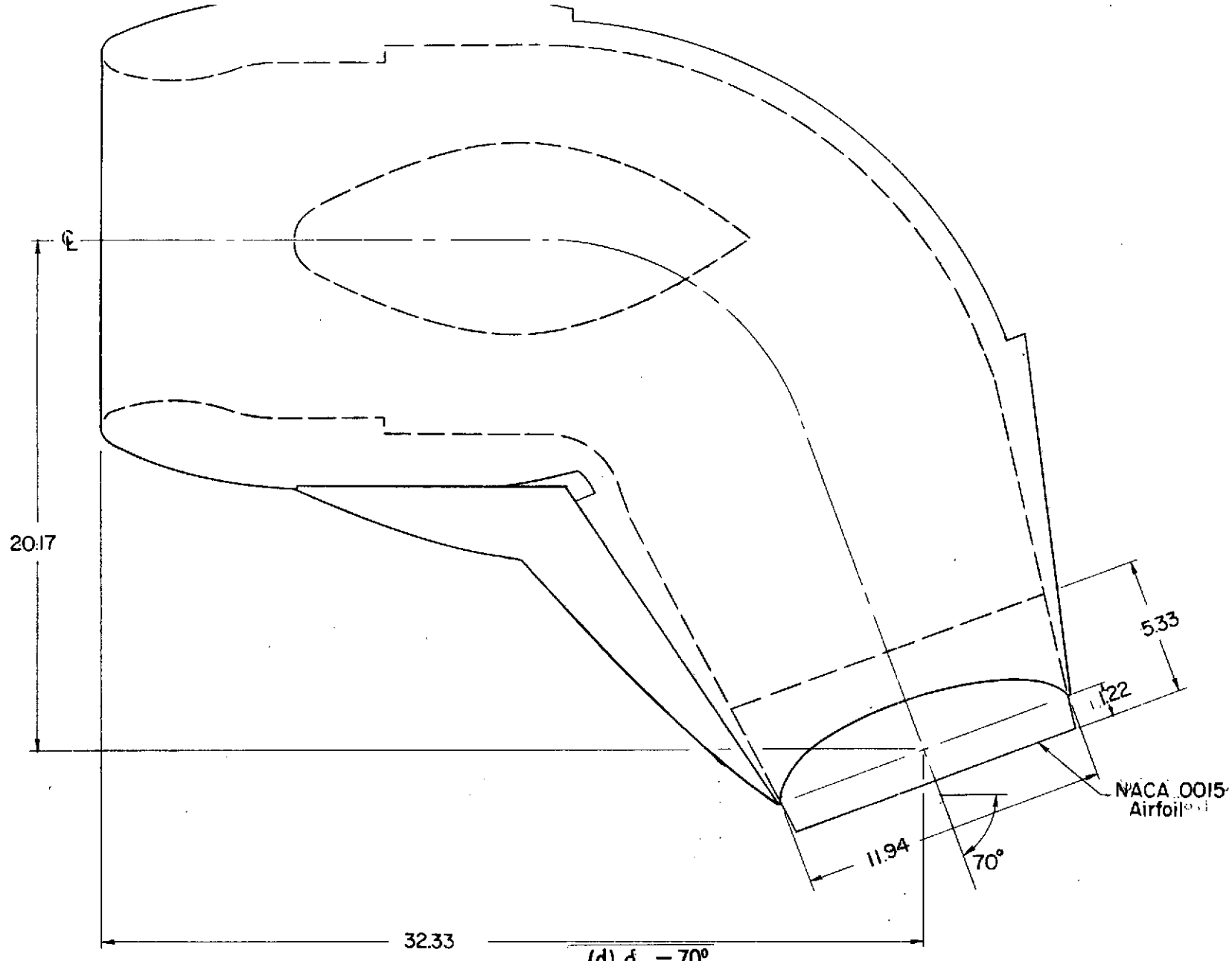

(d) $\delta_{LC} = 70°$

Figure 10. - Continued.

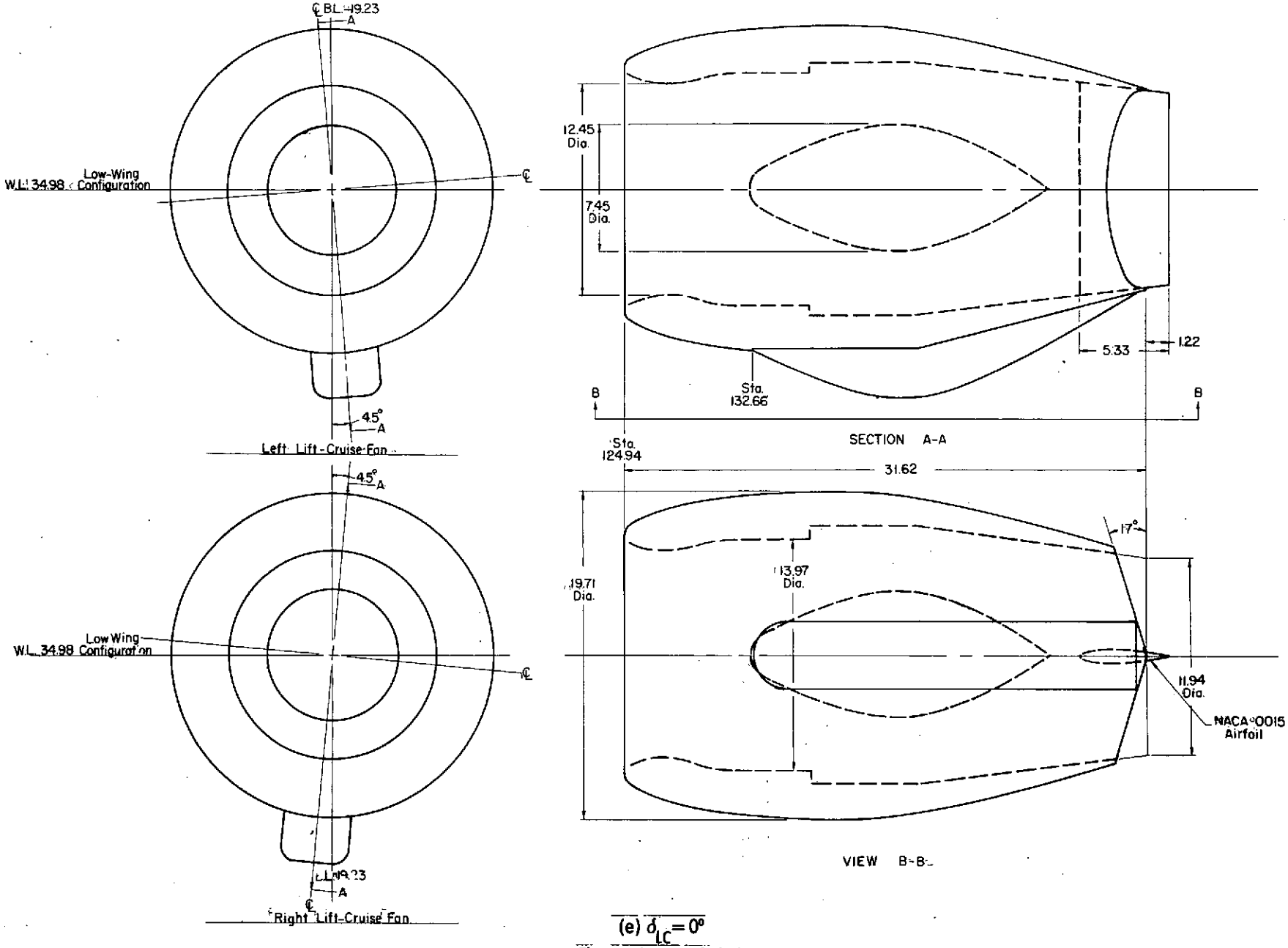

(e) $\delta_{LC} = 0°$

Figure 10. - Concluded.

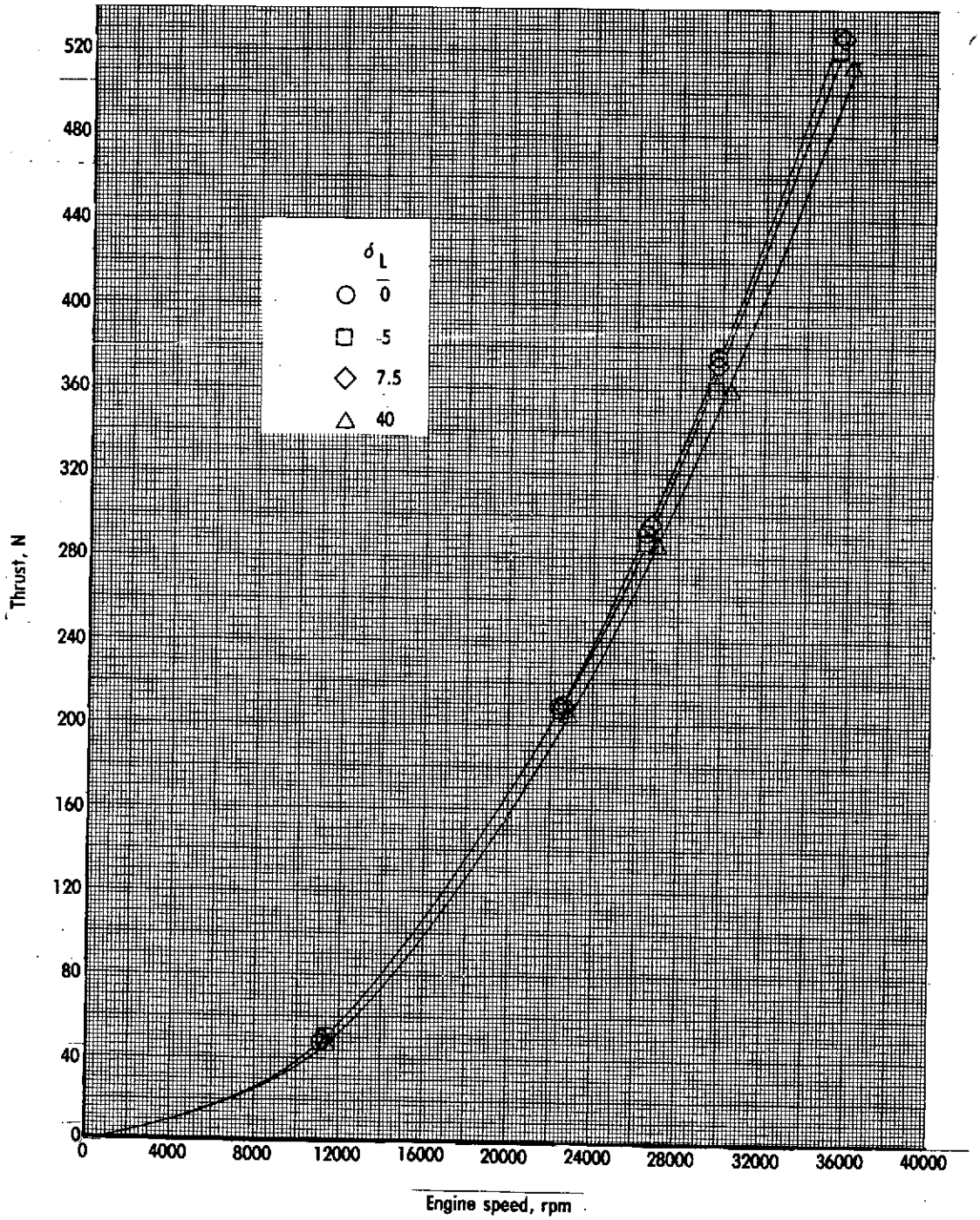

(a) Lift fan

Figure 11. - Typical thrust calibration as a function of engine speed.

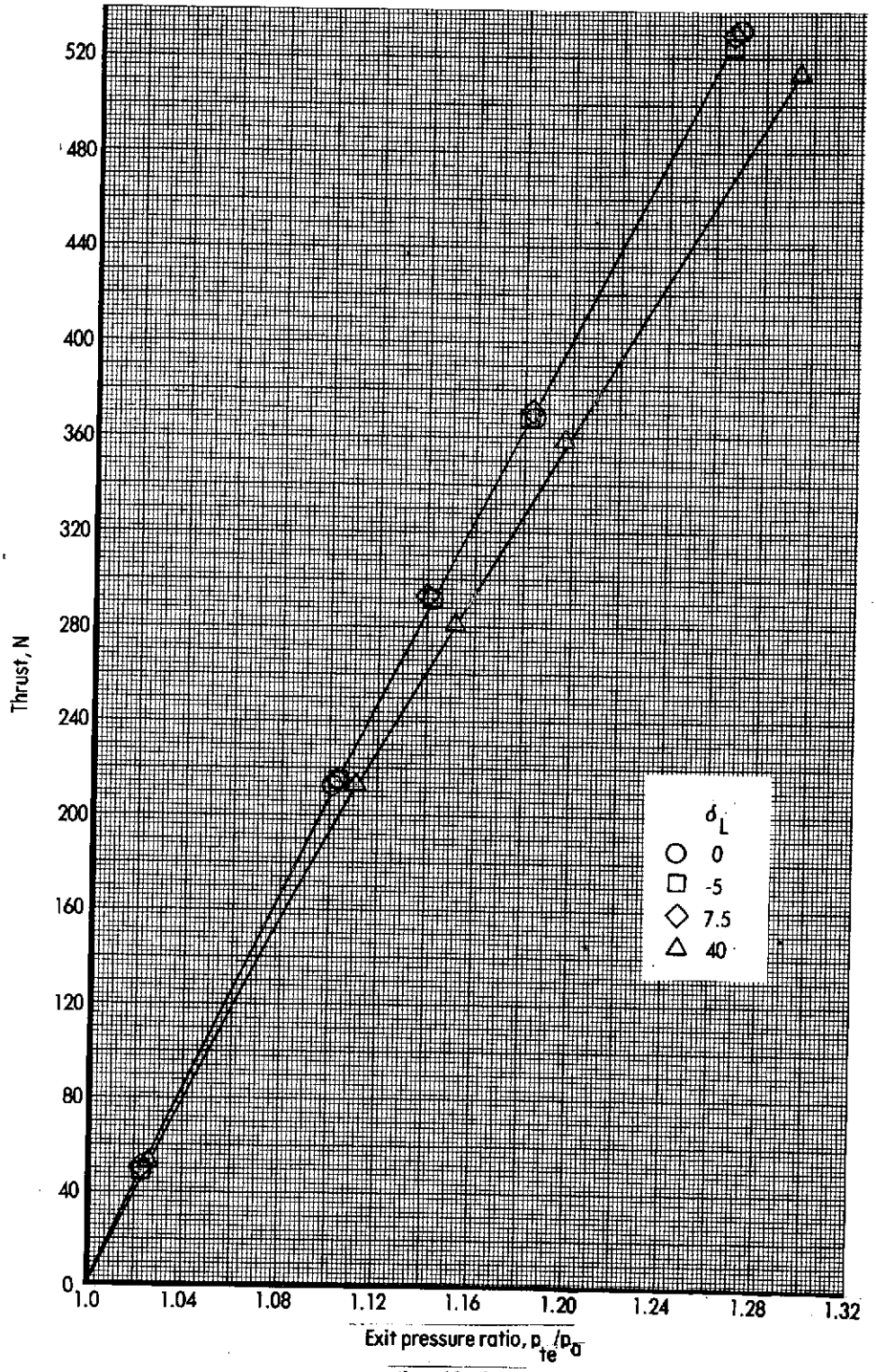

(b) Lift-fan

Figure 11. - Continued

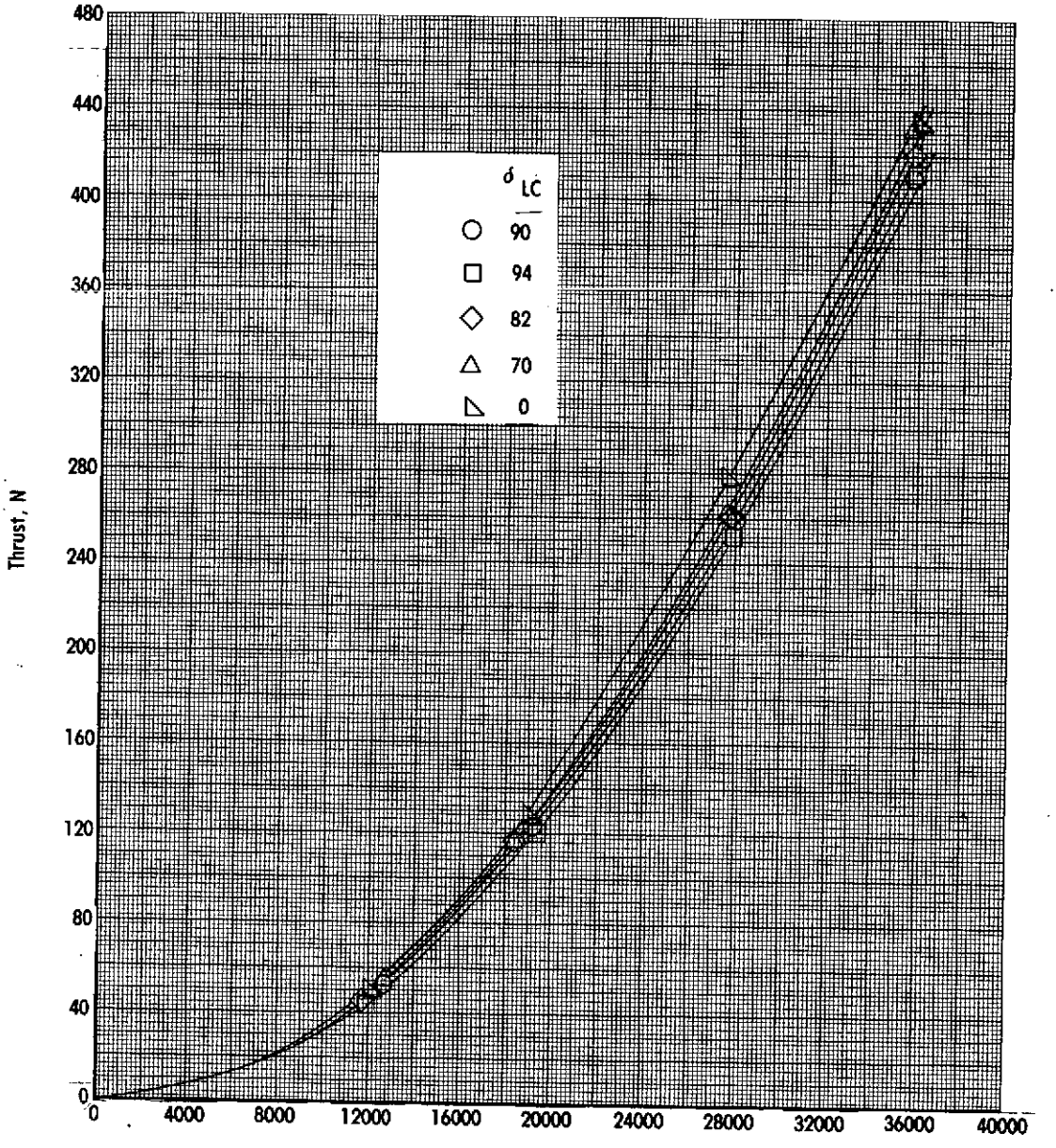

(c) Lift-cruise fan

Figure 11.-CONTINUED

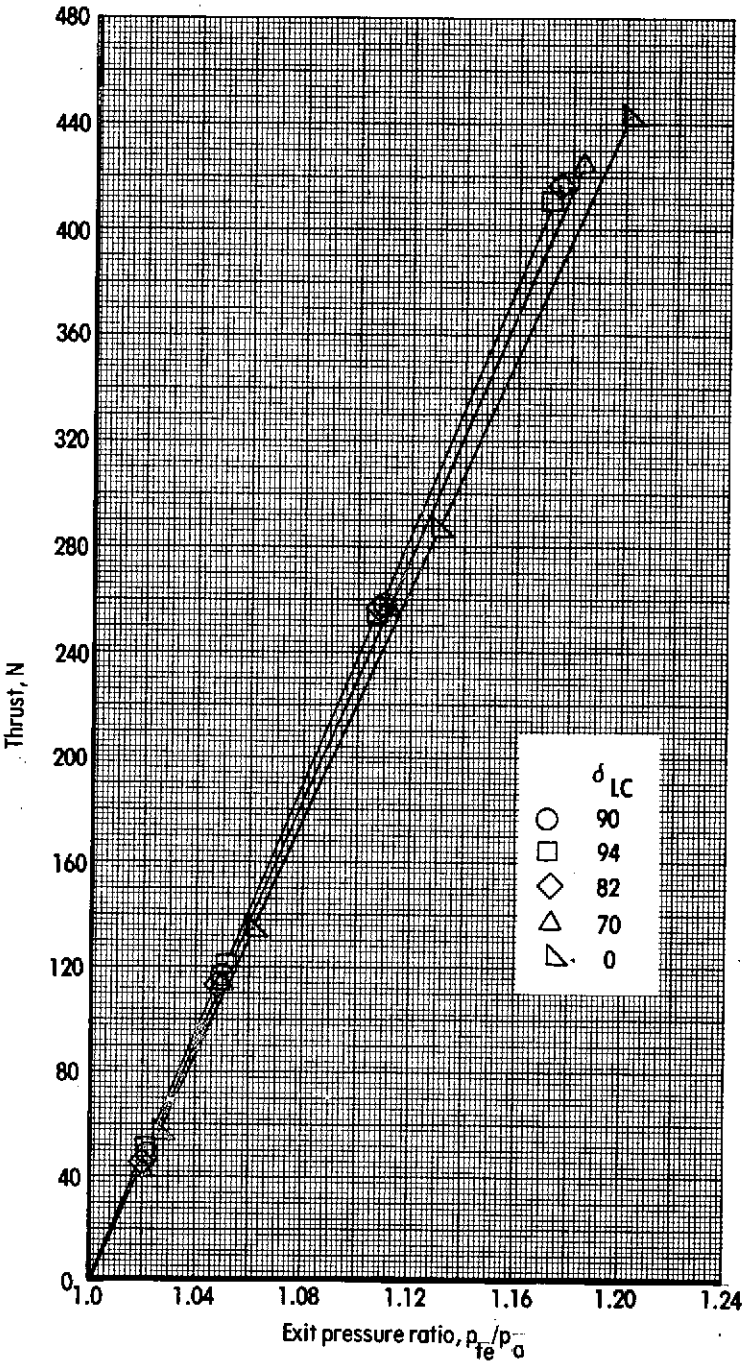

(d) Lift-cruise fan

Figure 11. - Concluded.

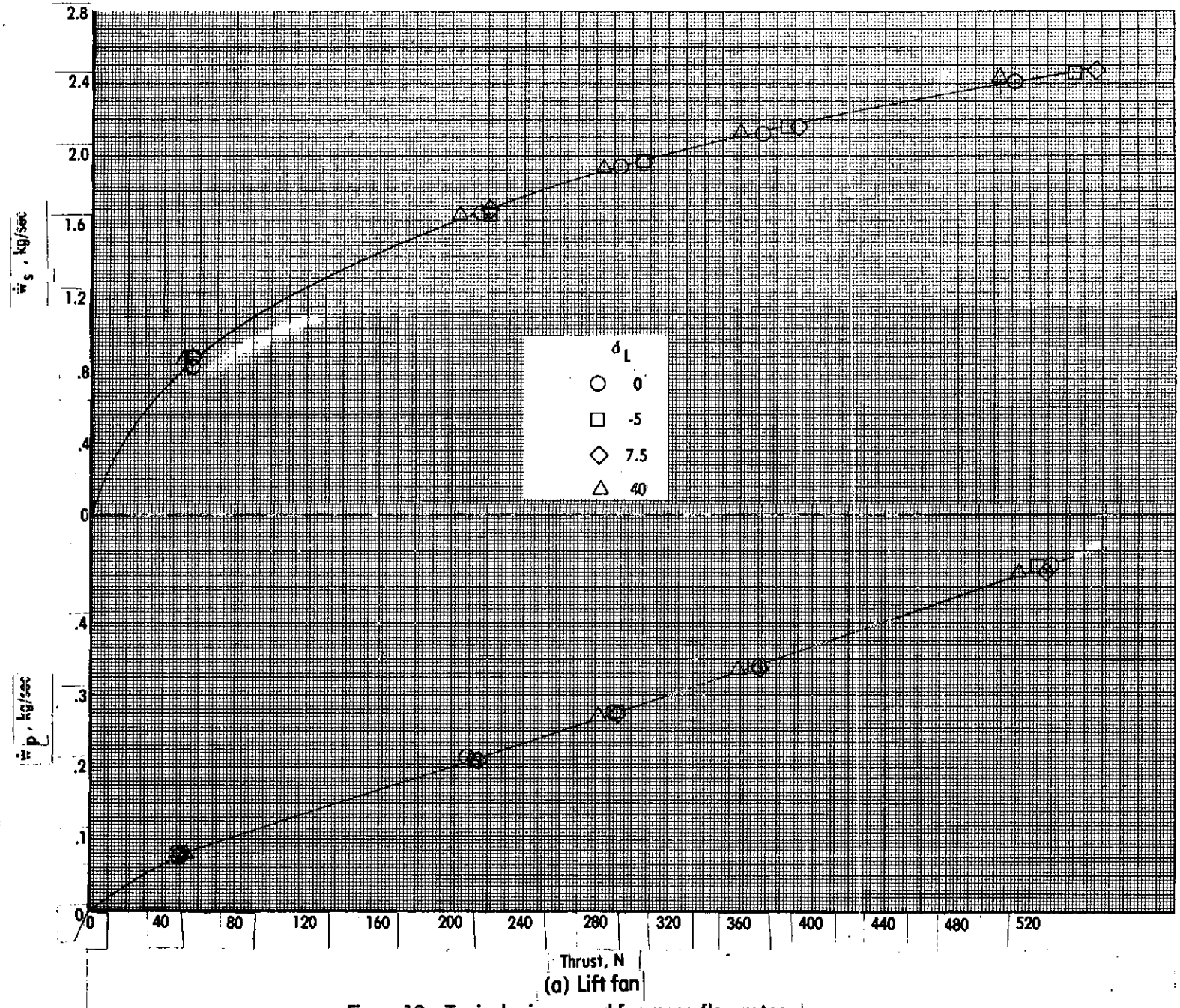

(a) Lift fan

Figure 12. - Typical primary and fan mass-flow rates.

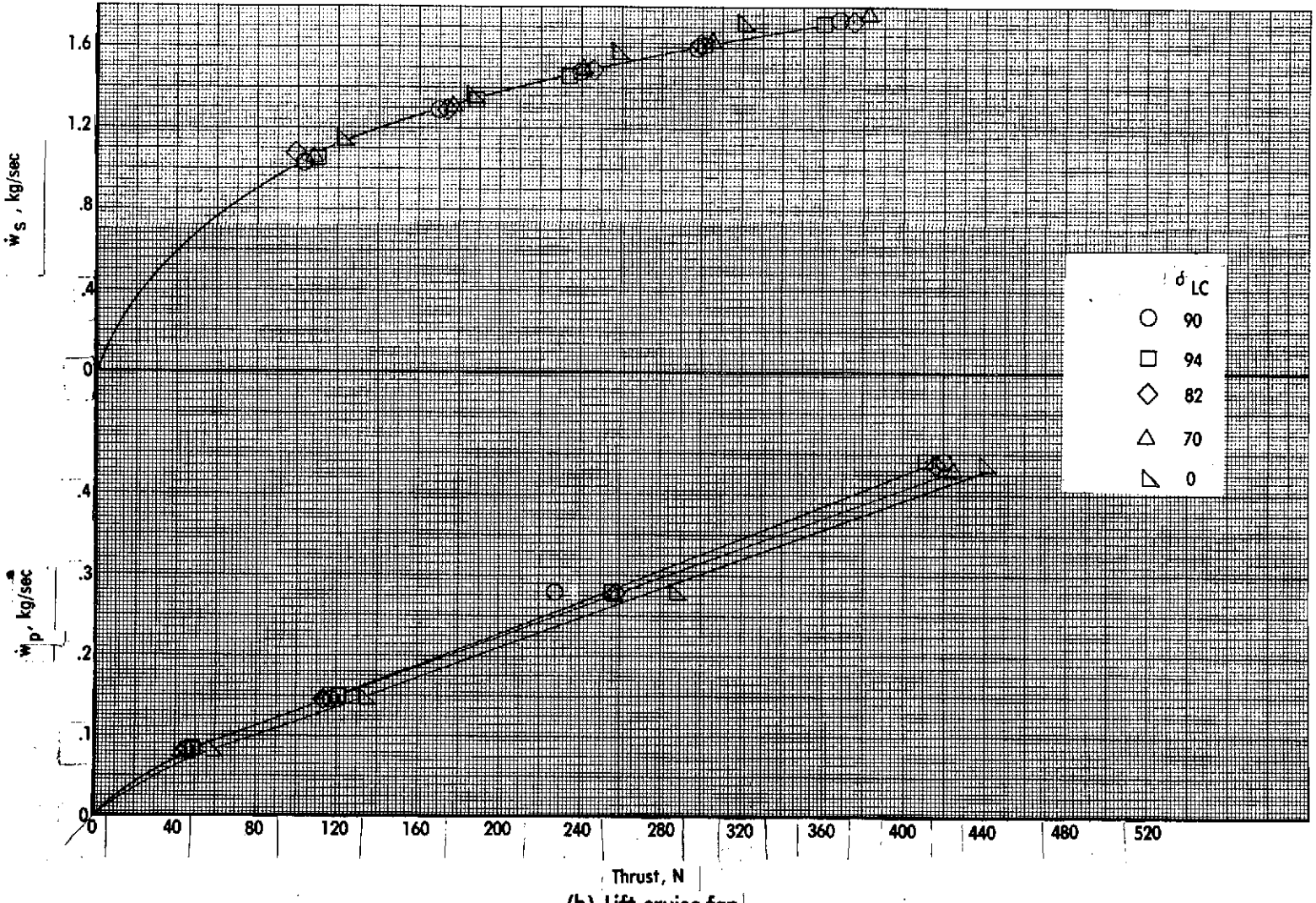

(b) Lift-cruise fan

Figure 12. - Concluded.

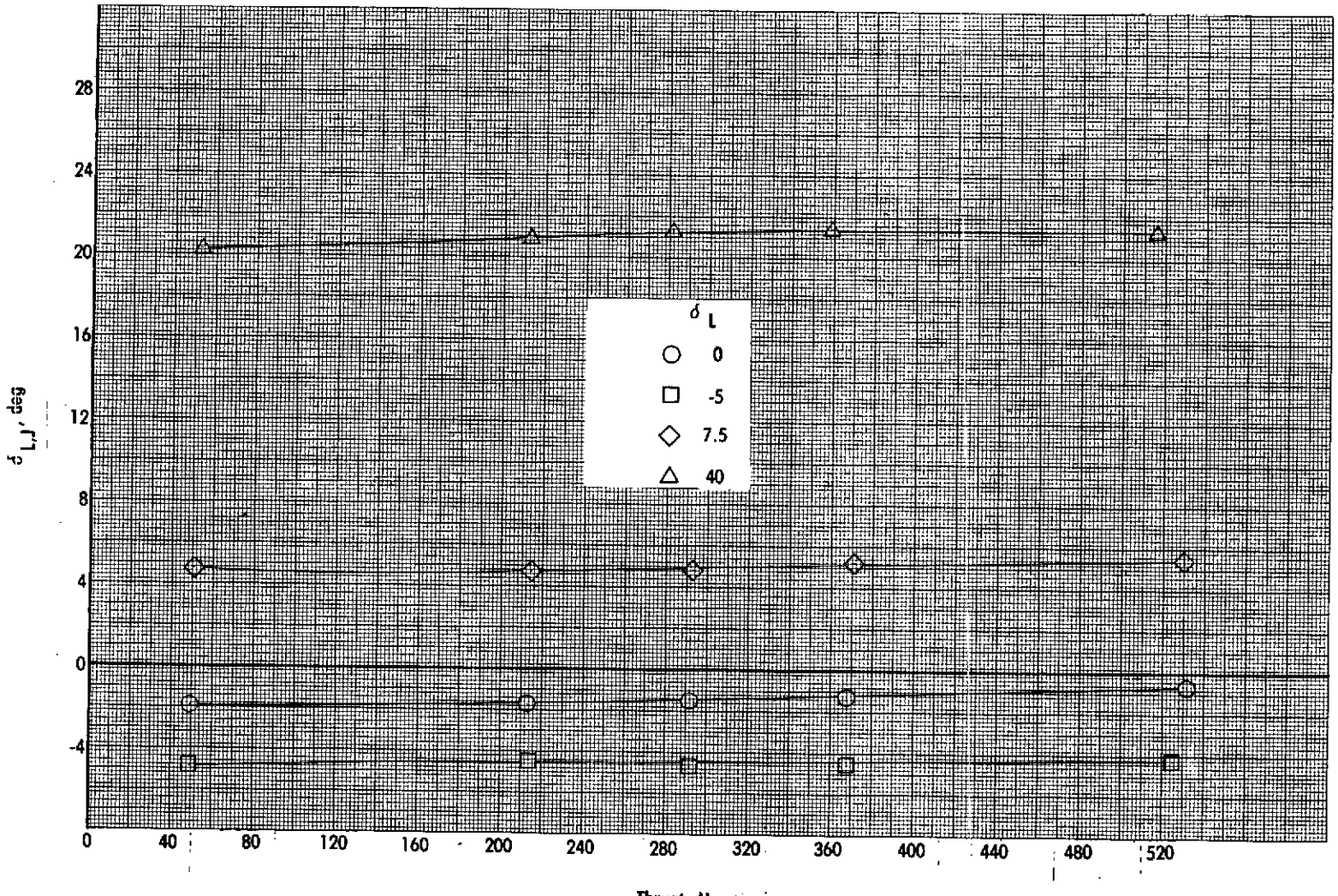

(a) Lift fan

Figure 13. - Typical fan-exhaust deflection angle.

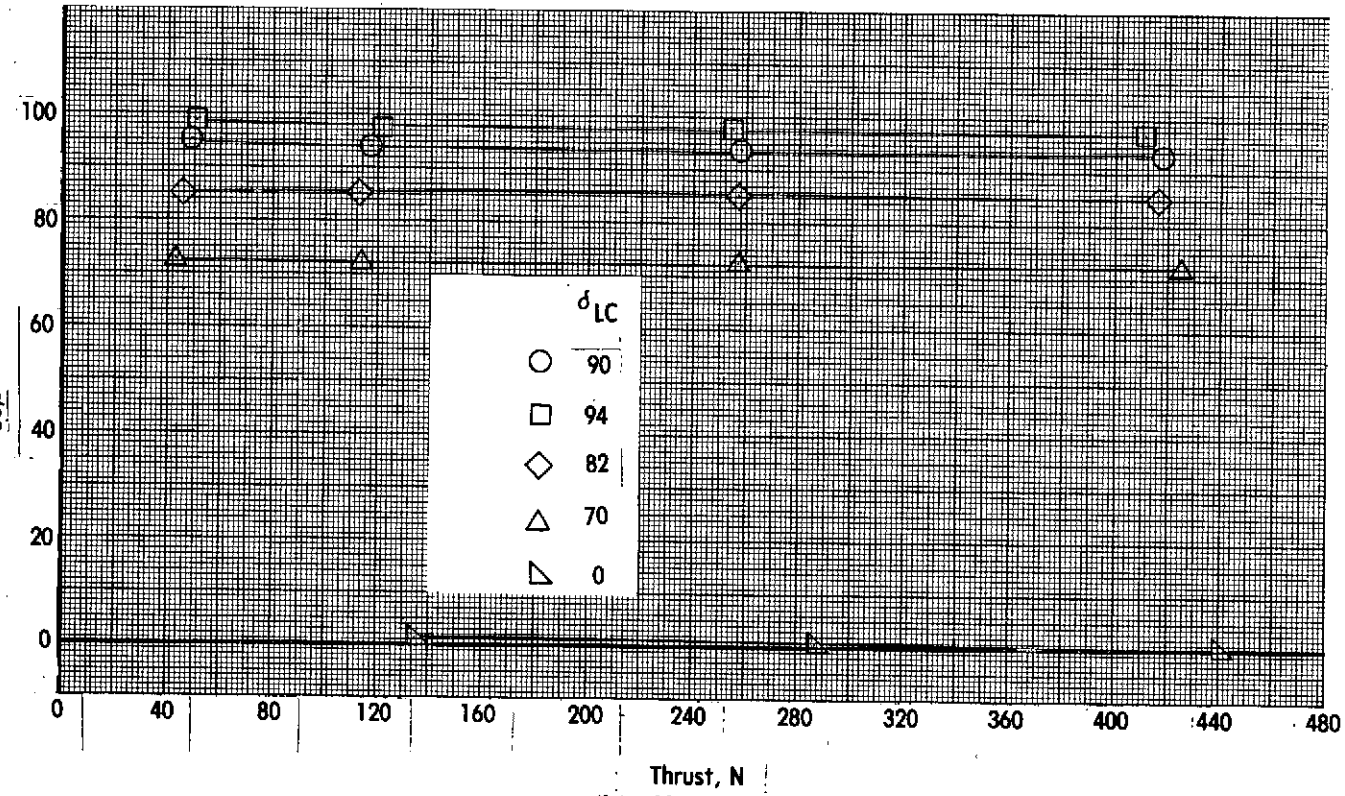

(b) Lift-cruise fan

Figure 13. - Concluded.

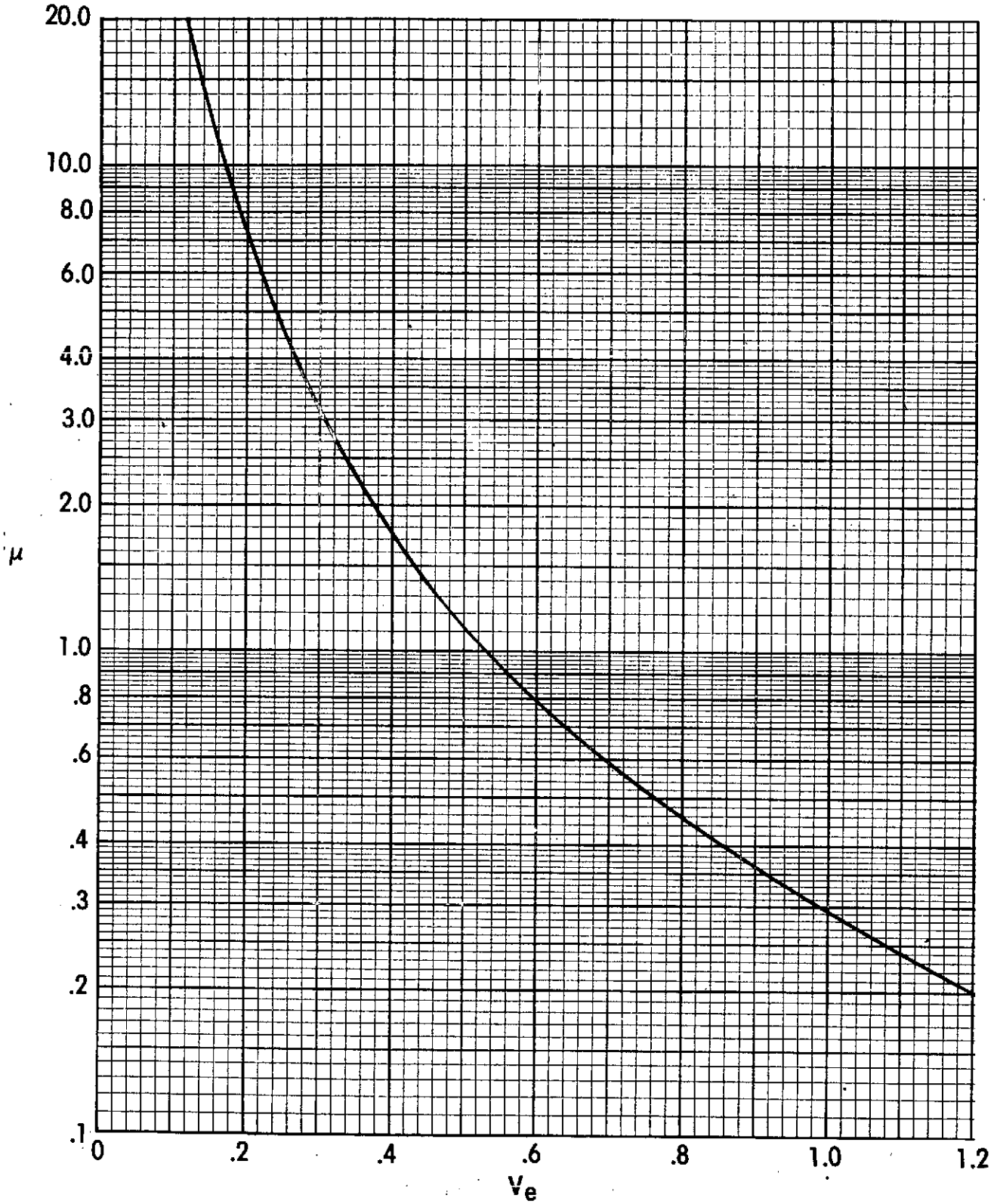

Figure 14. - Variation of thrust coefficient with velocity ratio. All six fans operating.

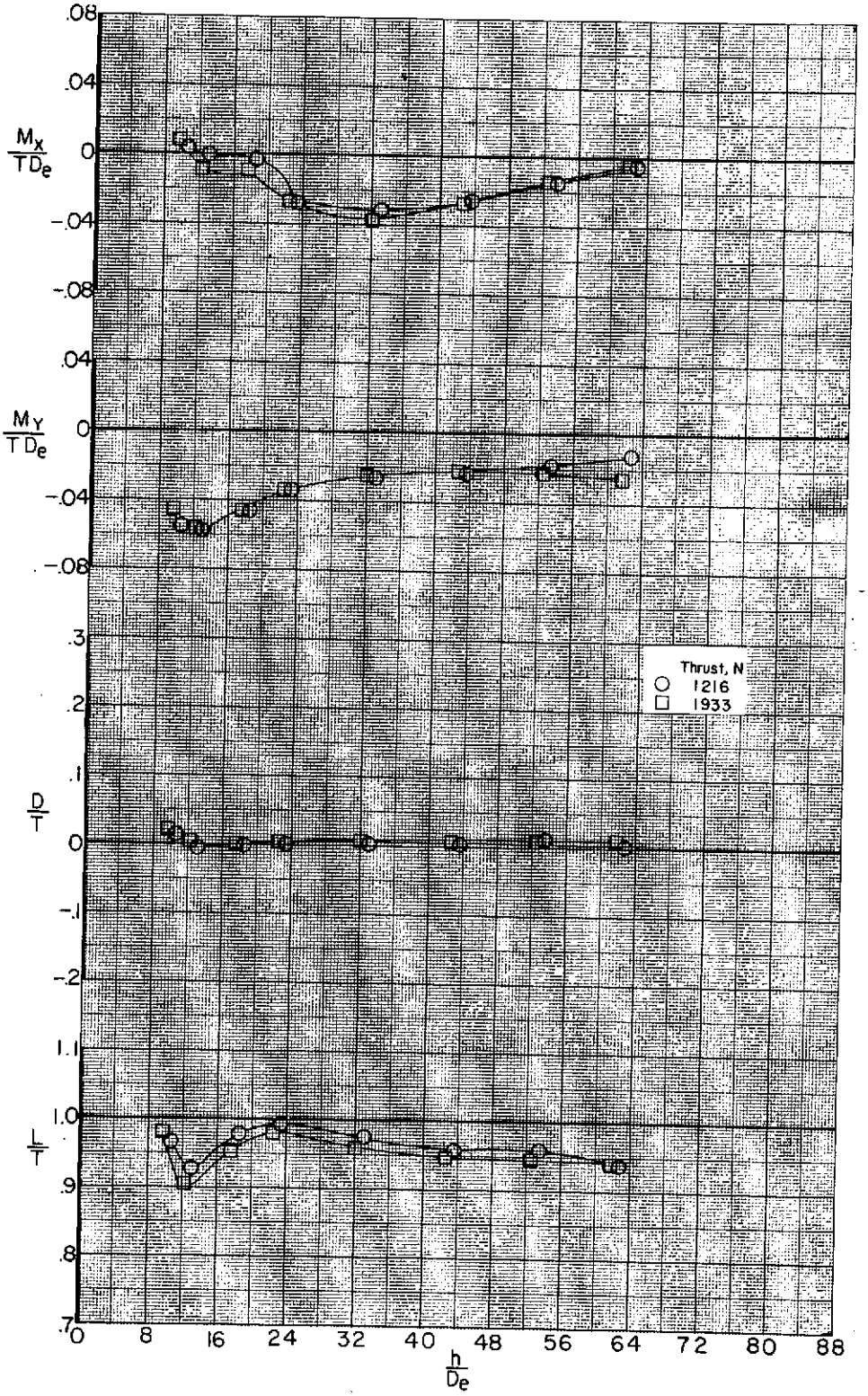

Figure 15. - Effect of ground proximity on the induced loads of configuration in hover. $\delta_L = 0°$ $\delta_{LC} = 90°$ $\delta_f = 40°$ tail off $\alpha = 0°$ $\beta = 0°$

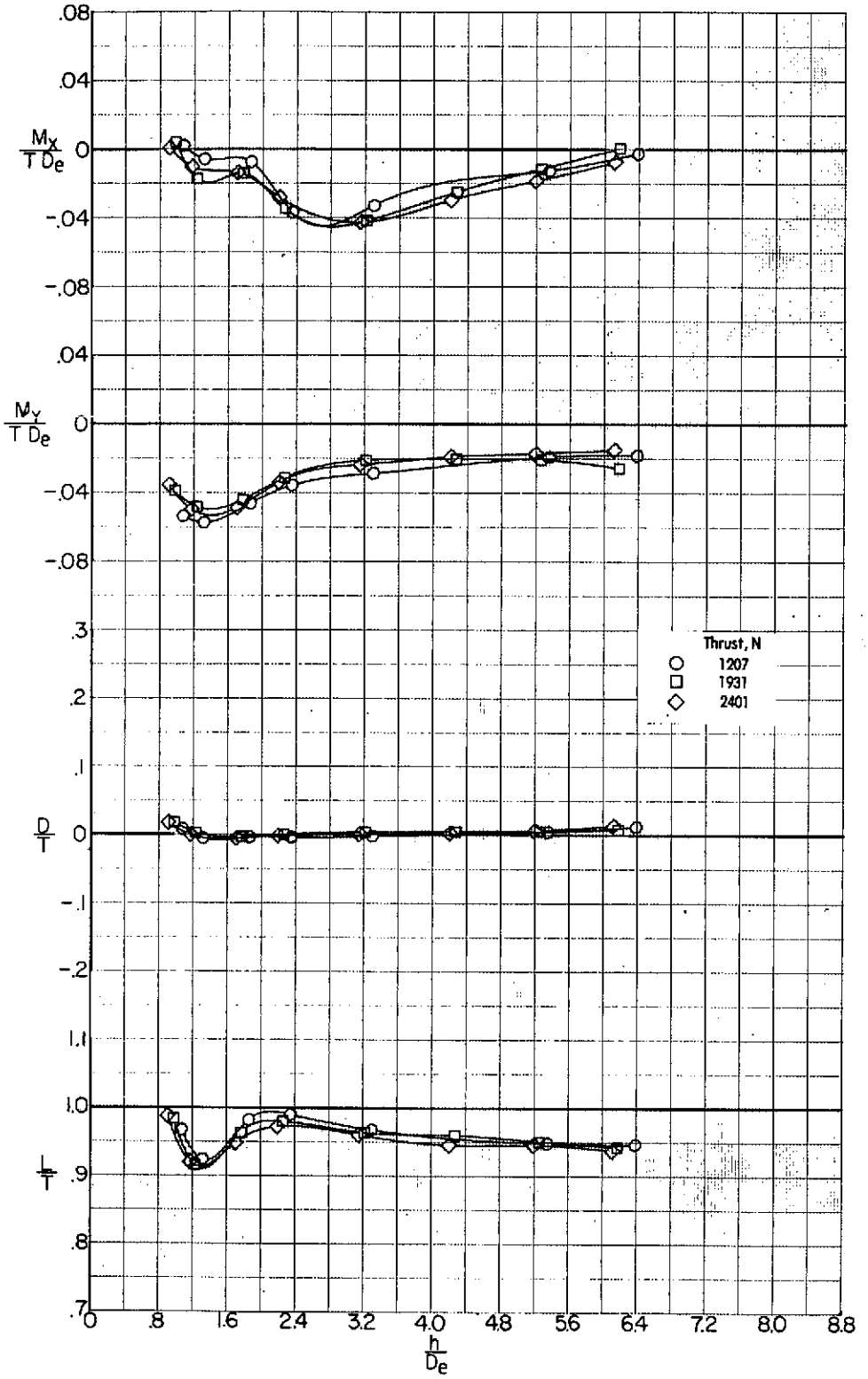

Figure 16. - Effect of ground proximity on the induced loads of configuration in hover.
$\delta_L = 0°$ $\delta_{LC} = 90°$ $\delta_f = 40°$ $i_t = 0°$ $\delta_e = 0°$ $\alpha = 0°$ $\phi = 0°$

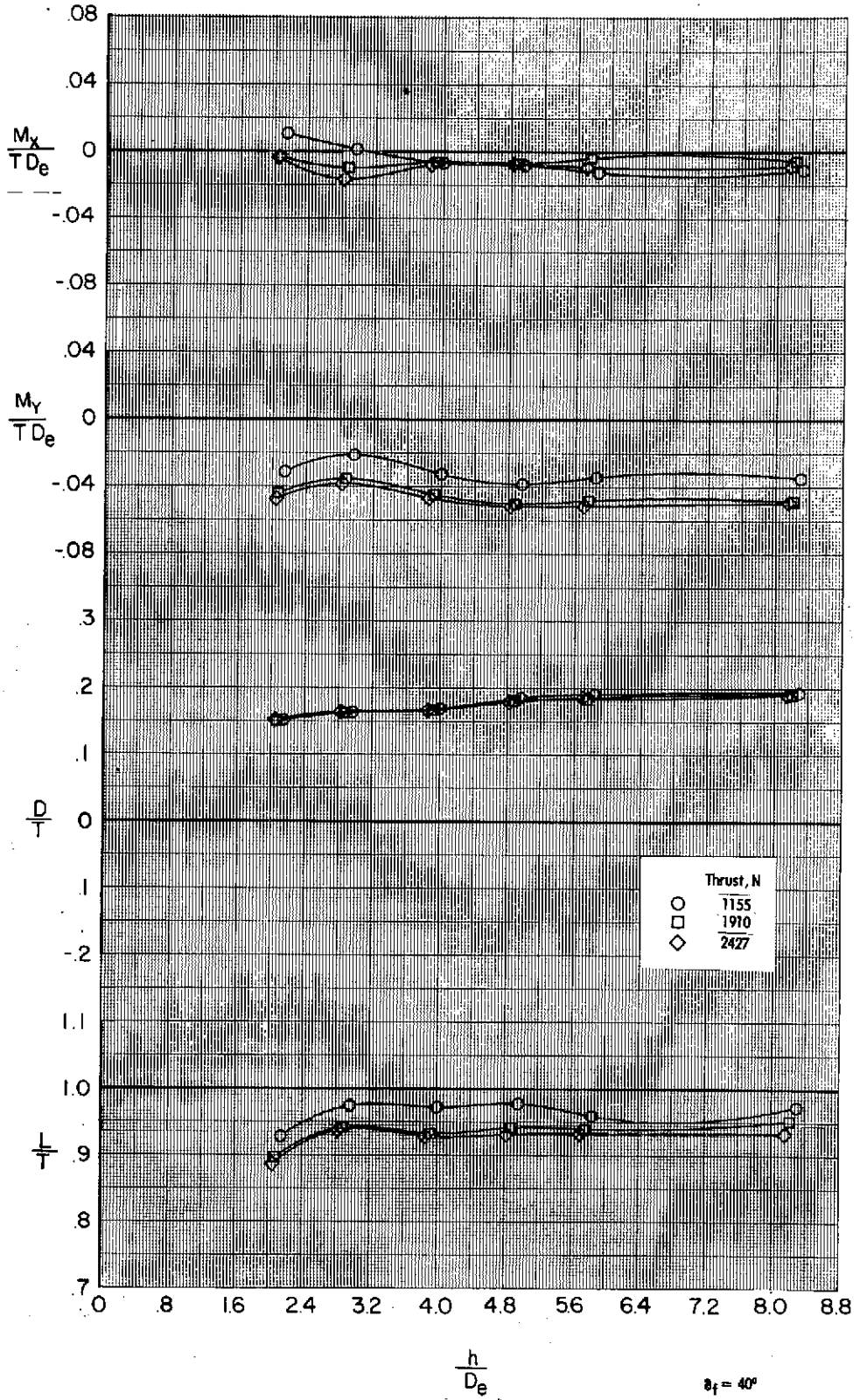

Figure 17. - Effect of ground proximity on the induced loads of configuration in hover. $\delta_L = 0°$ $\delta_{LC} = 90°$ tail off $\alpha = 10°$ $\phi = 0°$

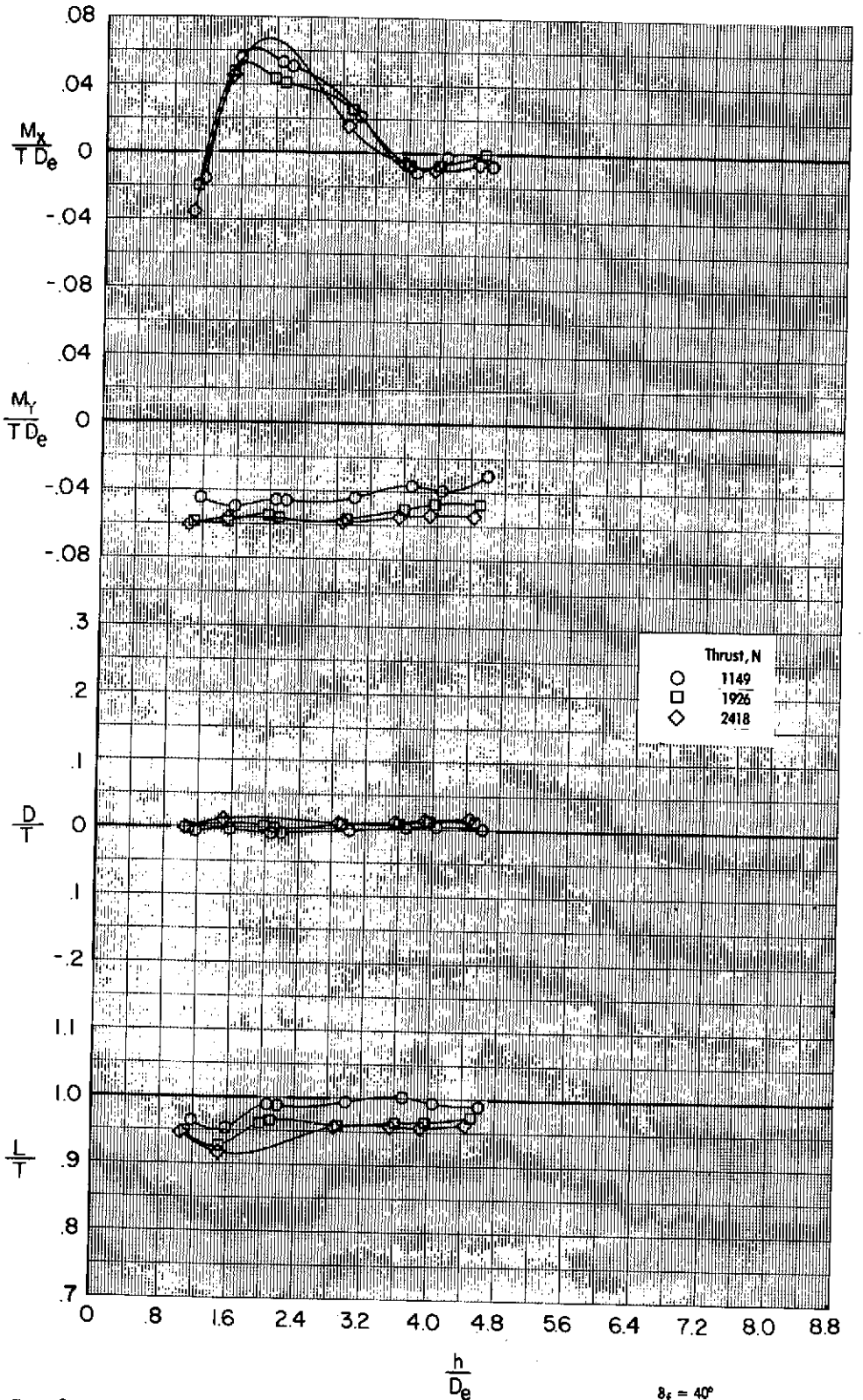

Figure 18. - Effect of ground proximity on the induced loads of configuration in hover. $\delta_L = 0°$ $\delta_{LC} = 90°$ tail off $\alpha = 0°$ $\phi = 10°$ $\delta_f = 40°$

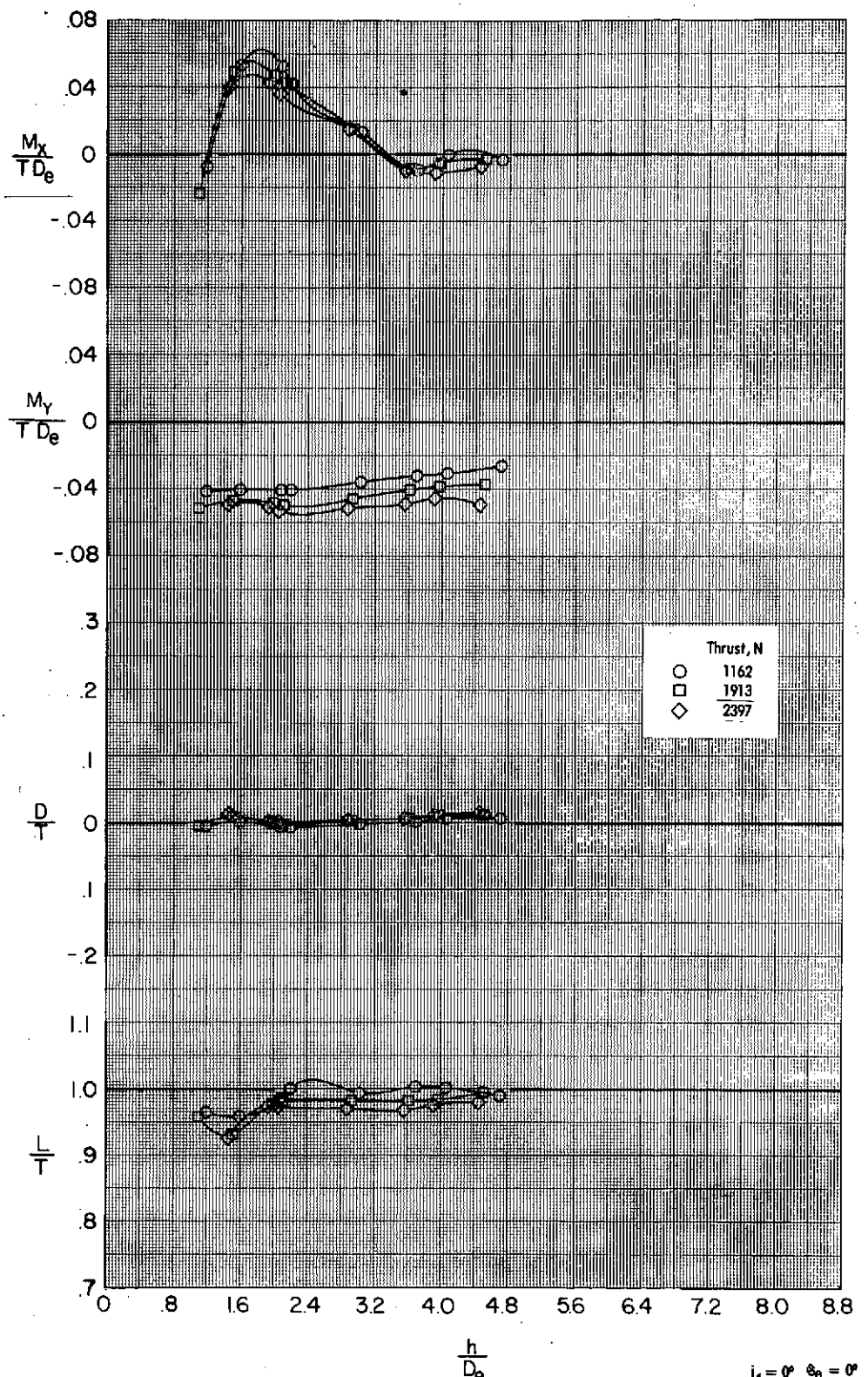

Figure 19. - Effect of ground proximity on the induced loads of configuration in hover. $\delta_L = 0°$ $\delta_{LC} = 90°$ $\delta_f = 40°$ $\alpha = 0°$ $i_f = 0°$ $\theta_e = 0°$ $\varnothing = 10°$

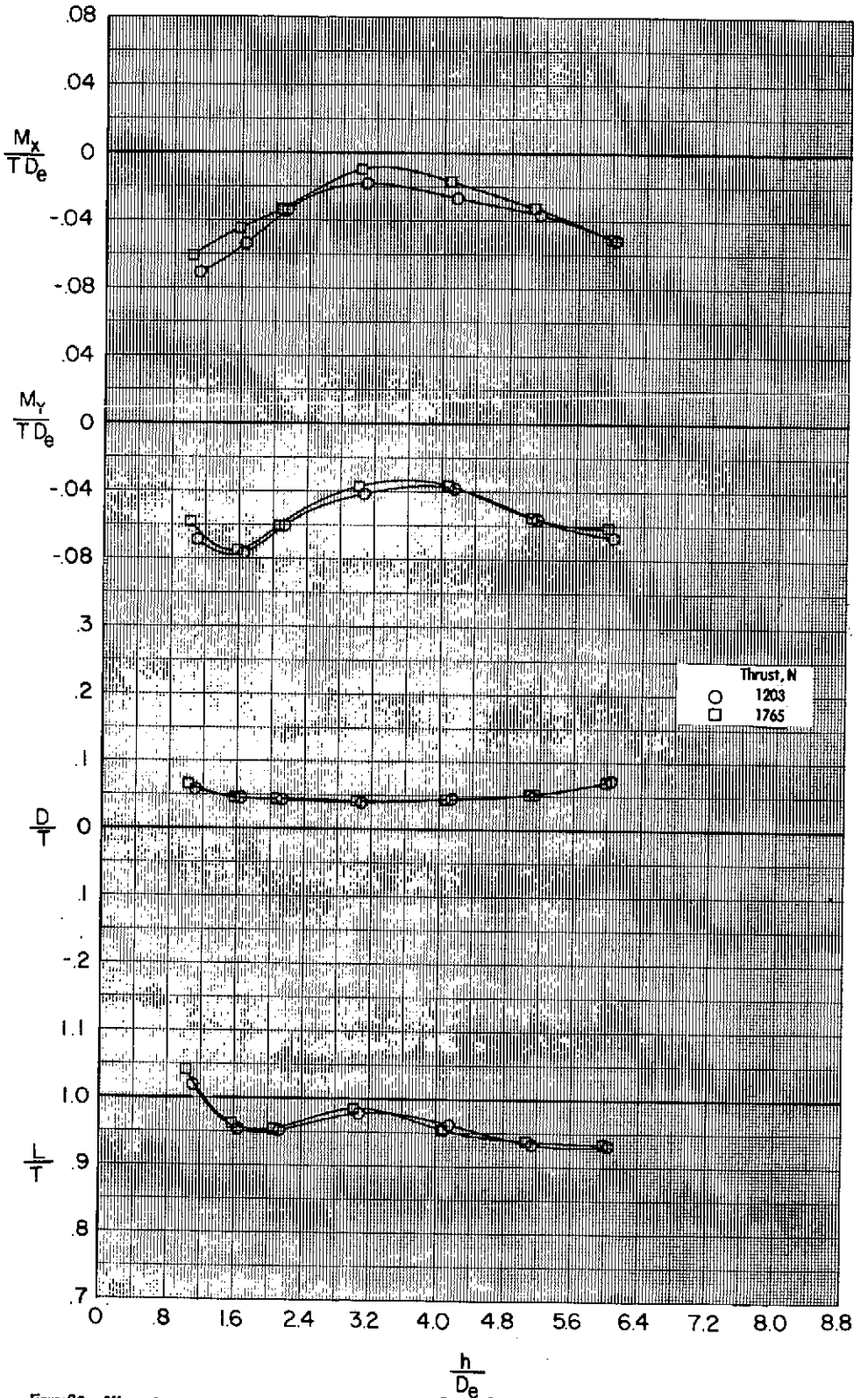

Figure20. - Effect of ground proximity on the induced loads of configuration in hover. $\delta_L = -5°$ $\delta_{LC} = 94°$ $\delta_f = 40°$ tail off $\alpha = 0°$
——— $\phi = 0°$

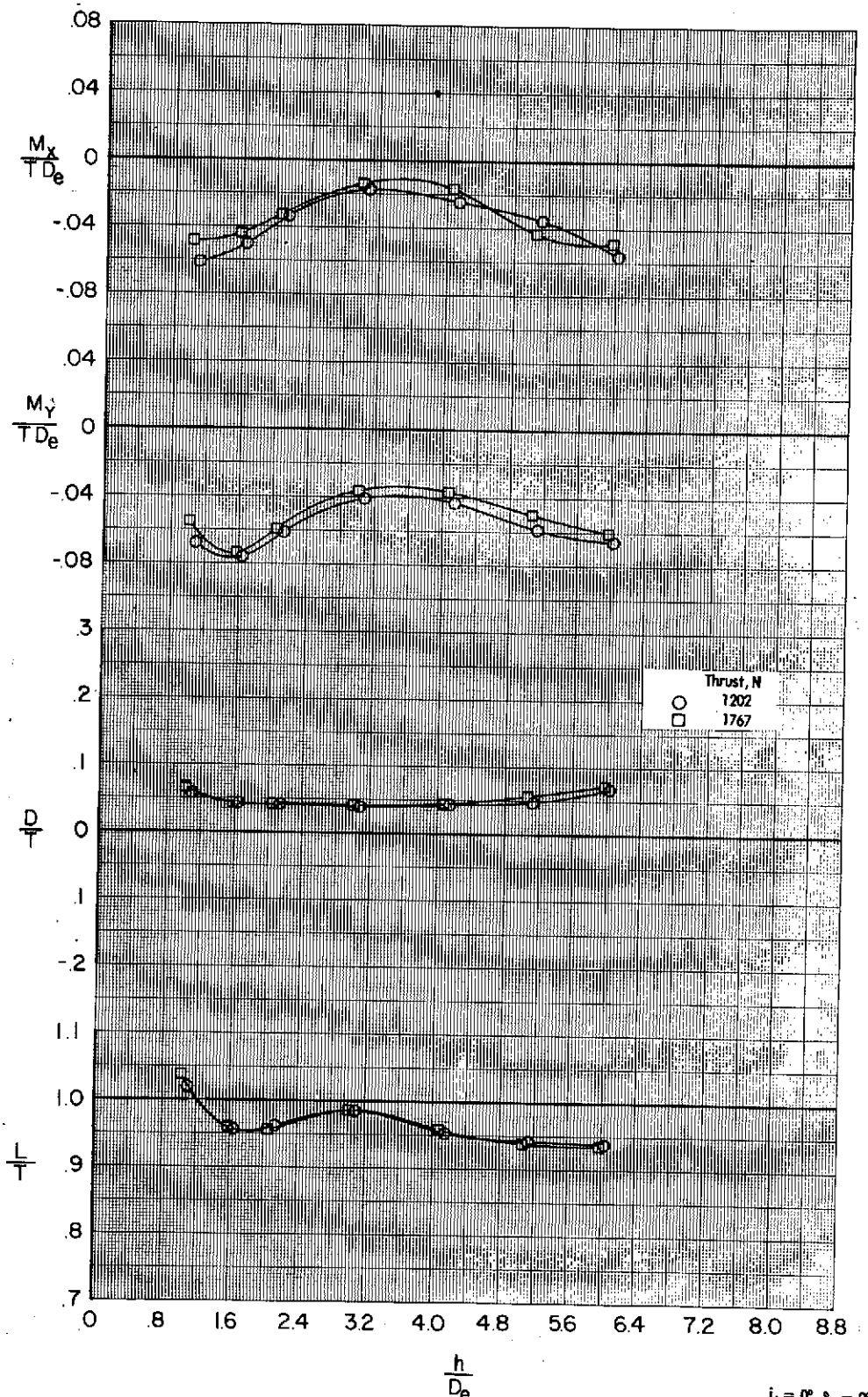

Figure 21. - Effect of ground proximity on the induced loads of configuration in hover. $\delta_L = -5°$ $\delta_{LC} = 94°$ $\delta_f = 40°$ $i_f = 0°$ $\delta_e = 0°$ $\alpha = 0°$ $\phi = 0°$

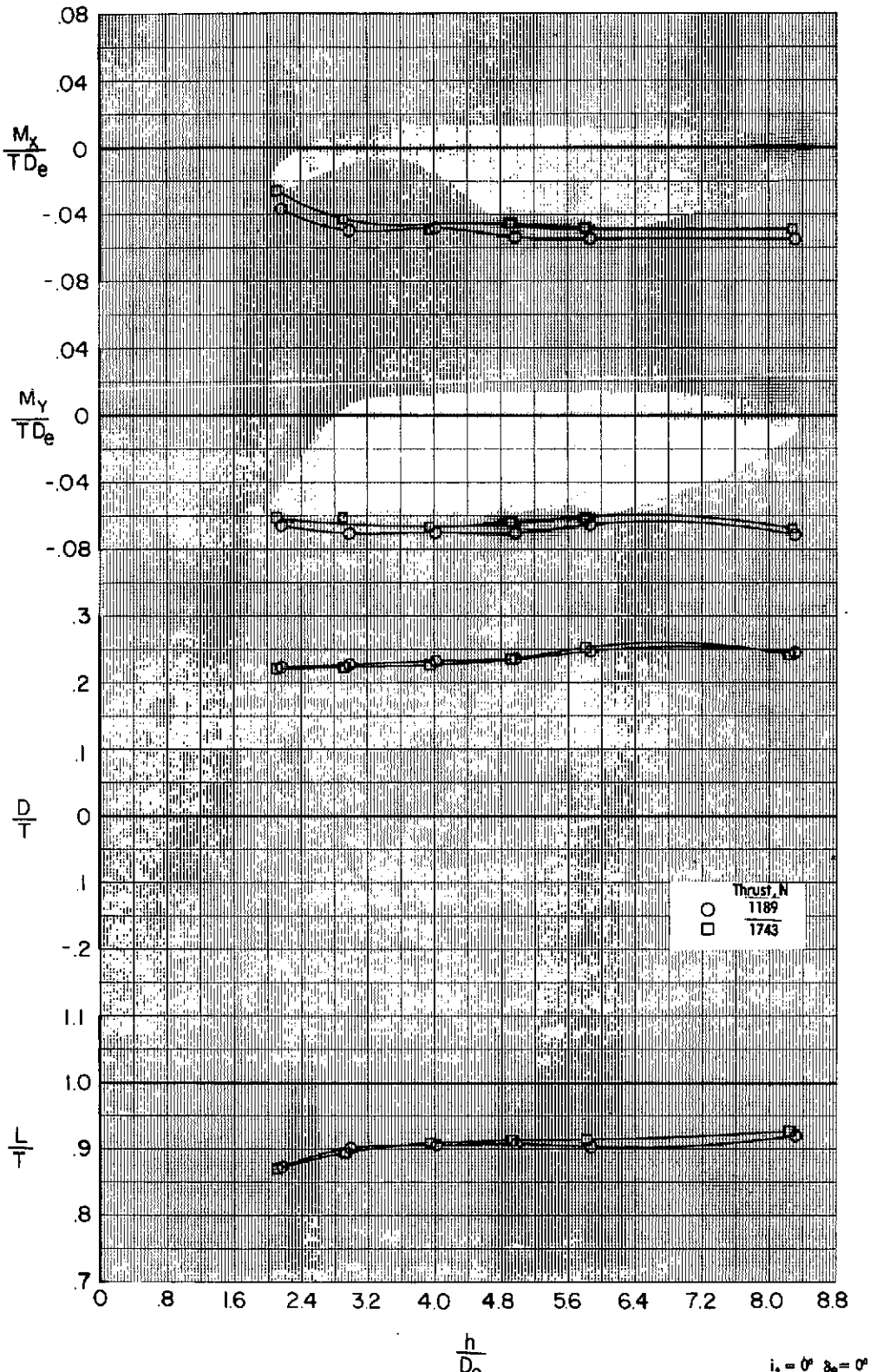

Figure 22. - Effect of ground proximity on the induced loads of configuration in hover. $\delta_L = -5°$ $\delta_{LC} = 94°$ $\delta_f = 40°$ $\alpha = 10°$ $\phi = 0°$ $i_t = 0°$ $\delta_e = 0°$

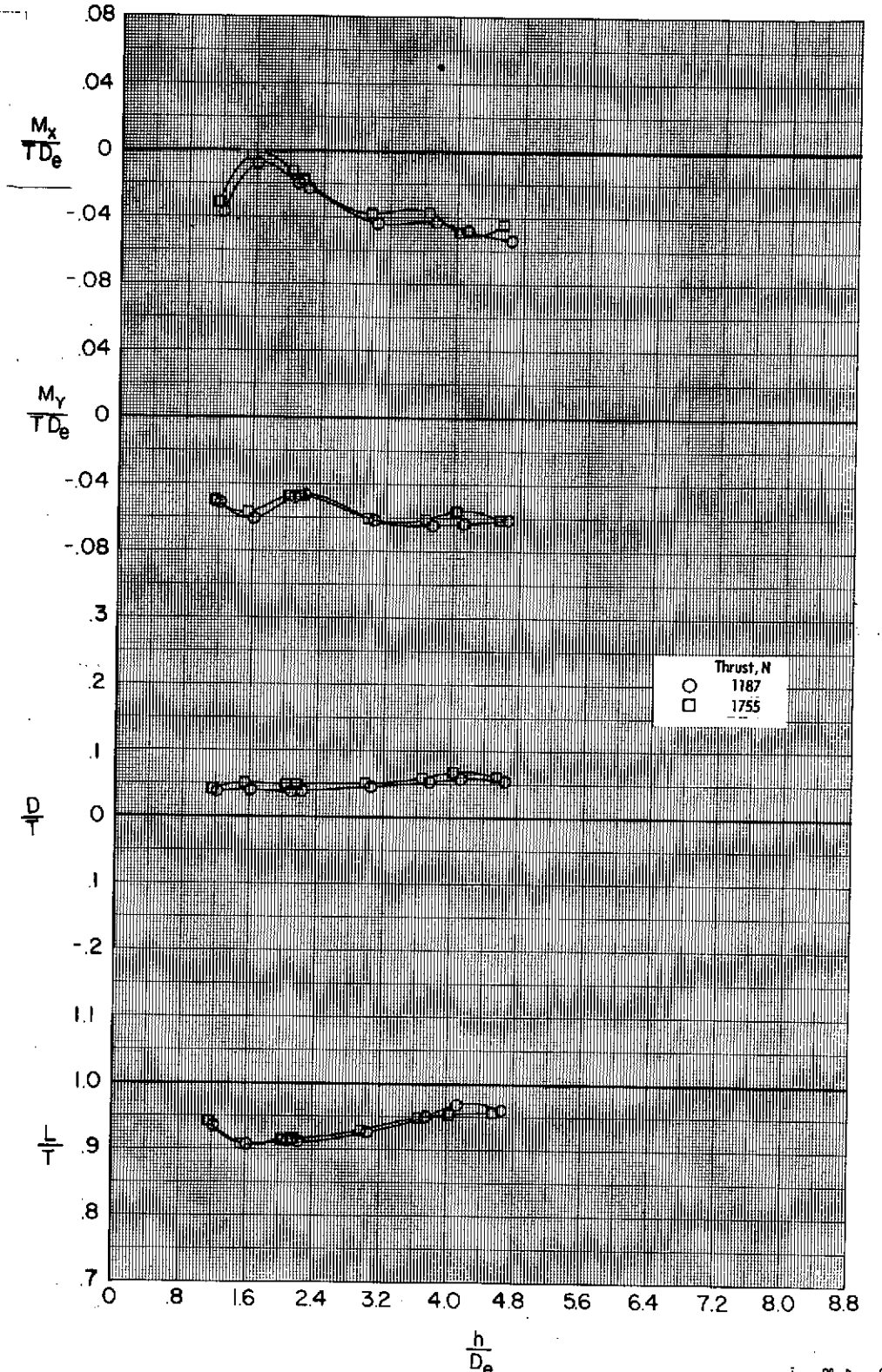

Figure23. - Effect of ground proximity on the induced loads of configuration in hover. $\delta_L = -5°$ $\delta_{LC} = 94°$ $\delta_f = 40°$ $i_t = 0°$ $\delta_e = 0°$ $\alpha = 0°$ $\emptyset = 10°$

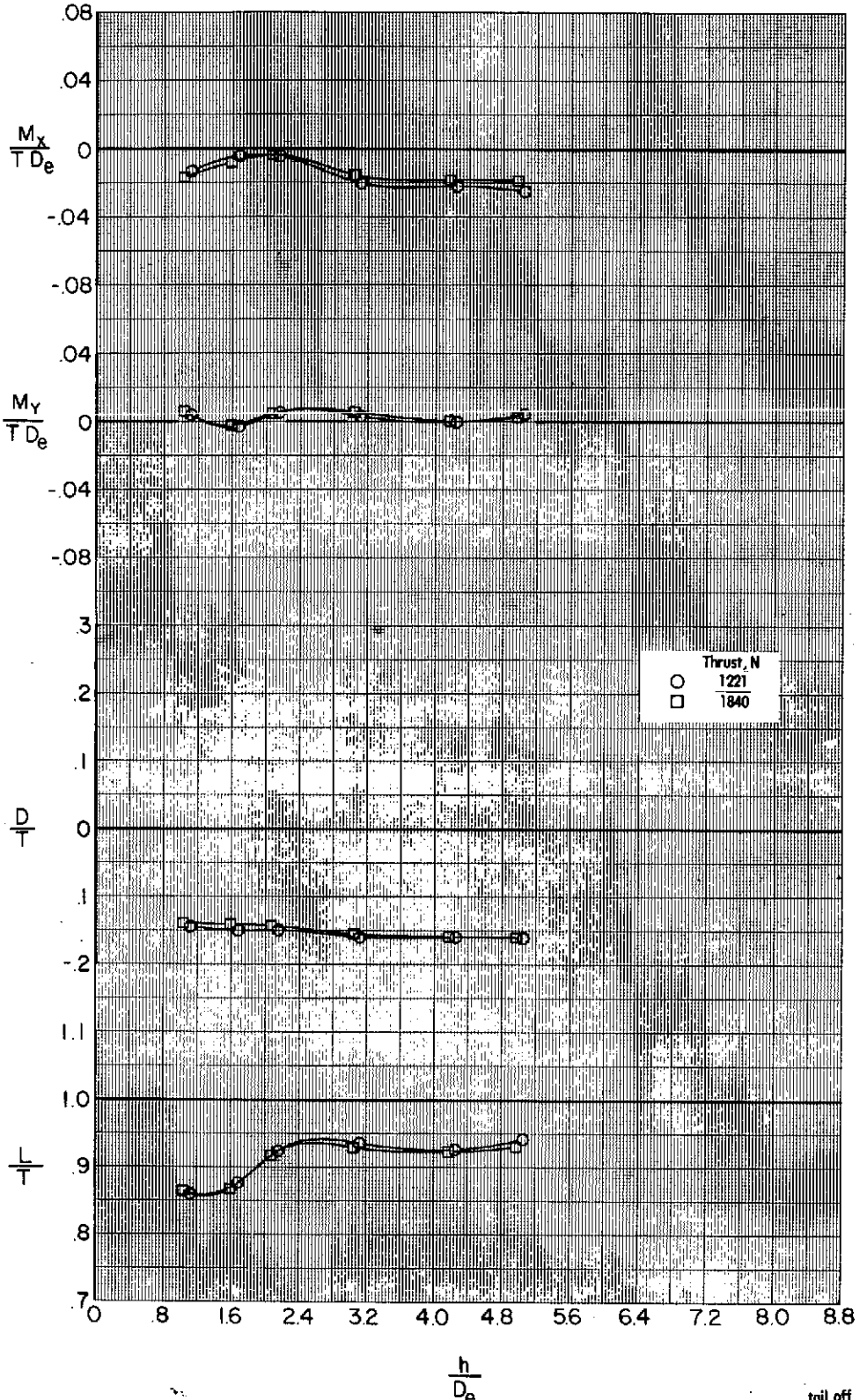

Figure24. - Effect of ground proximity on the induced loads of configuration in hover. $\delta_L = 7.5°$ $\delta_{LC} = 82°$ $\delta_f = 40°$ $\alpha = -4°$ $\phi = 0°$ tail off

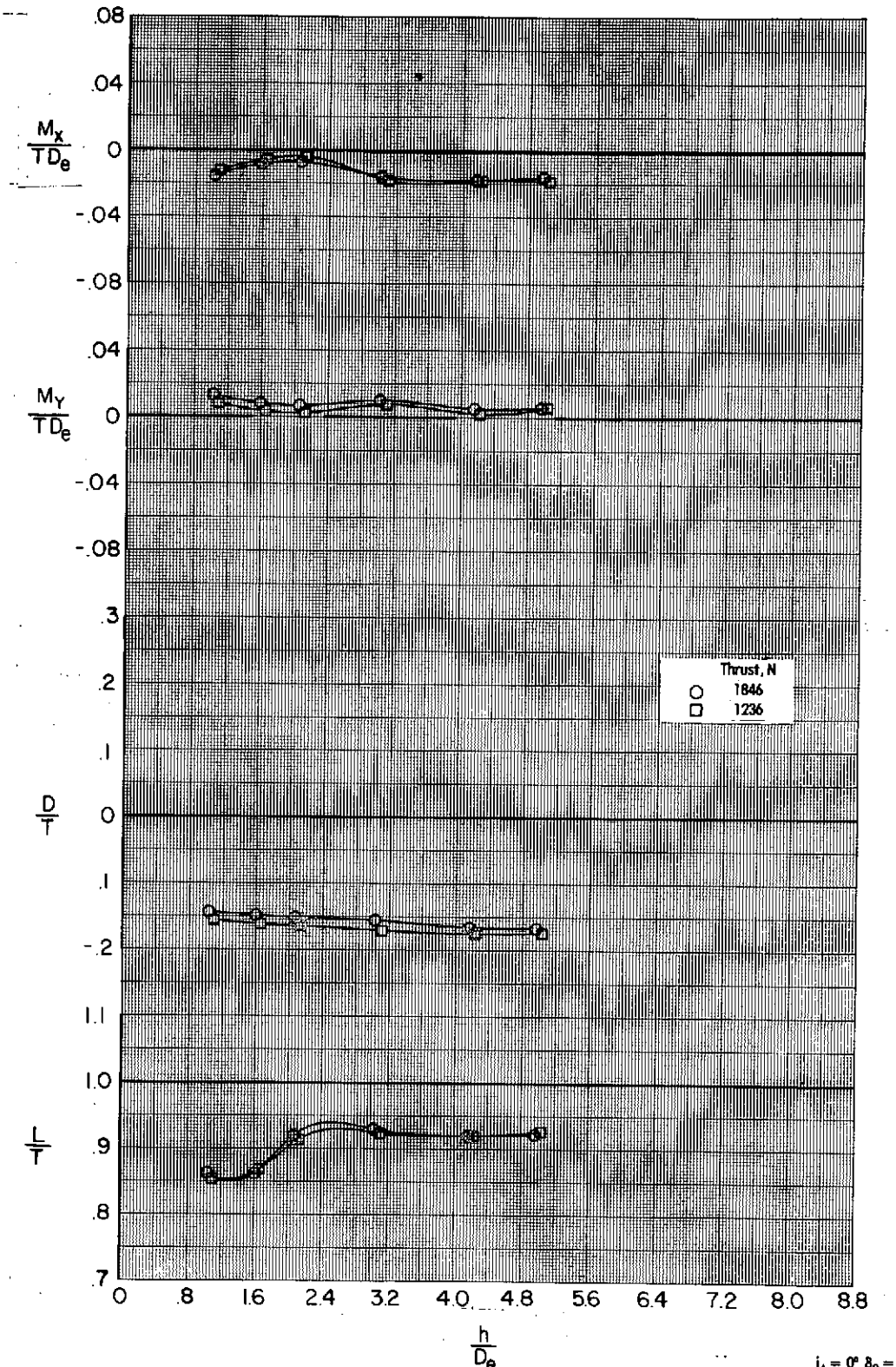

Figure25. - Effect of ground proximity on the induced loads of configuration in hover. $\delta_L = 7.5°$ $\delta_{LC} = 82°$ $\delta_f = 40°$ $\alpha = -4°$ $\emptyset = 0°$ $i_t = 0°$ $\delta_e = 0°$

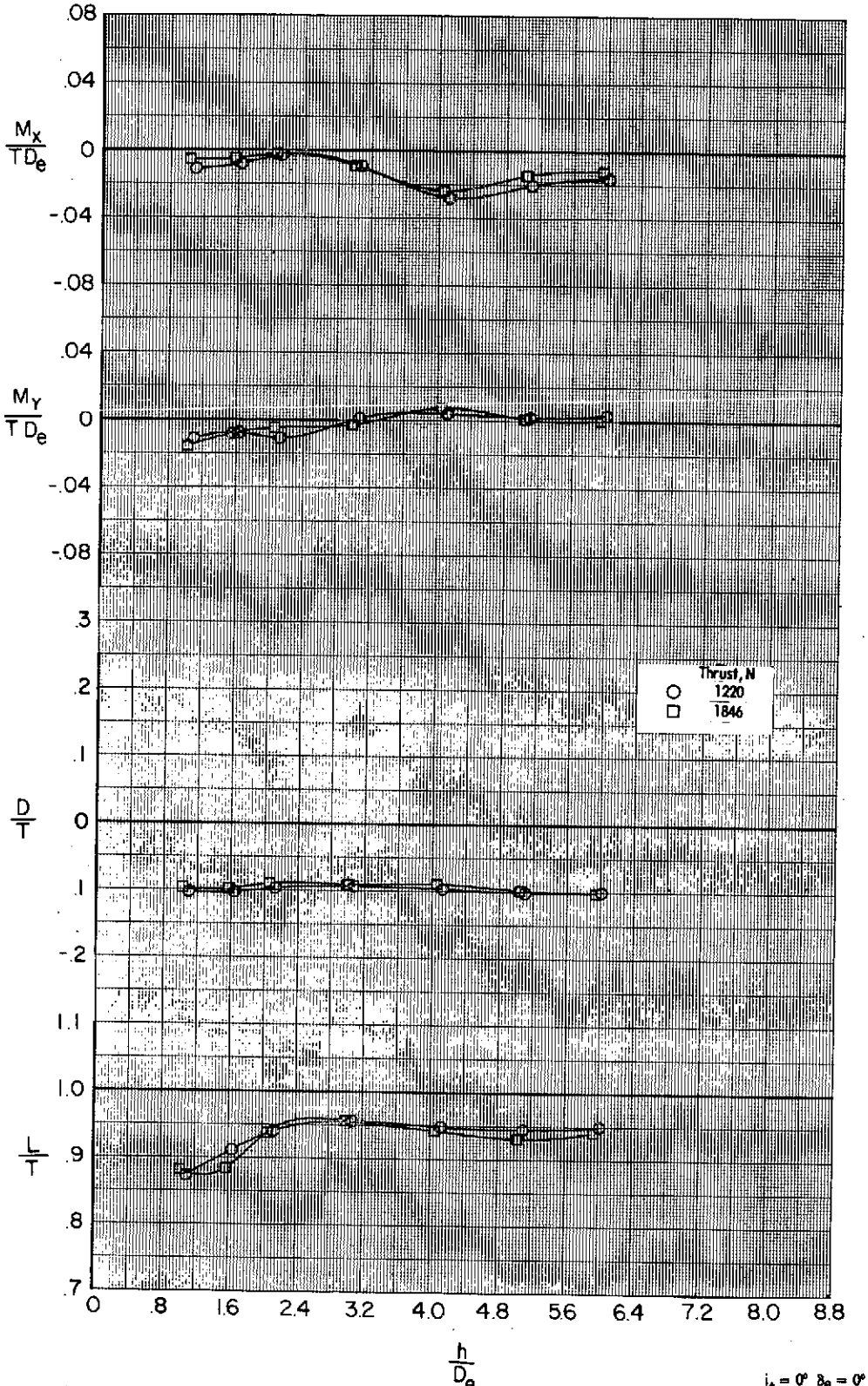

Figure26. - Effect of ground proximity on the induced loads of configuration in hover. $\delta_L = 7.5°$ $\delta_{LC} = 82°$ $\delta_f = 40°$ $\alpha = 0°$ $\phi = 0°$ $i_t = 0°$ $\delta_e = 0°$

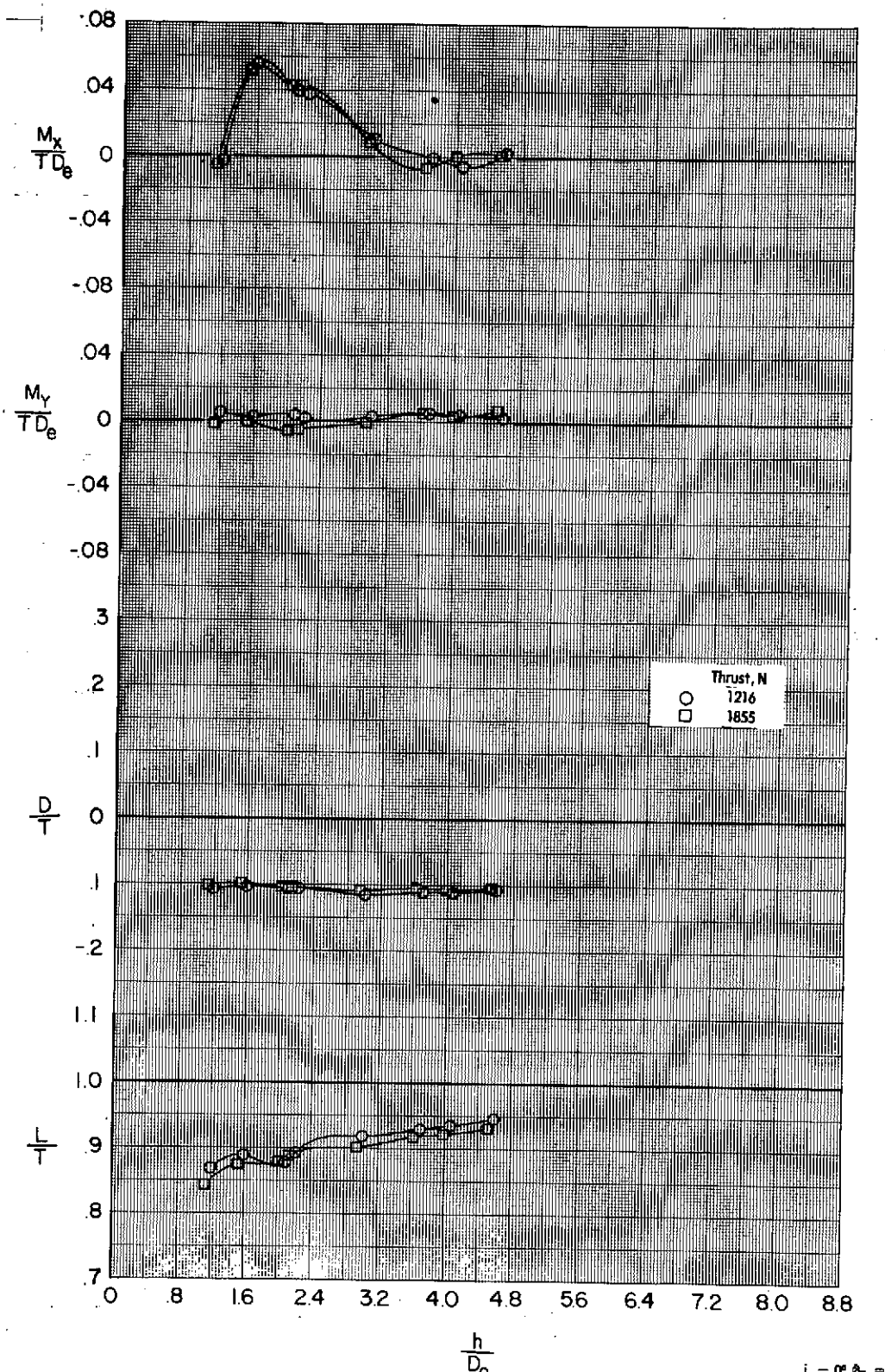

Figure27. - Effect of ground proximity on the induced loads of configuration in hover. $\delta_L = 7.5°$ $\delta_{LC} = 82°$ $\delta_f = 40°$ $i_t = 0°$ $\delta_e = 0°$ $\alpha = 0°$ $\varnothing = 10°$

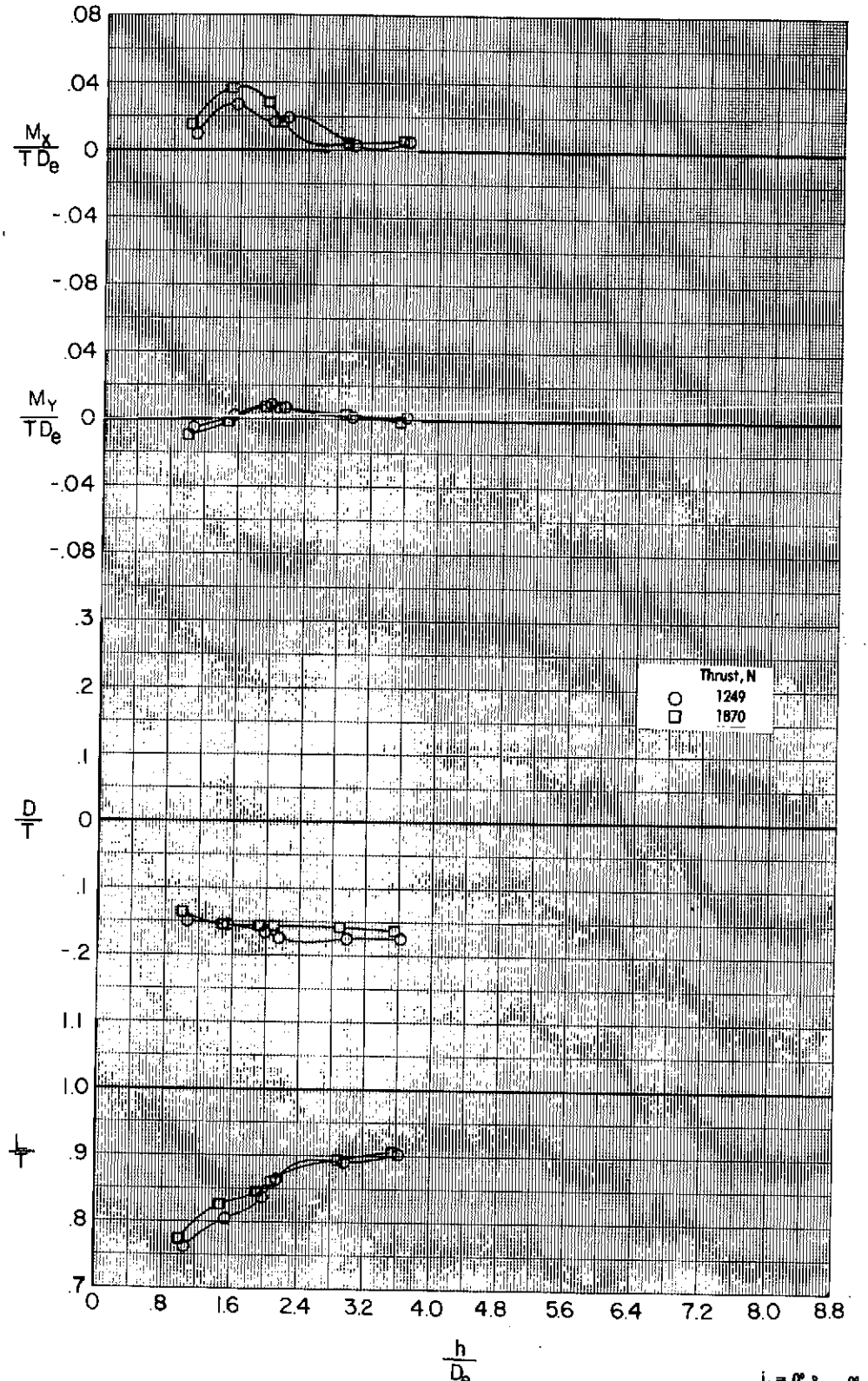

Figure28 - Effect of ground proximity on the induced loads of configuration in hover. $\delta_L = 7.5°$ $\delta_{LC} = 82°$ $\delta_f = 40°$ $i_t = 0°$ $\delta_e = 0°$ $\alpha = -4°$ $\phi = 10°$

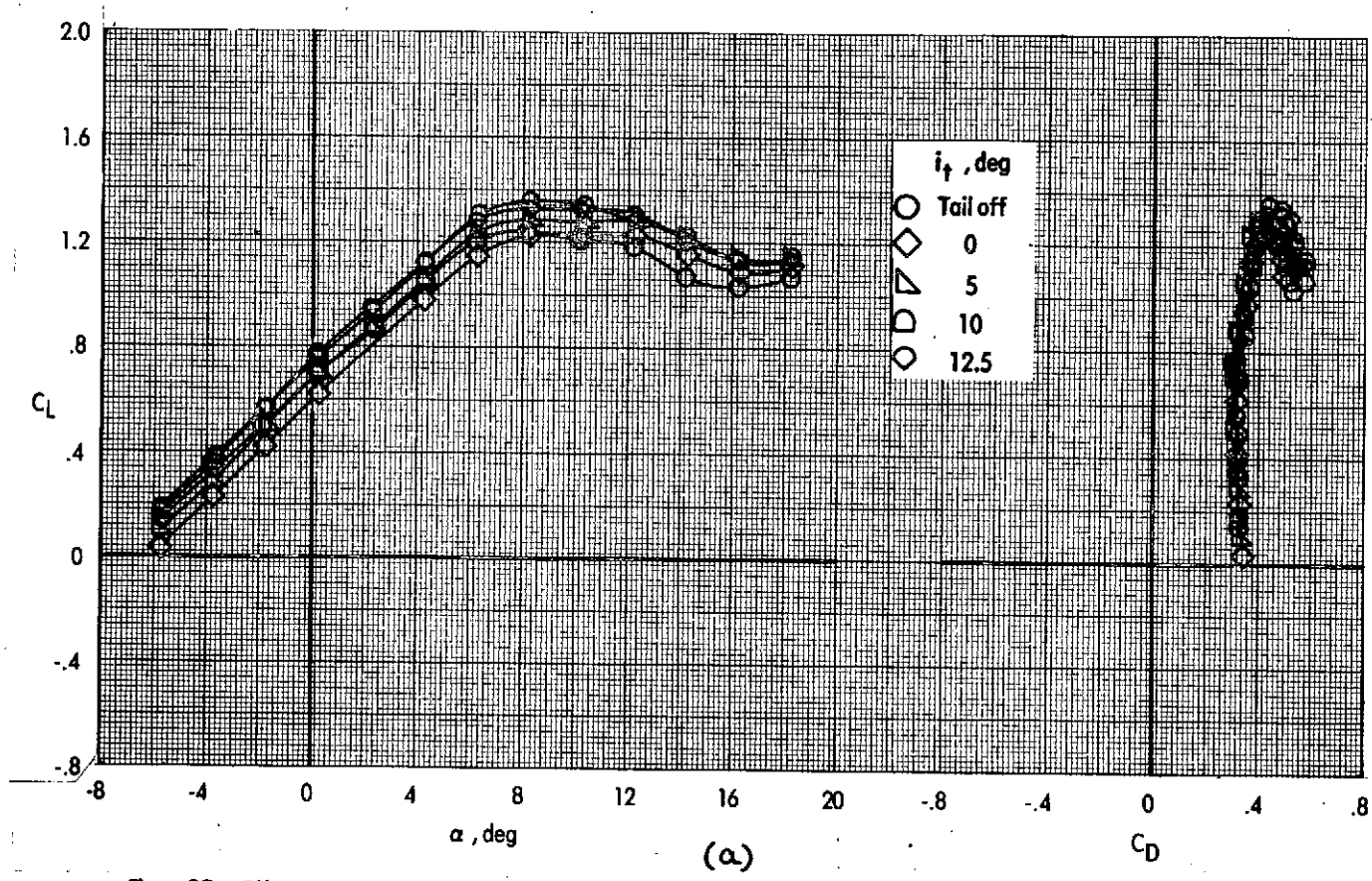

Figure29. - Effect of tail incidence on longitudinal aerodynamic characteristics of the VTOL transition configuration.
$\delta_L = 0°$ $\delta_{LC} = 90°$ $\delta_f = 40°$ $\delta_e = 0°$ $C_\mu = 0$ $q_\infty = 239$ N/m² (5.0 lb/ft²)

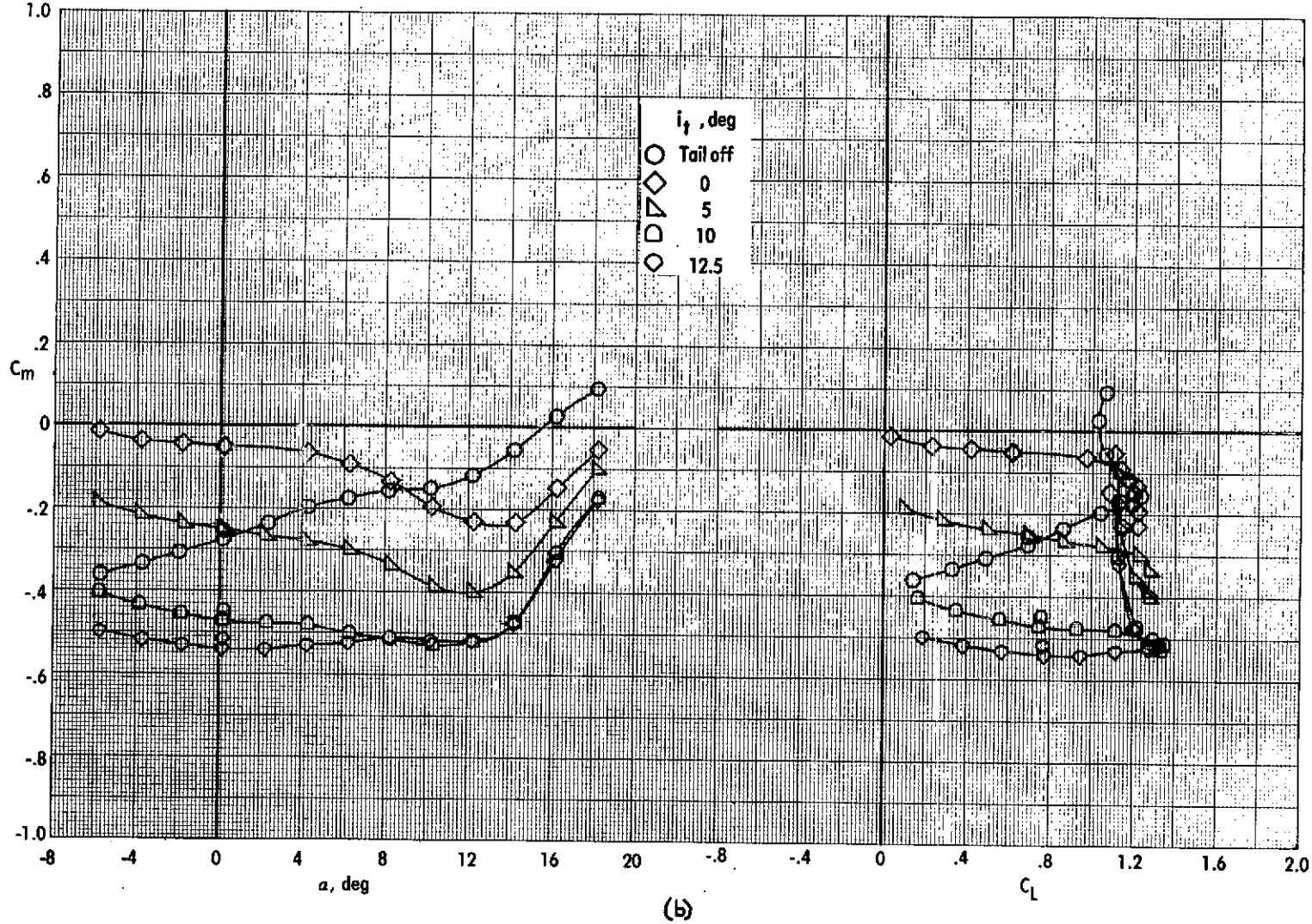

(b)

Figure 29. - Concluded.

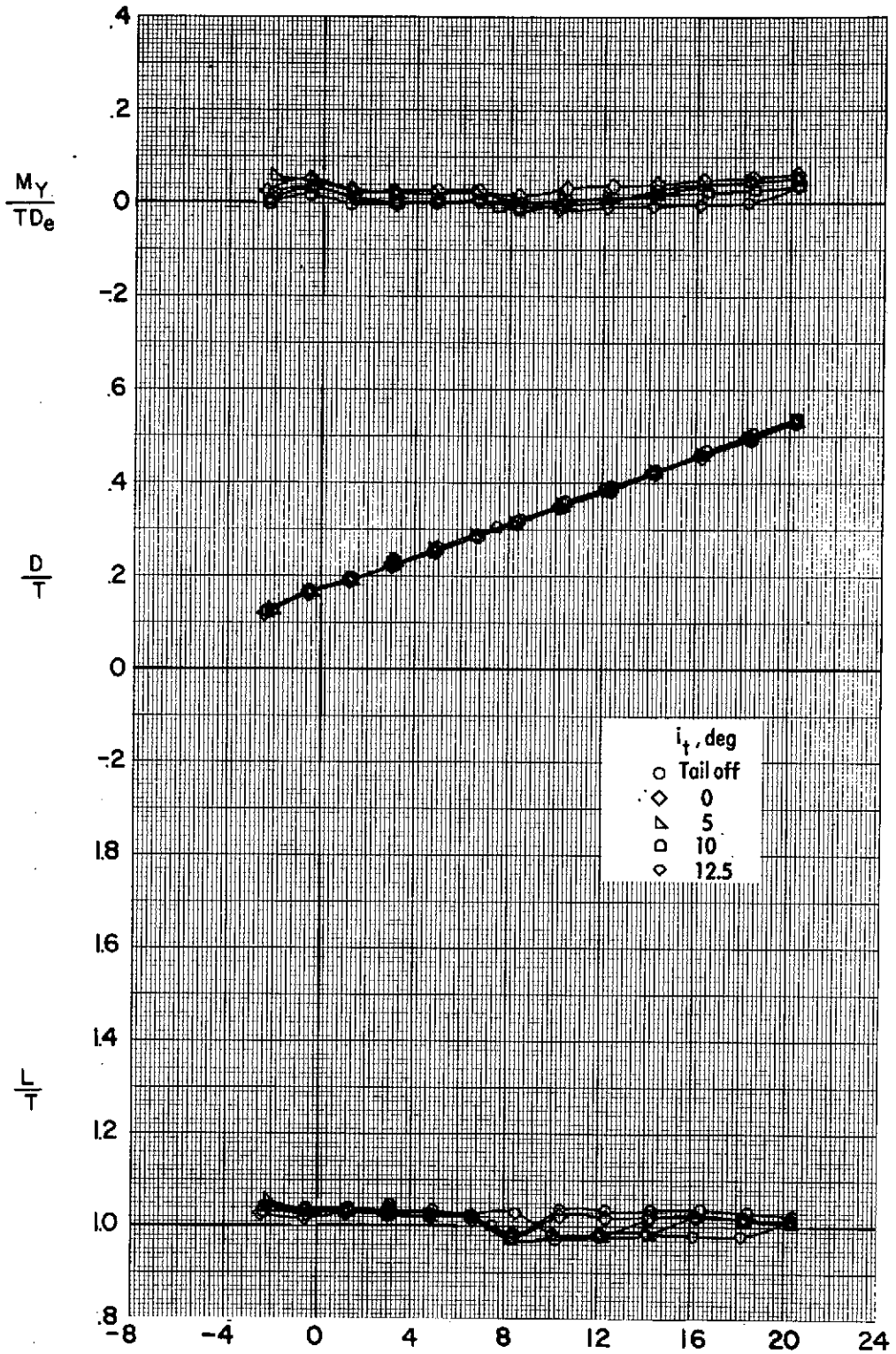

Figure30. - Effect of tail incidence on longitudinal aerodynamic characteristics of the VTOL transition configuration. $\delta_L = 0°$ $\delta_{LC} = 90°$ $\delta_f = 40°$ $\delta_e = 0°$ $V_e = 0.12$ $q_\infty = 239$ N/m² (5.0 lb/ft²)

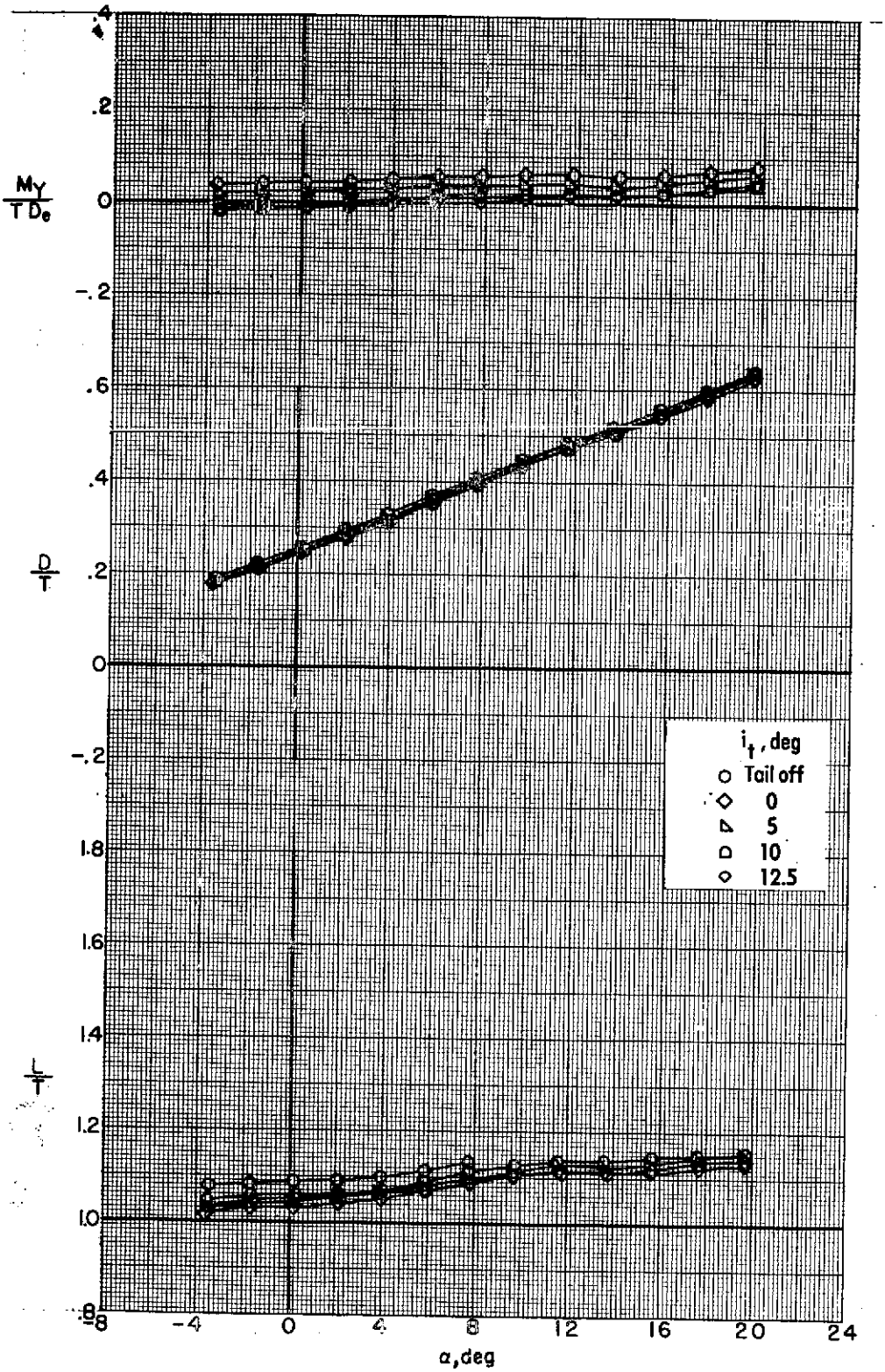

Figure 31. - Effect of tail incidence on longitudinal aerodynamic characteristics of the VTOL transition configuration. $\delta_L = 0°$ $\delta_{LC} = 90°$ $\delta_f = 40°$ $\delta_e = 0°$ $V_e = 0.18$ $q_\infty = 239$ N/m² (5.0 lb/ft²)

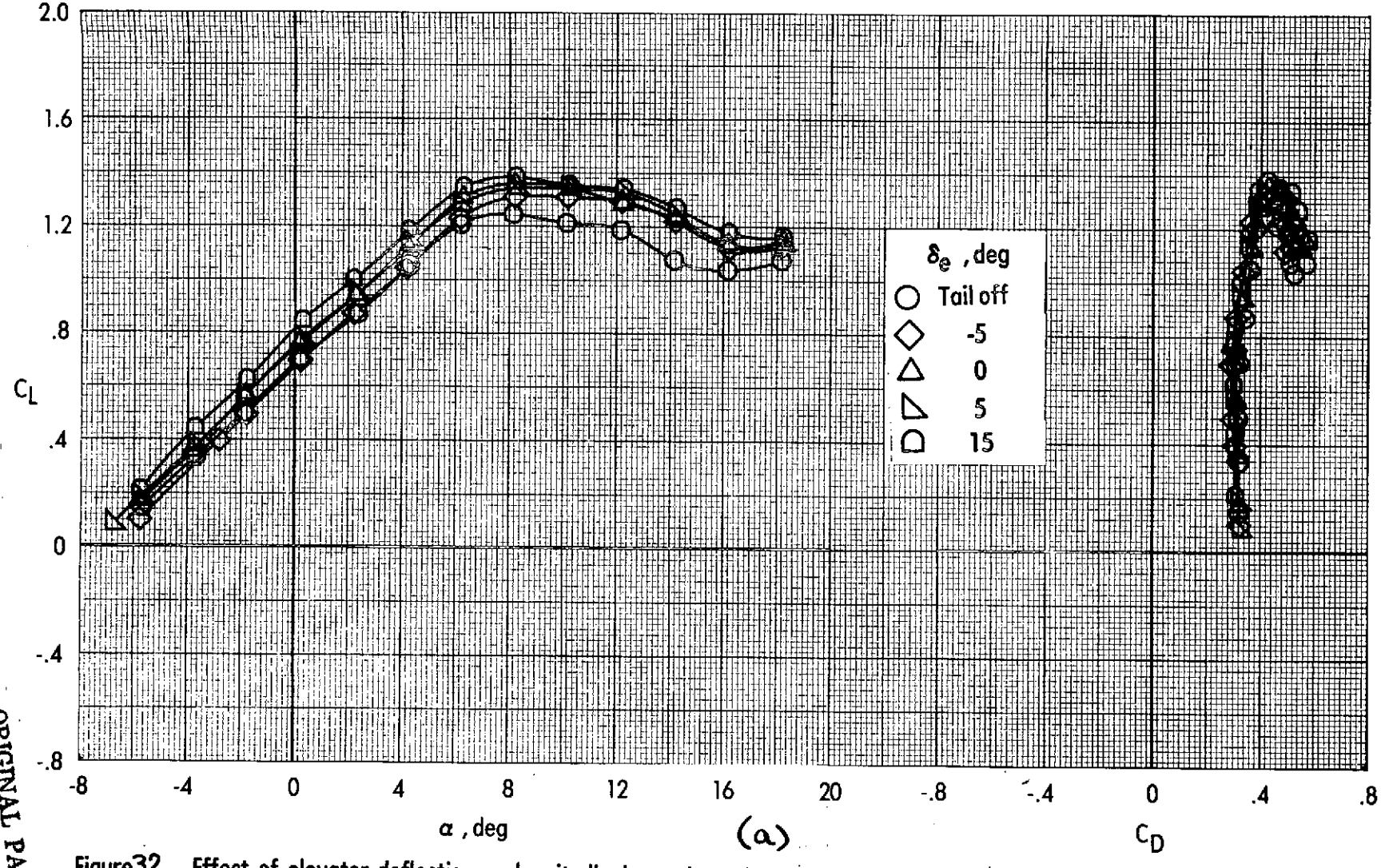

Figure32. - Effect of elevator deflection on longitudinal aerodynamic characteristics of the VTOL transition configuration.

$\delta_L = 0°$ $\delta_{LC} = 90°$ $\delta_f = 40°$ $i_t = 10°$ $C_\mu = 0$ $q_\infty = 239\ N/m^2$ (5.0 lb/ft^2)

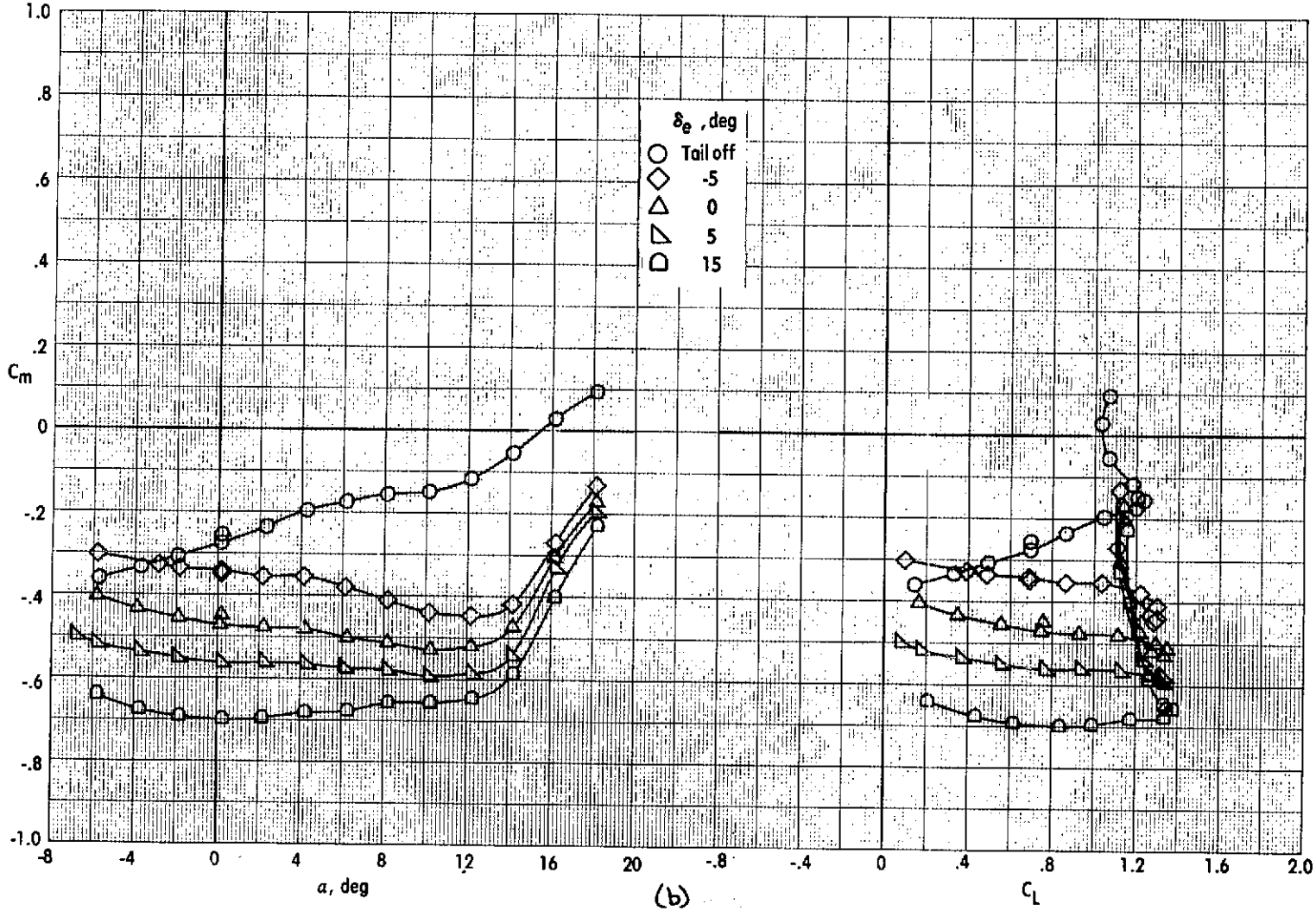

Figure32. - Concluded.

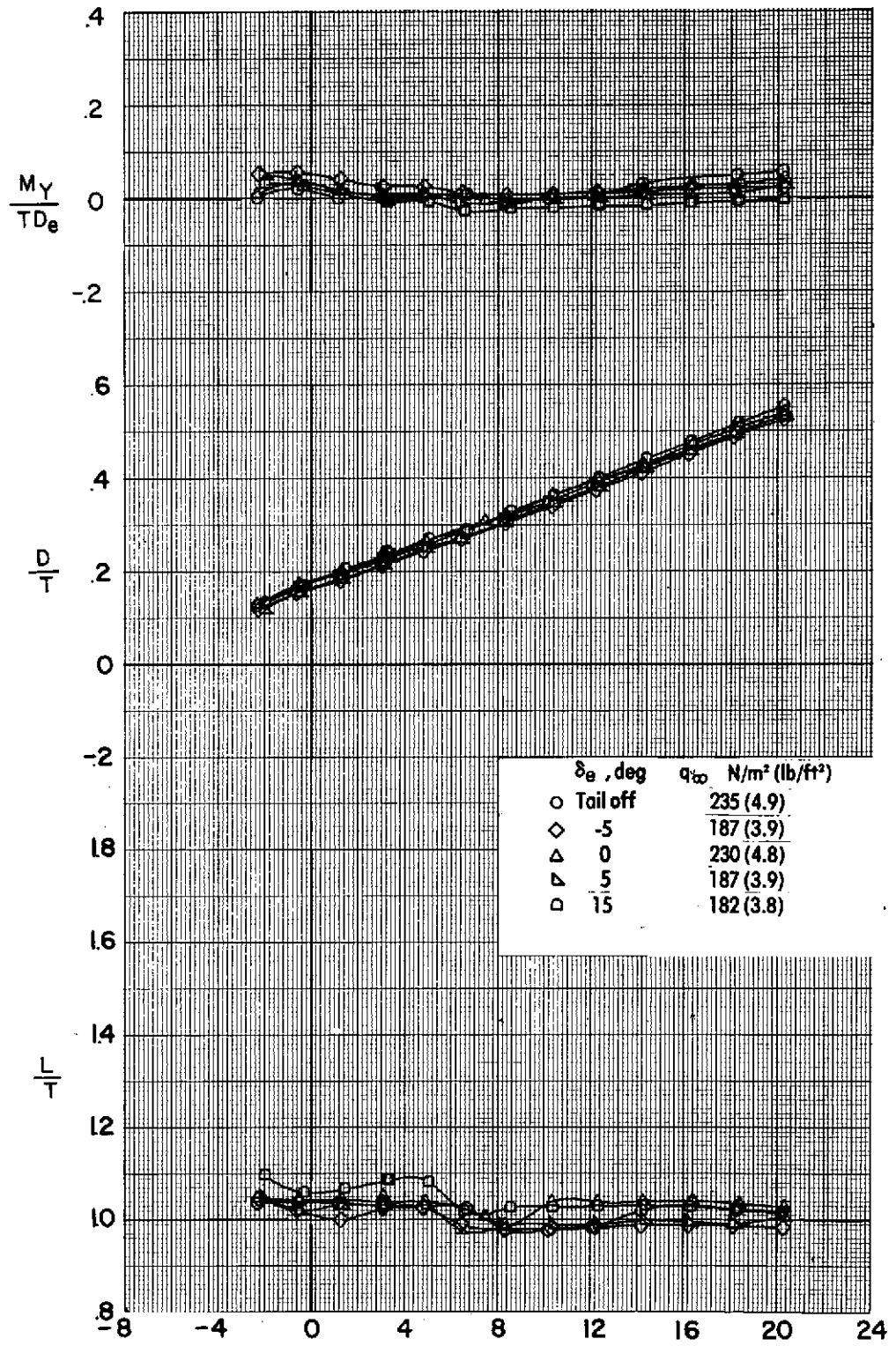

Figure33. - Effect of elevator deflection on longitudinal aerodynamic characteristics of the VTOL transition configuration. $\delta_L = 0°$ $\delta_{LC} = 90°$ $\delta_f = 40°$ $i_t = 10°$ $V_e = 0.12$

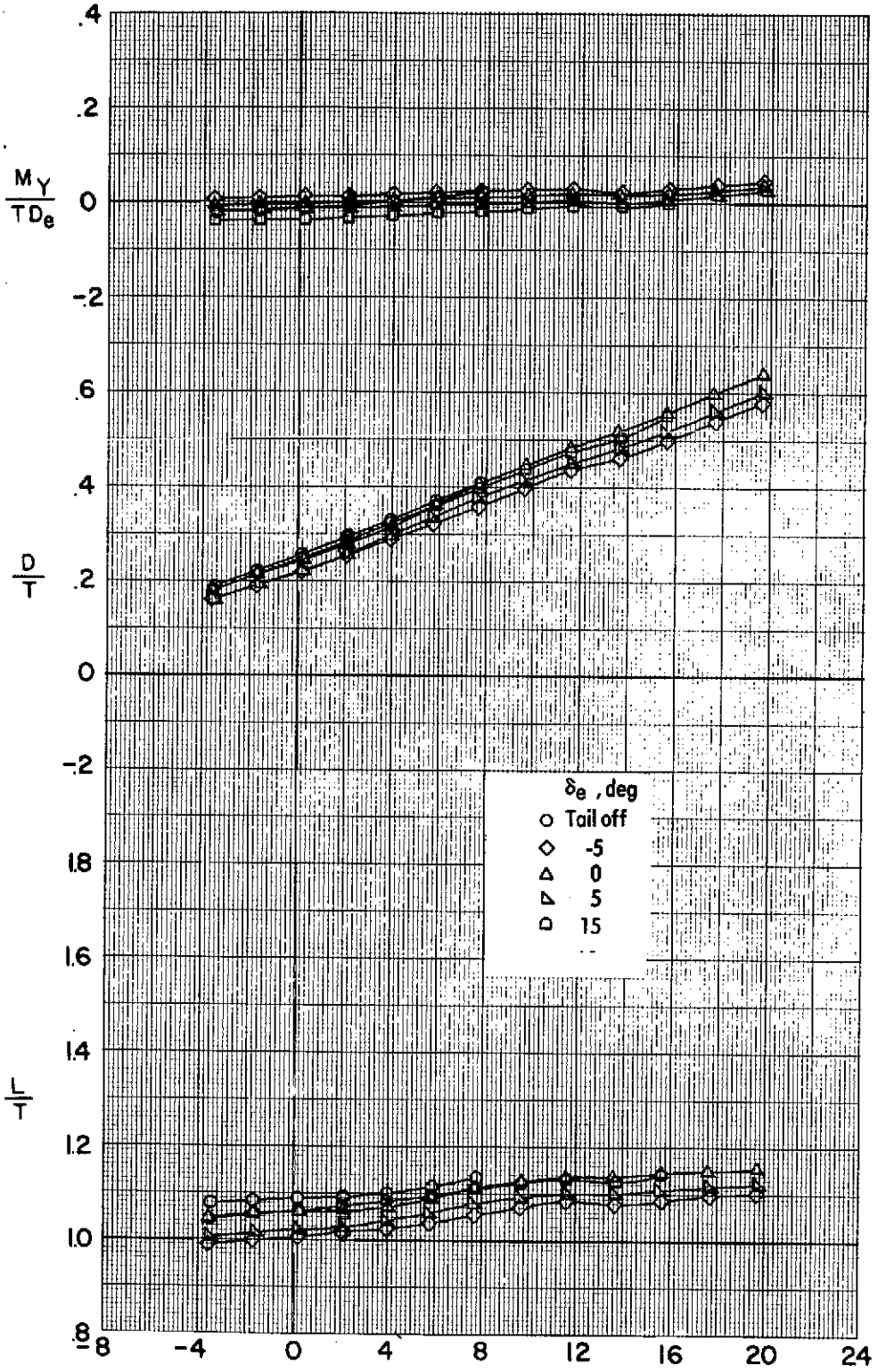

Figure 34 - Effect of elevator deflection on longitudinal aerodynamic characteristics of the VTOL transition configuration. $\delta_L = 0°$ $\delta_{LC} = 90°$ $\delta_f = 40°$ $i_t = 10°$ $V_e = 0.18$ $q_\infty = 239$ N/m² (5.01 lb/ft²)

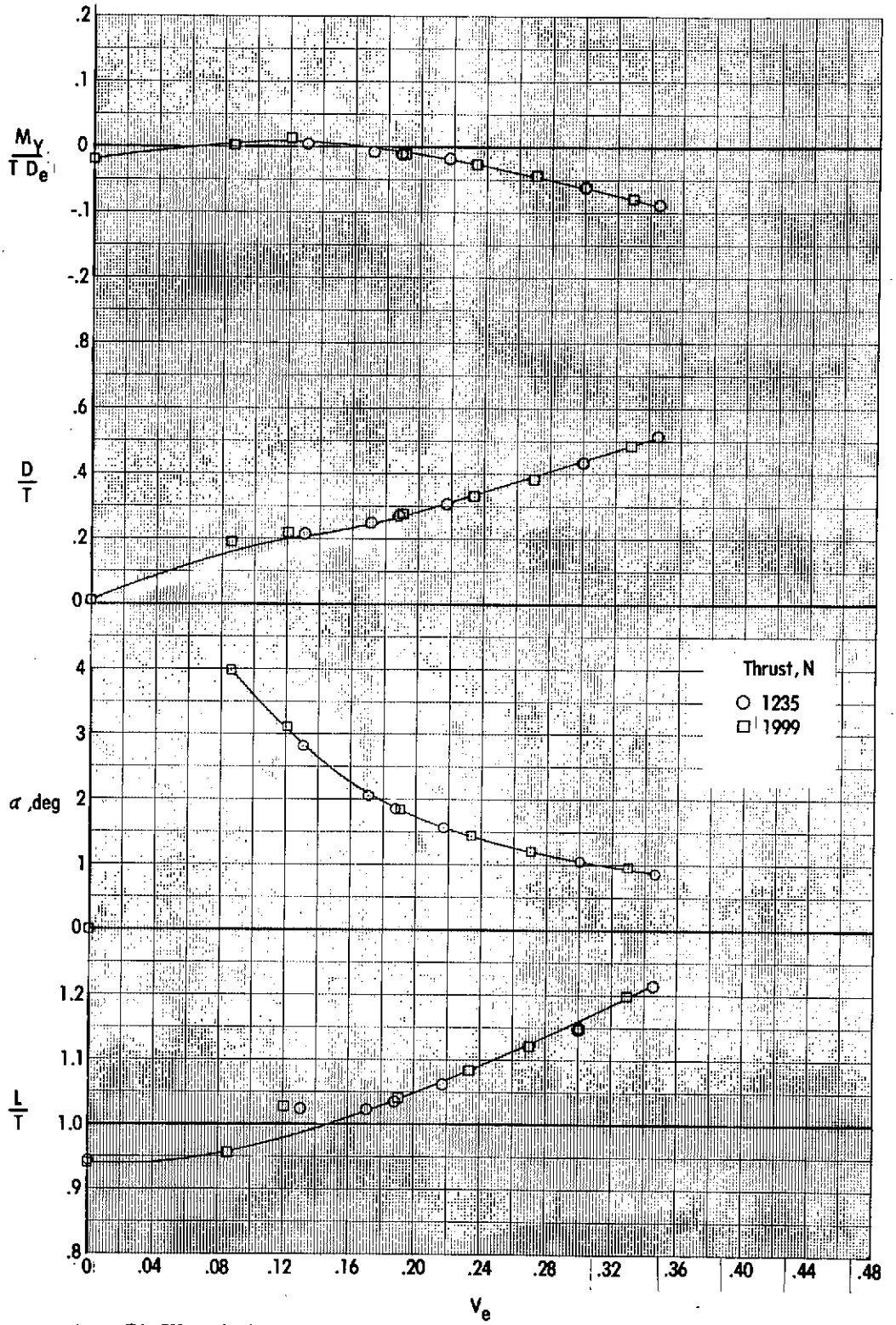

Figure 35. Effect of velocity ratio on longitudinal aerodynamic characteristics of the VTOL transition configuration.

$\delta_L = 0°$ $\delta_{LC} = 90°$ $\delta_f = 40°$ $i_t = 10°$ $\delta_e = 0°$

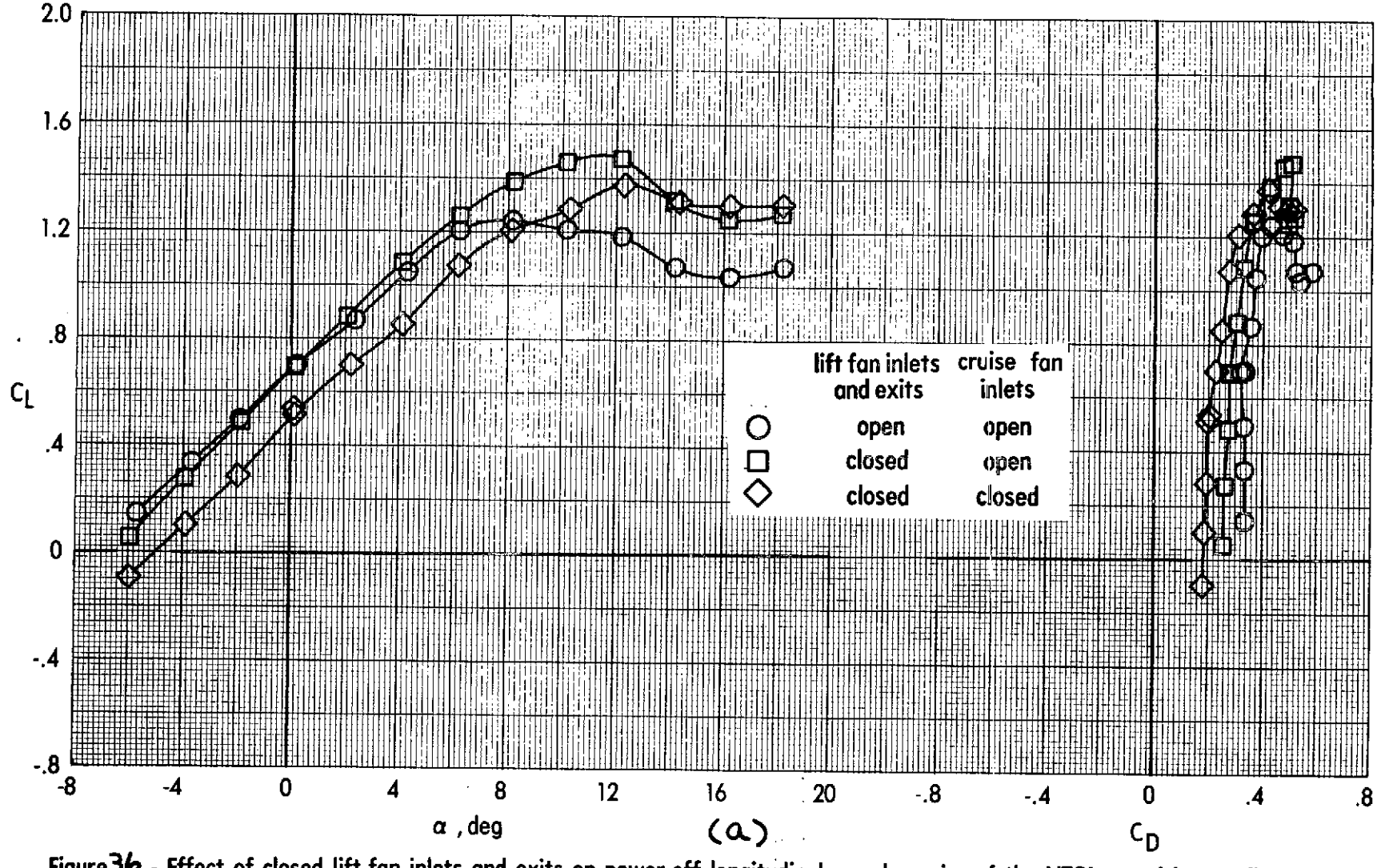

Figure 36 - Effect of closed lift-fan inlets and exits on power-off longitudinal aerodynamics of the VTOL transition configuration.

$\delta_L = 0°$ $\delta_{LC} = 90°$ $\delta_f = 40°$ tail off $C_\mu = 0$ $q_\infty = 239\ N/m^2\ (5.0\ lb/ft^2)$

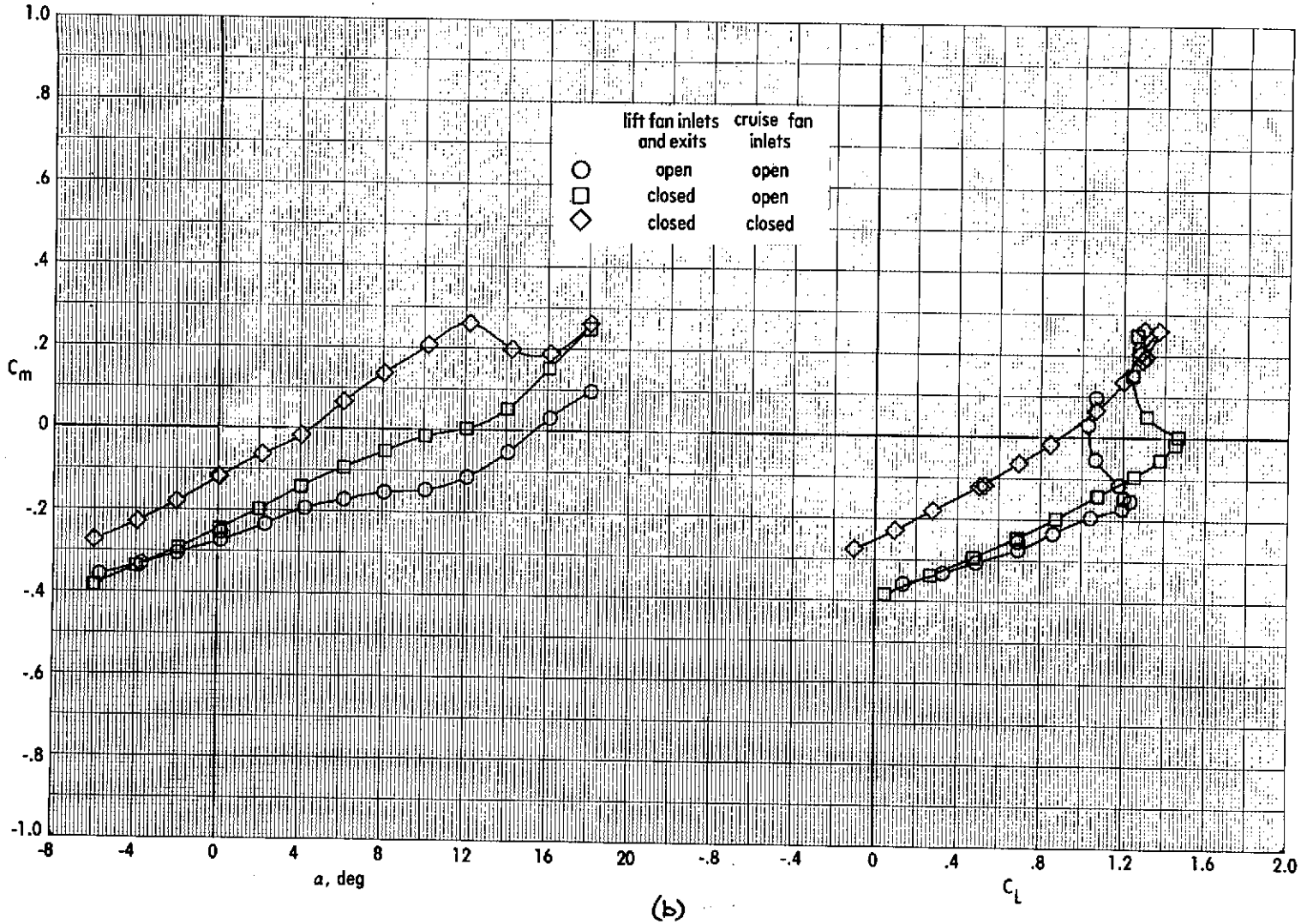

(b)

Figure 36. - Concluded.

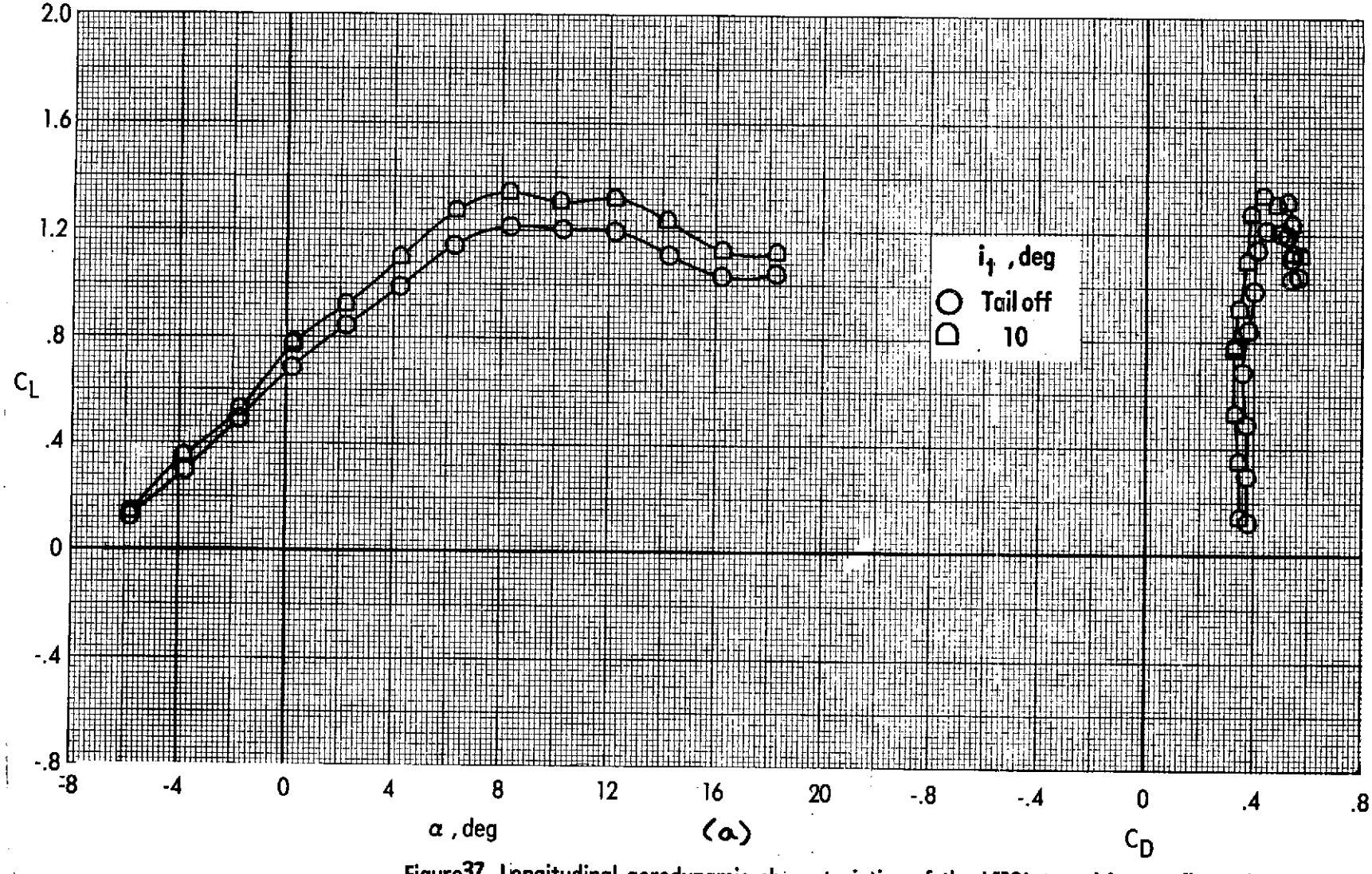

Figure 37 - Longitudinal aerodynamic characteristics of the VTOL transition configuration.

$\delta_L = -5°$ $\delta_{LC} = 94°$ $\delta_f = 40°$ $\delta_e = 0°$ $C_\mu = 0$ $q_\infty = 168\ N/m^2\ (3.5\ lb/ft^2)$

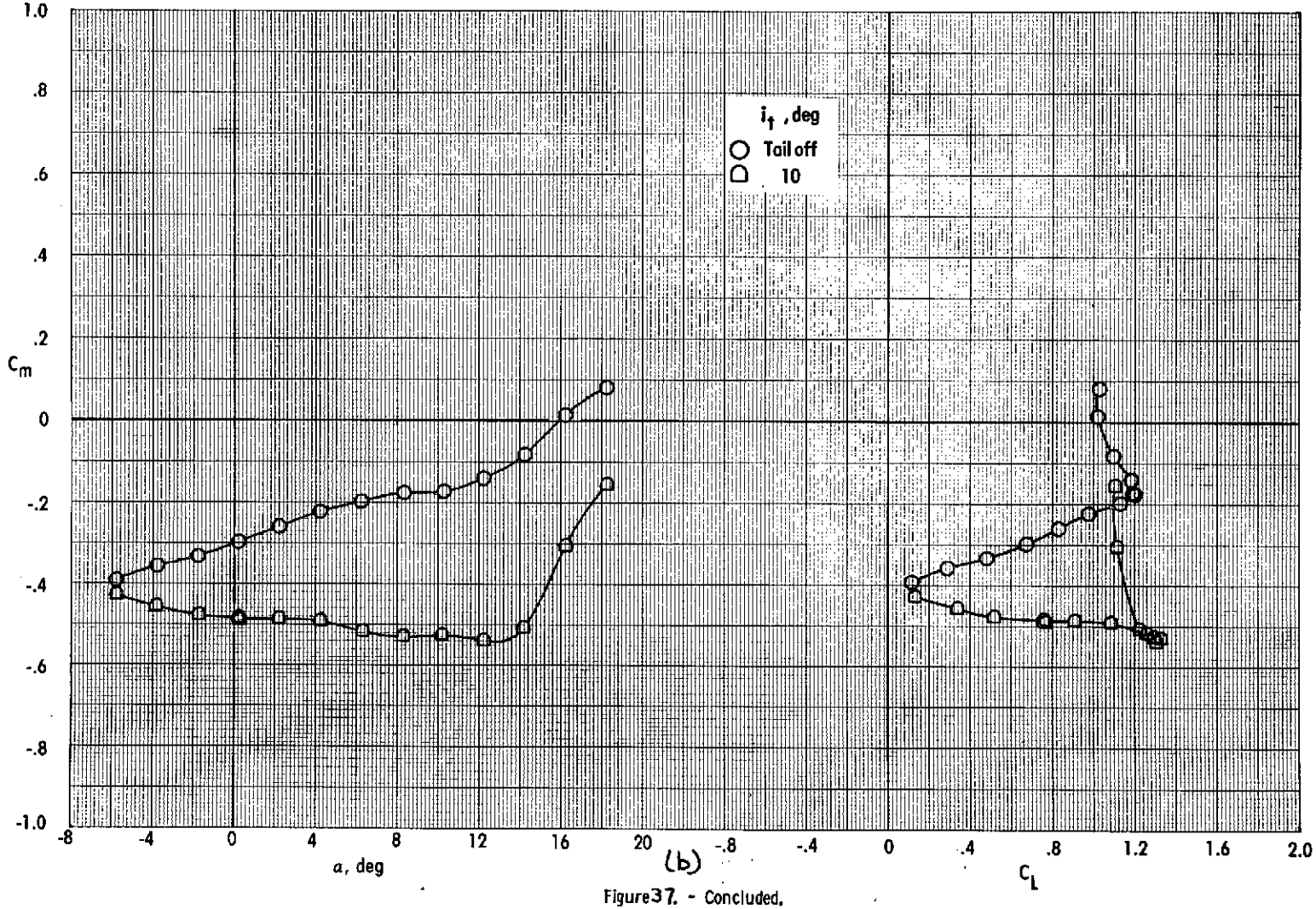

Figure 37. - Concluded.

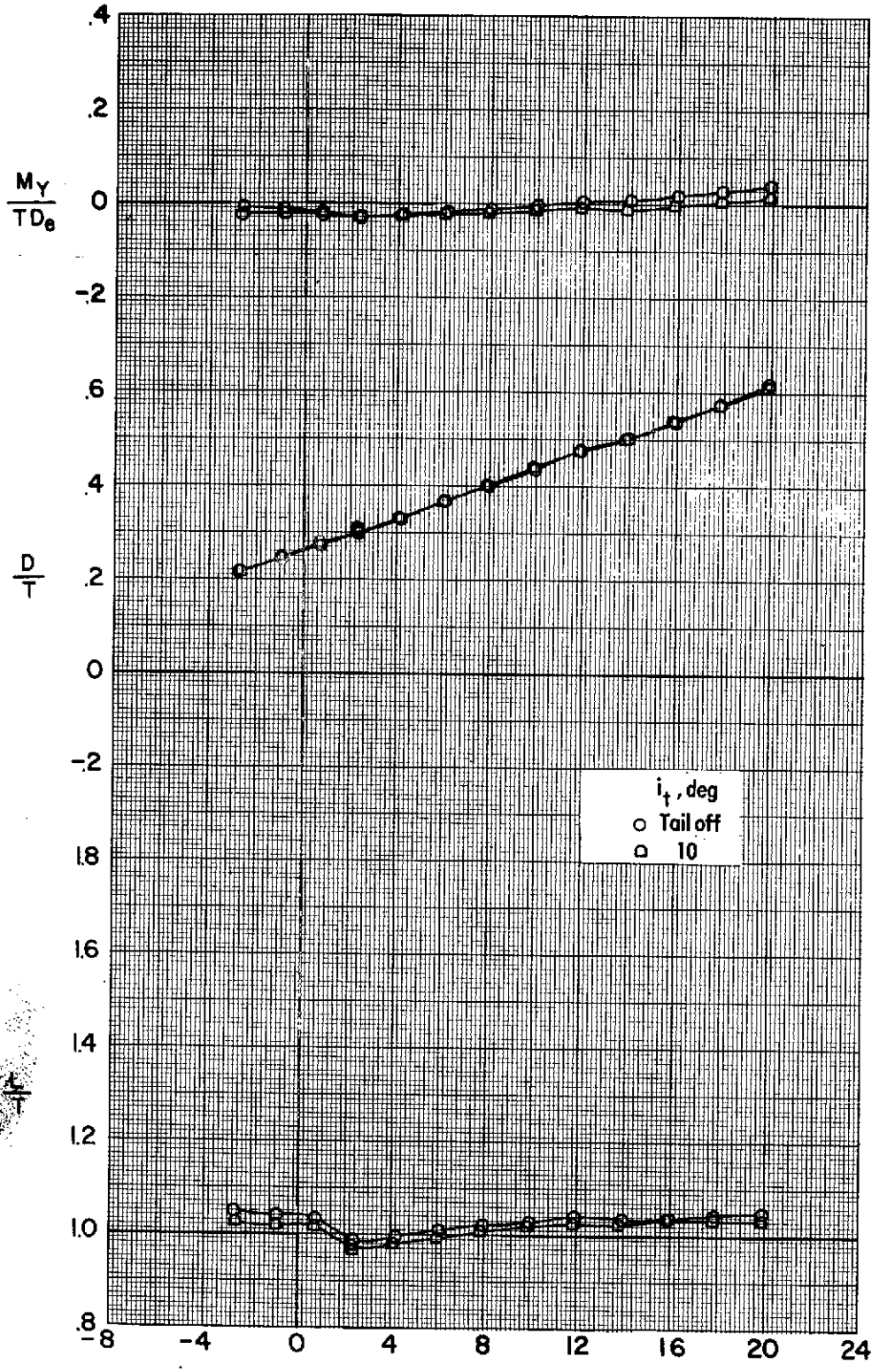

Figure 38 - Longitudinal aerodynamic characteristics of the VTOL transition configuration. $\delta_L = -5°$ $\delta_{LC} = 94°$ $\delta_f = 40°$ $\delta_e = 0°$ $V_c = 0.12$ $q_\infty = 168\ N/m^2\ (3.5\ lb/ft^2)$

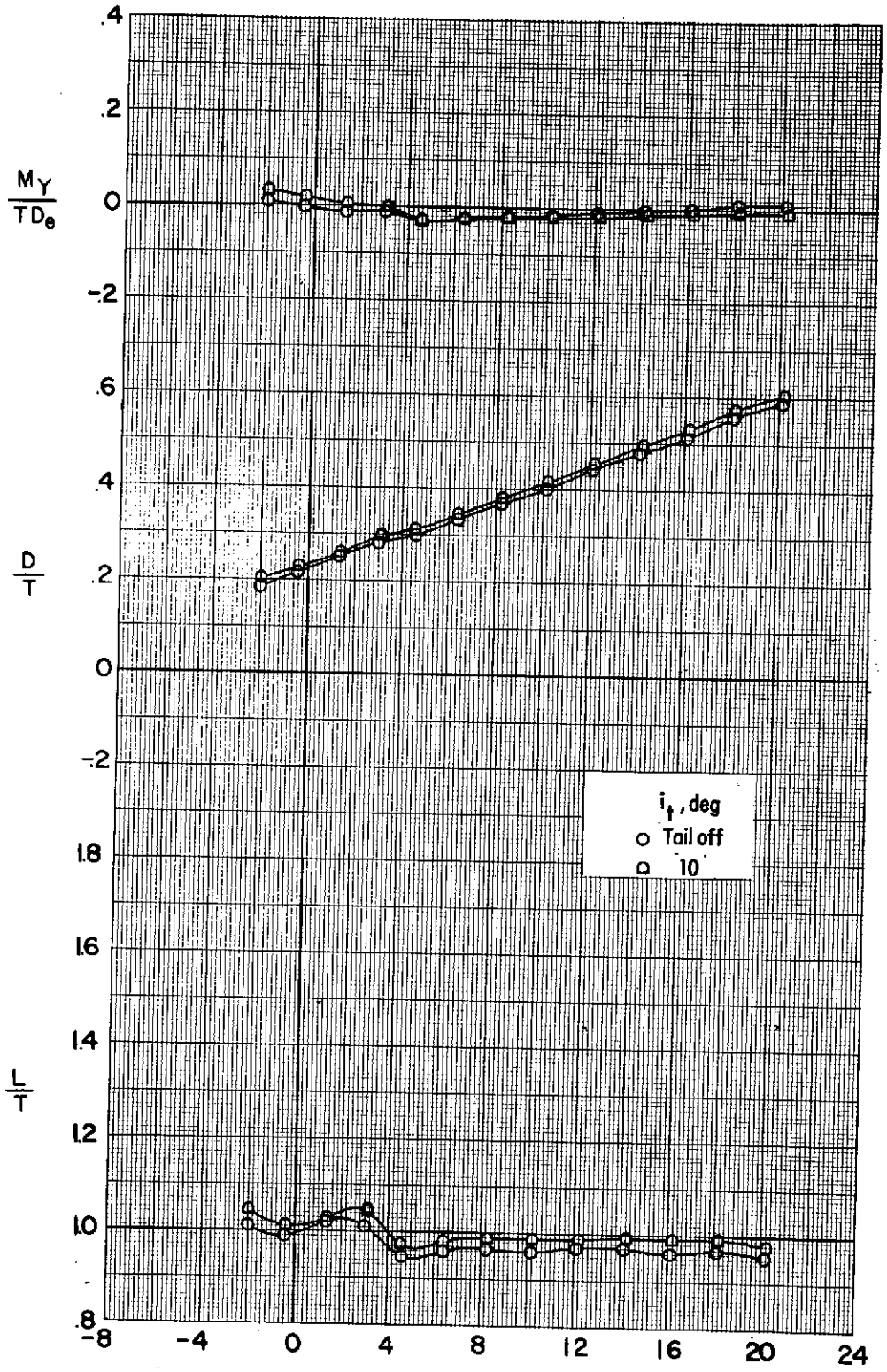

Figure 39 - Longitudinal aerodynamic characteristics of the VTOL transition configuration. $\delta_L = -5°$ $\delta_{LC} = 94°$ $\delta_f = 40°$ $\delta_s = 0°$ $V_e = 0.15$ $q_\infty = 168$ N/m² (3.5 lb/ft²)

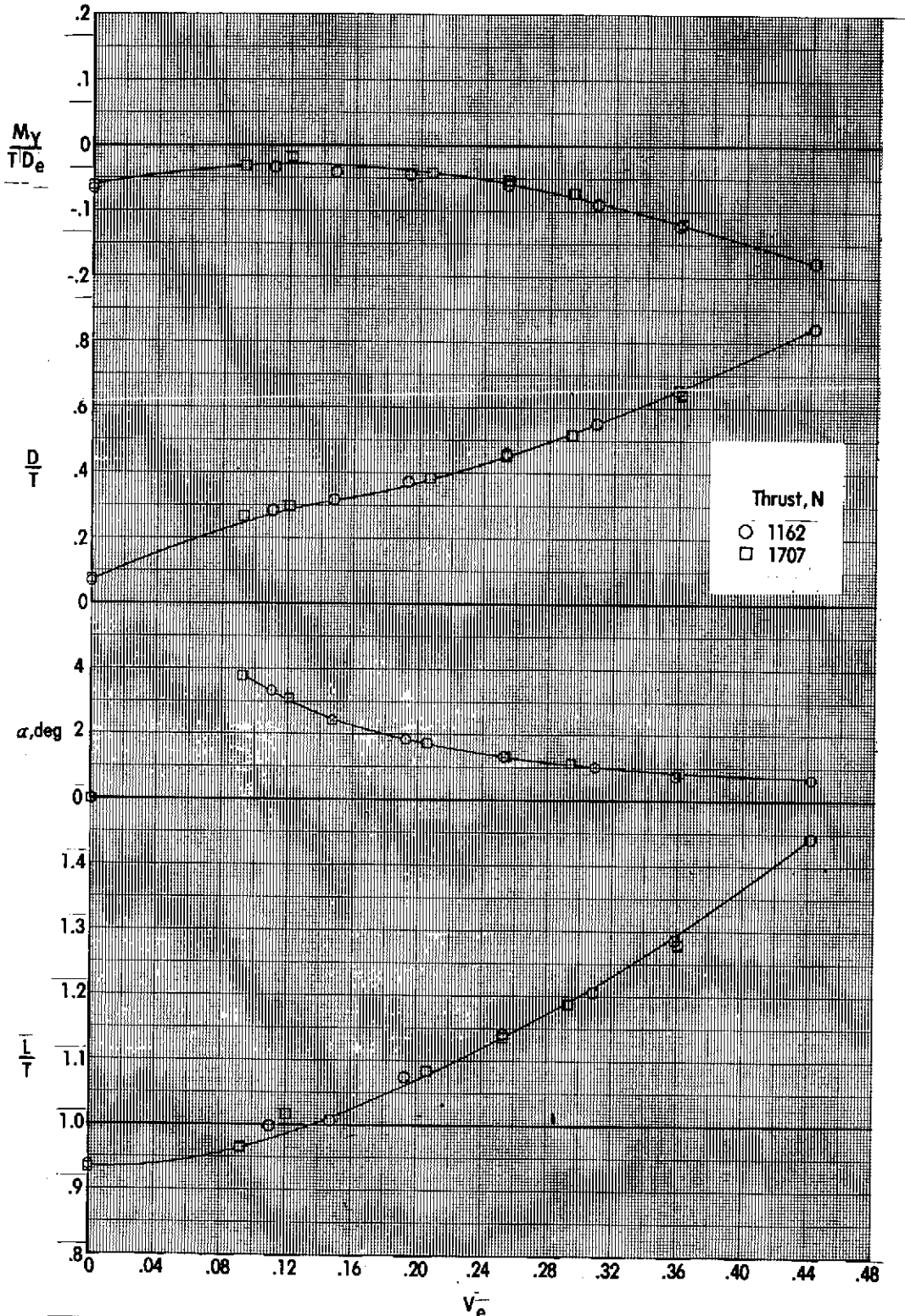

Figure 40 . Effect of velocity ratio on longitudinal aerodynamic characteristics of the VTOL transition configuration.

$\delta_L = -5°$ $\delta_{LC} = 94°$ $\delta_f = 40°$ $i_t = 10°$ $\theta_e = 0°$

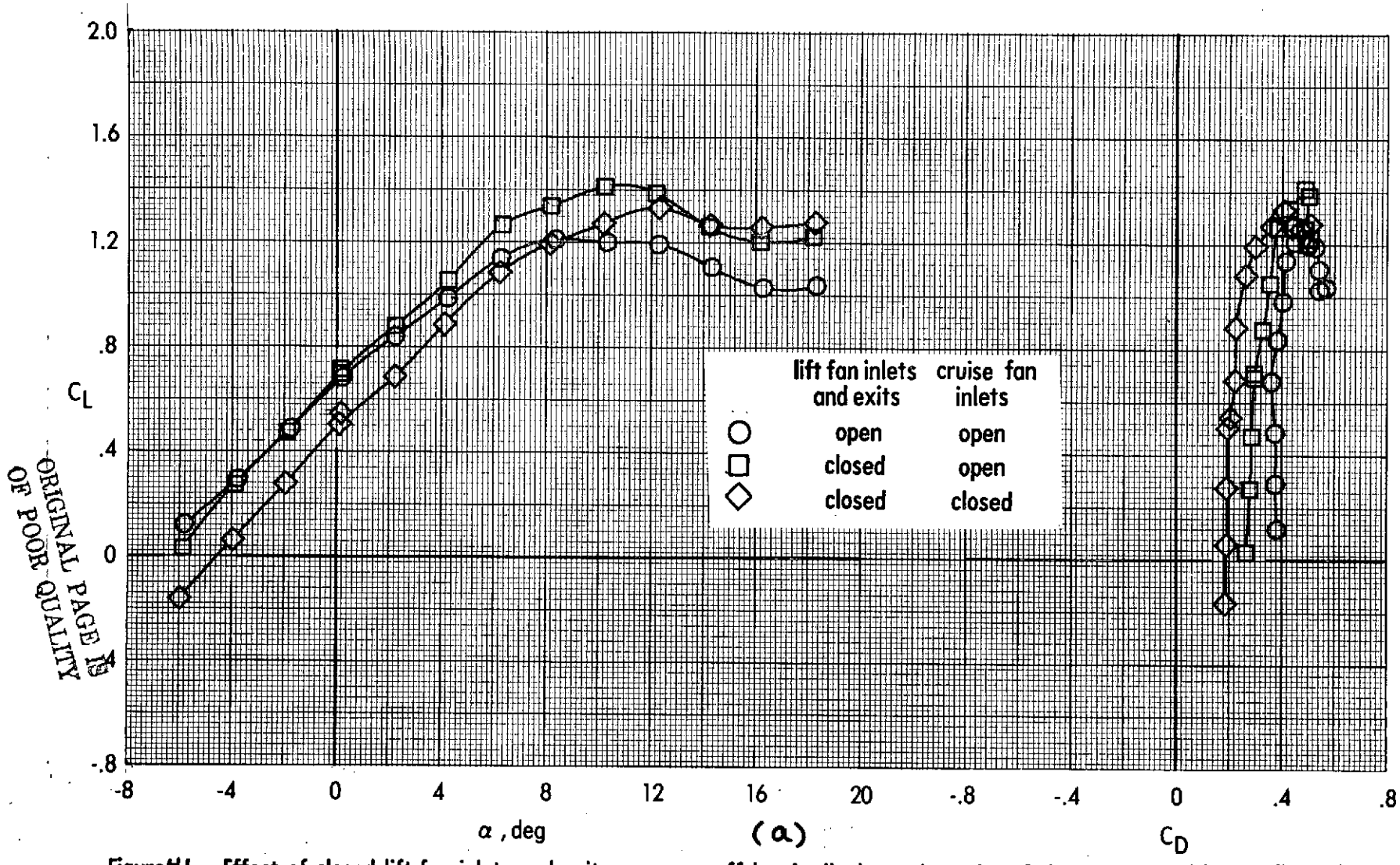

Figure 41. - Effect of closed lift-fan inlets and exits on power-off longitudinal aerodynamics of the VTOL transition configuration.

$\delta_L = -5°$ $\delta_{LC} = 94°$ $\delta_f = 40°$ tail off $C_\mu = 0$ $q_\infty = 168\ N/m^2$ (3.5 lb/ft²)

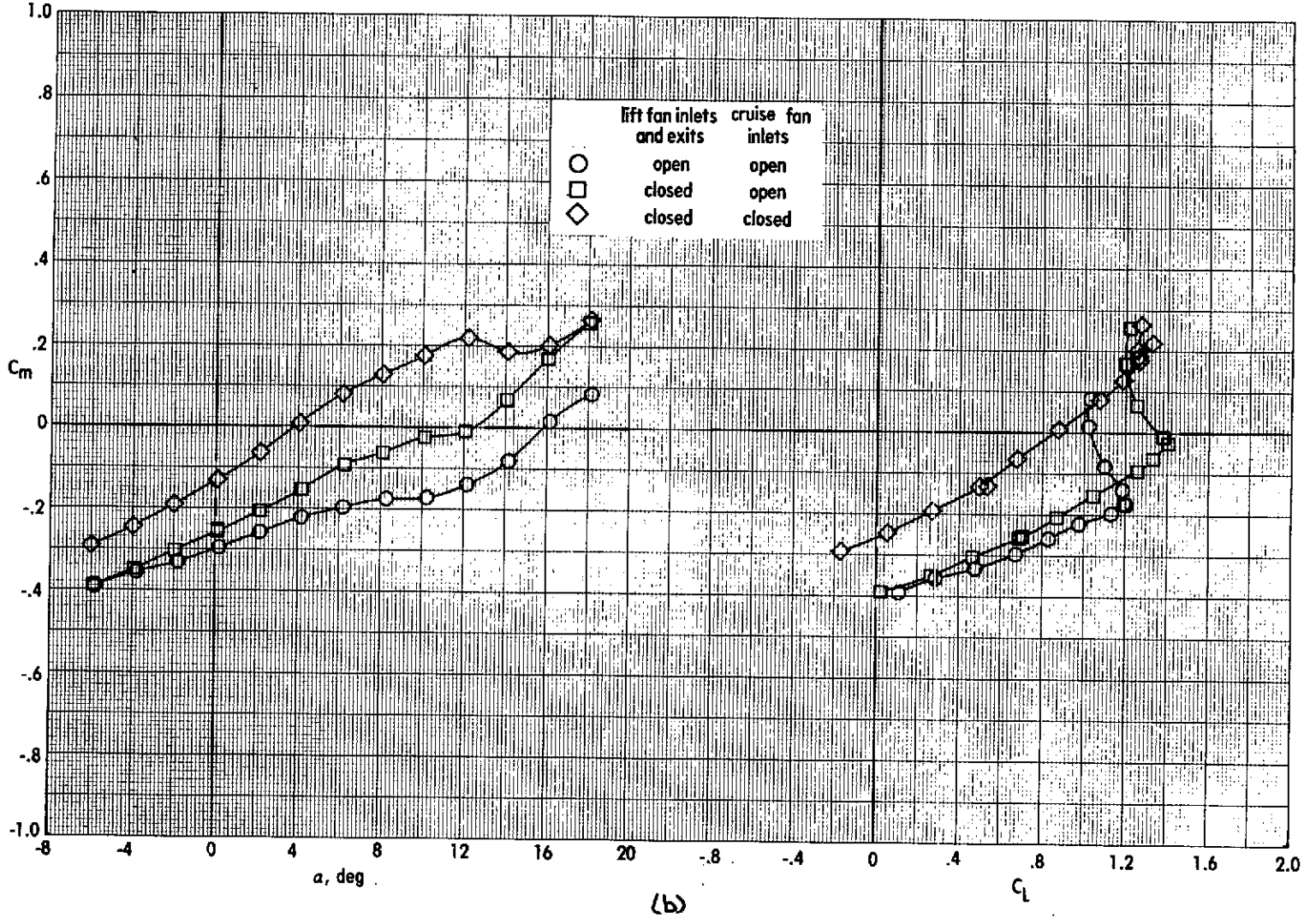

(b)

Figure 41. - Concluded.

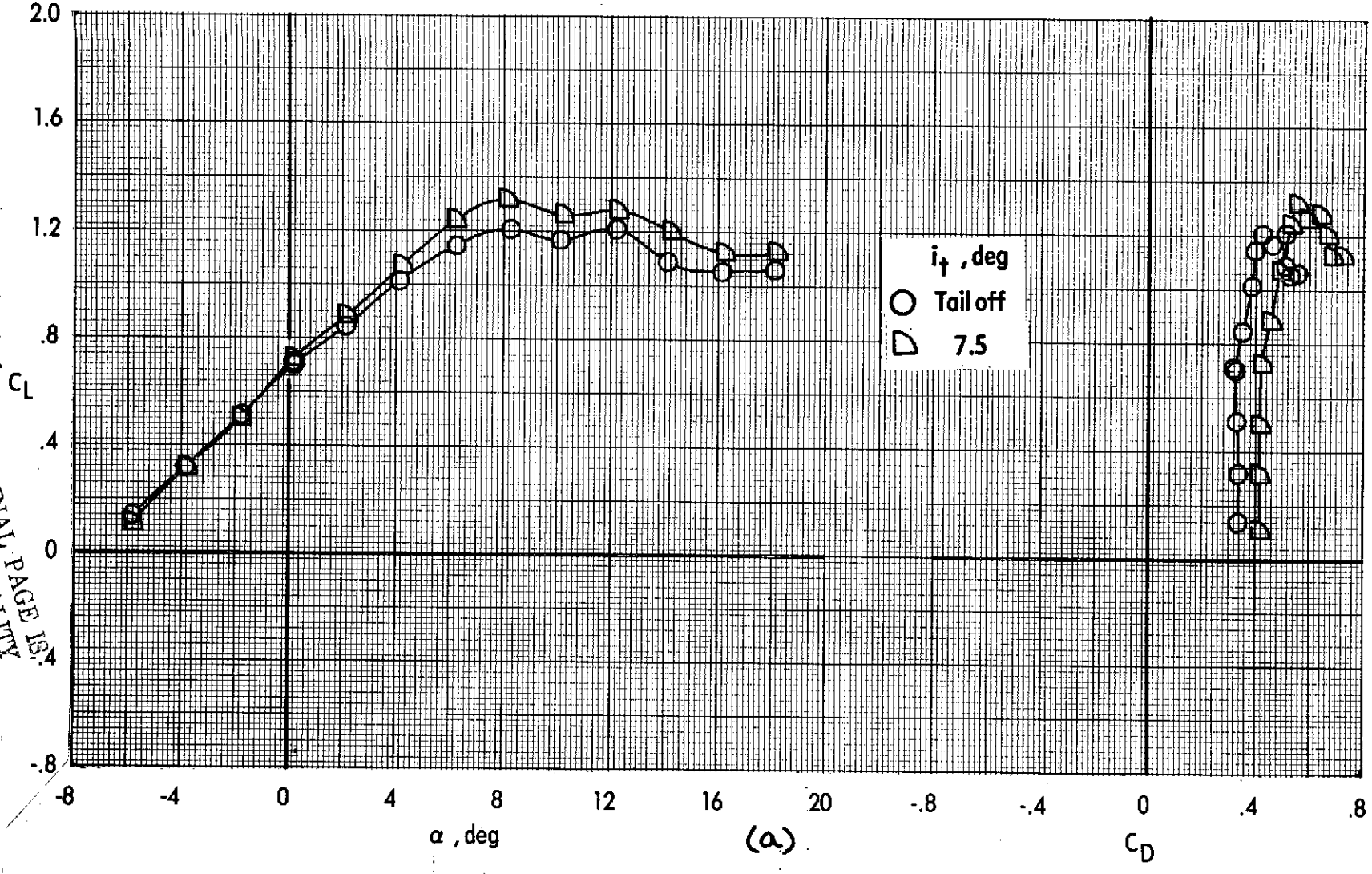

Figure 12 - Longitudinal aerodynamic characteristics of the VTOL transition configuration.

$\delta_L = 7.5°$ $\delta_{LC} = 82°$ $\delta_f = 40°$ $\delta_e = 0°$ $C_\mu = 0$ $q_\infty = 187\ N/m^2$ (3.9 lb/ft^2)

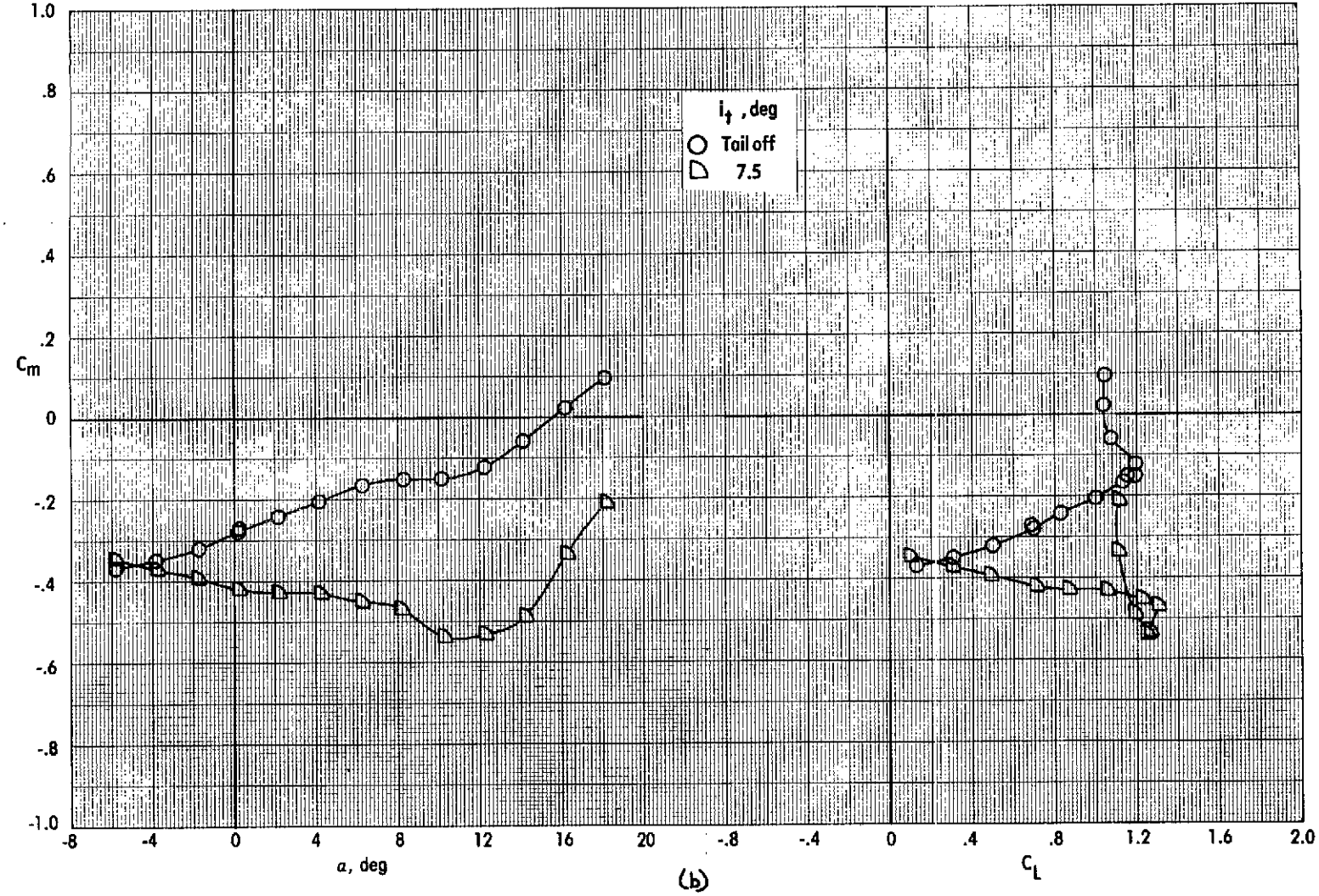

(b)

Figure 42. - Concluded.

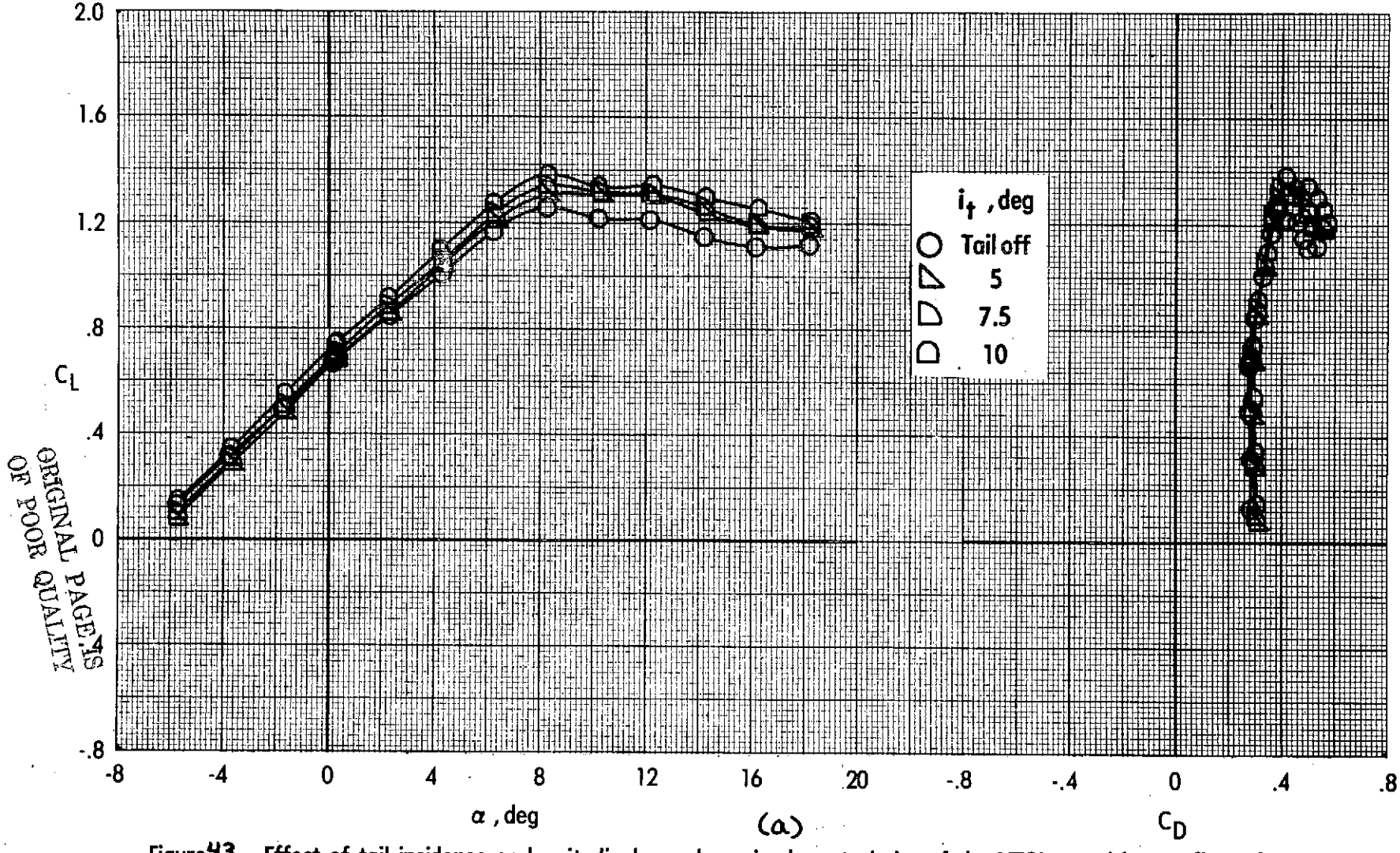

Figure 43. - Effect of tail incidence on longitudinal aerodynamic characteristics of the VTOL transition configuration.

$\delta_L = 7.5°$ $\delta_{LC} = 82°$ $\delta_f = 40°$ $\delta_e = 0°$ $C_\mu = 0$ $q_\infty = 455\ N/m^2 (9.5\ lb/ft^2)$

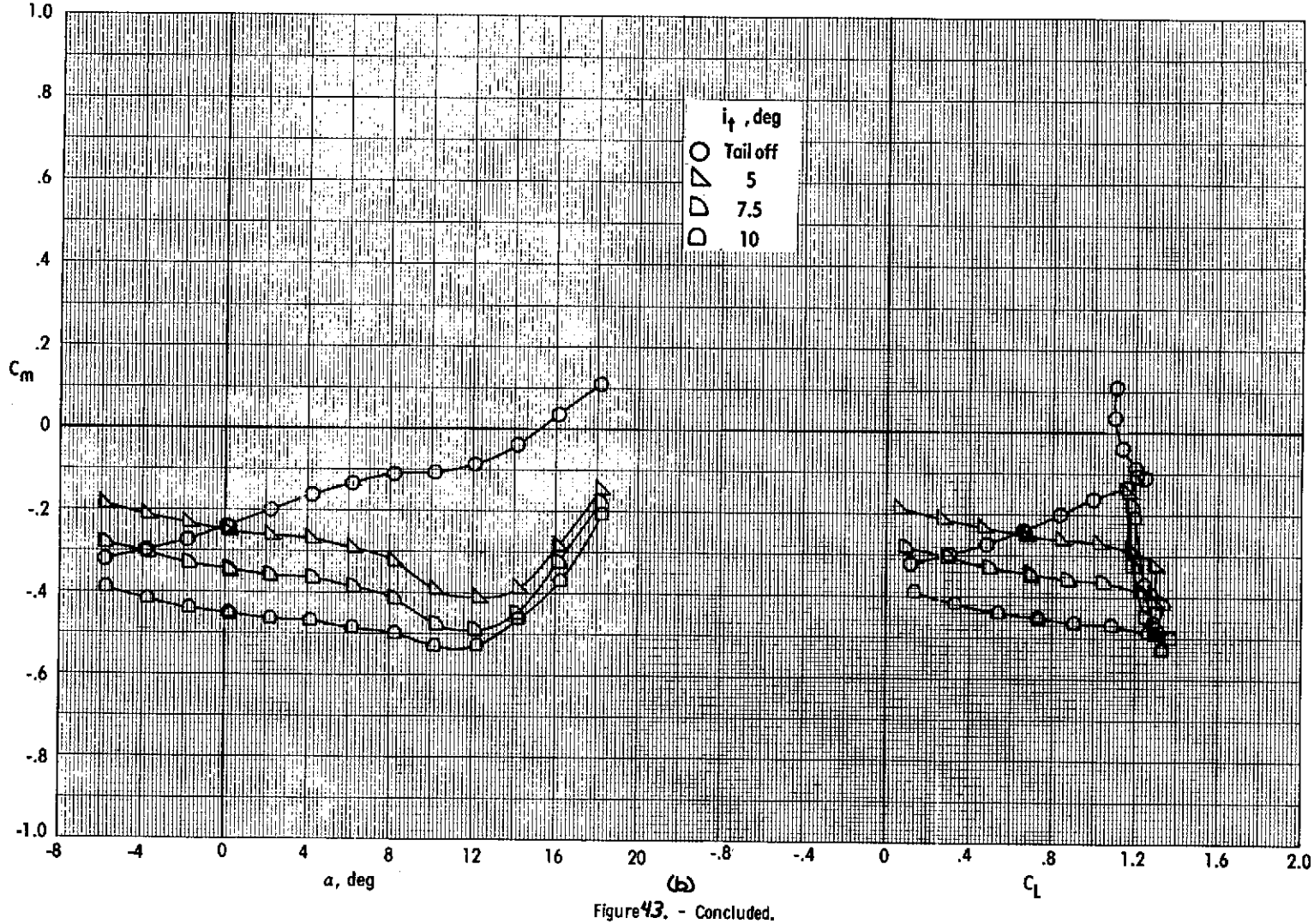

(b)

Figure 43. - Concluded.

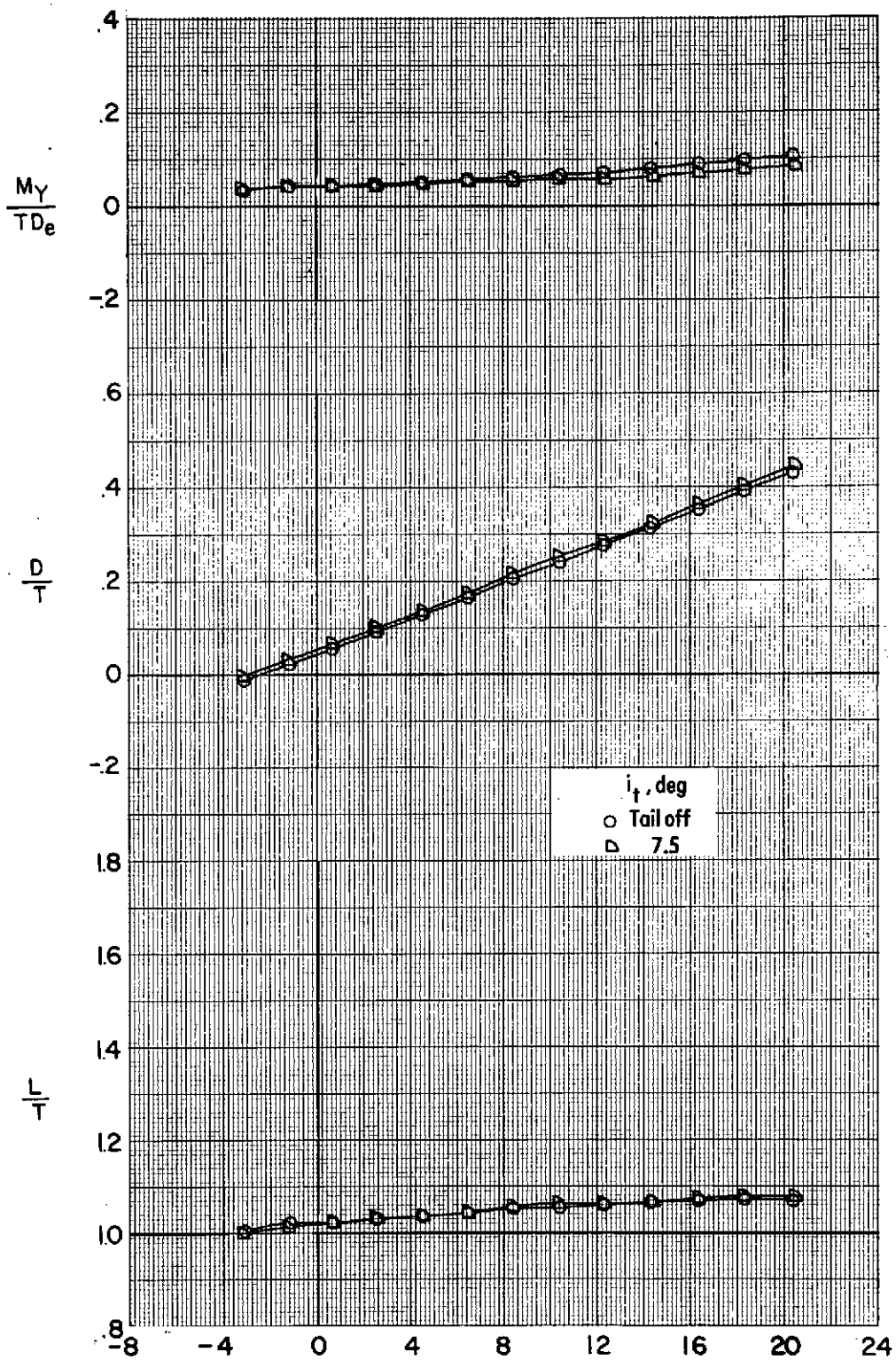

Figure 44 - Longitudinal aerodynamic characteristics of the VTOL transition configuration. $\delta_L = 7.5°$ $\delta_{LC} = 82°$ $\delta_f = 40°$ $\delta_e = 0°$ $V_e = 0.12$ $q_\infty = 177$ N/m² (3.7 lb/ft²)

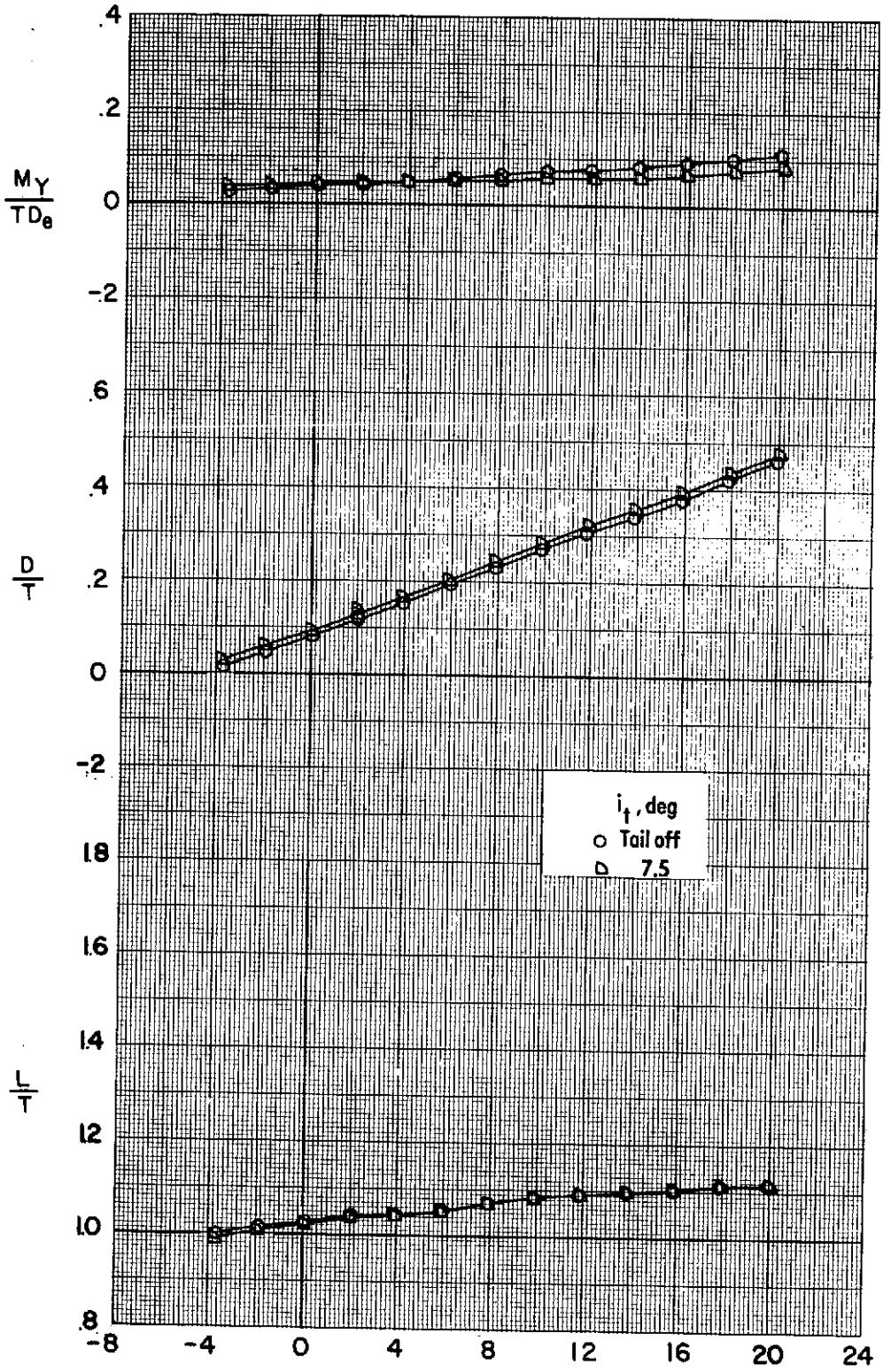

Figure 15- Longitudinal aerodynamic characteristics of the VTOL transition configuration. $\delta_L = 7.5°$ $\delta_{LC} = 82°$ $\delta_f = 40°$ $\delta_e = 0°$ $V_e = 0.15$ $q_\infty = 177$ N/m² (3.7 lb/ft²)

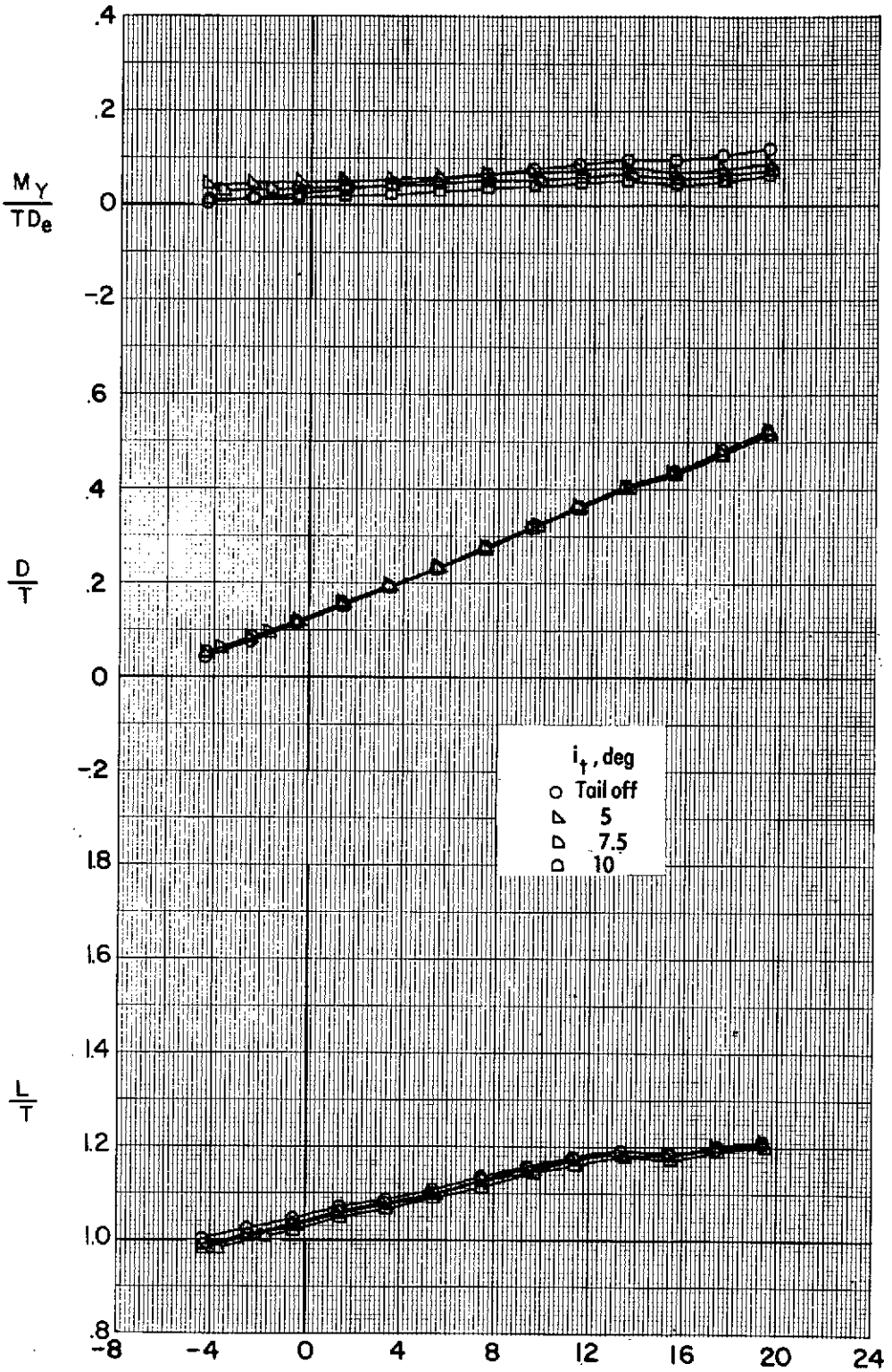

Figure 46. - Effect of tail incidence on longitudinal aerodynamic characteristics of the VTOL transition configuration. $\delta_L = 7.5°$ $\delta_{LC} = 82°$ $\delta_f = 40°$ $V_e = 0.20$ $q_\infty = 440$ N/m² (9.2 lb/ft²)

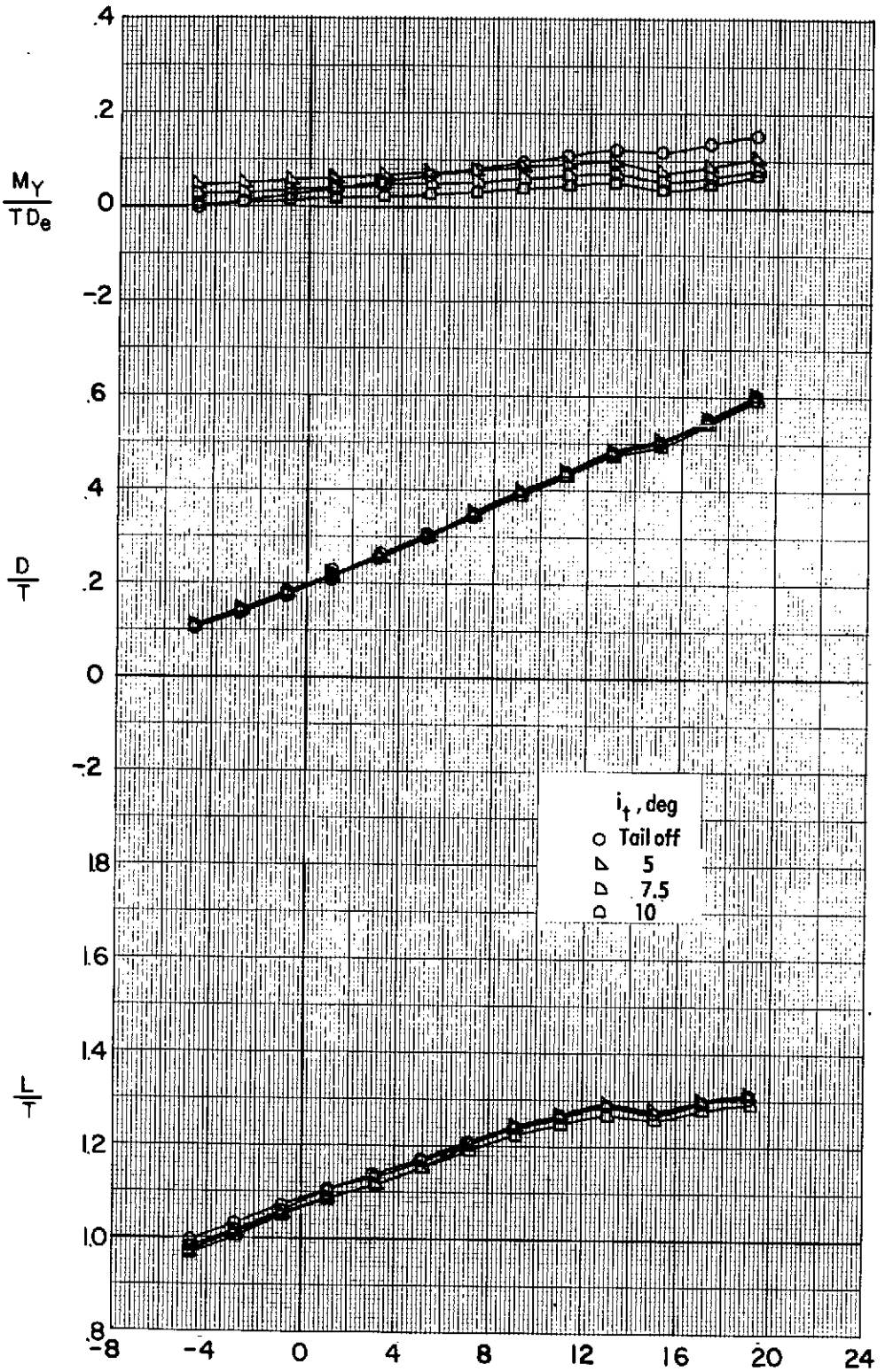

Figure 47. - Effect of tail incidence on longitudinal aerodynamic characteristics of the VTOL transition configuration. $\delta_L = 7.5°$ $\delta_{LC} = 82°$ $\delta_f = 40°$ $\delta_e = 0°$ $V_\infty = 0.24$ $q_\infty = 440$ N/m² (9.2 lb/ft²).

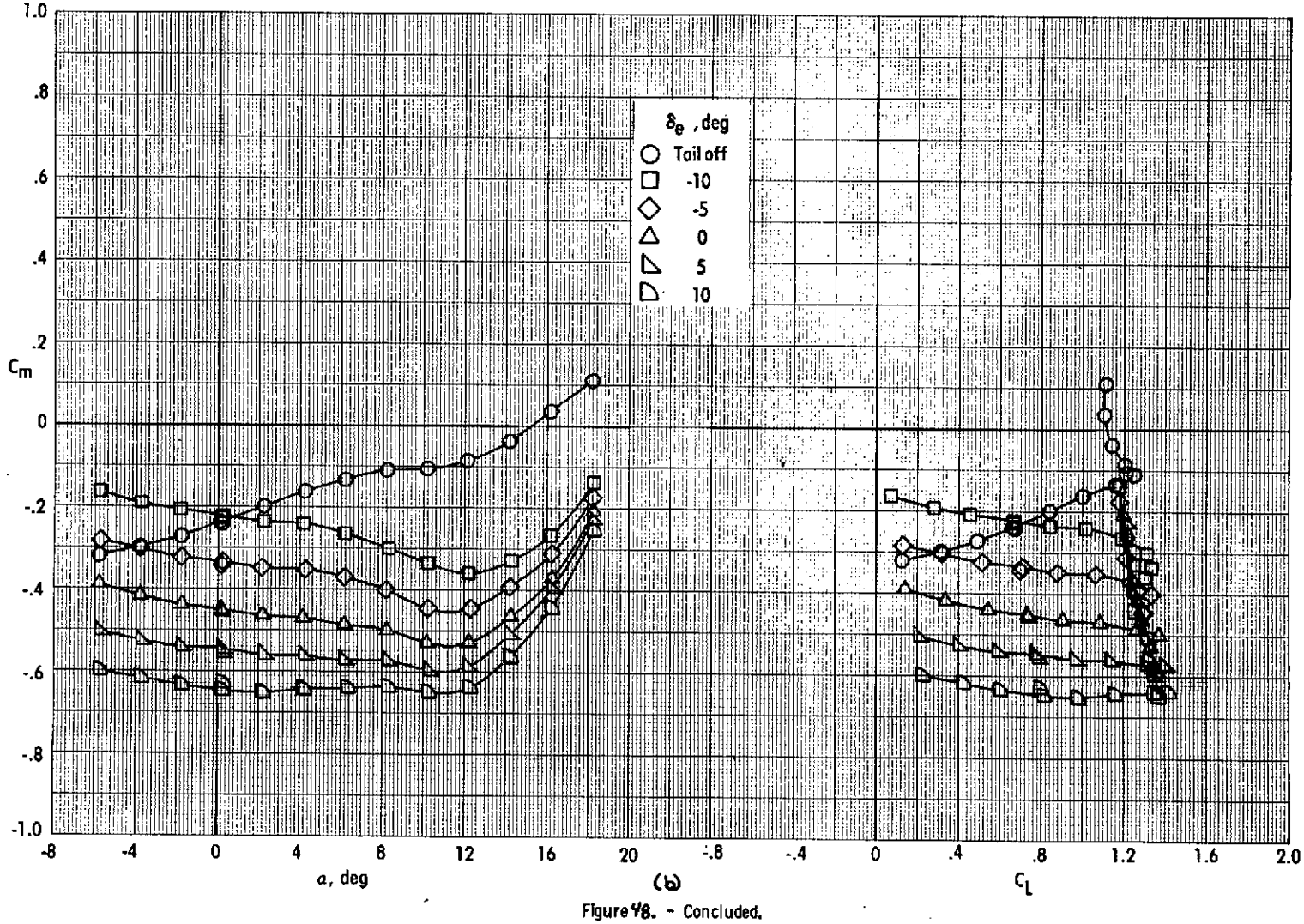

Figure 48. - Concluded.

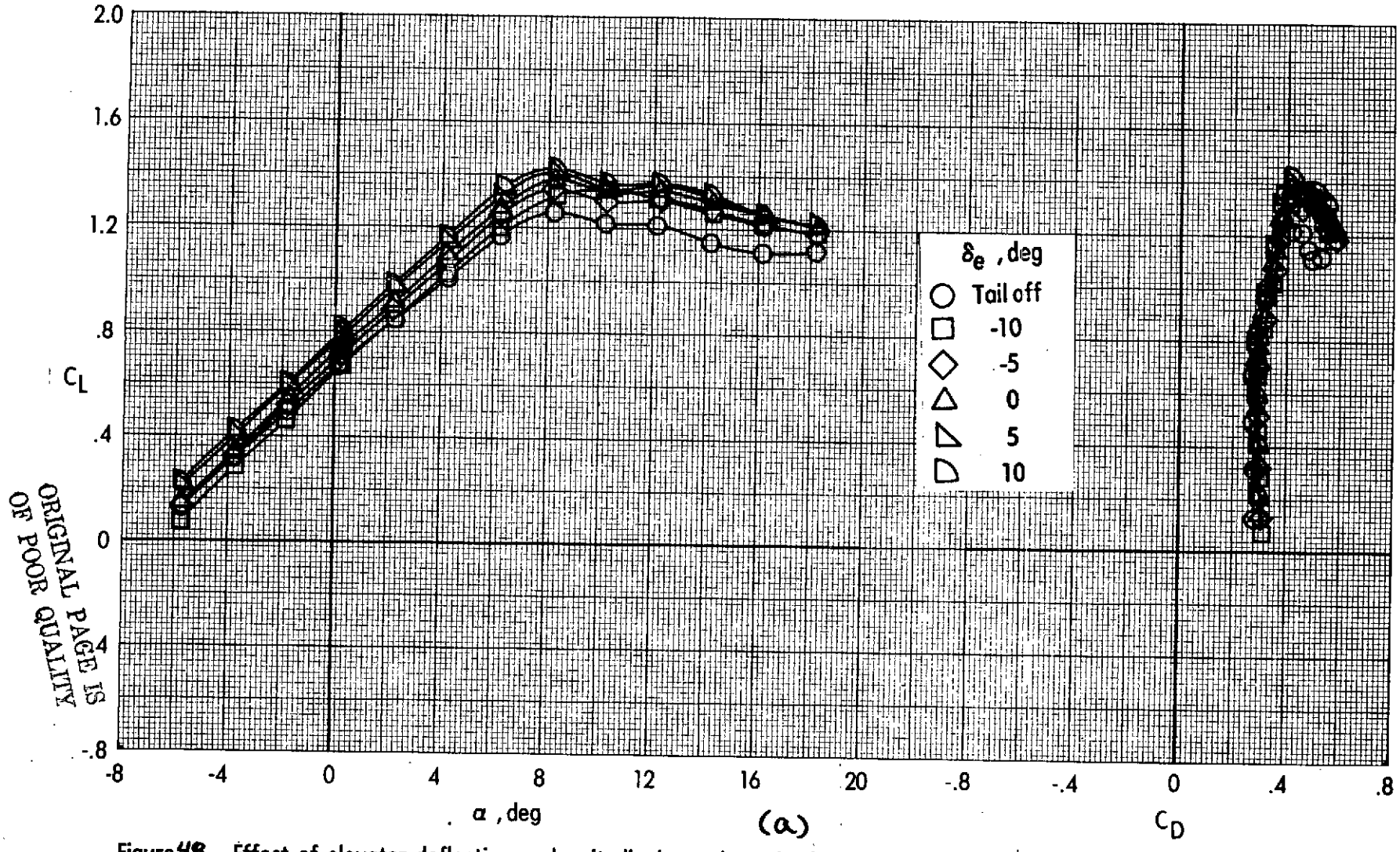

Figure 48 - Effect of elevator deflection on longitudinal aerodynamic characteristics of the VTOL transition configuration.

$\delta_L = 7.5°$ $\delta_{LC} = 82°$ $\delta_f = 40°$ $i_t = 10°$ $C_\mu = 0$ $q_\infty = 455\ N/m^2$ $(9.5\ lb/ft^2)$

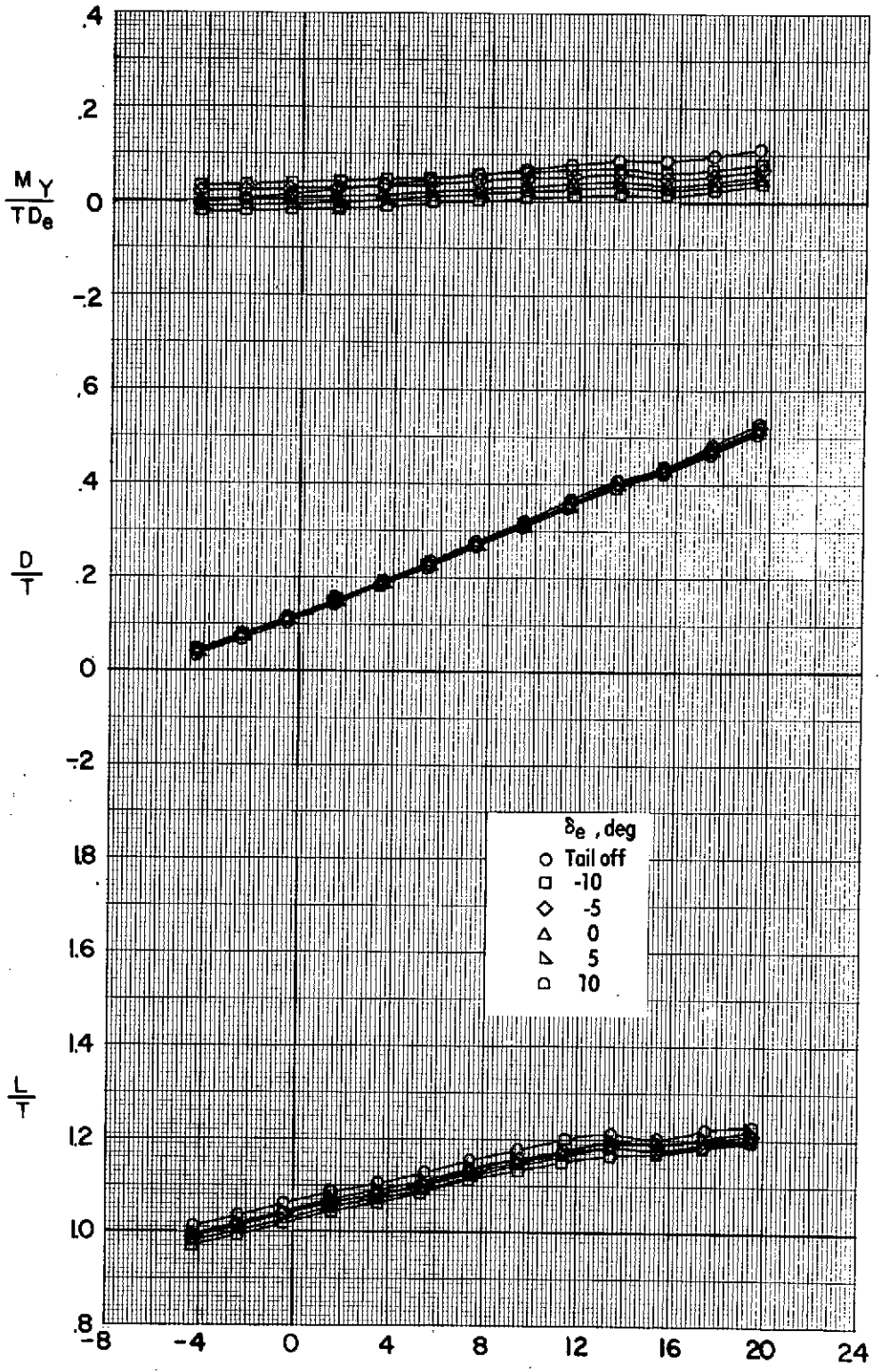

Figure 49. - Effect of elevator deflection on longitudinal aerodynamic characteristics of the VTOL transition configuration. $\delta_L = 7.5°$ $\delta_{LC} = 82°$ $\delta_f = 40°$ $i_t = 10°$ $V_e = 0.20$ $q_\infty = 440$ N/m² (9.5 lb/ft²)

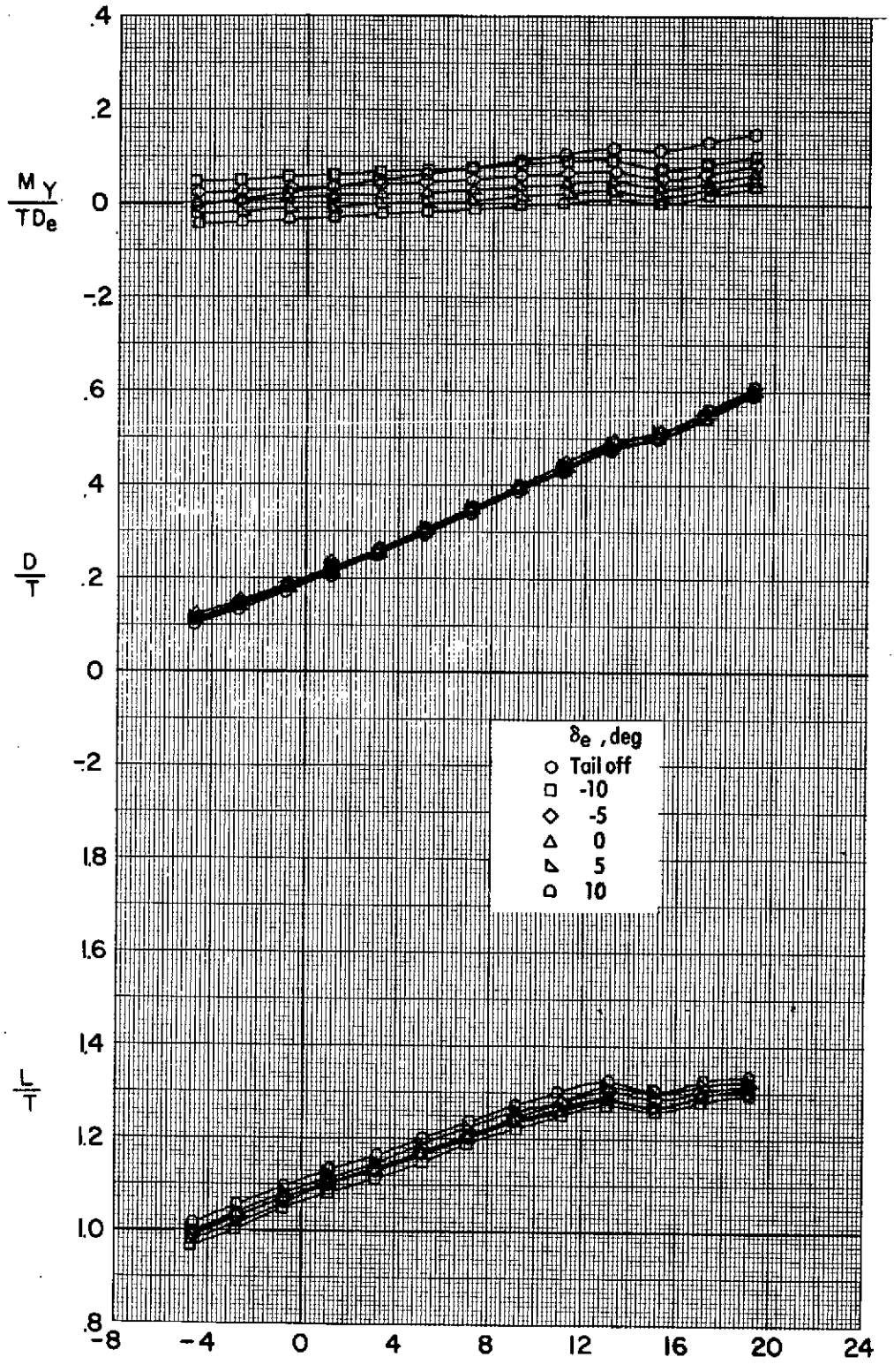

Figure 50 - Effect of elevator deflection on longitudinal aerodynamic characteristics of the VTOL transition configuration. $\delta_L = 7.5°$ $\delta_{LC} = 82°$ $\delta_f = 40°$ $i_t = 10°$ $V_e = 0.24$ $q_\infty = 440$ N/m² (9.5 lb/ft²)

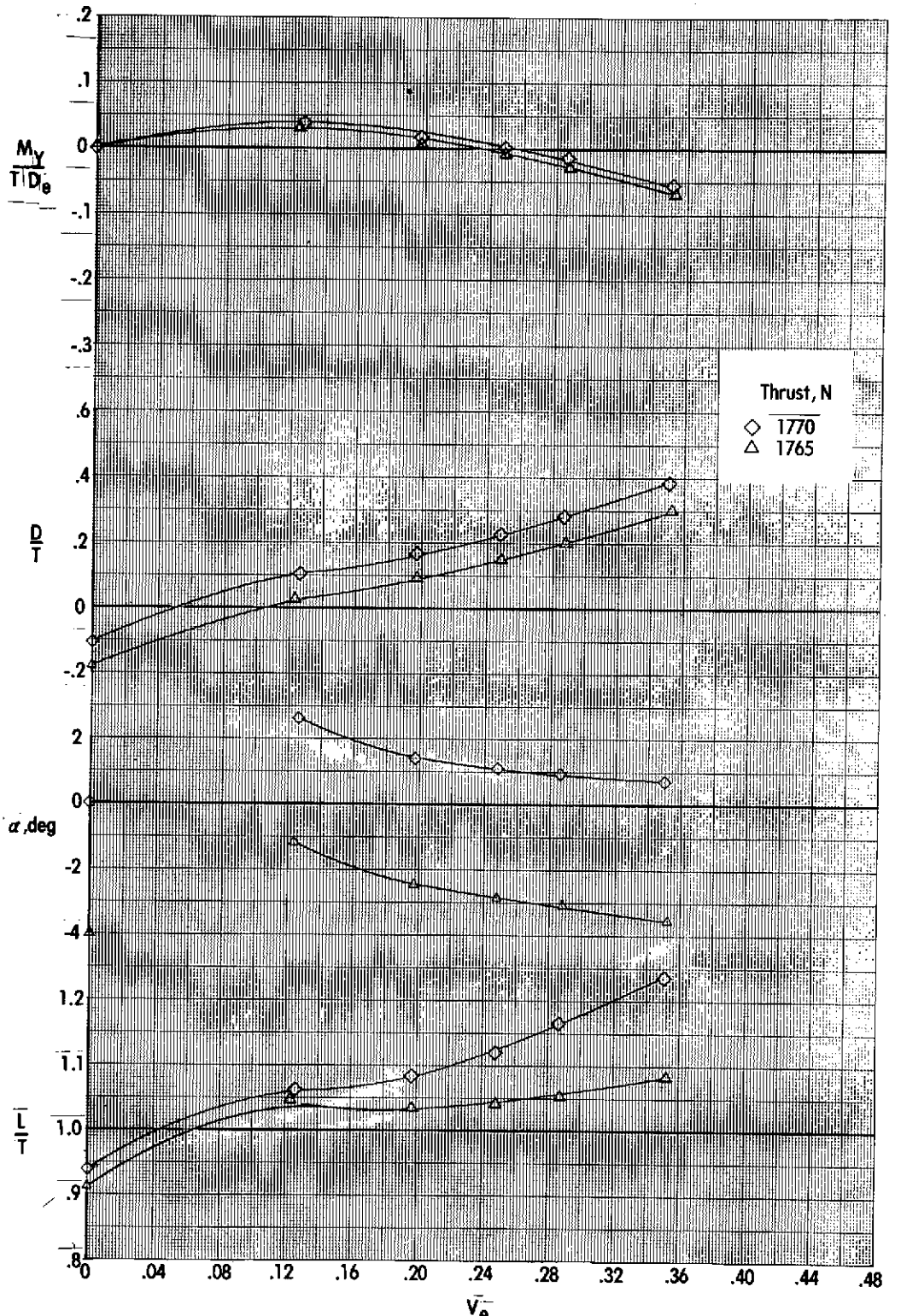

Figure 51. Effect of velocity ratio on longitudinal aerodynamic characteristics of the VTOL transition configuration.

$\delta_L = 7.5°$ $\delta_{LC} = 82°$ $\delta_f = 40°$ $i_t = 10°$ $\delta_e = 0°$

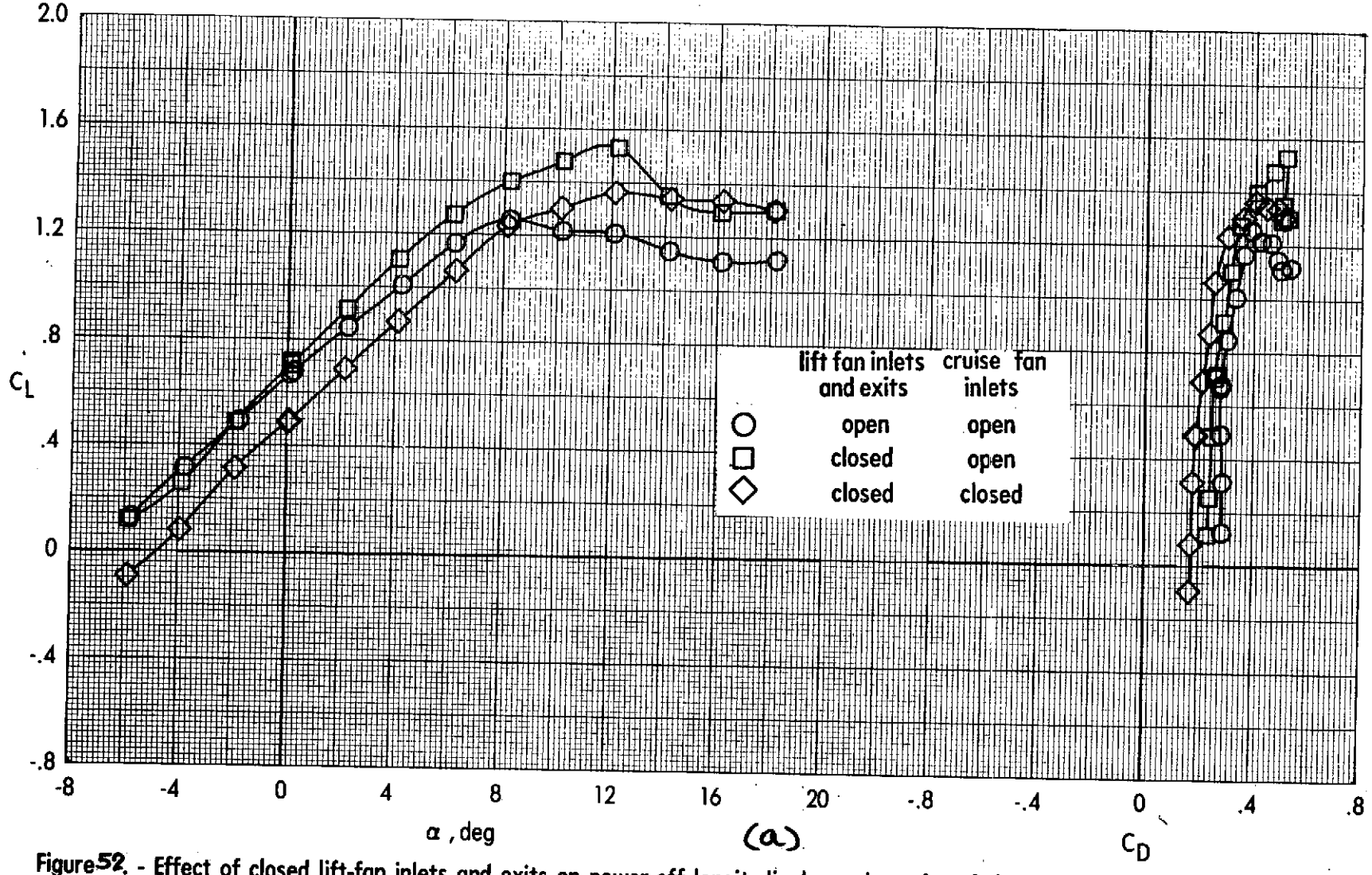

Figure 52. - Effect of closed lift-fan inlets and exits on power-off longitudinal aerodynamics of the VTOL transition configuration.

$\delta_L = 7.5°$ $\delta_{LC} = 82°$ $\delta_f = 40°$ tail off $C_\mu = 0$ $q_\infty = 455$ N/m² (9.5 lb/ft²)

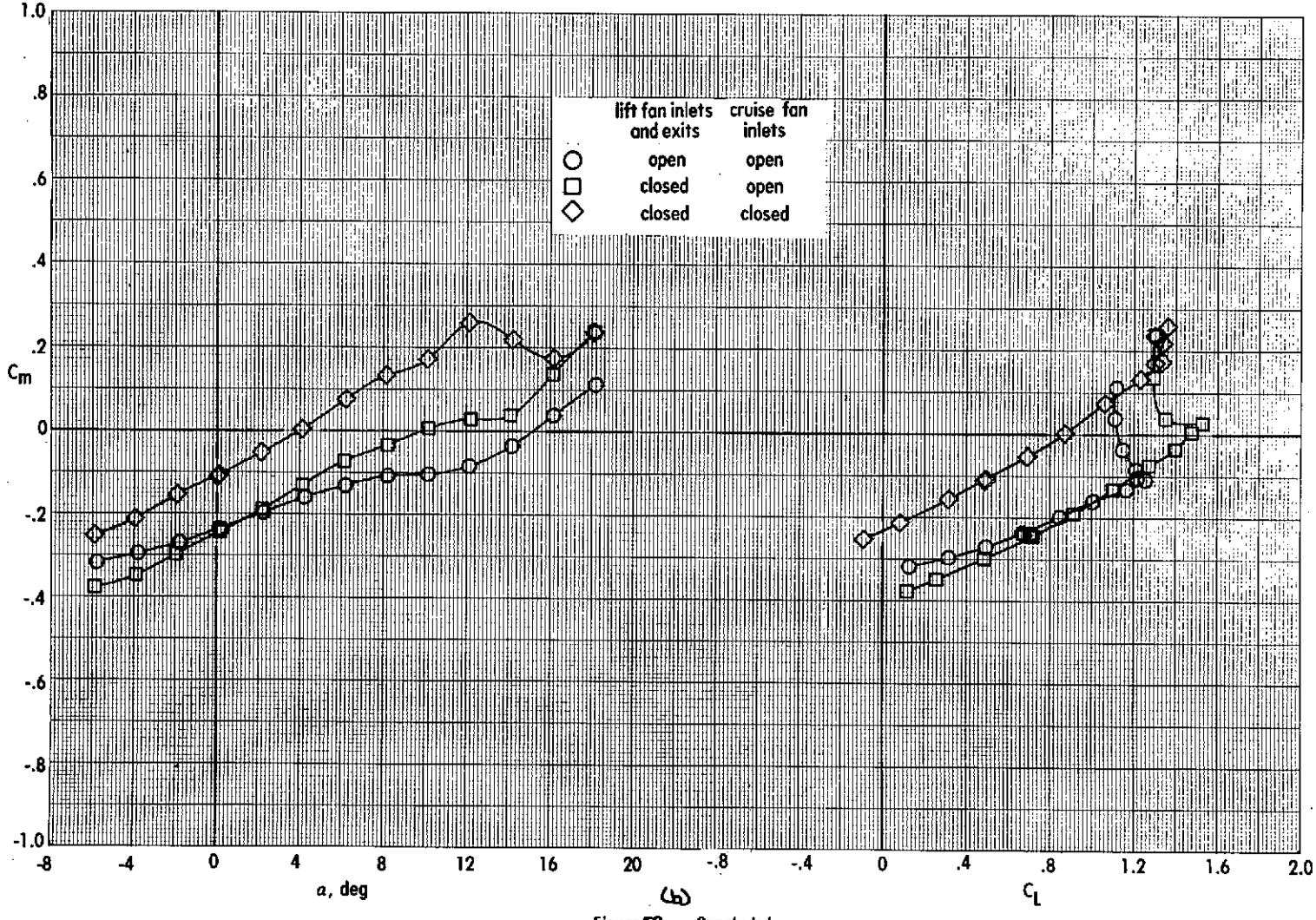

Figure 52. - Concluded.

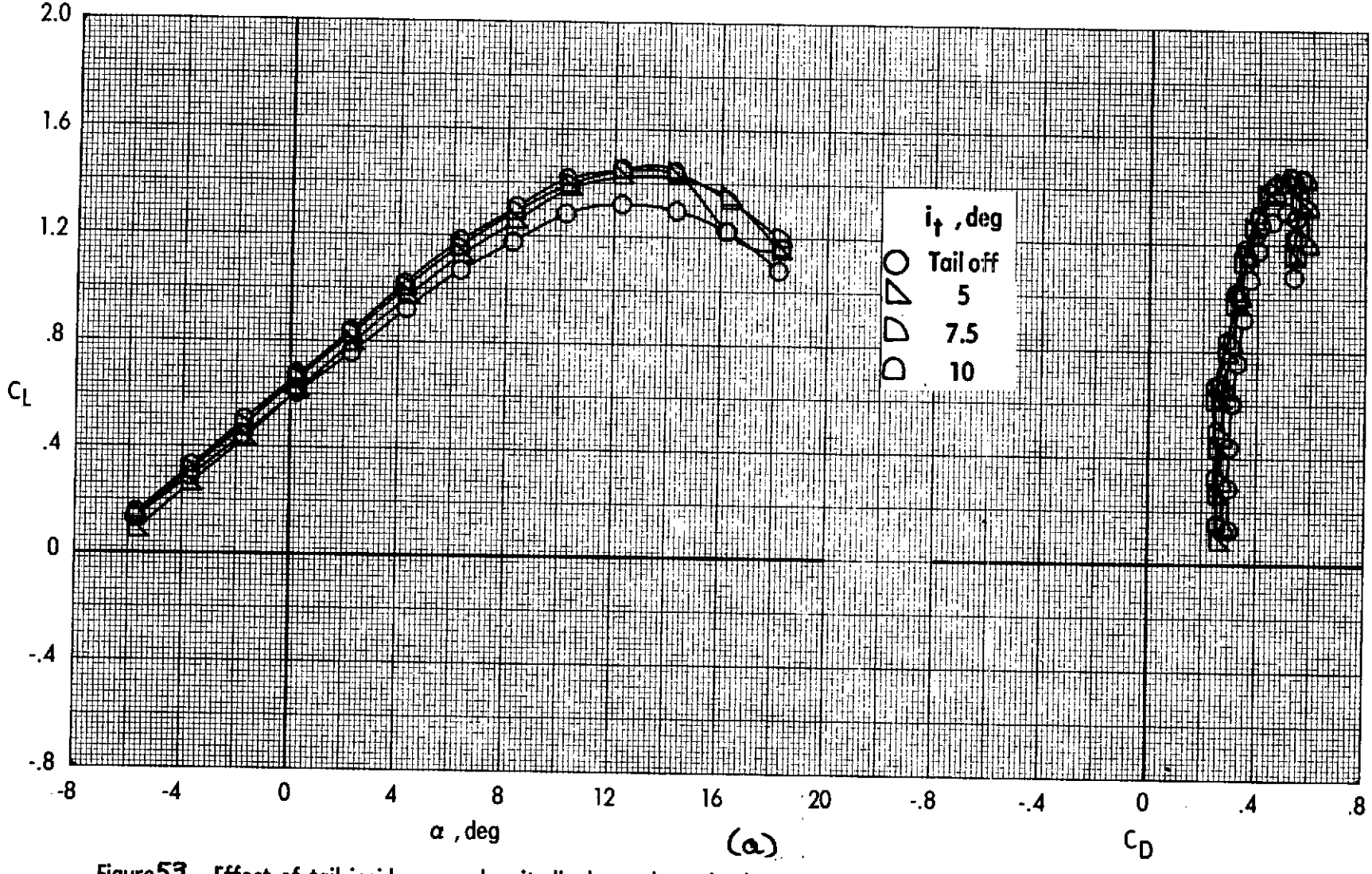

Figure 53. - Effect of tail incidence on longitudinal aerodynamic characteristics of the VTOL transition configuration.

$\delta_L = 40°$ $\delta_{LC} = 70°$ $\delta_f = 40°$ $\delta_e = 0°$ $C_\mu = 0$ $q_\infty = 728\ N/m^2$ (15.2 lb/ft^2)

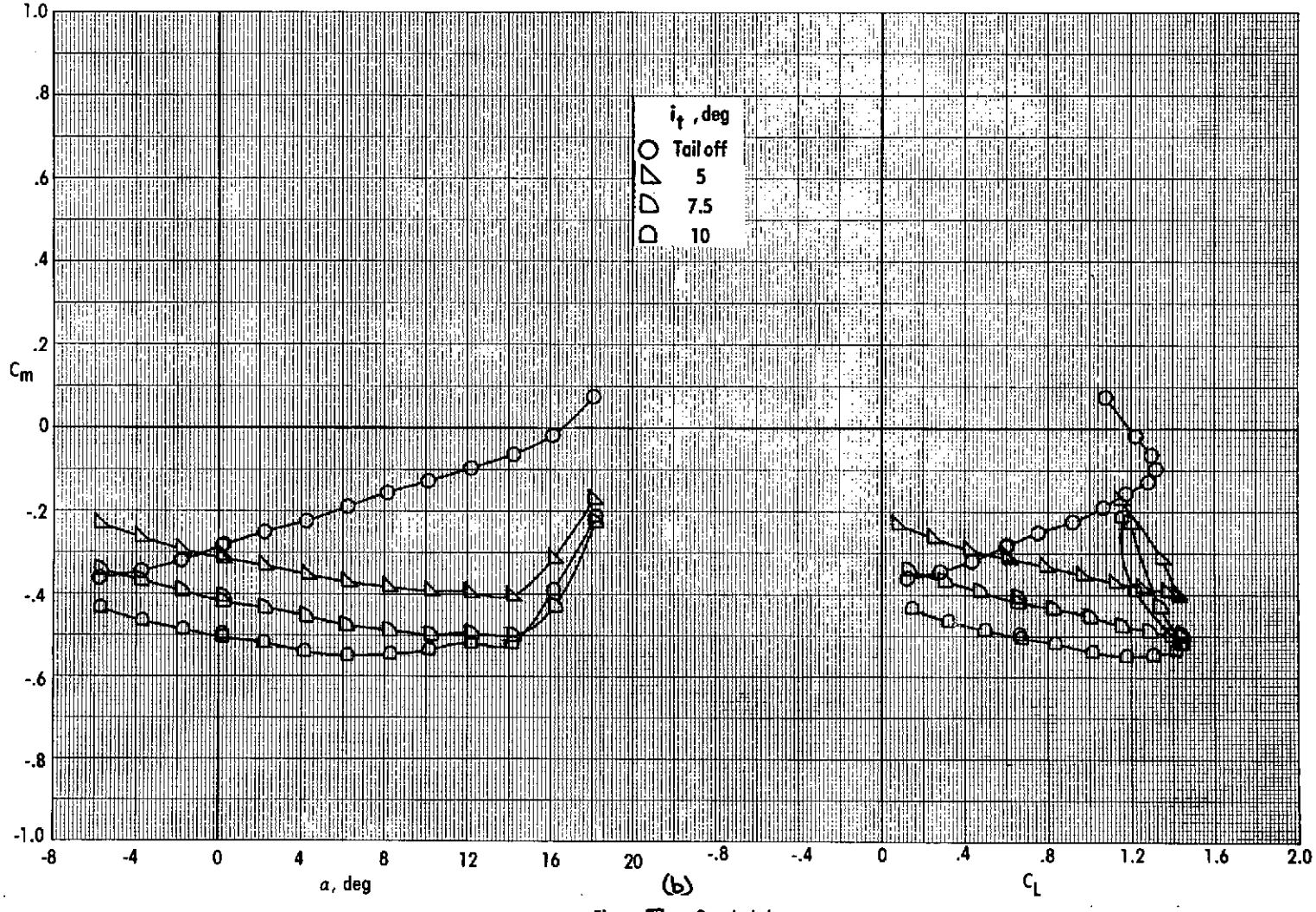

Figure 53. - Concluded.

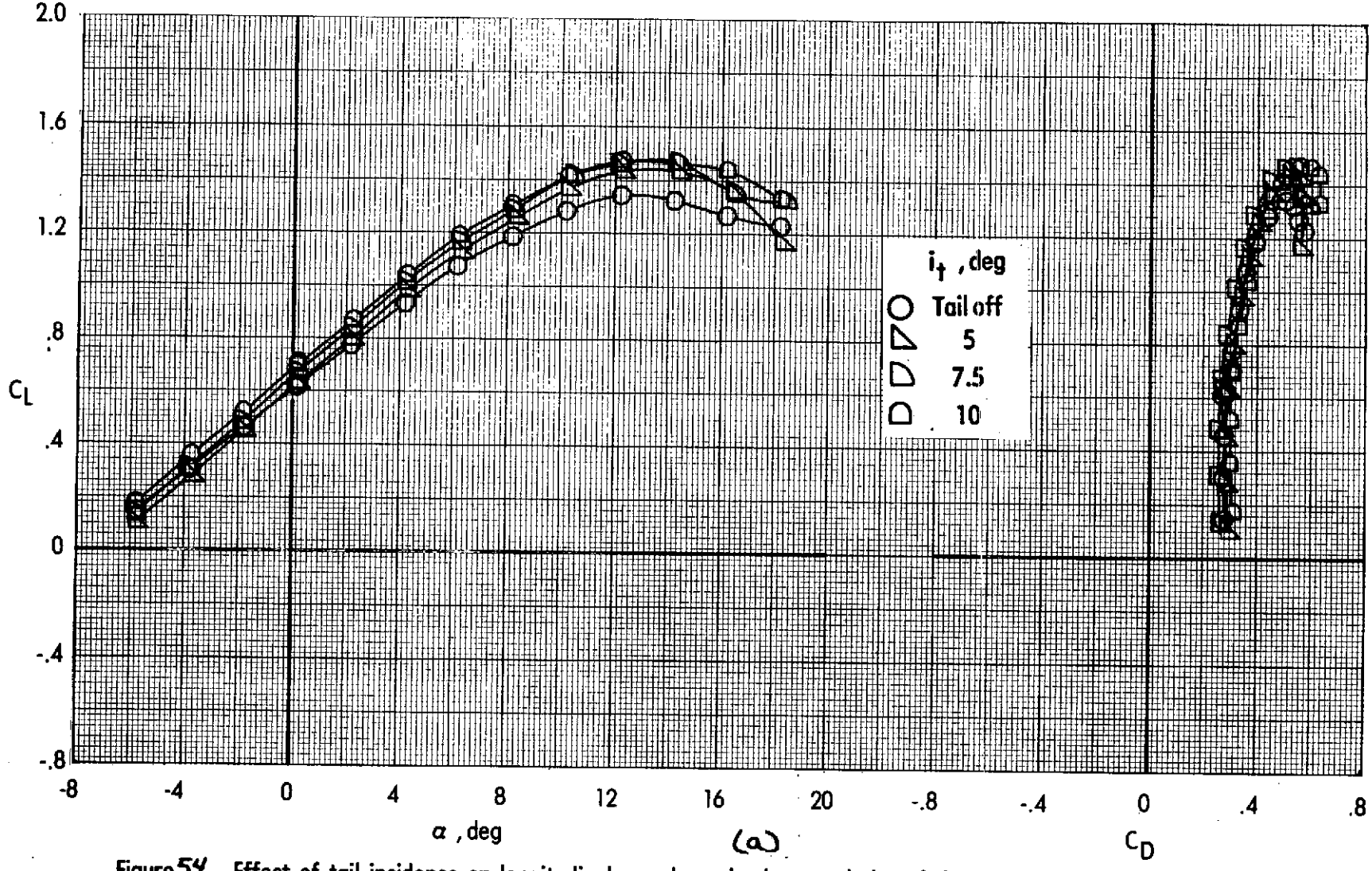

Figure 54. - Effect of tail incidence on longitudinal aerodynamic characteristics of the VTOL transition configuration.

$\delta_L = 40°$, $\delta_{LC} = 70°$, $\delta_f = 40°$ $\delta_e = 0°$ $C_\mu = 0$ $q_\infty = 1245\ N/m^2$ (26.0 lb/ft^2)

C-2

(b)

Figure 5. - Concluded.

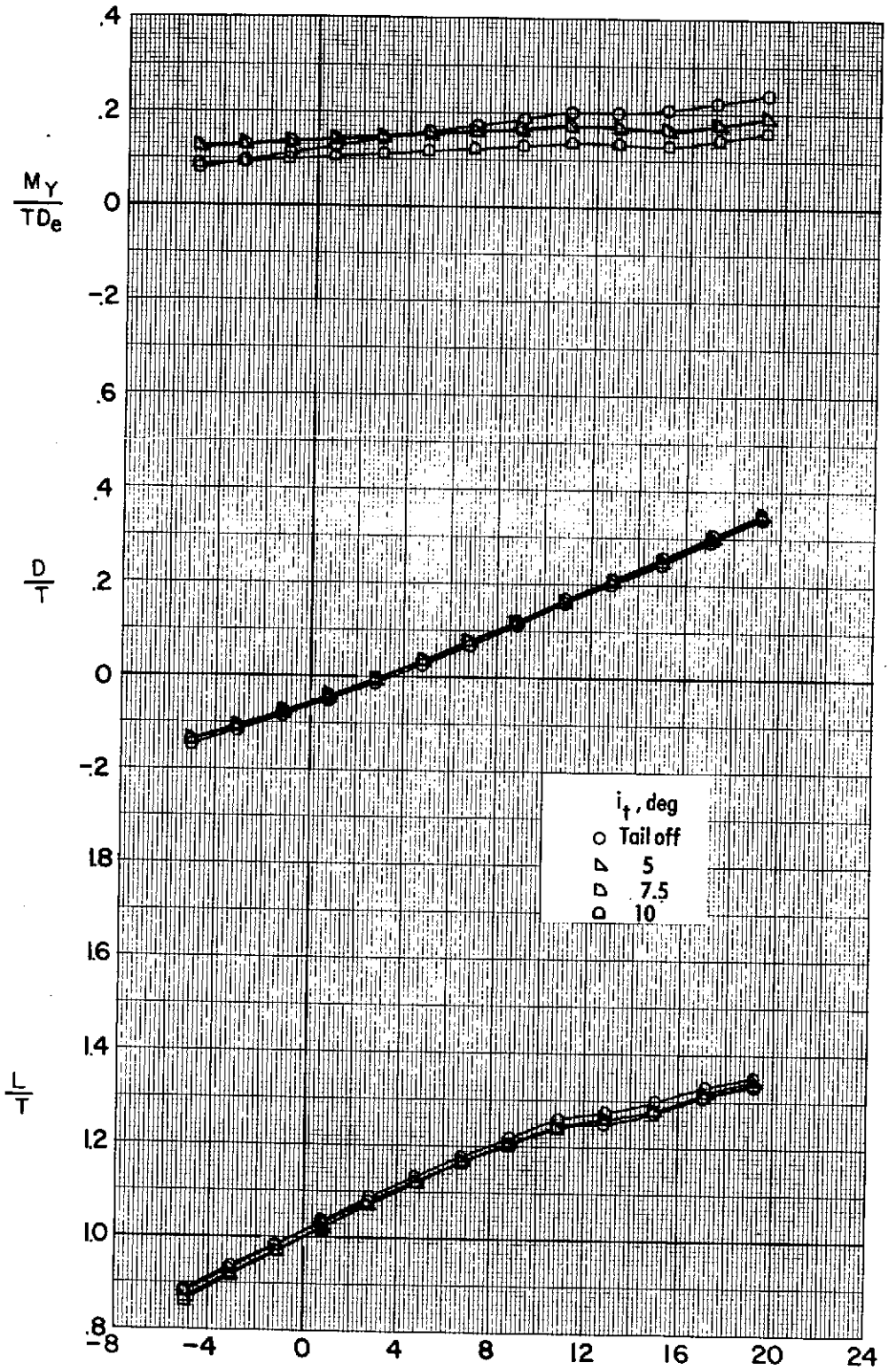

Figure 55 - Effect of tail incidence on longitudinal aerodynamic characteristics of the VTOL transition configuration. $\delta_L = 40°$ $\delta_{LC} = 70°$ $\delta_f = 40°$ $\delta_e = 0°$

$V_e = 0.24$ $q_\infty = 709$ N/m² (14.8 lb/ft²)

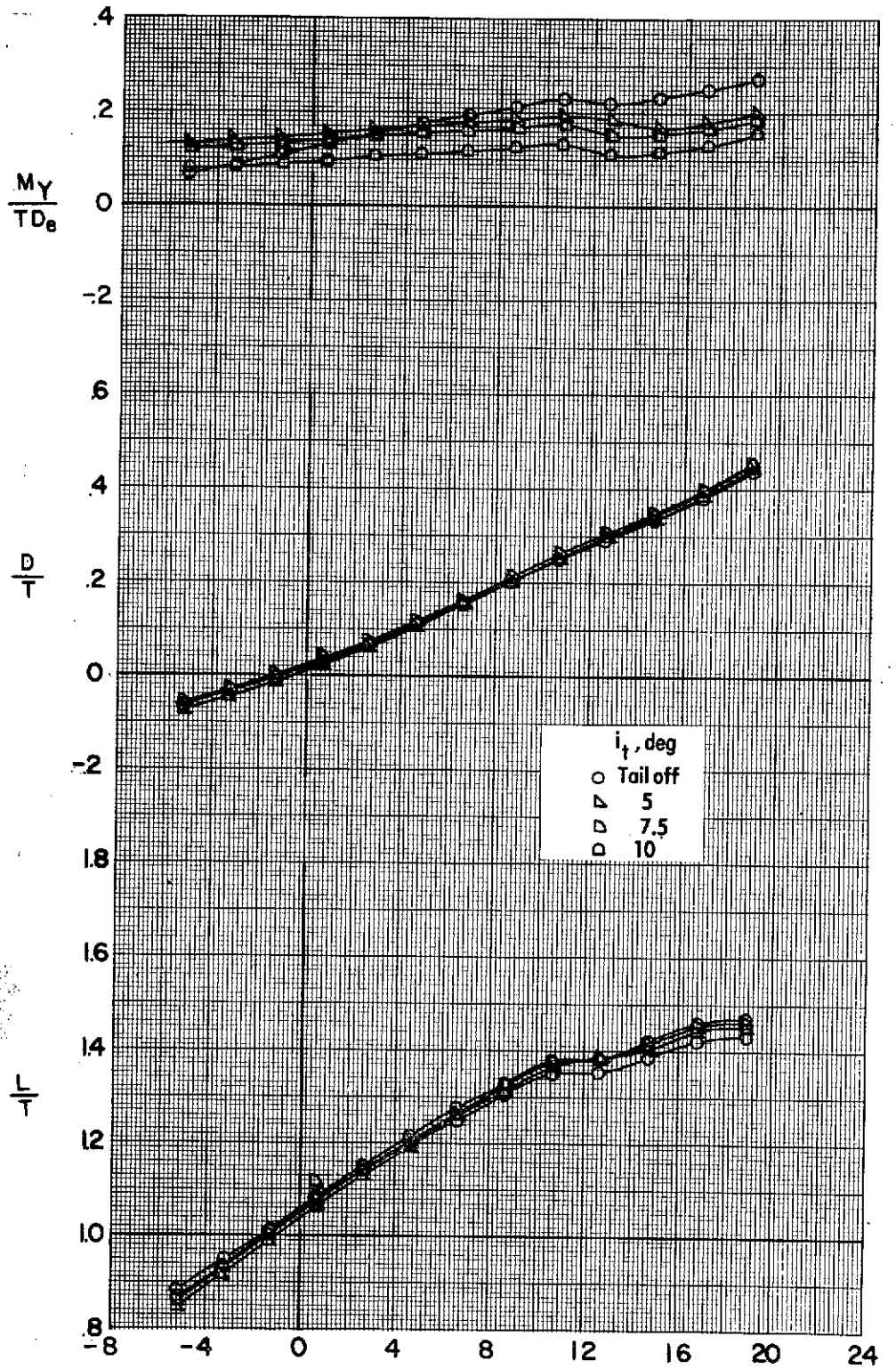

Figure 56. - Effect of tail incidence on longitudinal aerodynamic characteristics of the VTOL transition configuration. $\delta_l = 40°$ $\delta_{LC} = 70°$ $\delta_f = 40°$ $\delta_e = 0°$
$V_e = 0.29$ $q_\infty = 709$ N/m² (14.8 lb/ft²)

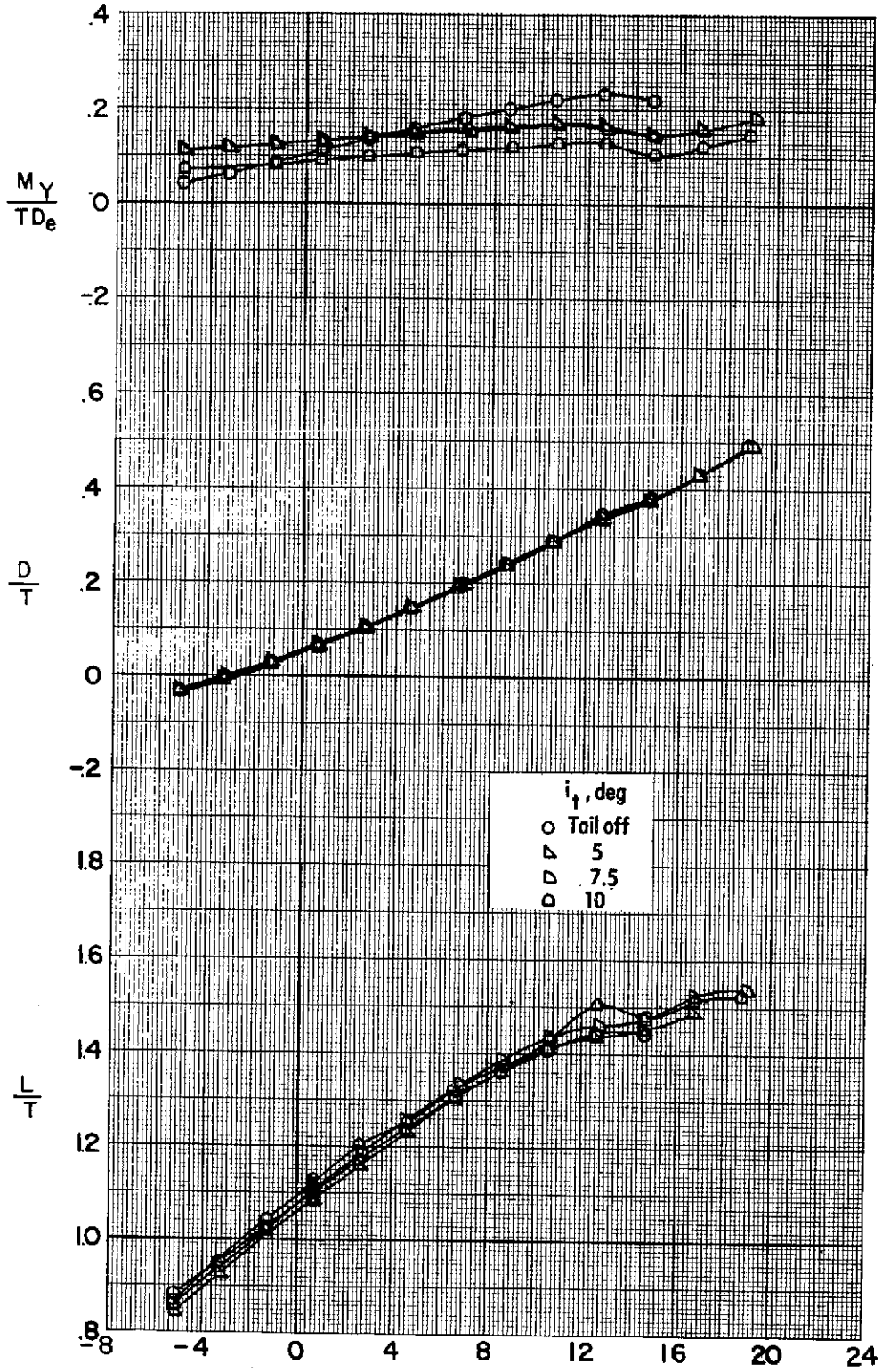

Figure 57. - Effect of tail incidence on longitudinal aerodynamic characteristics of the VTOL transition configuration. $\delta_l = 40°$ $\delta_{LC} = 70°$ $\delta_f = 40°$ $\delta_e = 0°$ $V_e = 0.31$ $q_\infty = 1230\ N/m^2 (25.7\ lb/ft^2)$

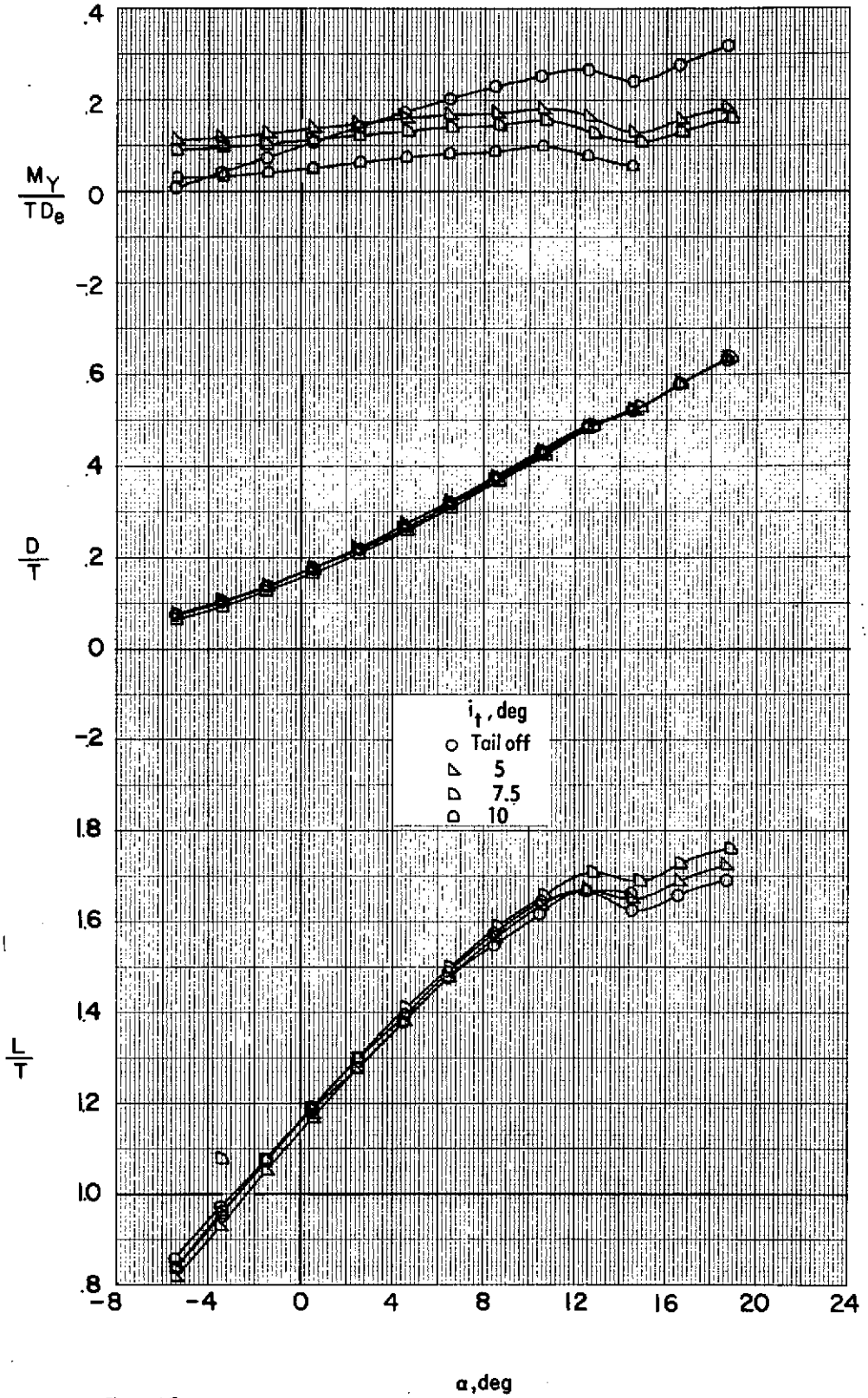

Figure 58. - Effect of tail incidence on longitudinal aerodynamic characteristics of the VTOL transition configuration. $\delta_L = 40°$ $\delta_{LC} = 70°$ $\delta_f = 40°$ $\delta_e = 0°$

$V_e = 0.38$

$q_\infty = 1230$ N/m^2 (25.7 lb/ft^2)

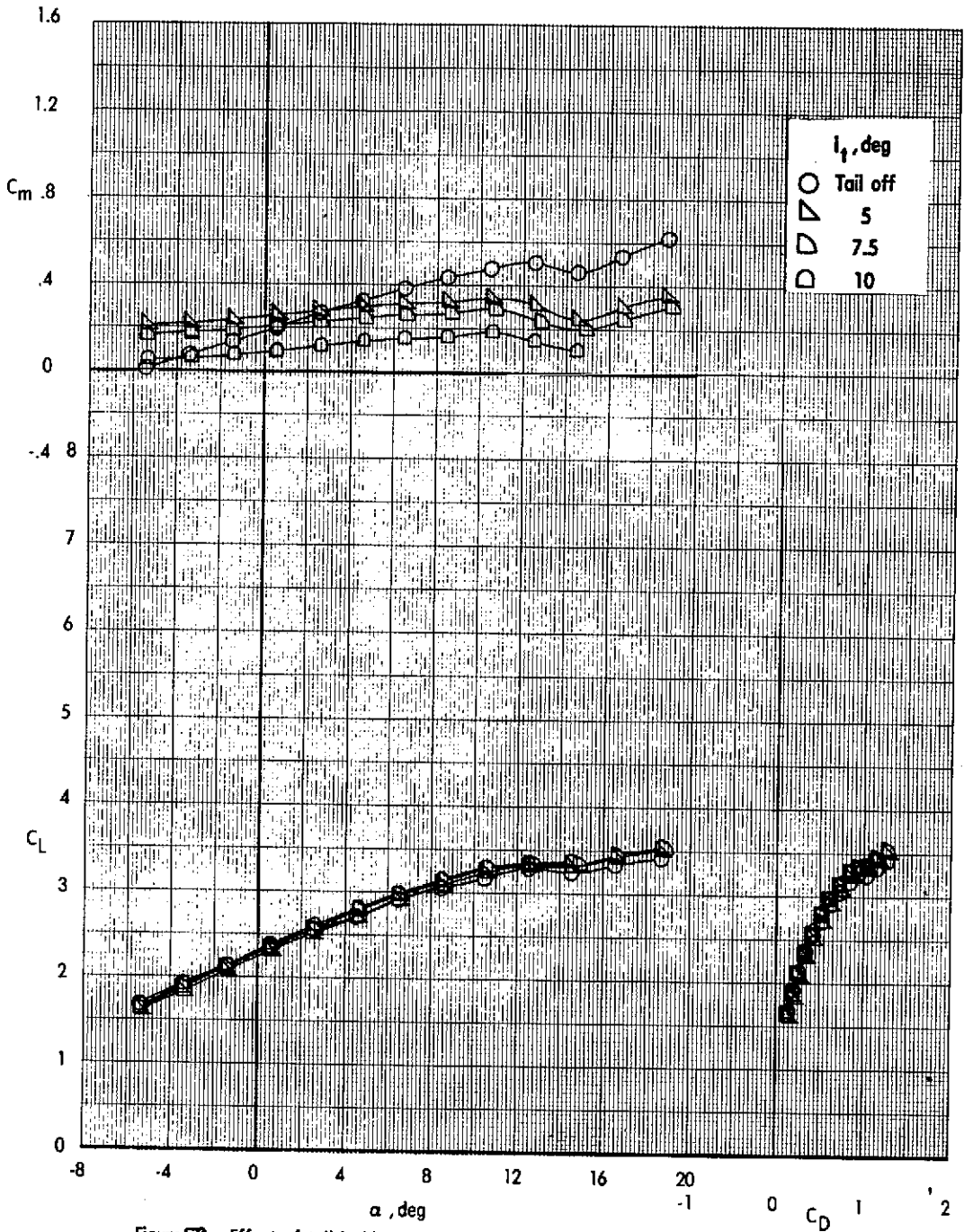

Figure 59 - Effect of tail incidence on longitudinal aerodynamic characteristics of the VTOL transition configuration. $\delta_L = 40°$ $\delta_{LC} = 70°$ $\delta_f = 40°$ $\delta_e = 0°$

$C_\mu = 2.0$ $q_\infty = 1230$ N/m² (25.7 lb/ft²)

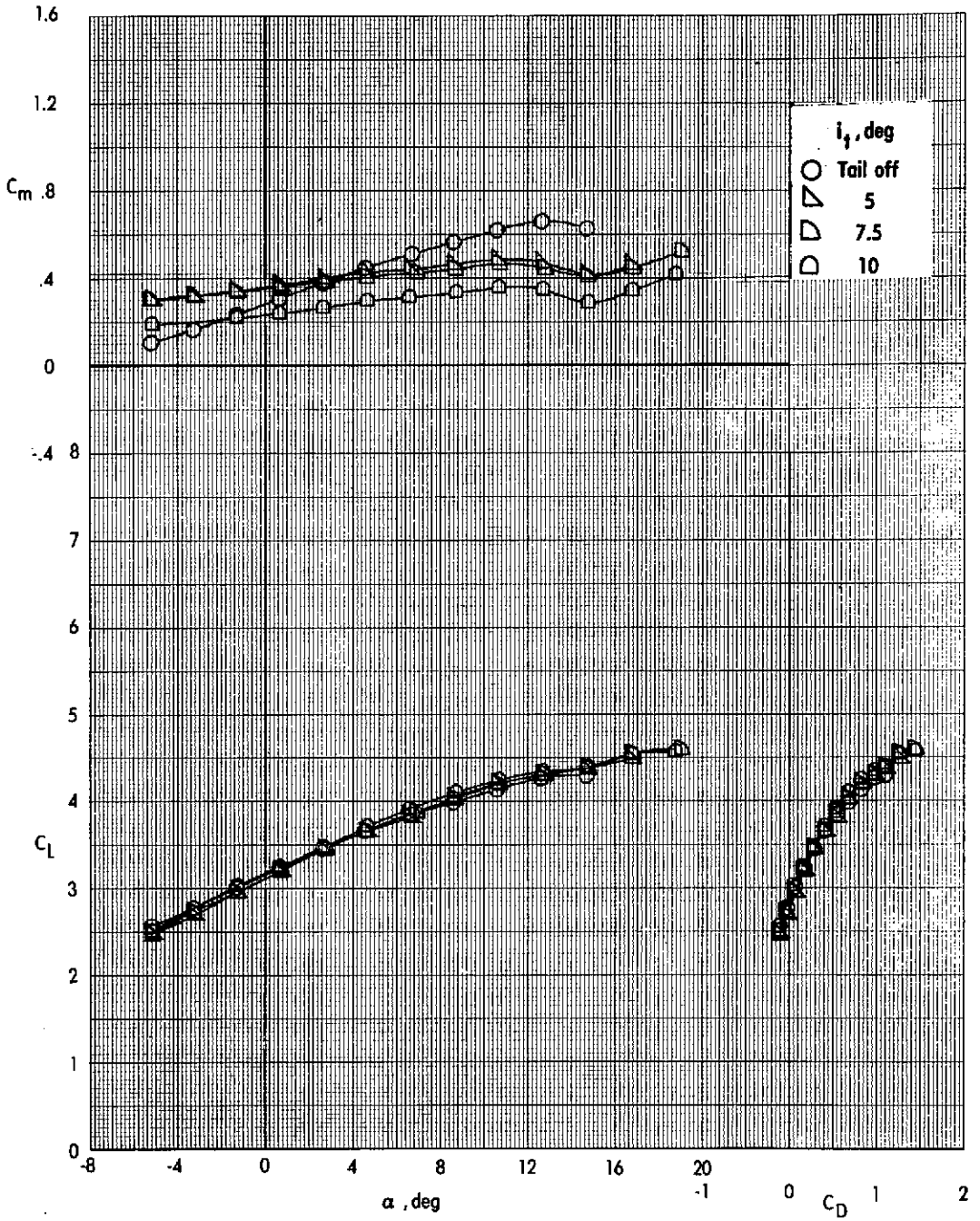

Figure 60. - Effect of tail incidence on longitudinal aerodynamic characteristics of the VTOL transition configuration. $\delta_L = 40°$ $\delta_{LC} = 70°$ $\delta_f = 40°$ $\delta_e = 0°$

$C_{\mu} = 2.9$ $q_\infty = 1230\ N/m^2$ (25.7 lb/ft^2)

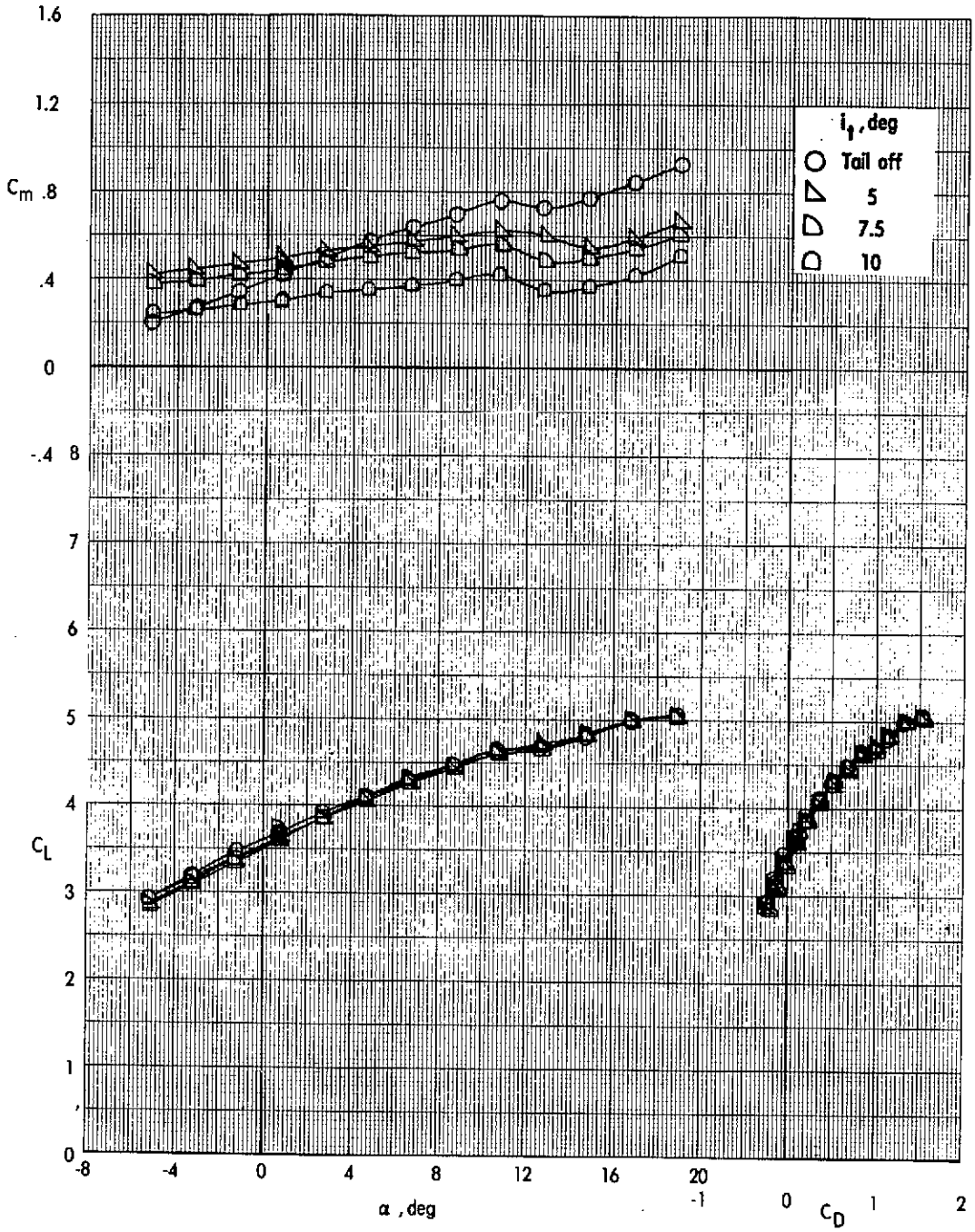

Figure 61. - Effect of tail incidence on longitudinal aerodynamic characteristics of the VTOL transition configuration. $\delta_L = 40°$ $\delta_{LC} = 70°$ $\delta_f = 40°$ $\delta_e = 0°$

$C_\mu = 3.4$ $q_\infty = 709\ N/m^2 (14.8\ lb/ft^2)$

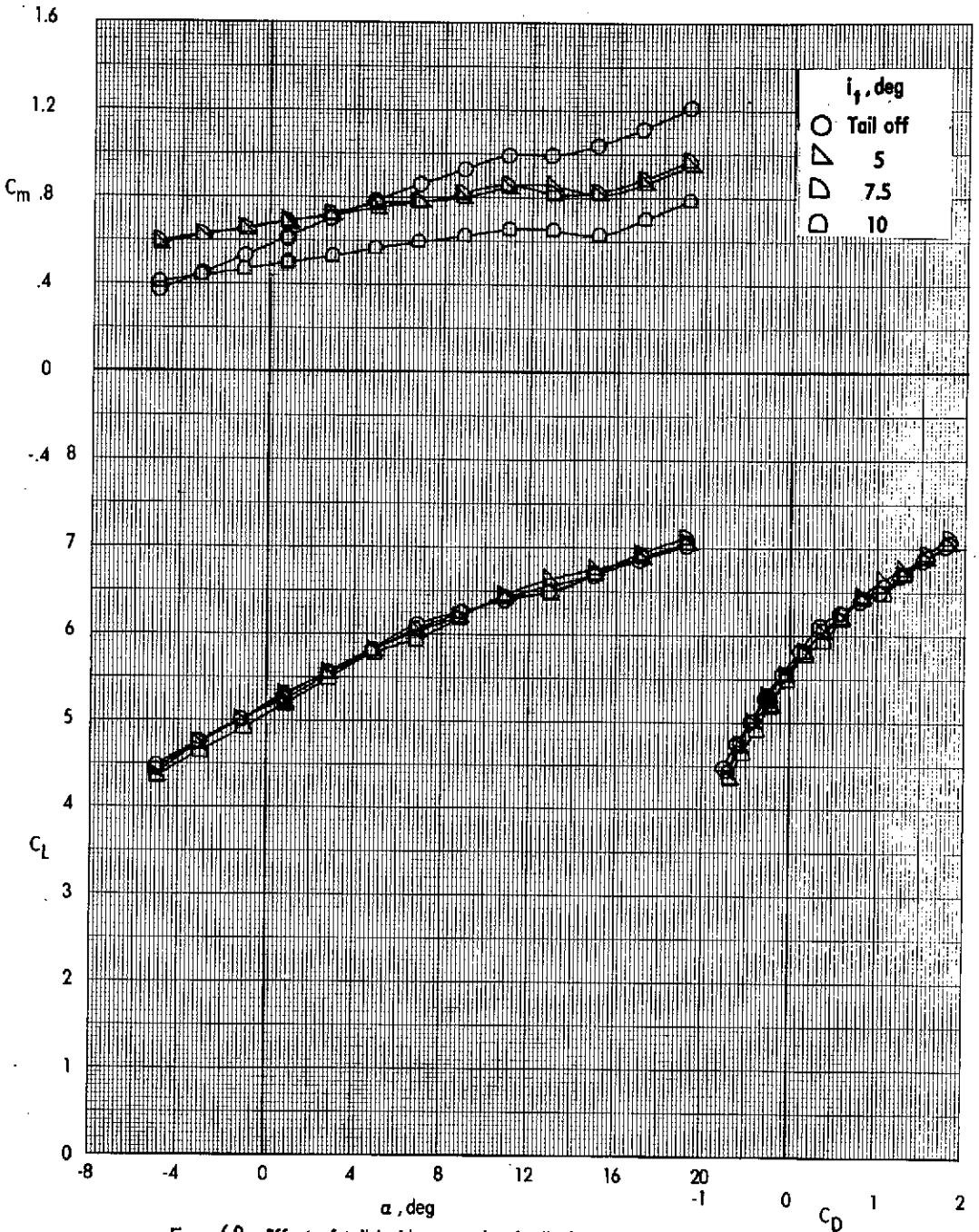

Figure 62 - Effect of tail incidence on longitudinal aerodynamic characteristics of the VTOL transition configuration. $\delta_L = 40°$ $\delta_{LC} = 70°$ $\delta_f = 40°$ $\delta_e = 0°$

$C_{\mu} = 5.1$ $q_\infty = 709\ N/m^2$ $(14.8\ lb/ft^2)$

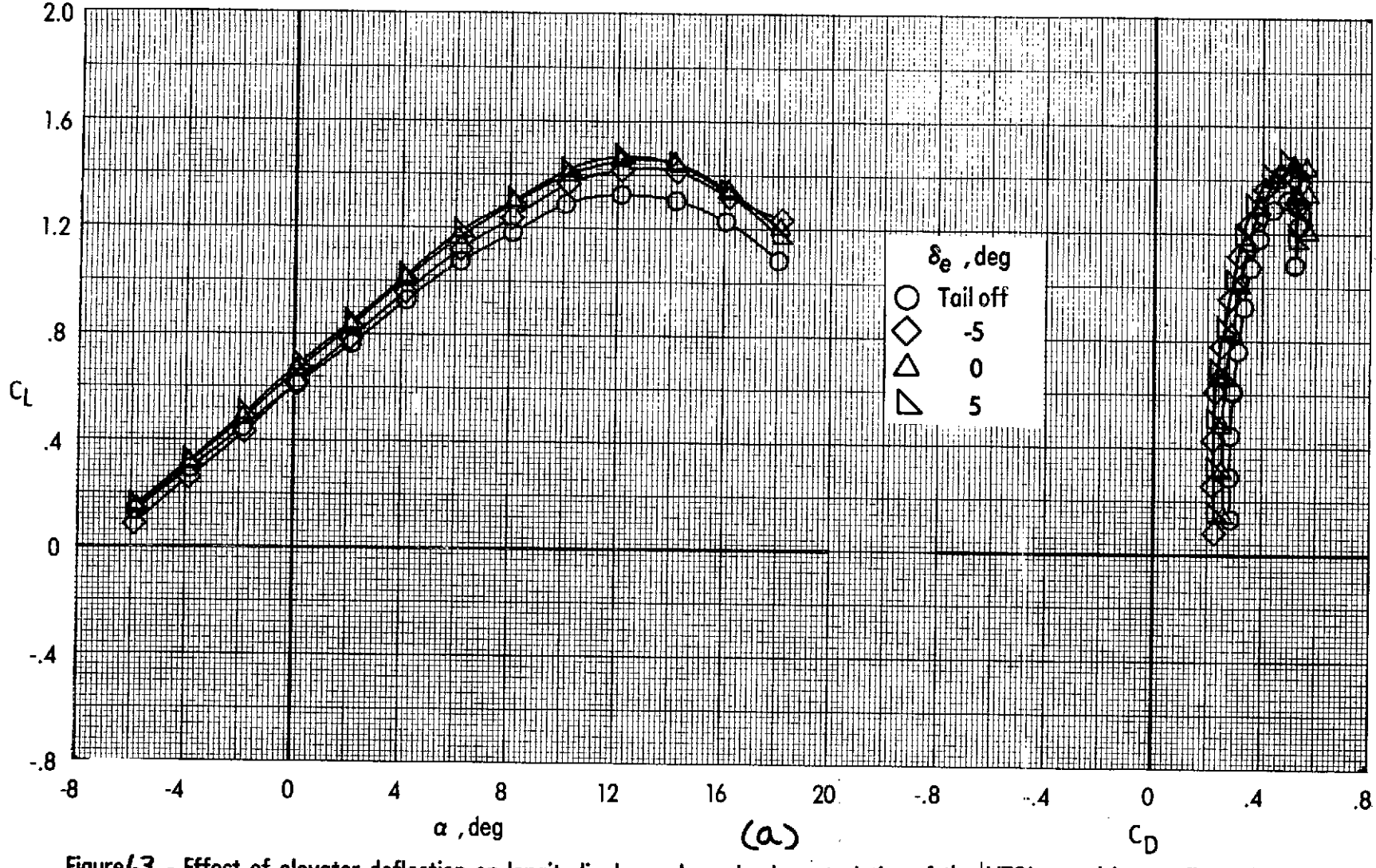

Figure 63. - Effect of elevator deflection on longitudinal aerodynamic characteristics of the VTOL transition configuration.

$\delta_L = 40°$ $\delta_{LC} = 70°$ $\delta_f = 40°$ $i_t = 7.5°$ $C_\mu = 0$ $q_\infty = 728\ N/m^2$ (15.2 lb/ft^2)

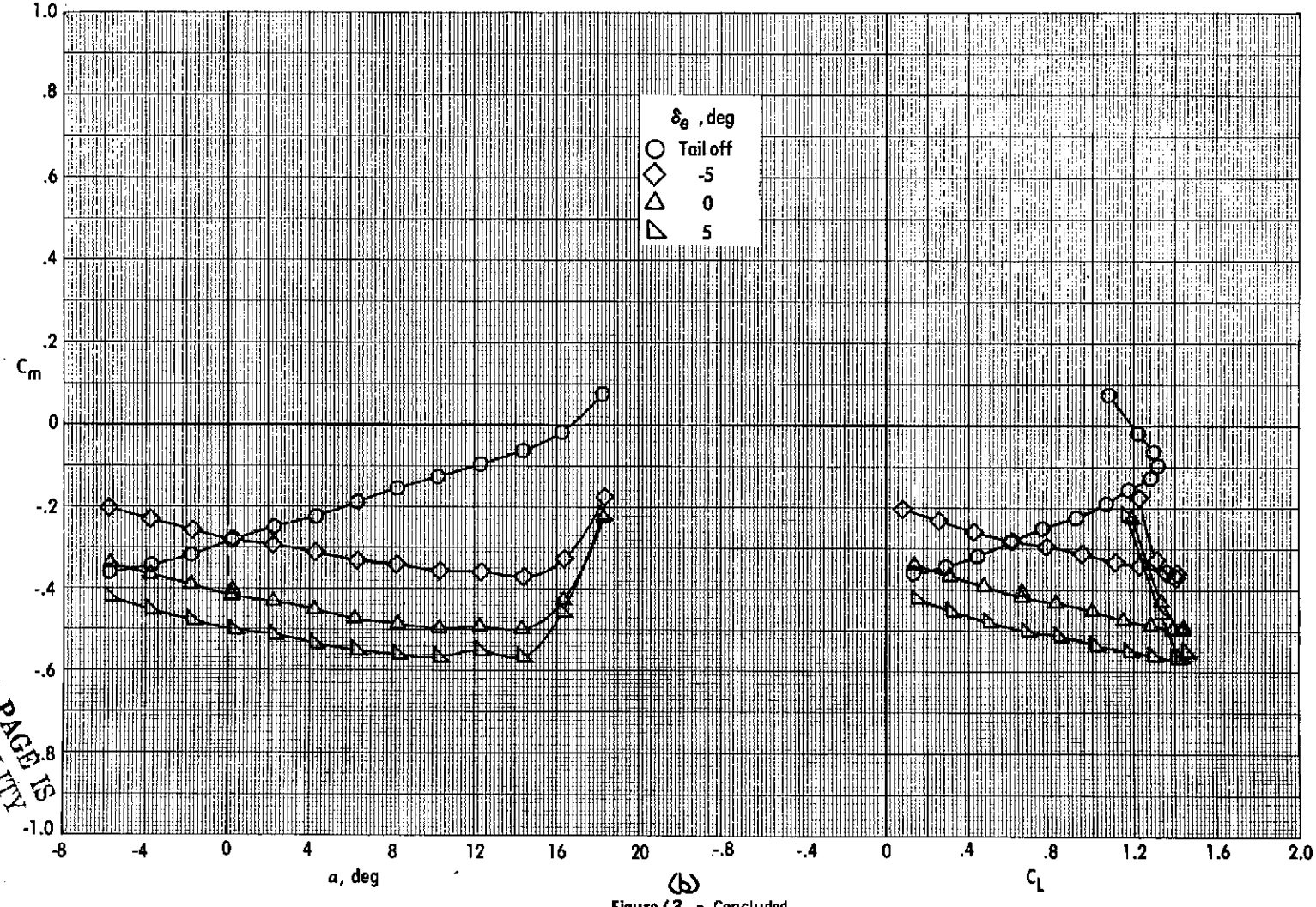

(b)

Figure 63. - Concluded.

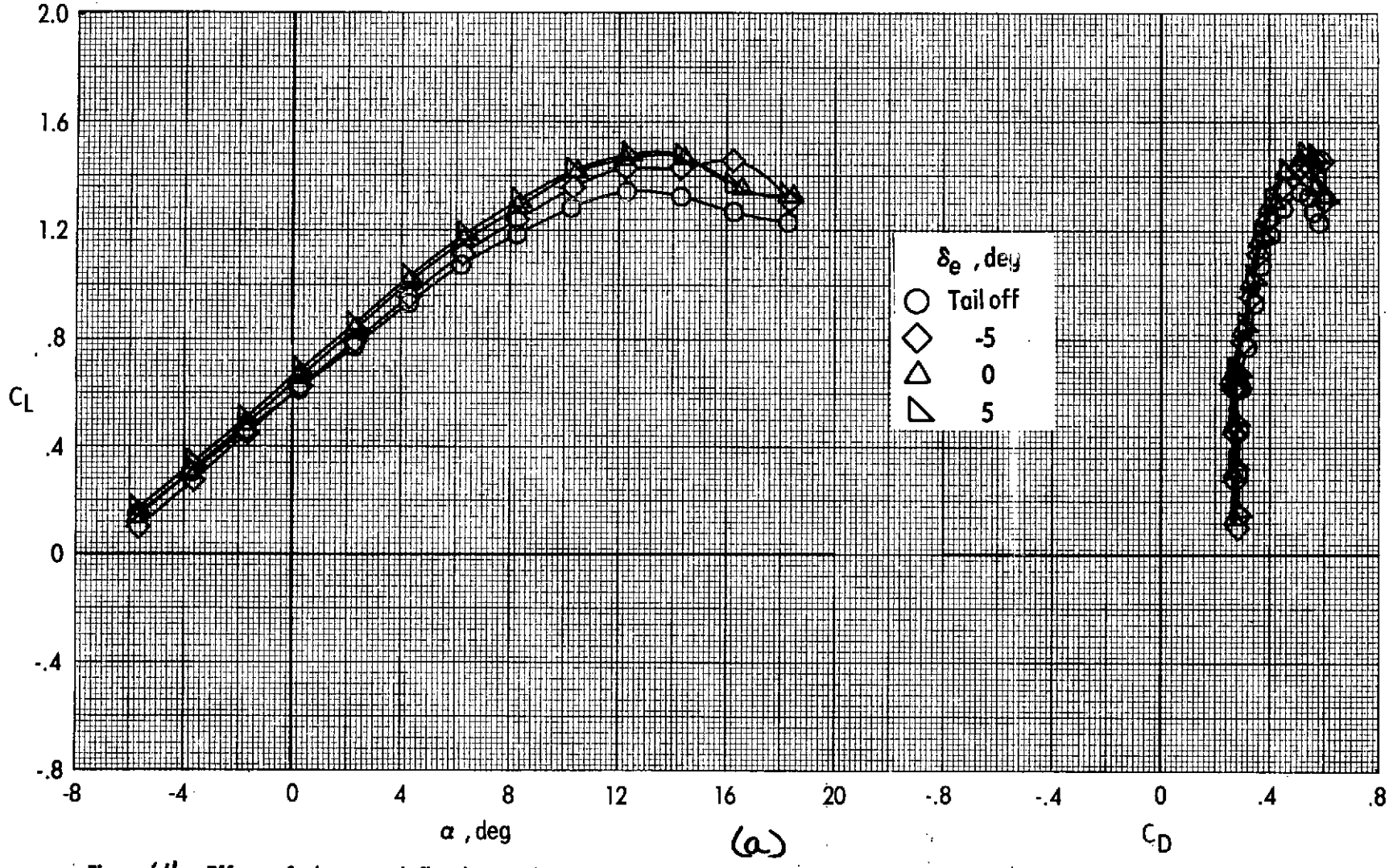

Figure 64. - Effect of elevator deflection on longitudinal aerodynamic characteristics of the VTOL transition configuration.

$\delta_L = 40°$ $\delta_{LC} = 70°$ $\delta_f = 40°$ $i_t = 7.5°$ $C_\mu = 0$ $q_\infty = 1245\ N/m^2$ $(26.0\ lb/ft^2)$

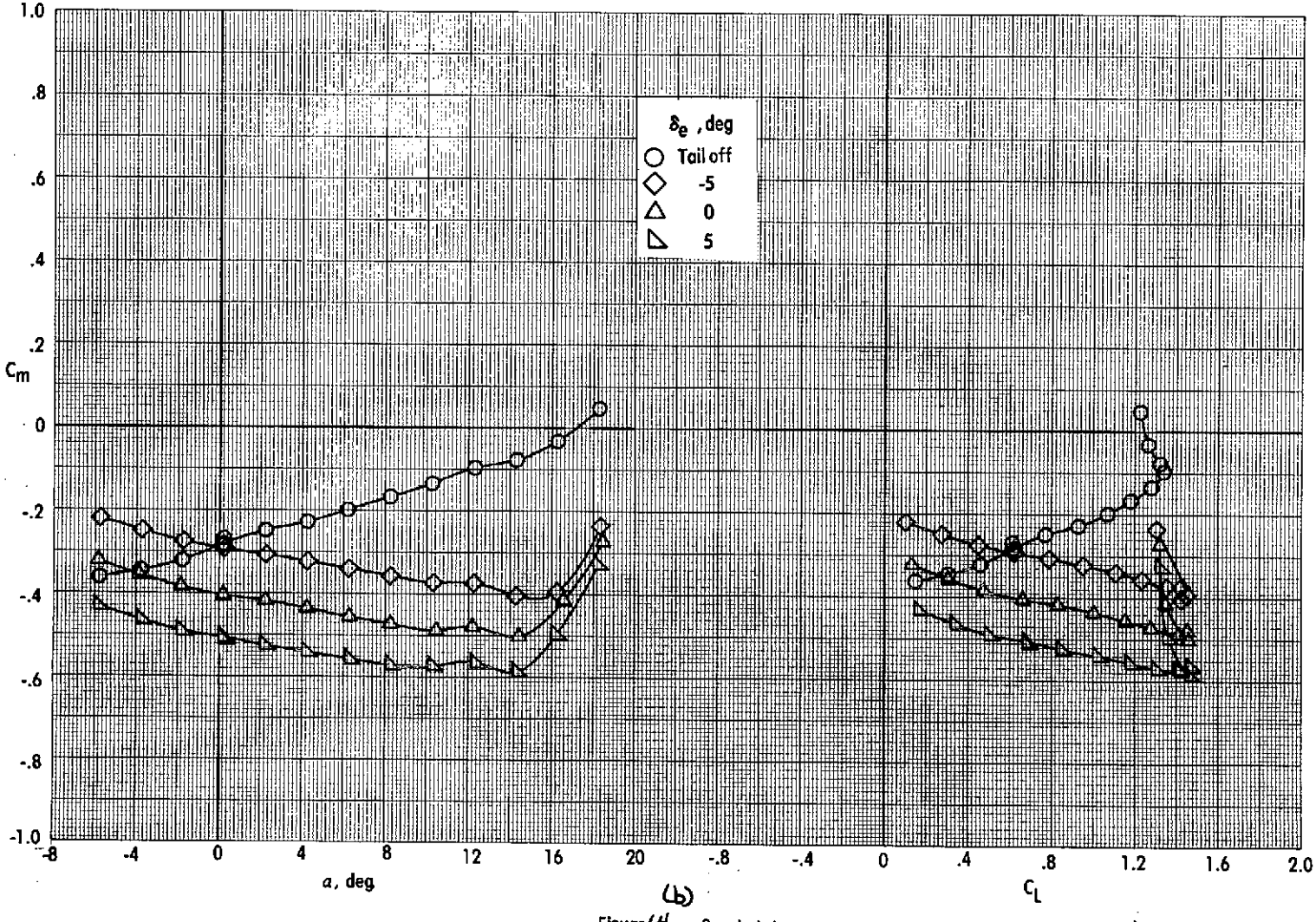

Figure 4. - Concluded.

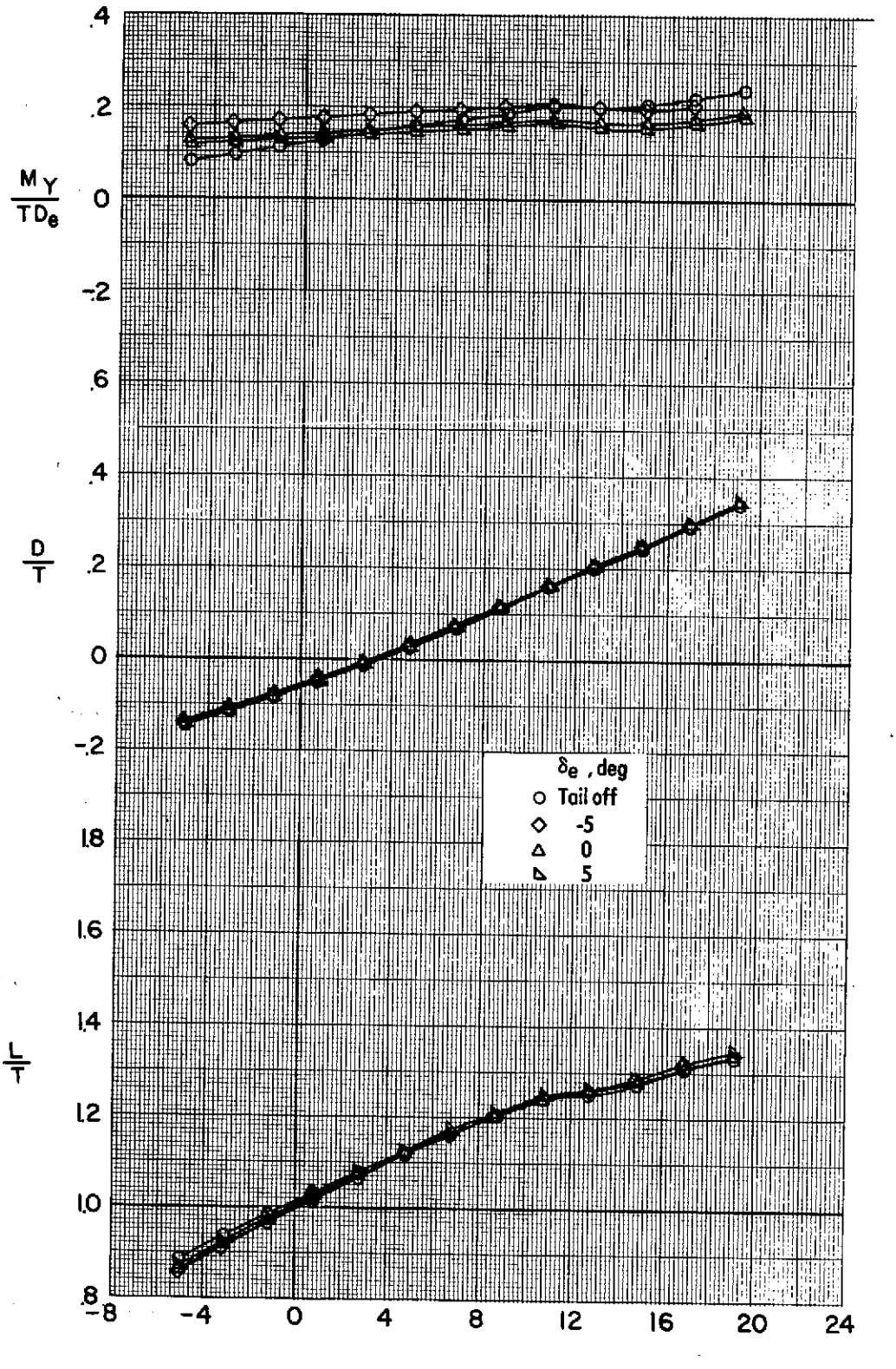

Figure 65. - Effect of elevator deflection on longitudinal aerodynamic characteristics of the VTOL transition configuration. $\delta_L = 40°$ $\delta_{LC} = 70°$ $\delta_f = 40°$ $i_t = 7.5°$ $V_e = 0.24$ $q_\infty = 709\ N/m^2 (14.8\ lb/ft^2)$

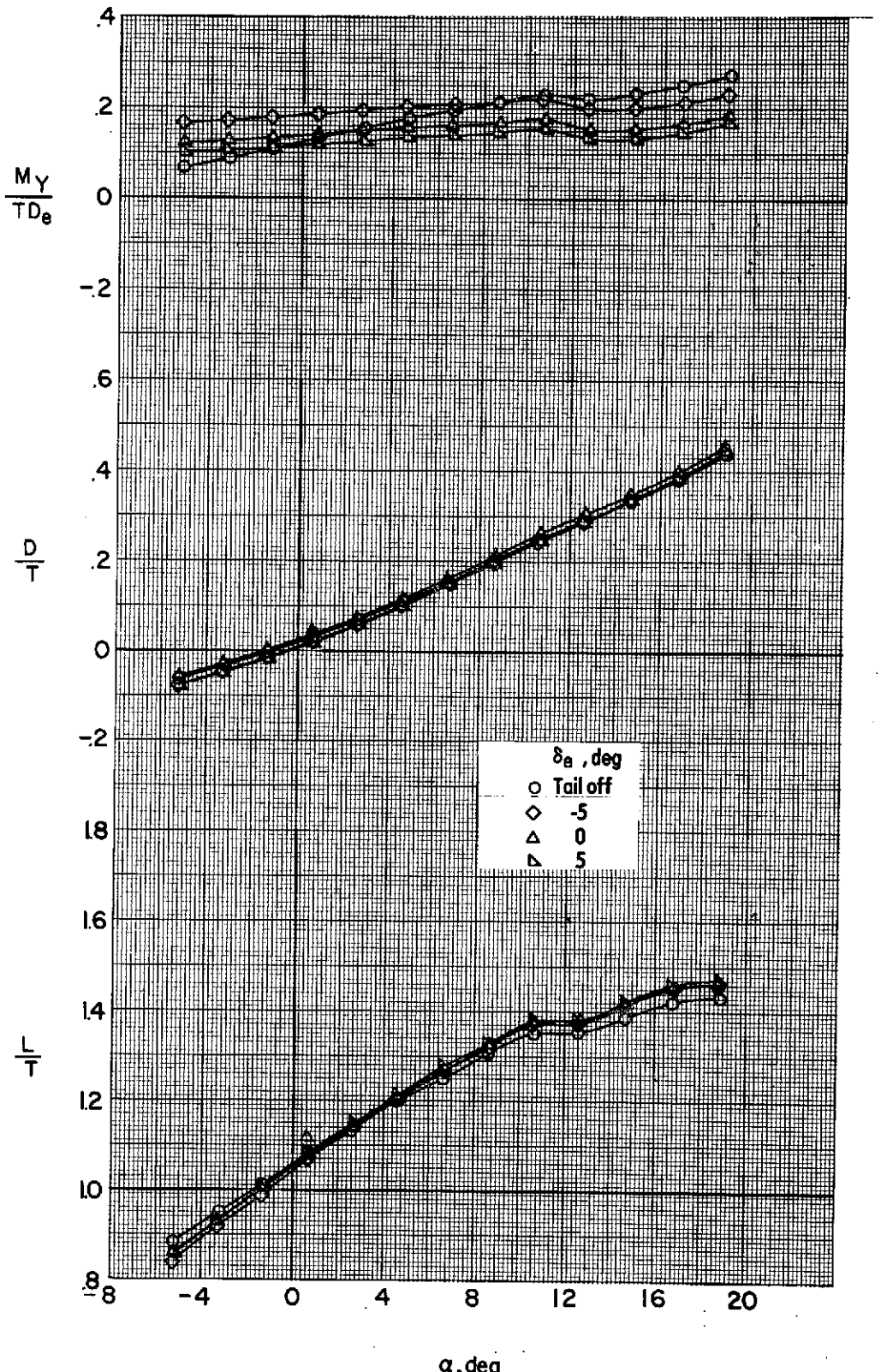

Figure 6a - Effect of elevator deflection on longitudinal aerodynamic characteristics of the VTOL transition configuration. $\delta_L = 40°$ $\delta_{LC} = 70°$ $\delta_f = 40°$ $i_t = 7.5°$

$V_e = 0.29$ $q_\infty = 709\ N/m^2\ (14.8\ lb/ft^2)$

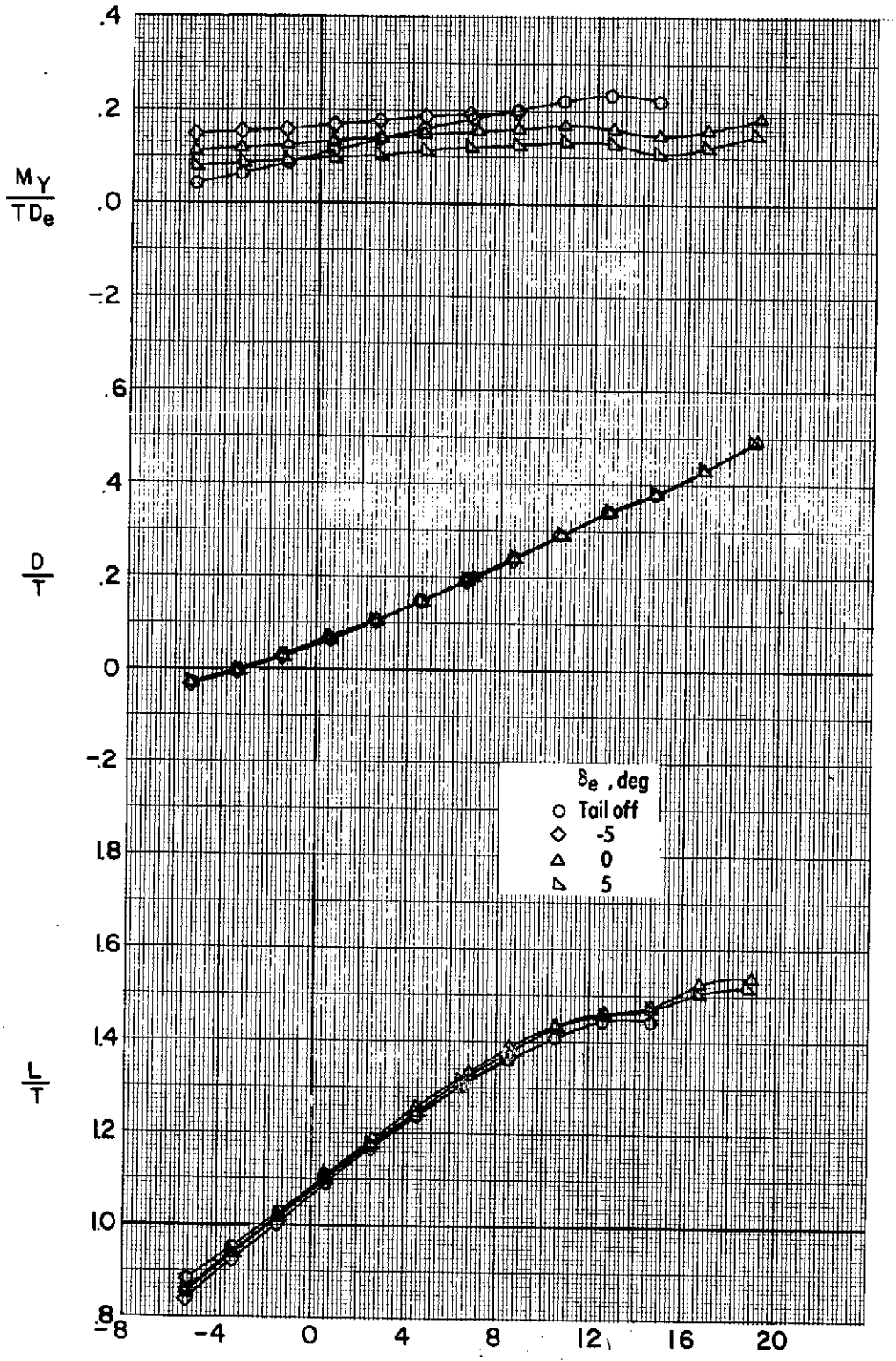

Figure 67. - Effect of elevator deflection on longitudinal aerodynamic characteristics of the VTOL transition configuration. $\delta_L = 40°$ $\delta_{LC} = 70°$ $\delta_f = 40°$ $i_t = 7.5°$

$V_e = 0.31$ $q_\infty = 1230\ N/m^2 (25.7\ lb/ft^2)$

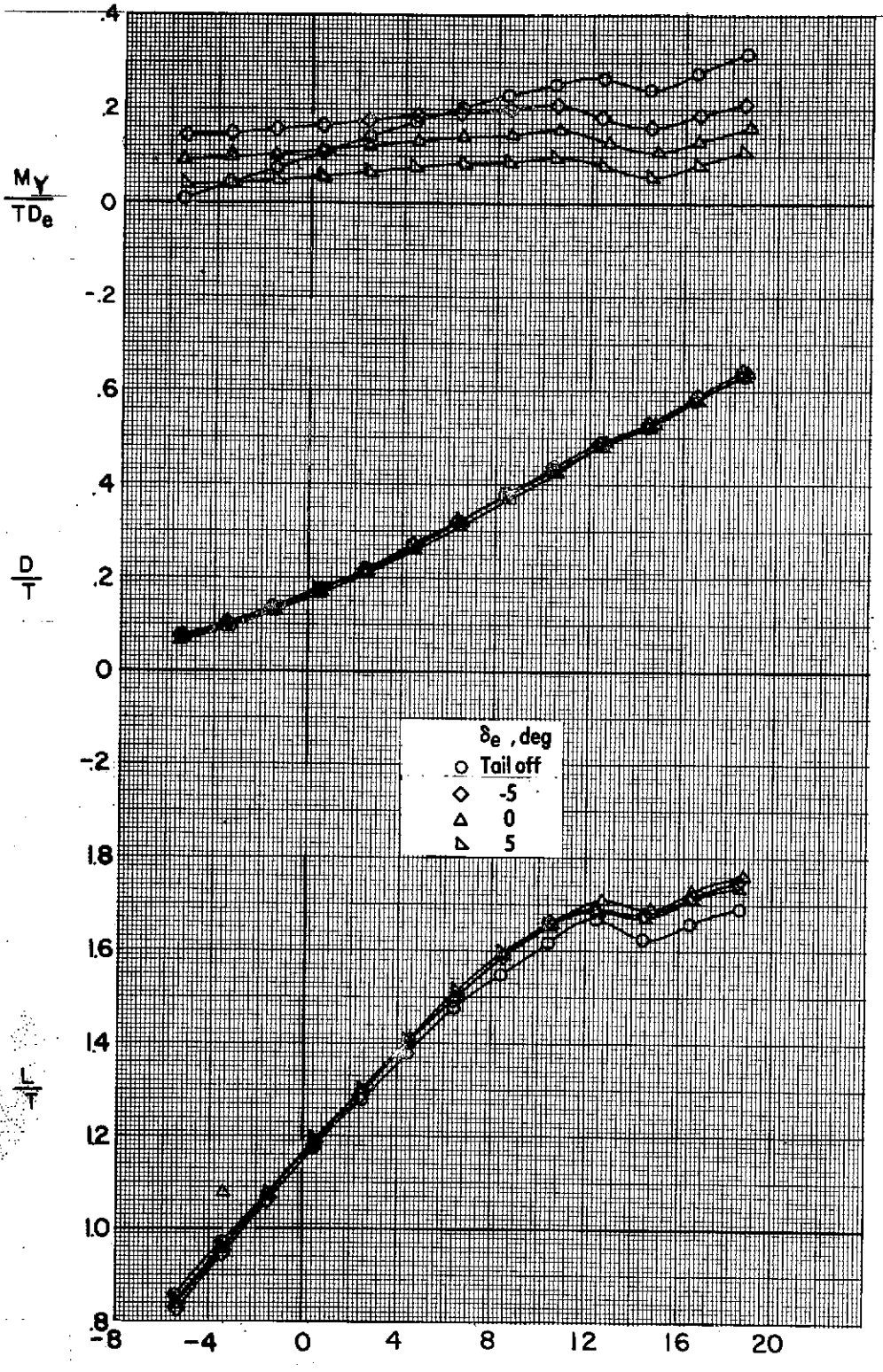

Figure 68 - Effect of elevator deflection on longitudinal aerodynamic characteristics of the VTOL transition configuration. $\delta_L = 40°$ $\delta_{LC} = 70°$ $\delta_f = 40°$ $i_t = 7.5°$

$V_e = 0.38$ $q_\infty = 1230\ N/m^2$ (25.7 lb/ft²)

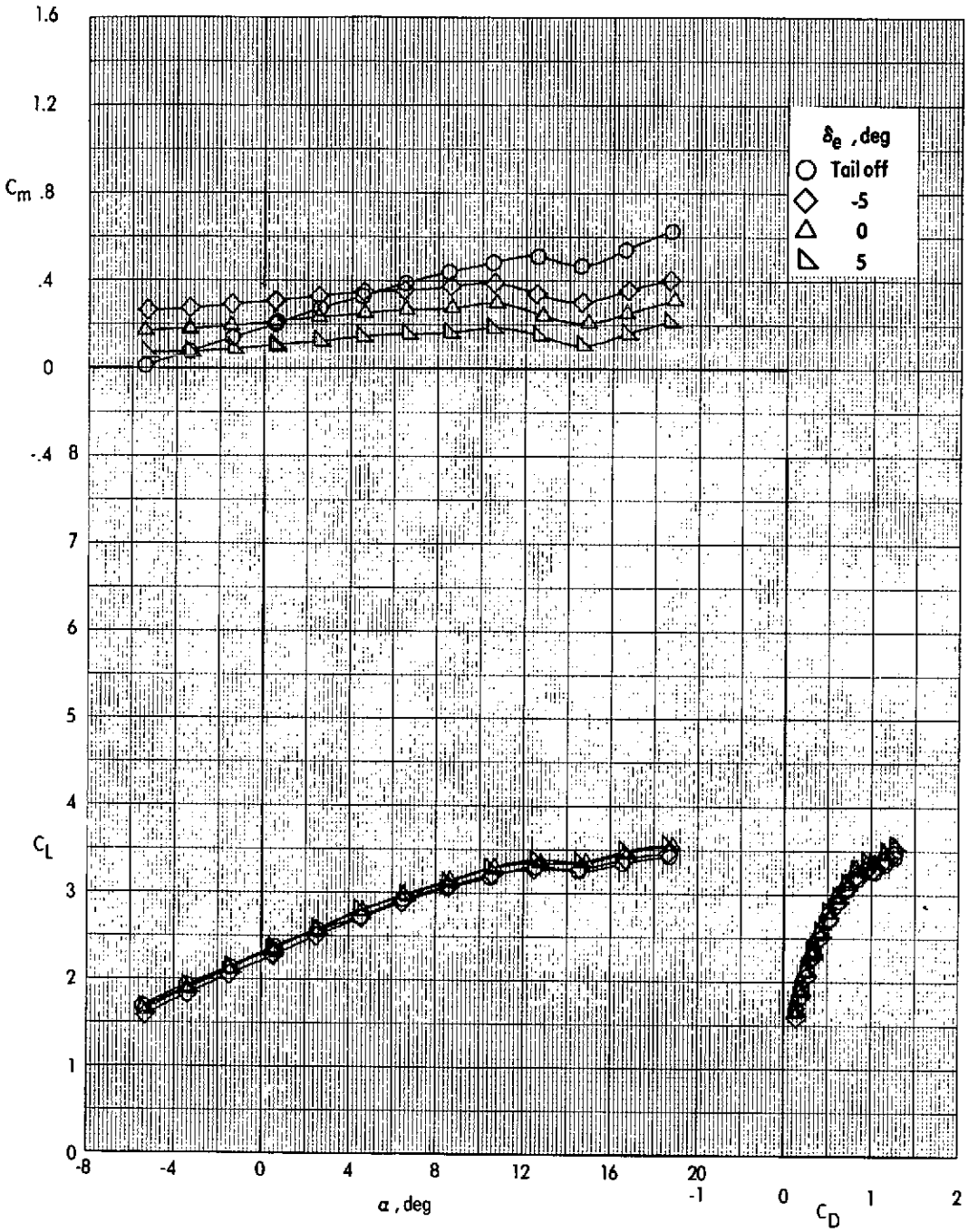

Figure 69. - Effect of elevator deflection on longitudinal aerodynamic characteristics of the VTOL transition configuration. $\delta_l = 40°$ $\delta_{LC} = 70°$ $\delta_f = 40°$ $i_t = 7.5°$

$C_\mu = 2.0$ $q_\infty = 1230$ N/m² (25.7 lb/ft²)

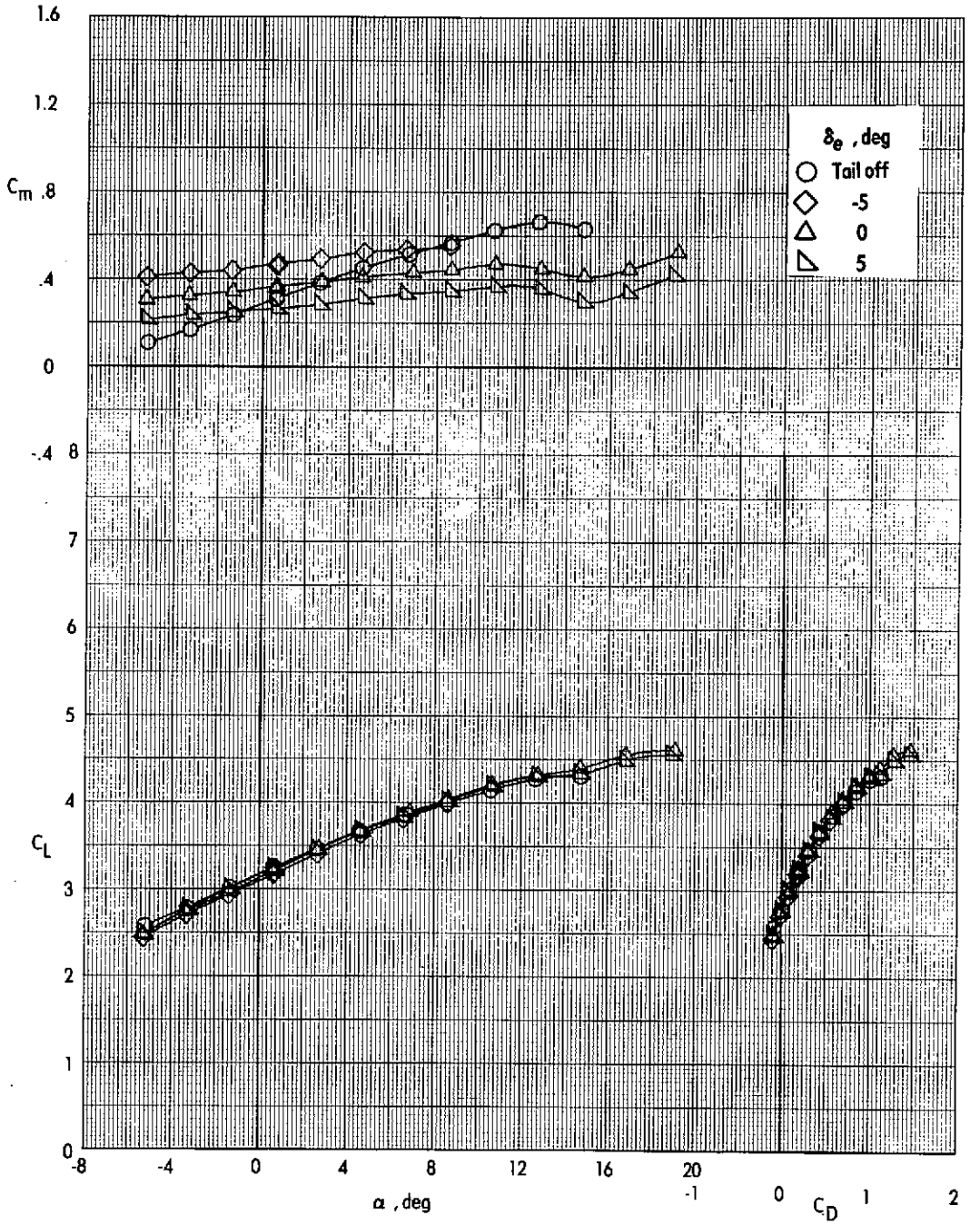

Figure 70. - Effect of elevator deflection on longitudinal aerodynamic characteristics of the VTOL transition configuration. $\delta_L = 40°$ $\delta_{LC} = 70°$ $\delta_f = 40°$ $i_t = 7.5°$

$C_\mu = 2.9$ $q_\infty = 1230\ N/m^2$ $(25.7\ lb/ft^2)$

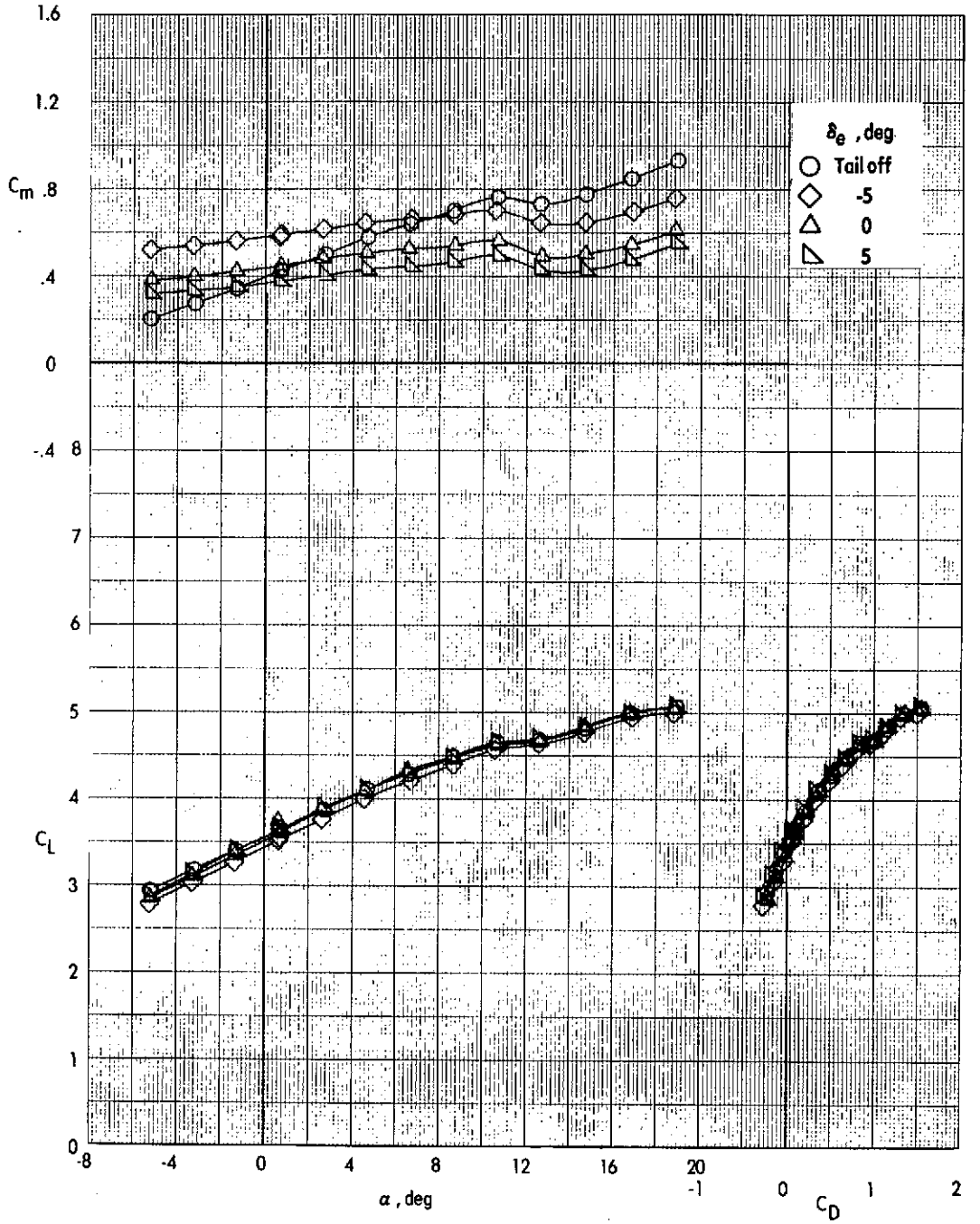

Figure 71. - Effect of elevator deflection on longitudinal aerodynamic characteristics of the VTOL transition configuration. $\delta_L = 40°$ $\delta_{LC} = 70°$ $\delta_f = 40°$ $i_t = 7.5°$

$C_\mu = 3.4$ $q_\infty = 709\ N/m^2$ $(14.8\ lb/ft^2)$

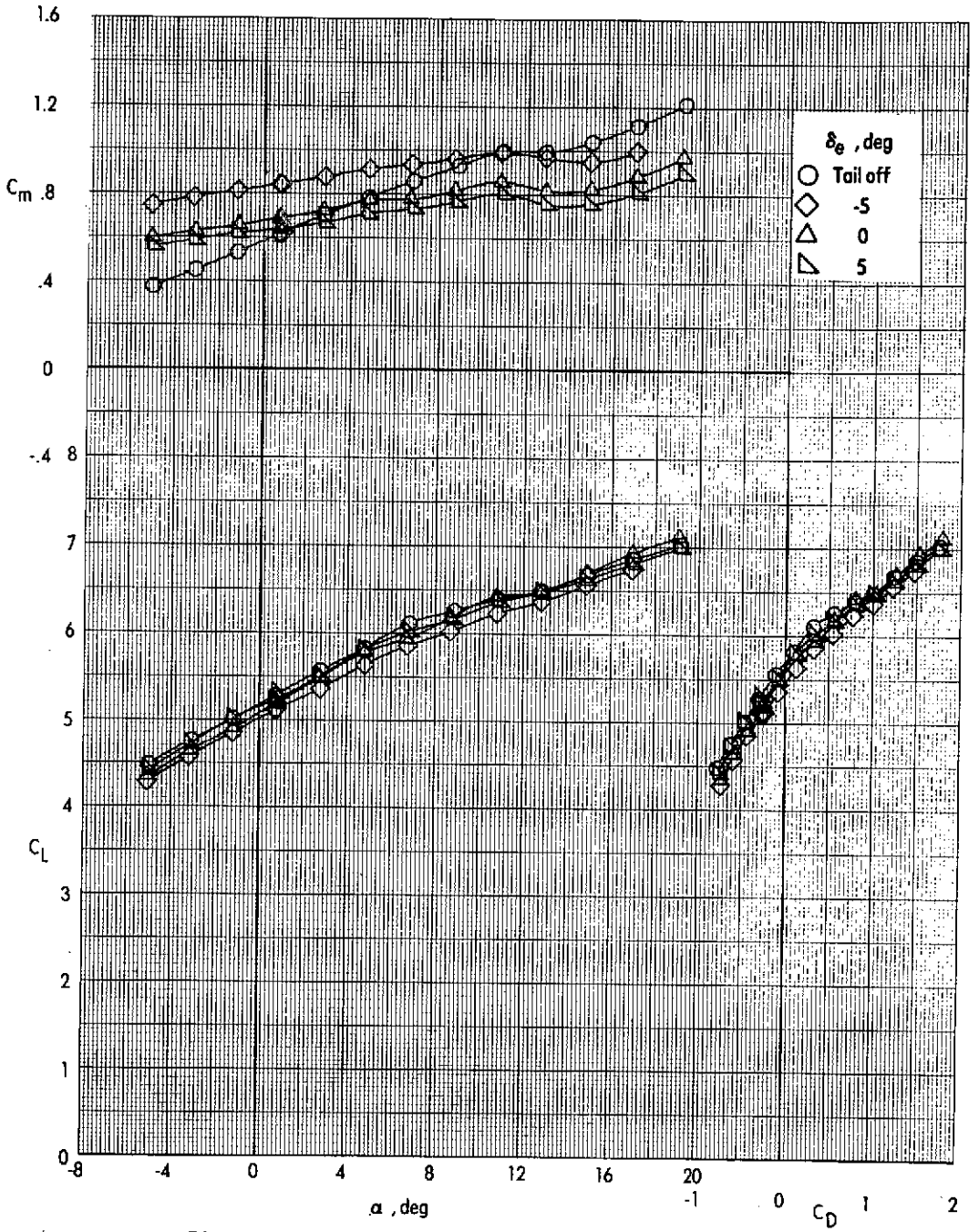

Figure 72 - Effect of elevator deflection on longitudinal aerodynamic characteristics of the VTOL transition configuration. $\delta_L = 40°$ $\delta_{LC} = 70°$ $\delta_f = 40°$ $i_t = 7.5°$

$C_\mu = 5.1$ $q_\infty = 709$ N/m² (14.8 lb/ft²)

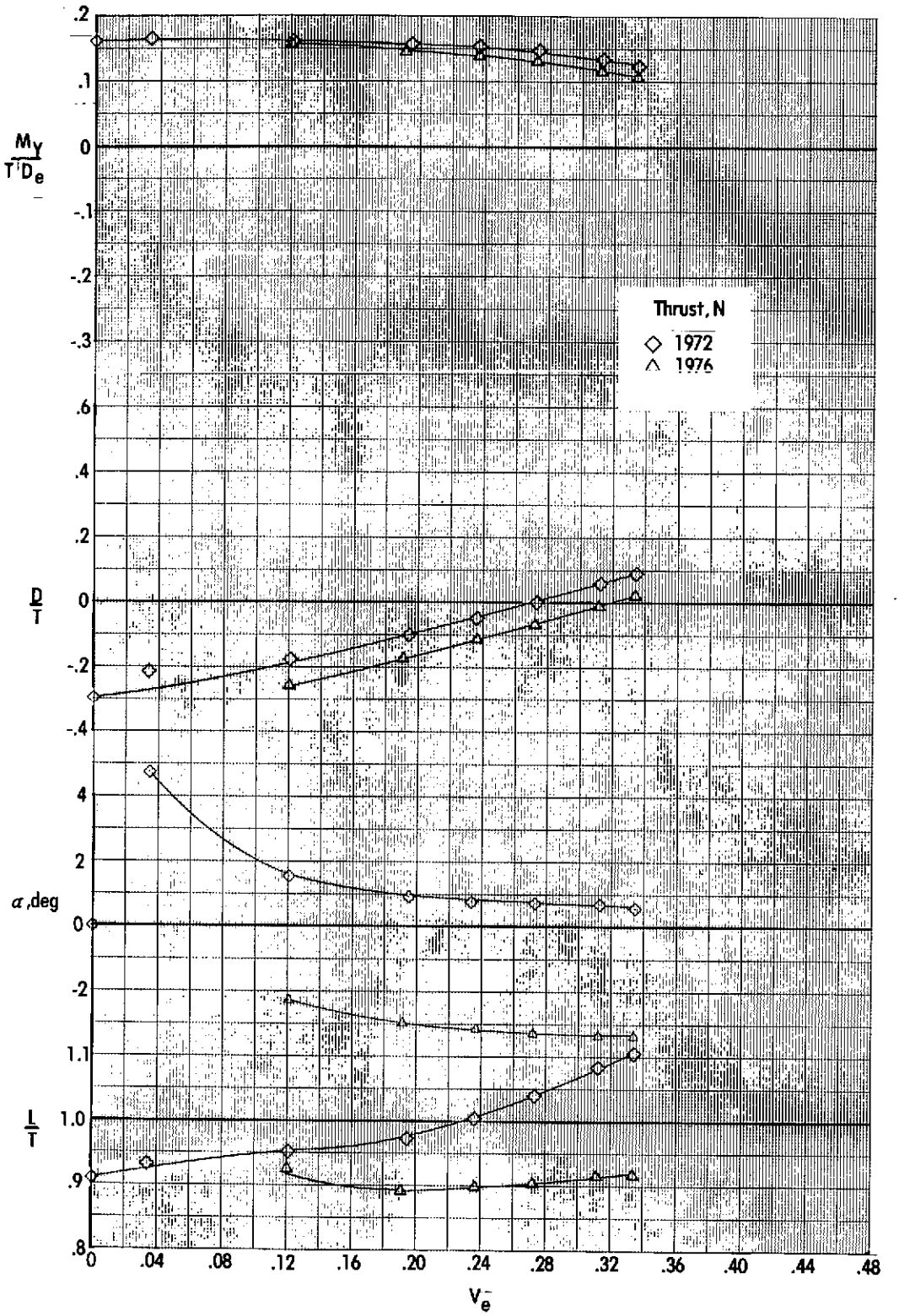

Figure 73. Effect of velocity ratio on longitudinal aerodynamic characteristics of the VTOL transition configuration.

$\delta_L = 40°$ $\delta_{LC} = 70°$ $\delta_f = 40°$ $i_t = 7.5°$ $\delta_e = 0°$

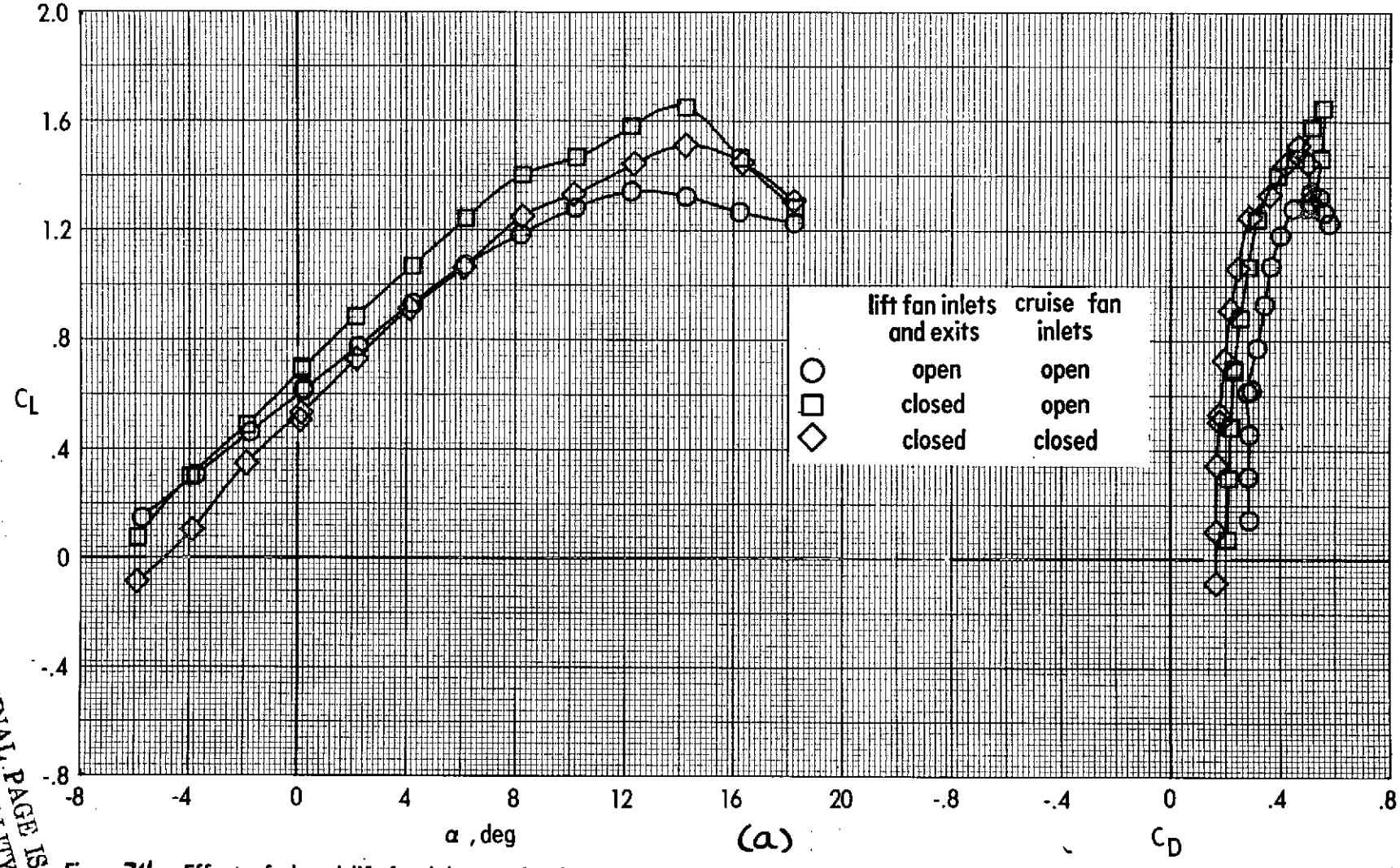

Figure 74. - Effect of closed lift-fan inlets and exits on power-off longitudinal aerodynamics of the VTOL transition configuration.

$\delta_L = 40°$ $\delta_{LC} = 70°$ $\delta_f = 40°$ tail off $C_\mu = 0$ $q_\infty = 1245\ N/m^2$ (26.0 lb/ft²)

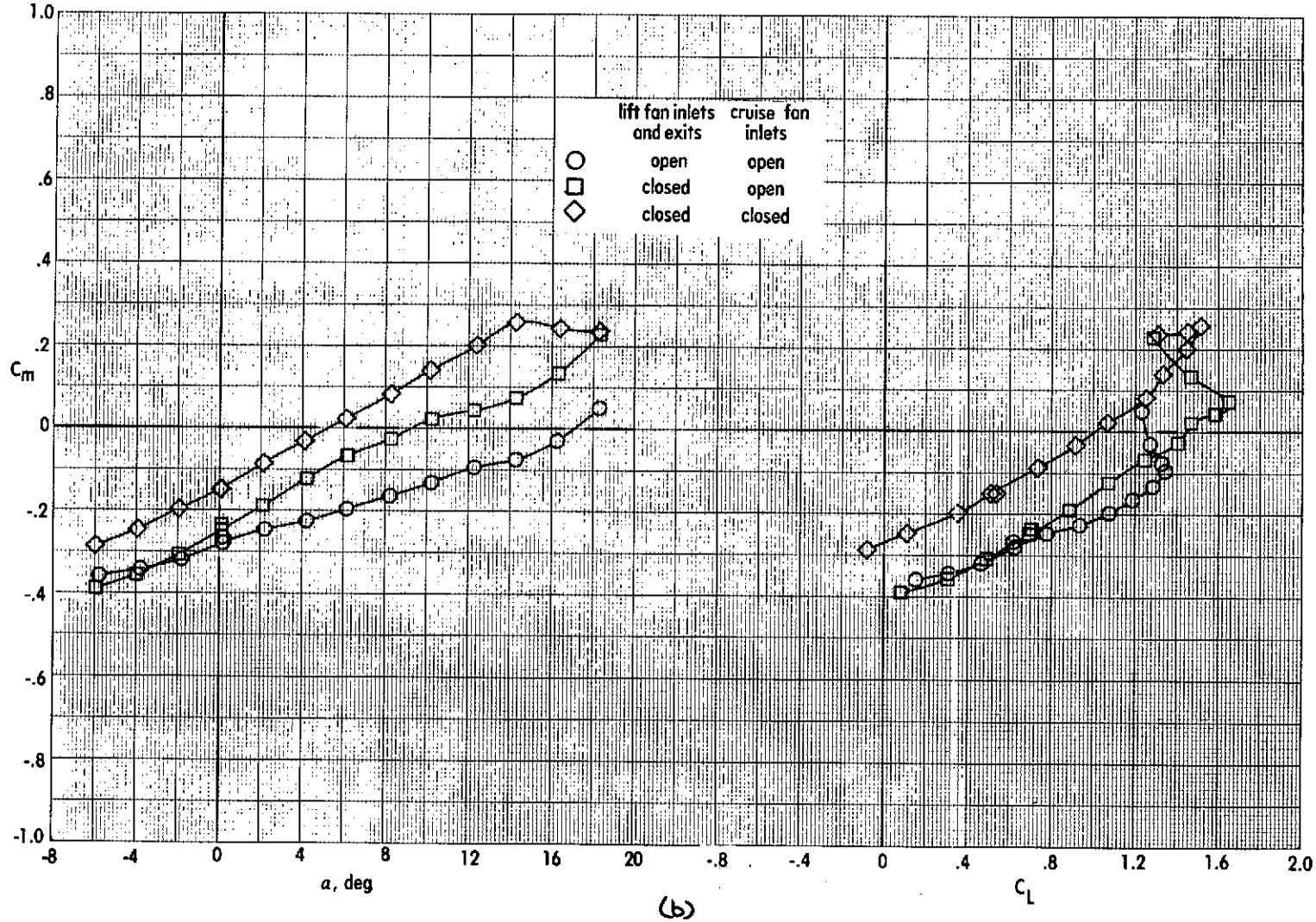

(b)

Figure 74. - Concluded.

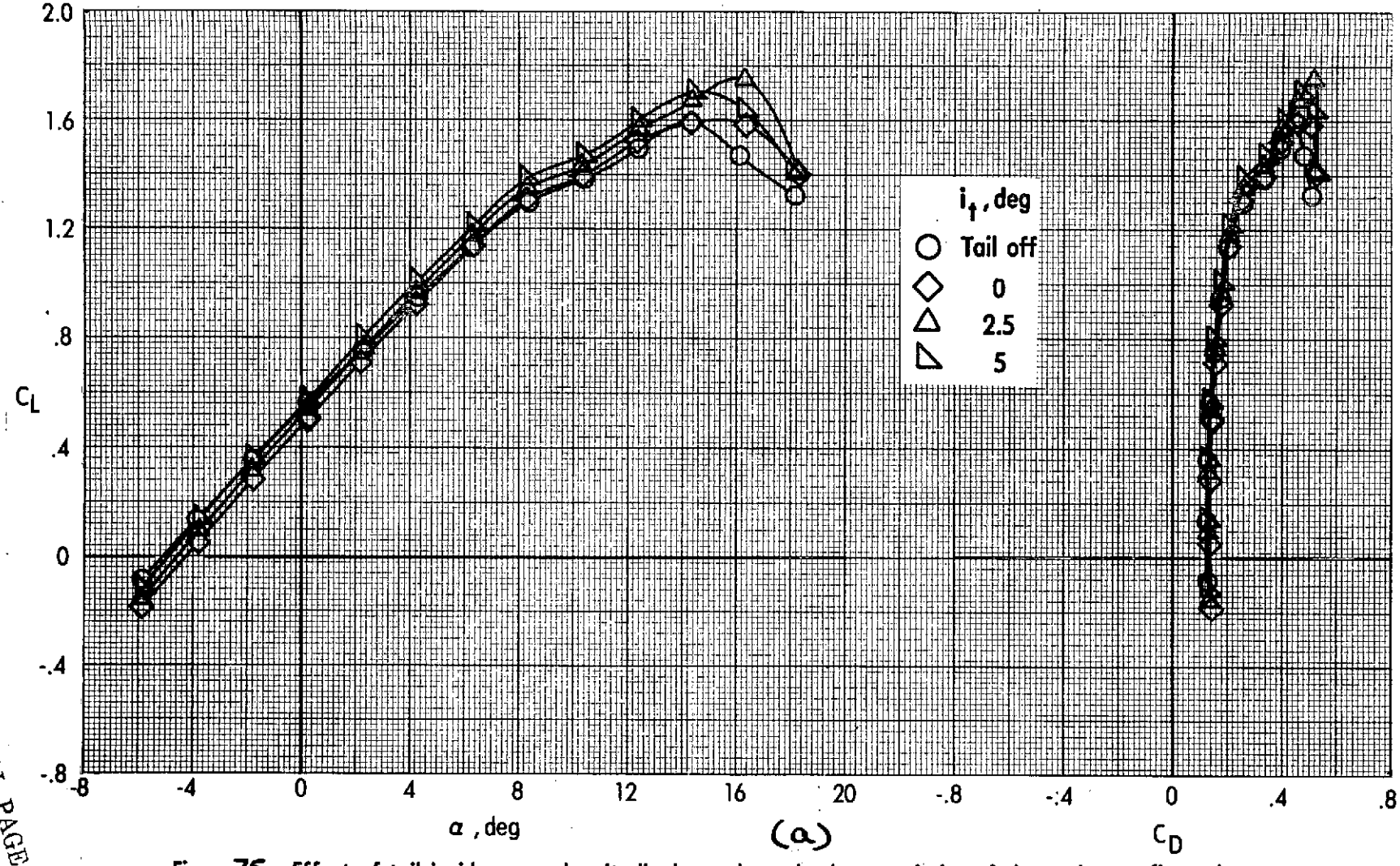

Figure 75. - Effect of tail incidence on longitudinal aerodynamic characteristics of the cruise configuration.

δ_L = closed $\delta_{LC} = 0°$ $\delta_f = 40°$ $\delta_e = 0°$ $C_{\mu} = 0$ $q_\infty = 2672\ N/m^2$ (55.8 lb/ft^2)

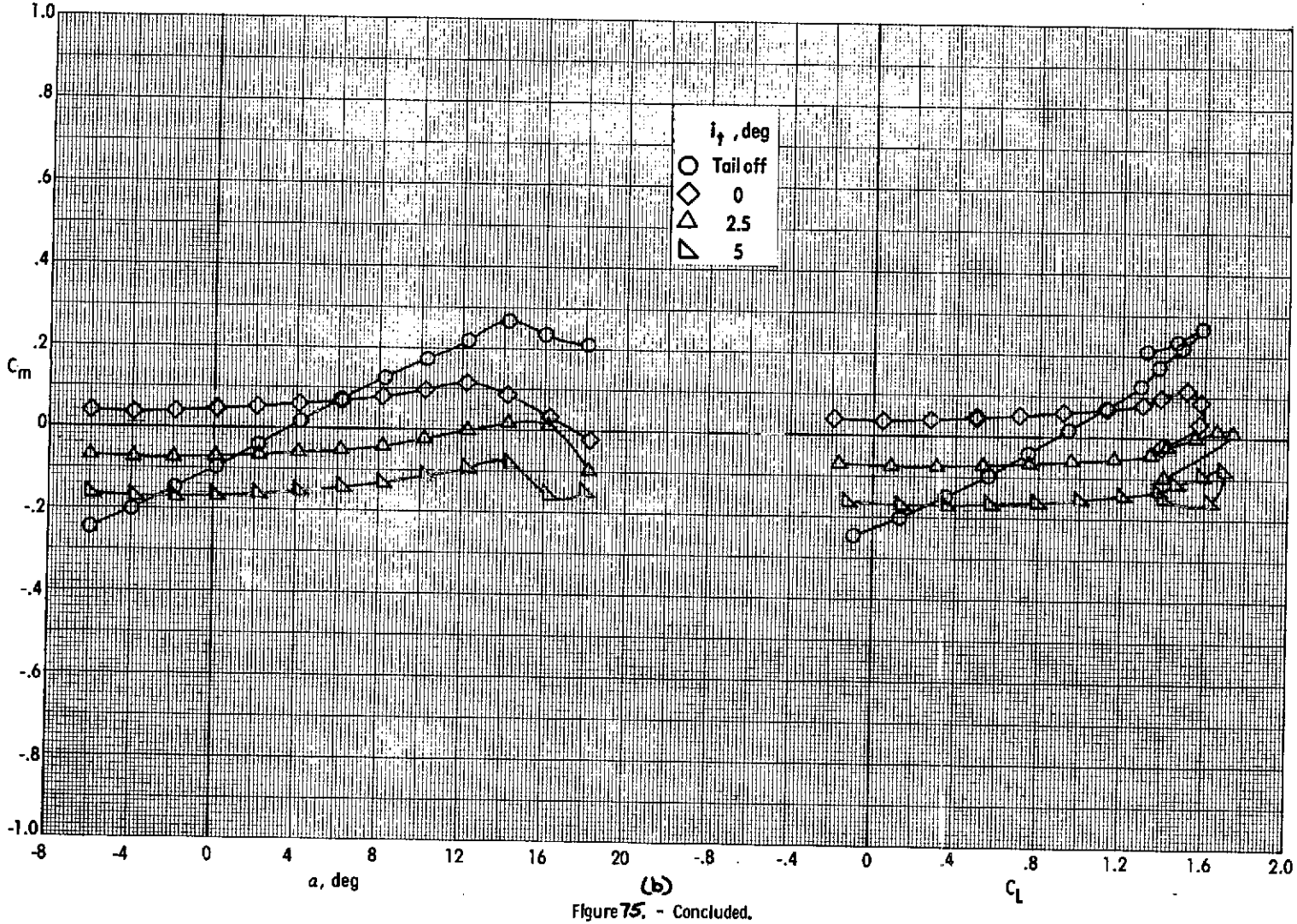

Figure 75. - Concluded.

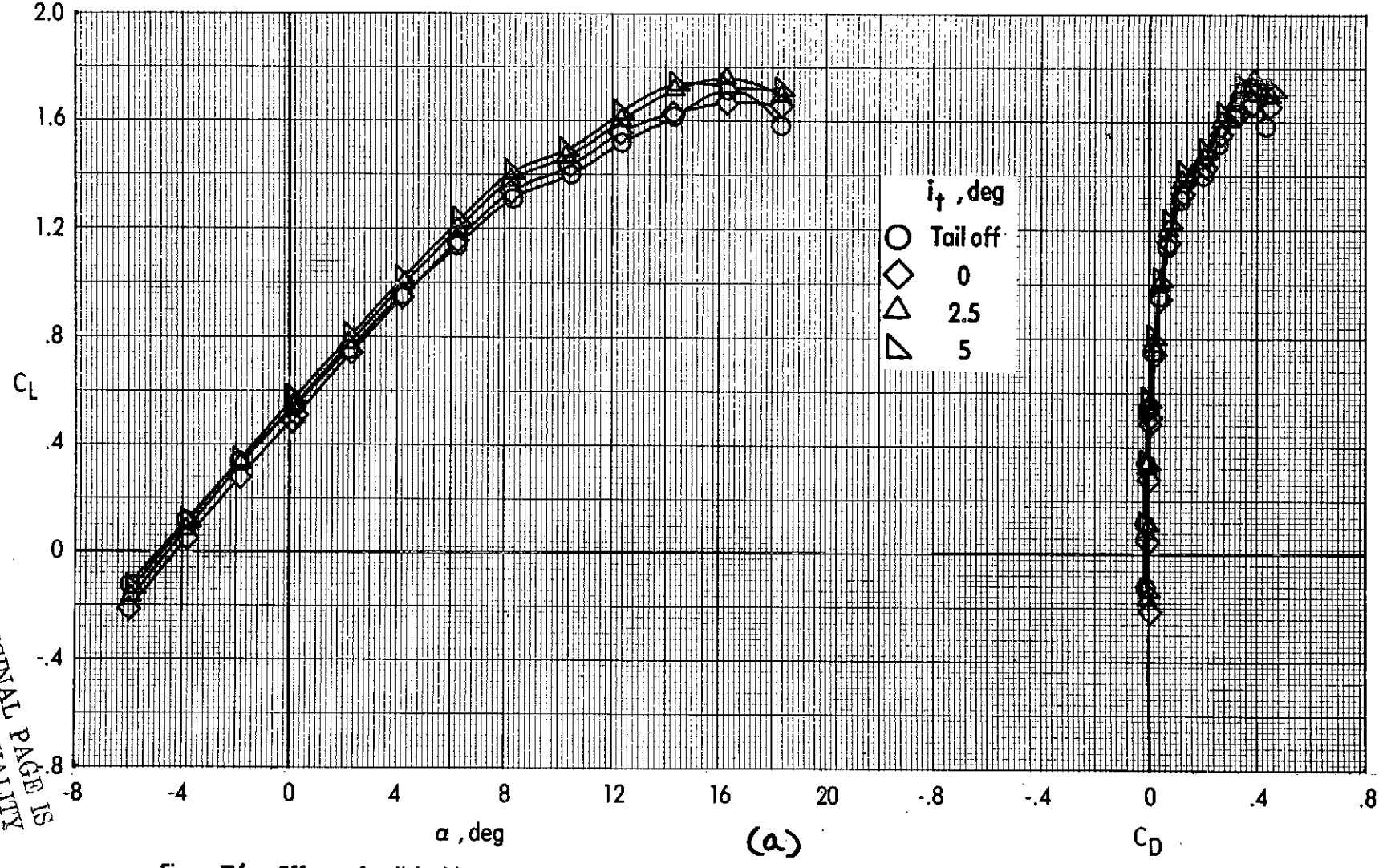

(a)

Figure 76 - Effect of tail incidence on longitudinal aerodynamic characteristics of the cruise configuration.

δ_L = closed $\delta_{LC} = 0°$ $\delta_f = 40°$ $\delta_e = 0°$ $C_\mu = 0.19$ $q_\infty = 2672\ N/m^2 (55.8\ lb/ft^2)$

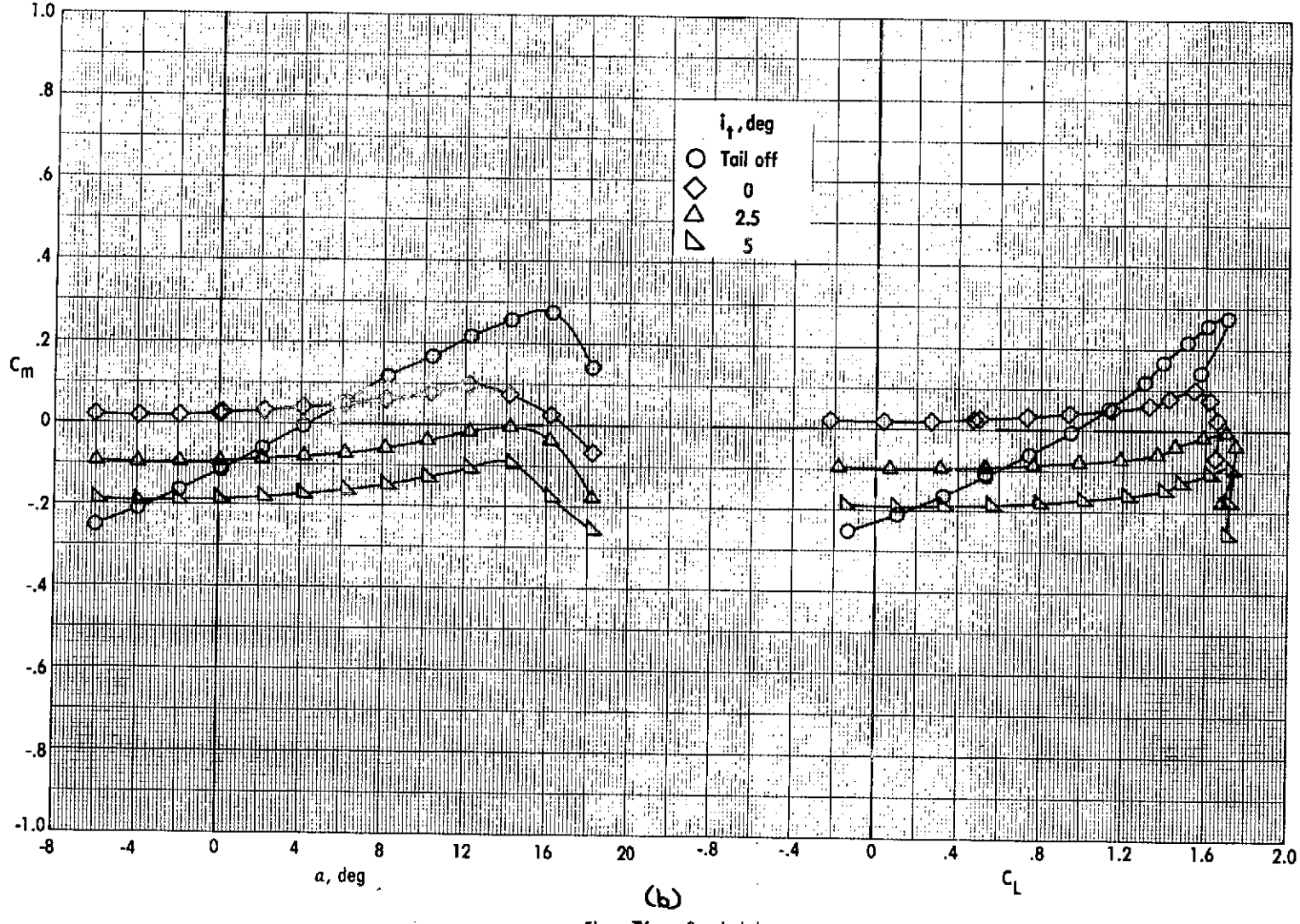

(b)

Figure 7b - Concluded.

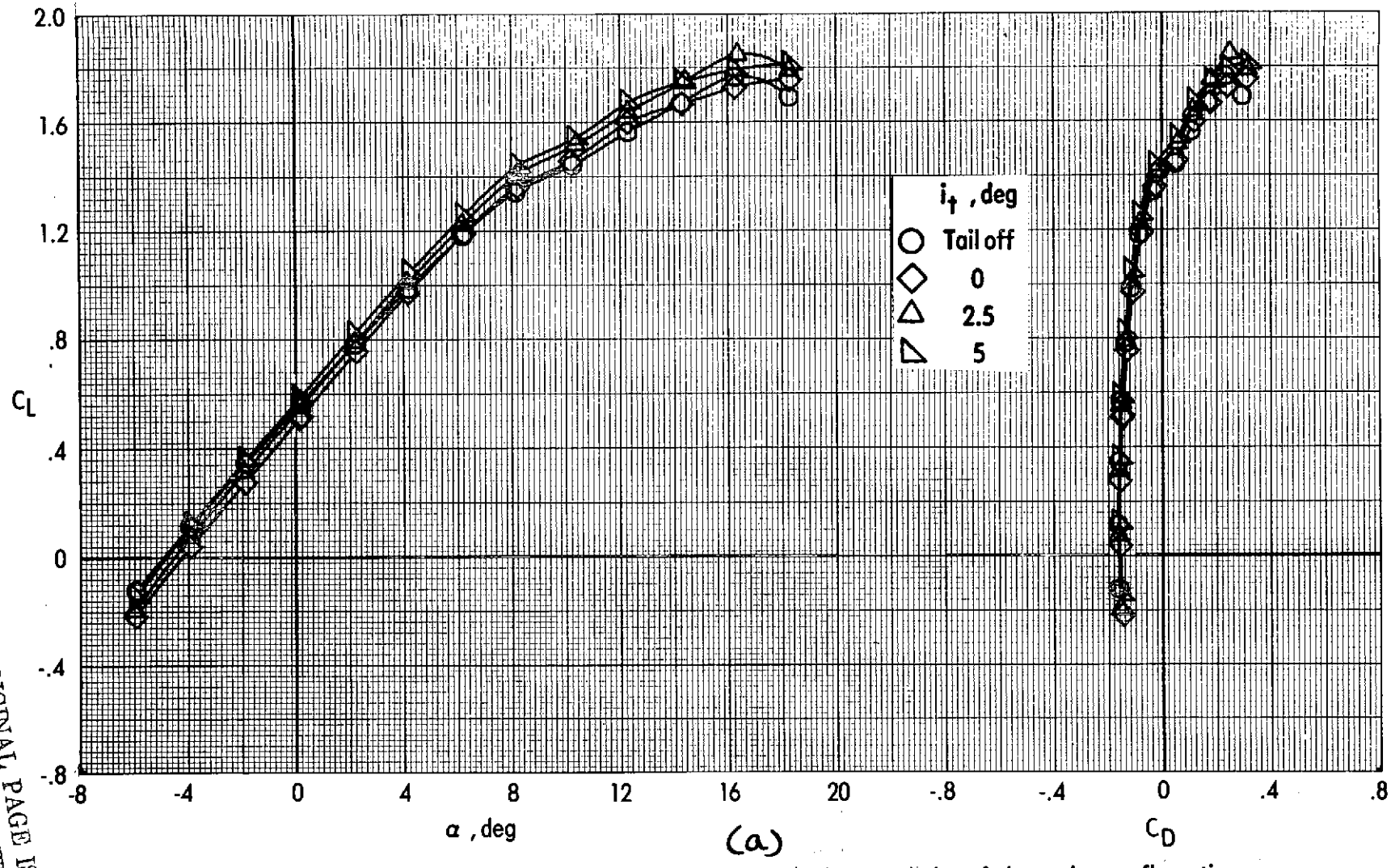

Figure 77. - Effect of tail incidence on longitudinal aerodynamic characteristics of the cruise configuration.

δ_L = closed $\delta_{LC} = 0°$ $\delta_f = 40°$ $\delta_e = 0°$ $C_\mu = 0.37$ $q_\infty = 2672$ N/m² (55.8 lb/ft²)

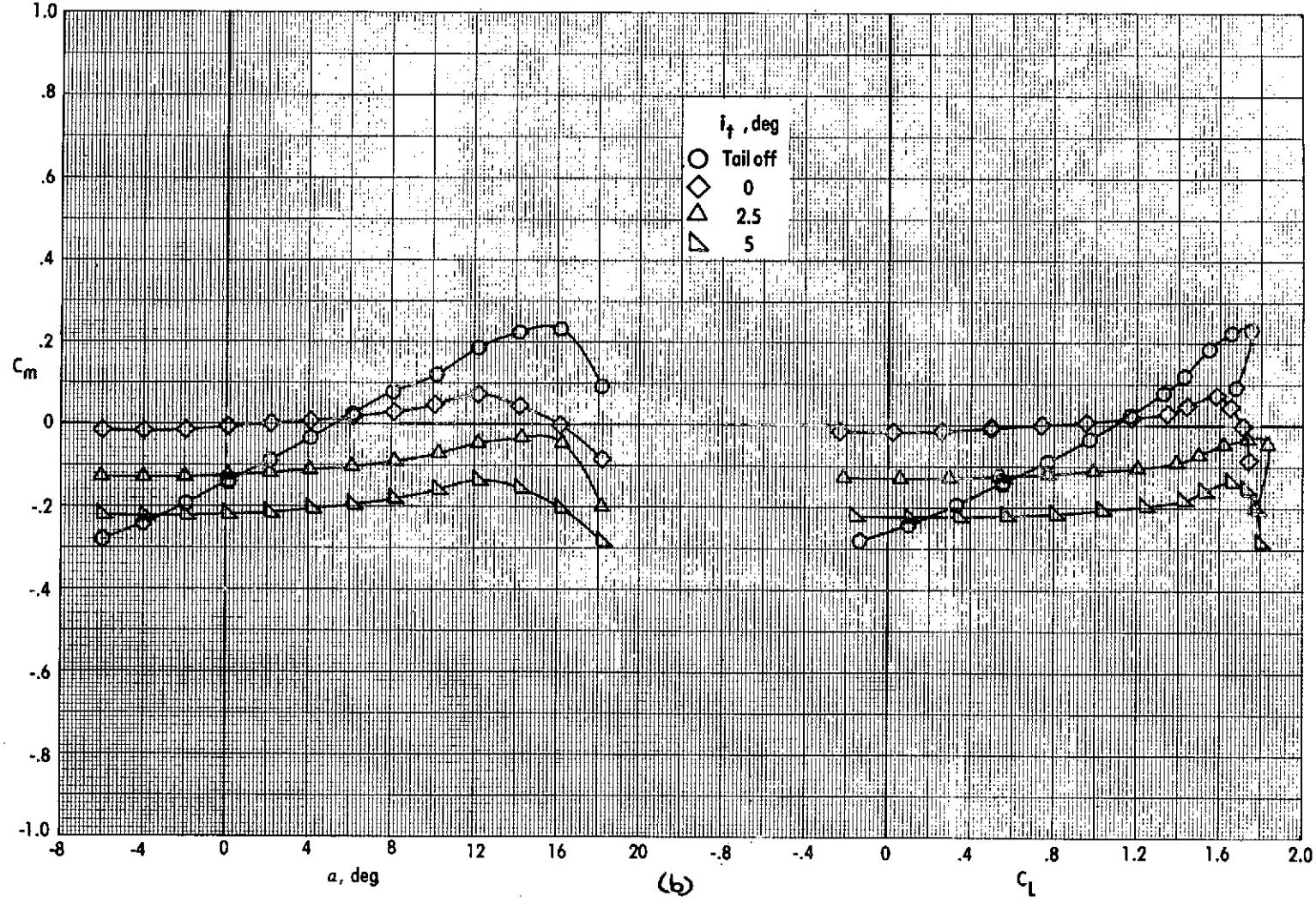

Figure 77. - Concluded.

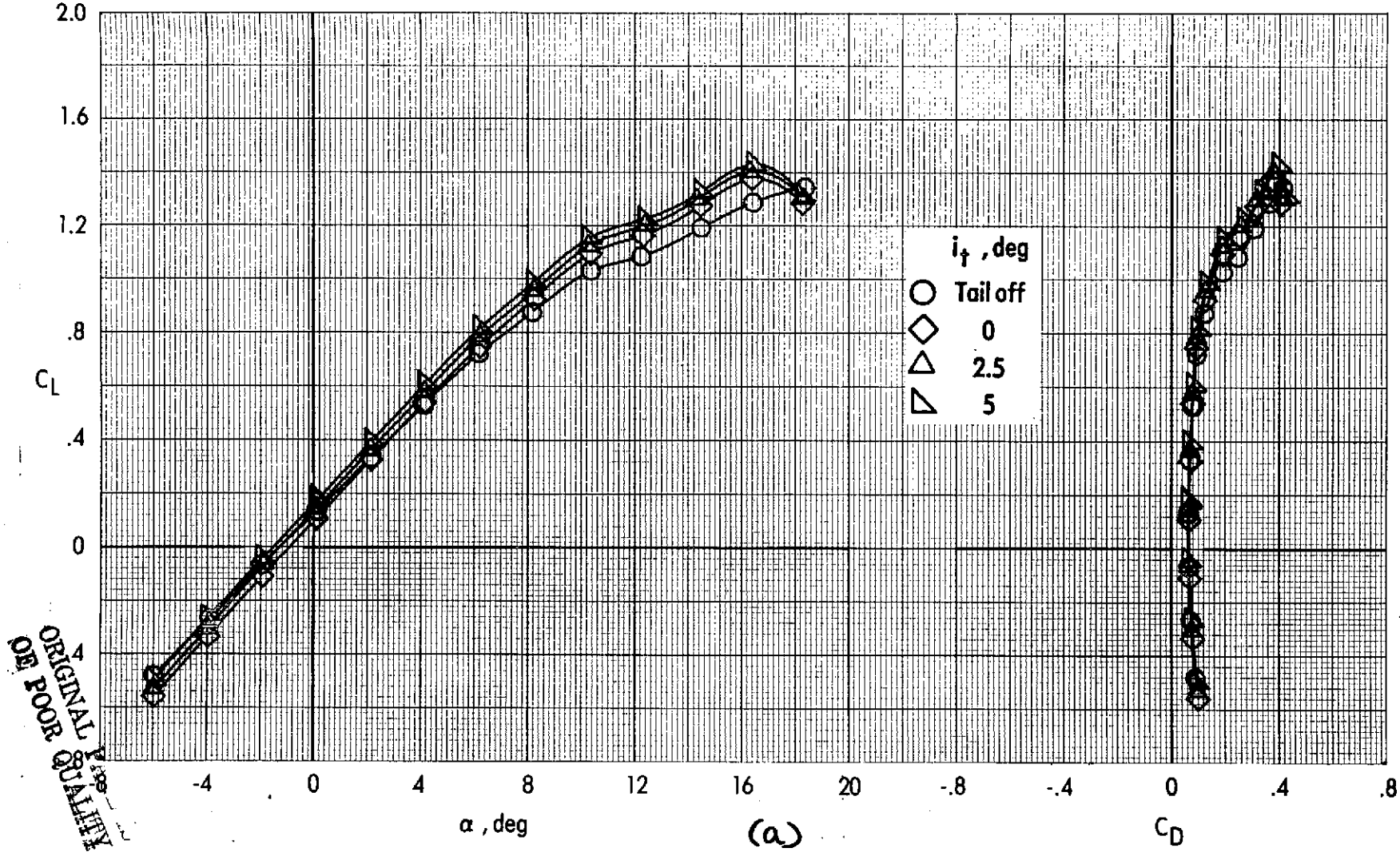

Figure 78. - Effect of tail incidence on longitudinal aerodynamic characteristics of the cruise configuration.
δ_L = closed δ_{LC}= 0° δ_f= 0° δ_e = 0° C_μ=0 q_∞= 2672 N/m² (55.8 lb/ft²)

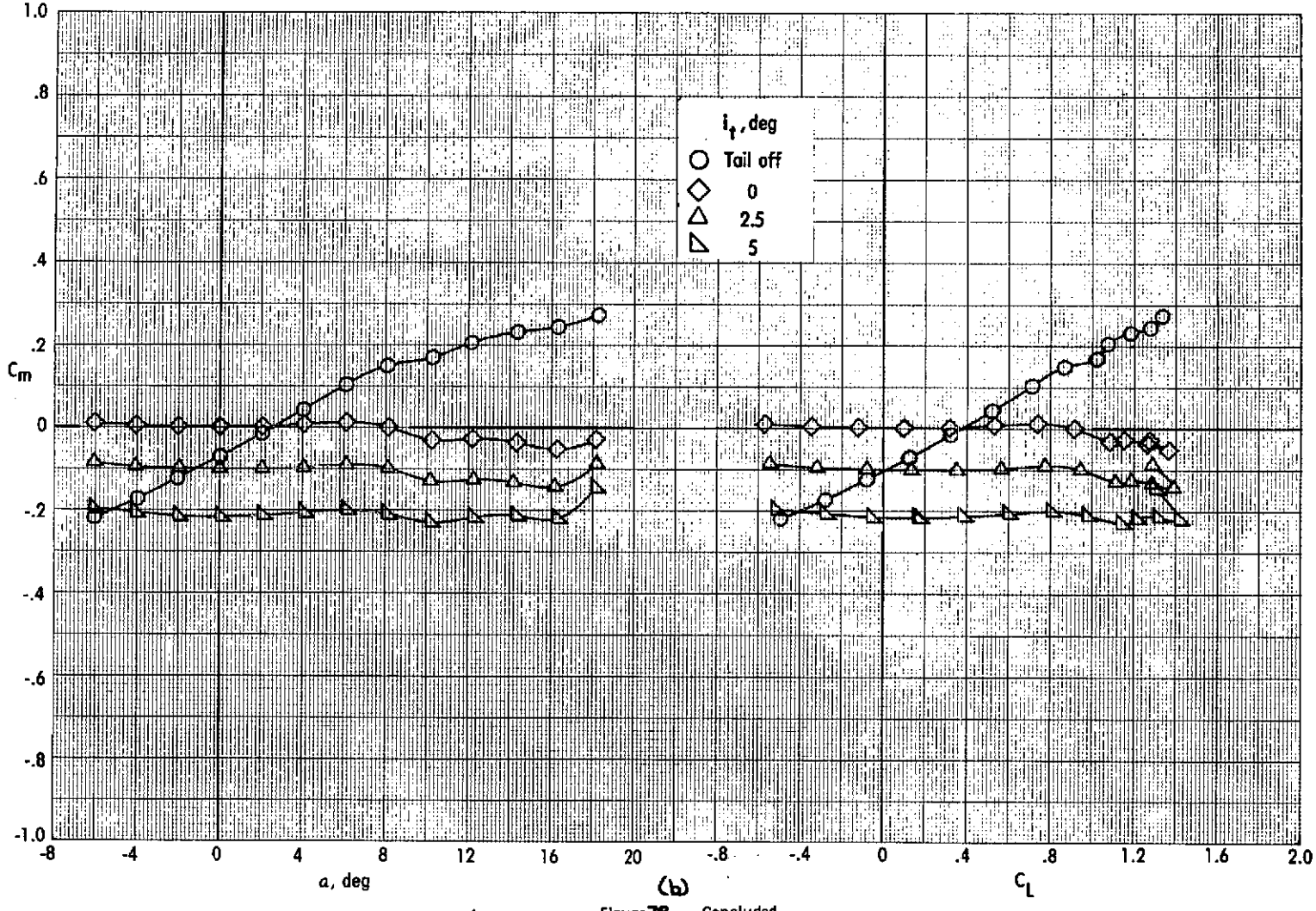

Figure 78. - Concluded.

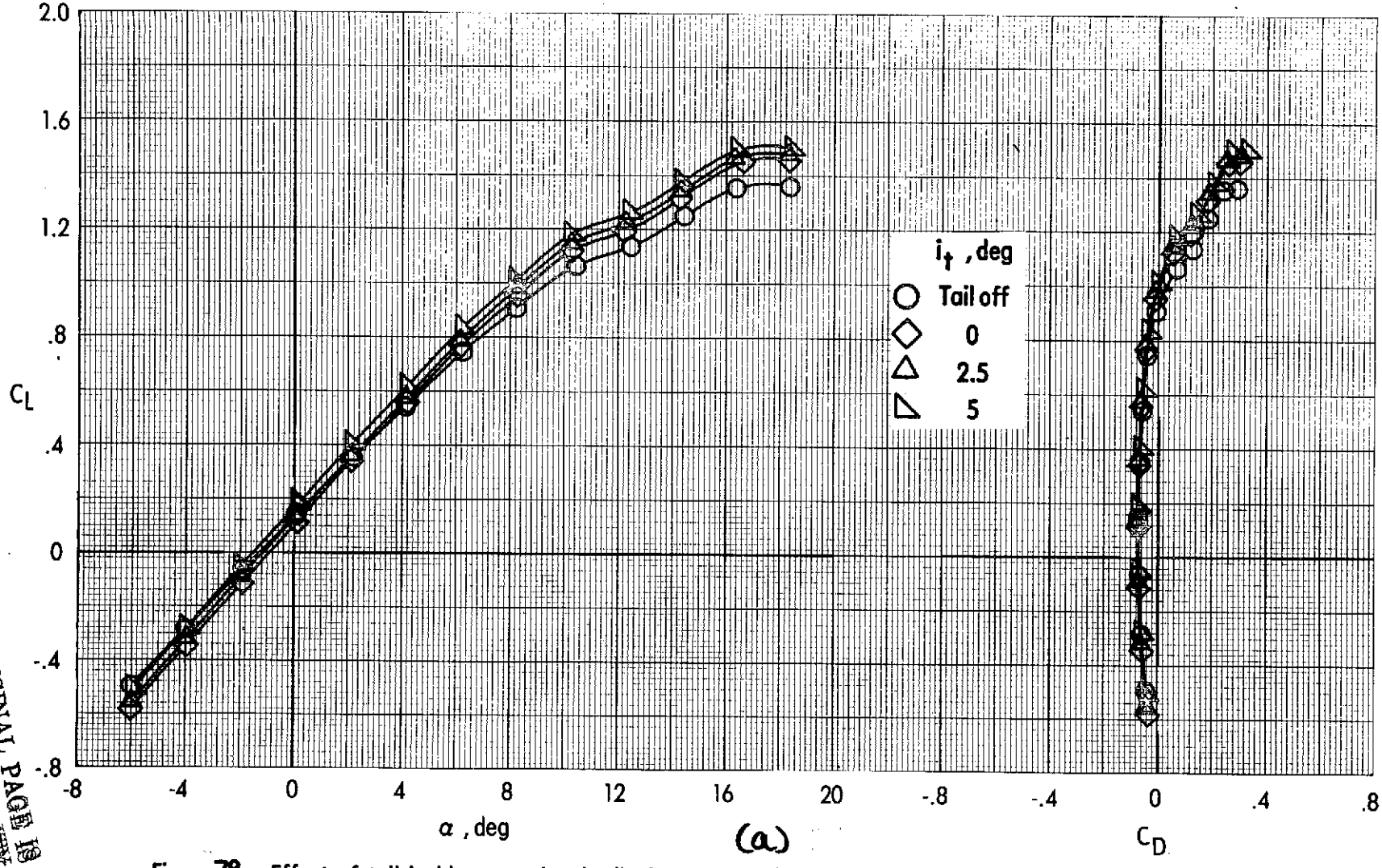

Figure 79. - Effect of tail incidence on longitudinal aerodynamic characteristics of the cruise configuration.

δ_L = closed δ_{LC} = 0° δ_f = 0° δ_e = 0° C_μ = 0.19 q_∞ = 2672 N/m² (55.8 lb/ft²)

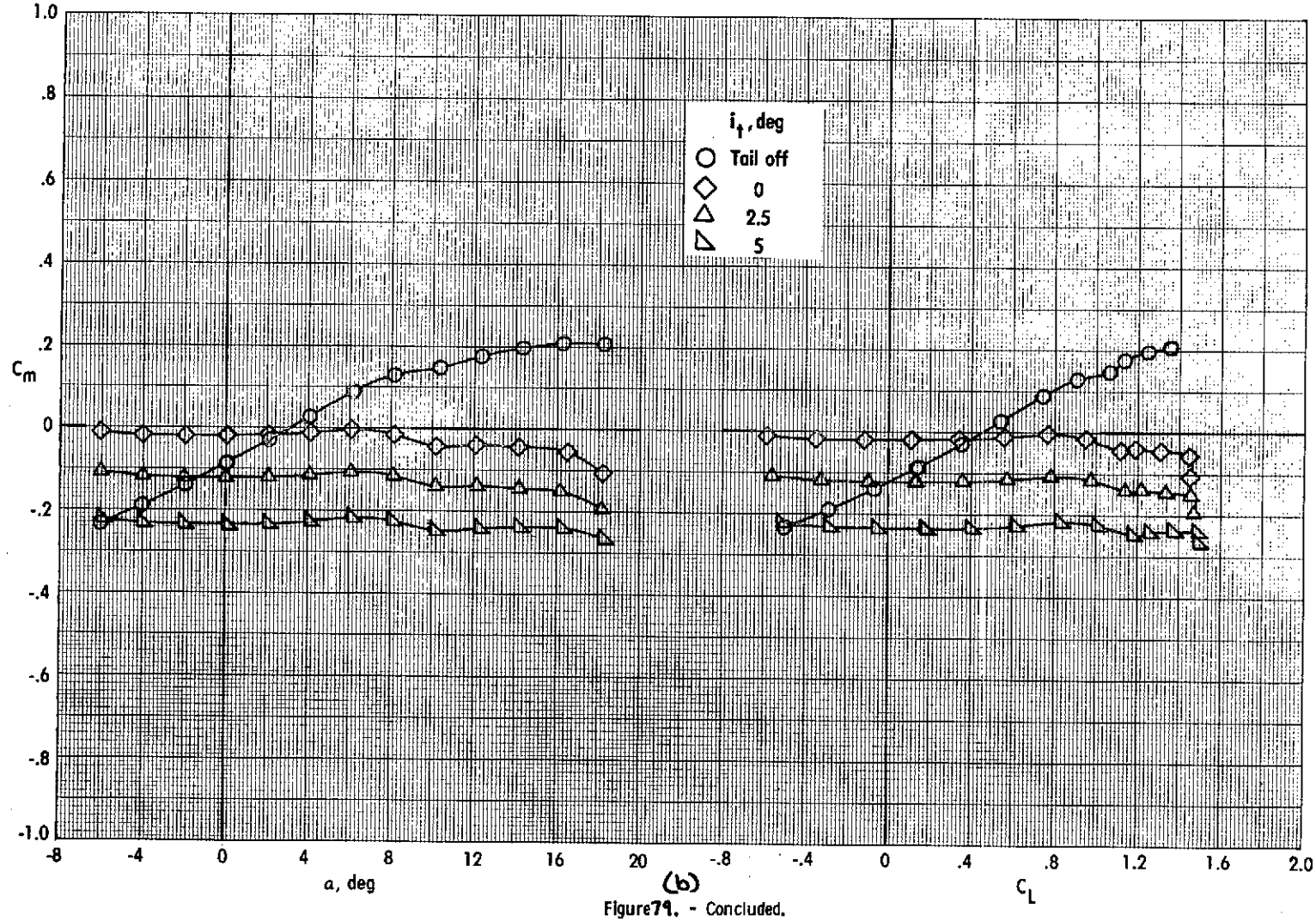

(b)

Figure 79. - Concluded.

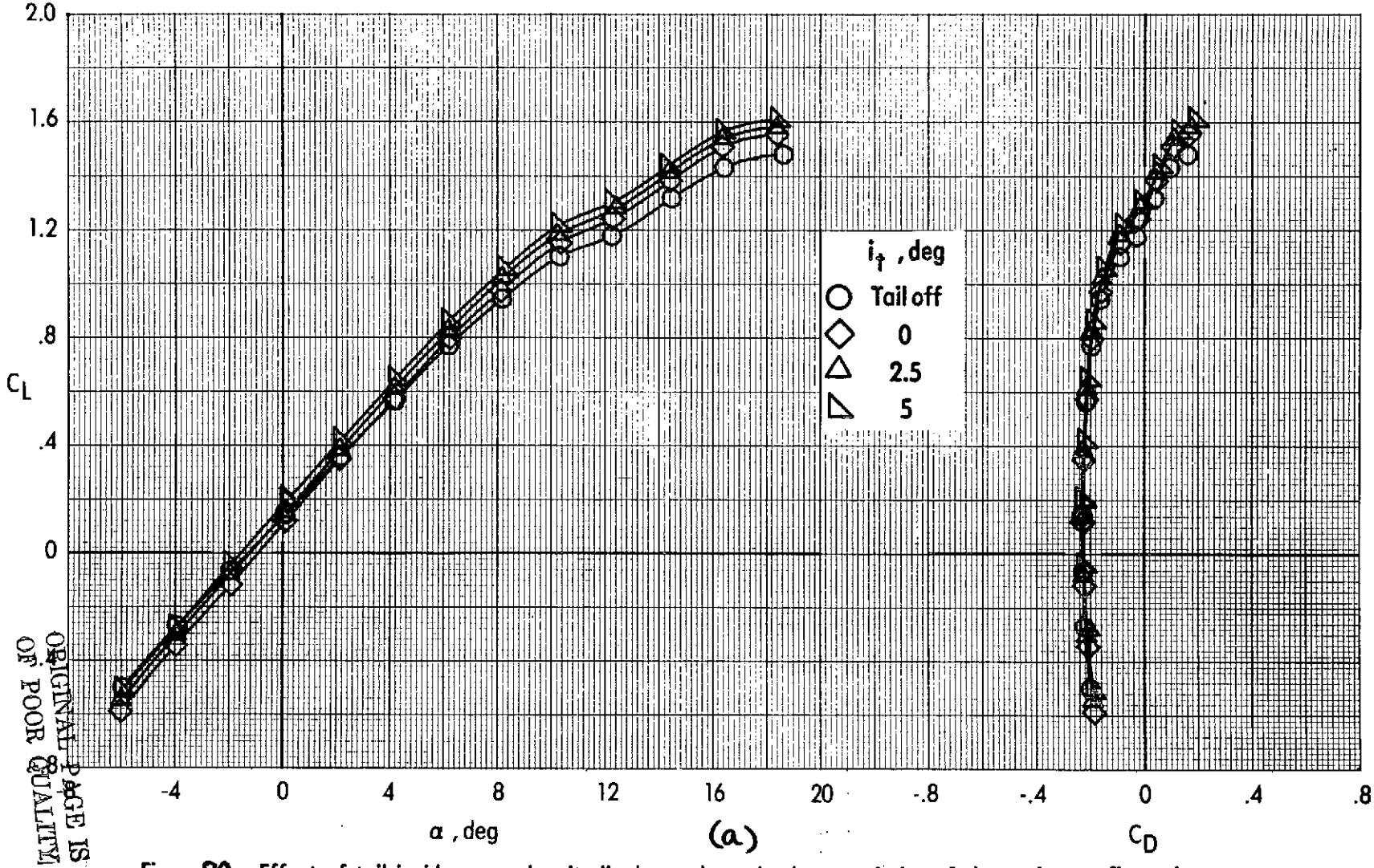

Figure 80. - Effect of tail incidence on longitudinal aerodynamic characteristics of the cruise configuration.

δ_L = closed δ_{LC}= 0° δ_f= 0° δ_e= 0° C_μ = 0.37 q_∞ = 2672 N/m^2 (55.8 lb/ft^2)

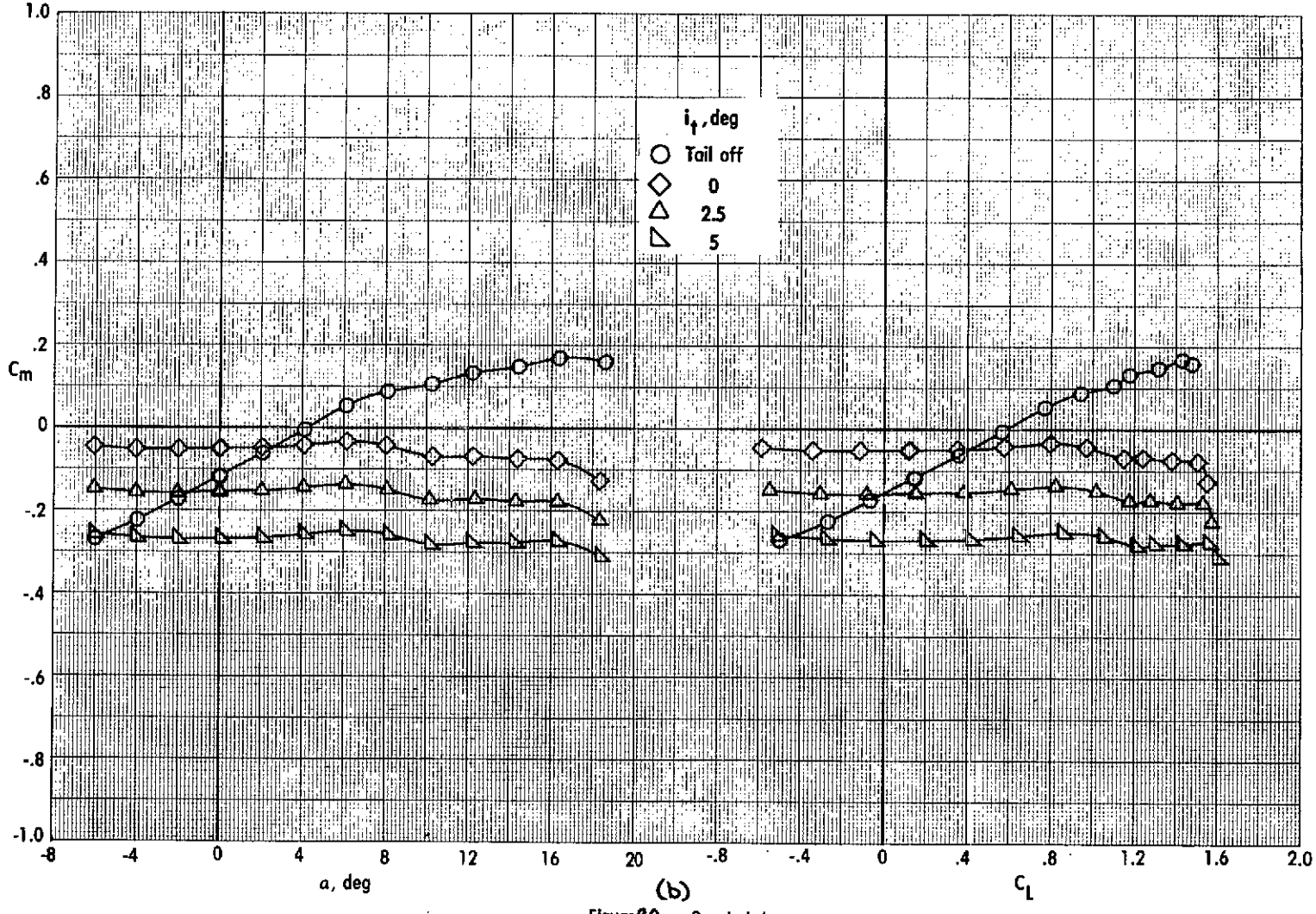

Figure 60. - Concluded.

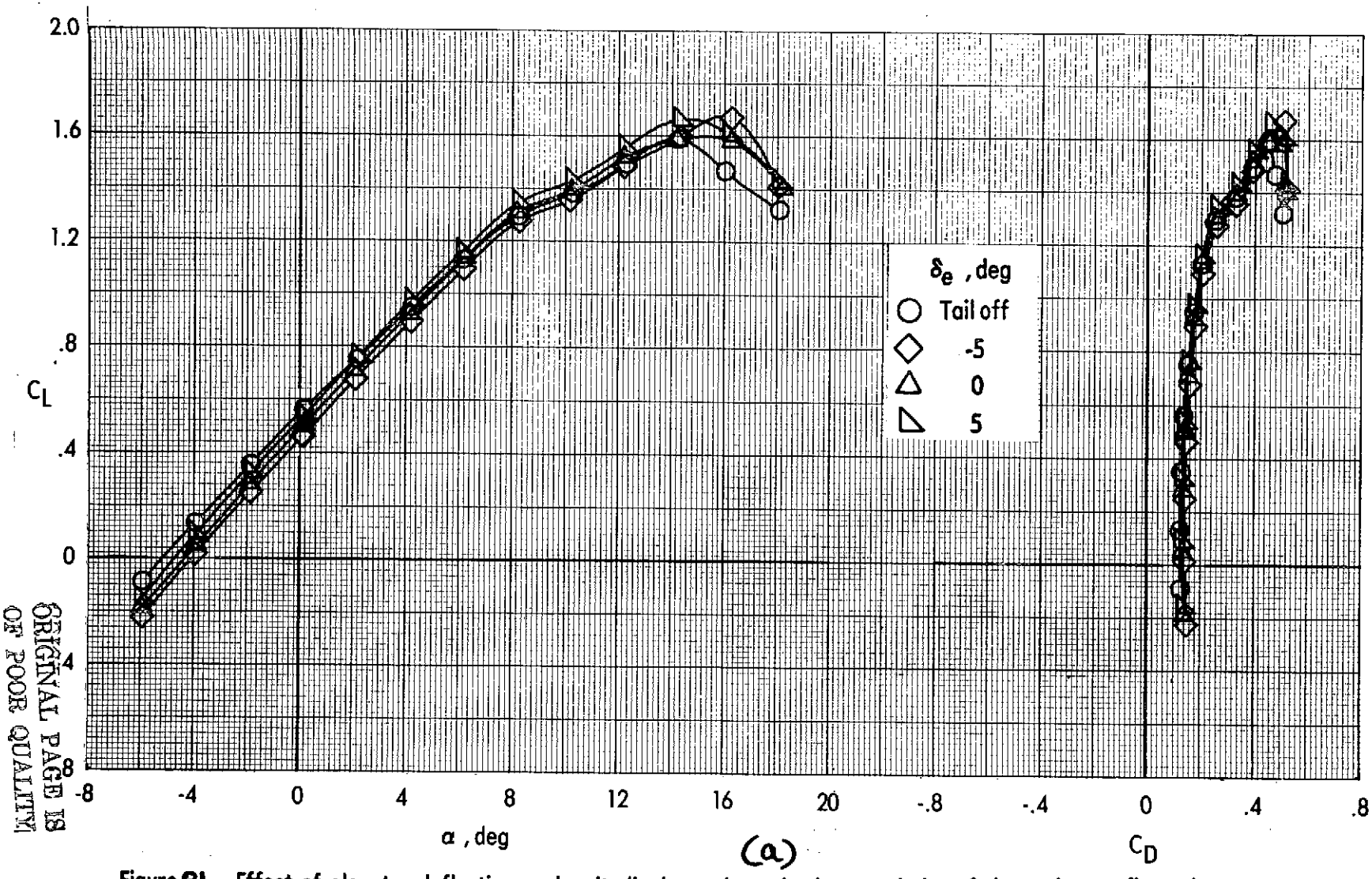

Figure 81. - Effect of elevator deflection on longitudinal aerodynamic characteristics of the cruise configuration.

δ_L = closed δ_{LC} = 0° δ_f = 40° i_t = 0° $C_\mu = 0$ $q_\infty = 2672\ N/m^2$ (55.8 lb/ft²)

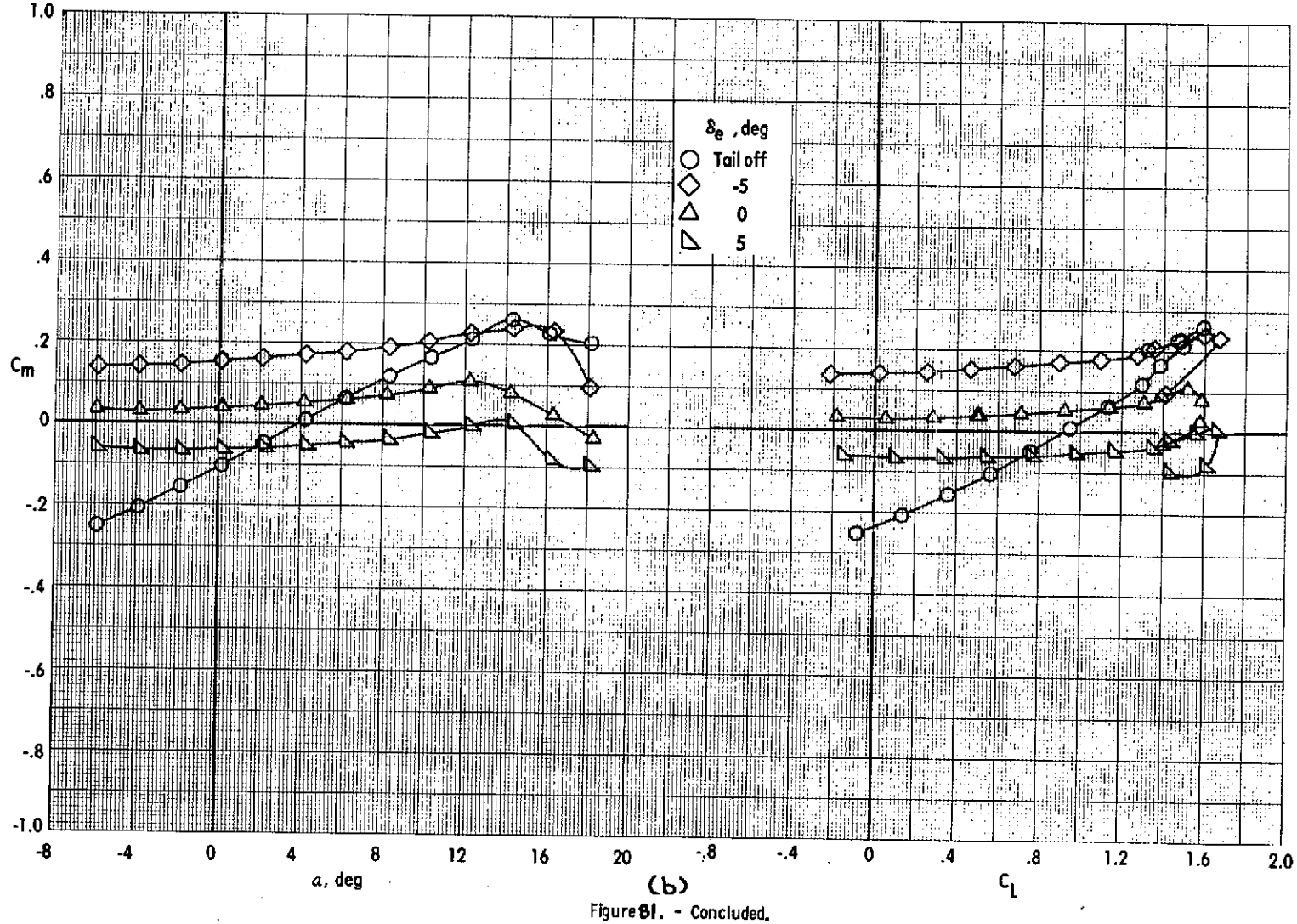

Figure 81. - Concluded.

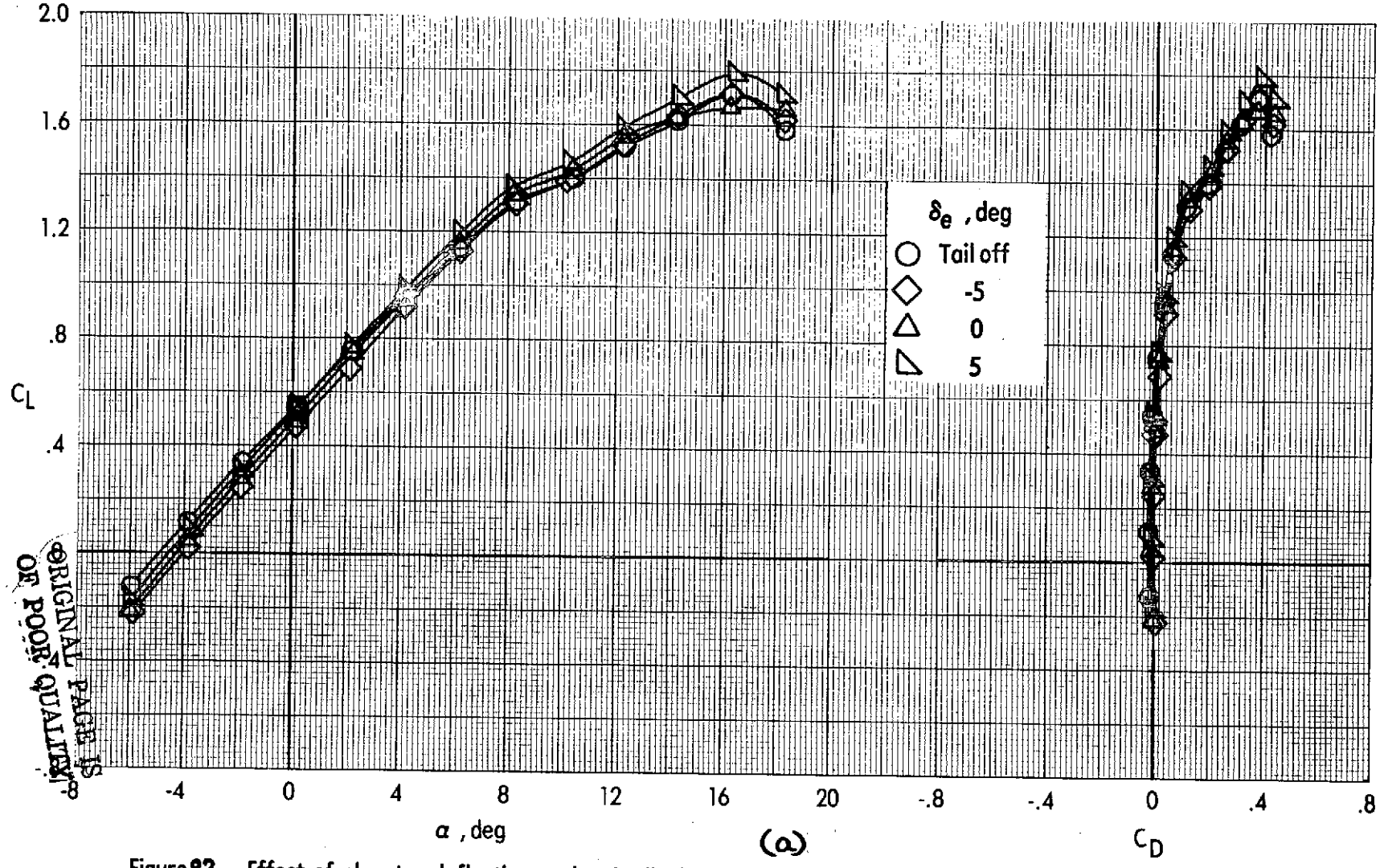

Figure 82. - Effect of elevator deflection on longitudinal aerodynamic characteristics of the cruise configuration.

δ_L = closed $\delta_{LC} = 0°$ $\delta_f = 40°$ $i_t = 0°$ $C_{\mu} = 0.19$ $q_\infty = 2672\ N/m^2 (55.8\ lb/ft^2)$

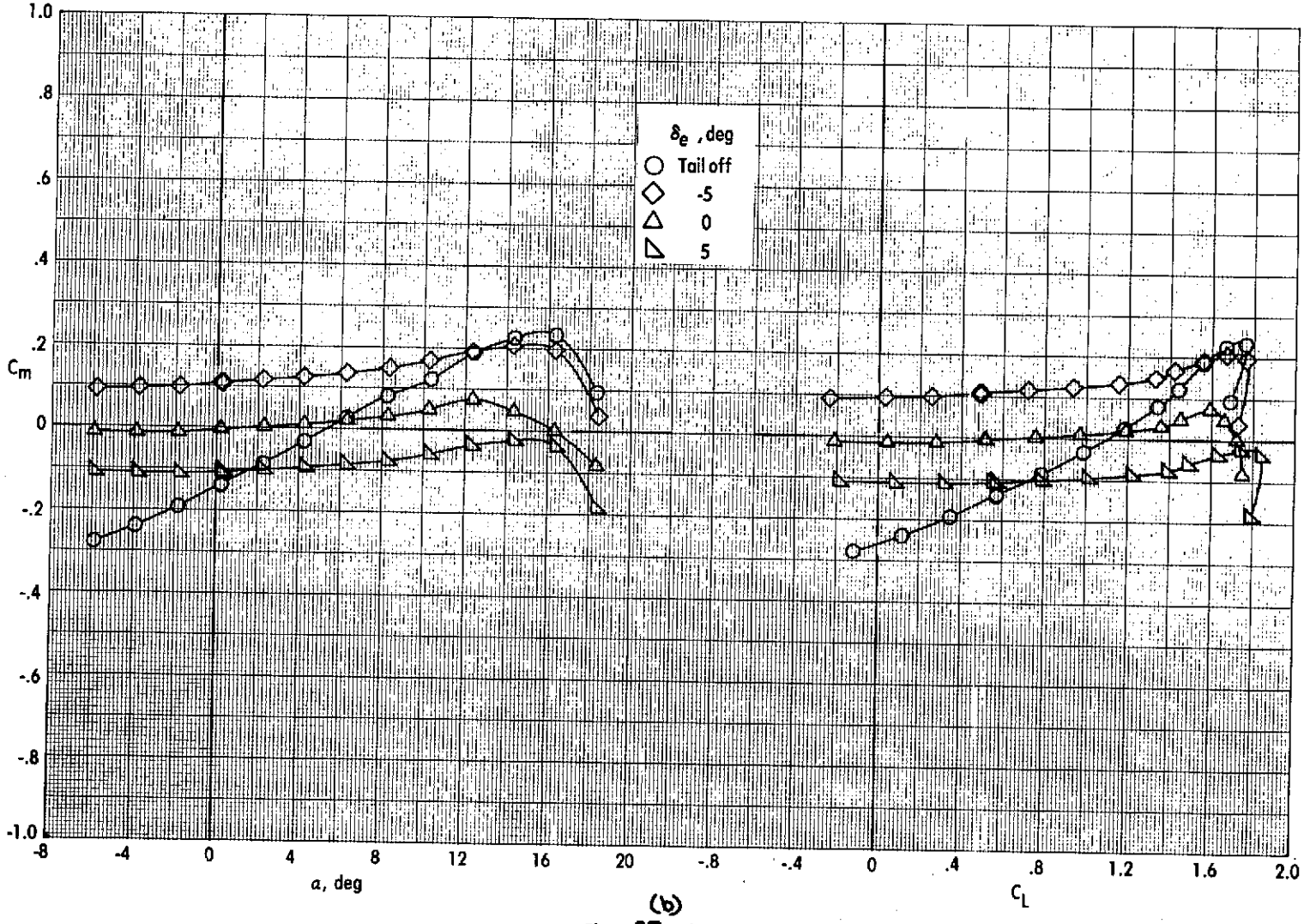

(b)

Figure 82 - Concluded.

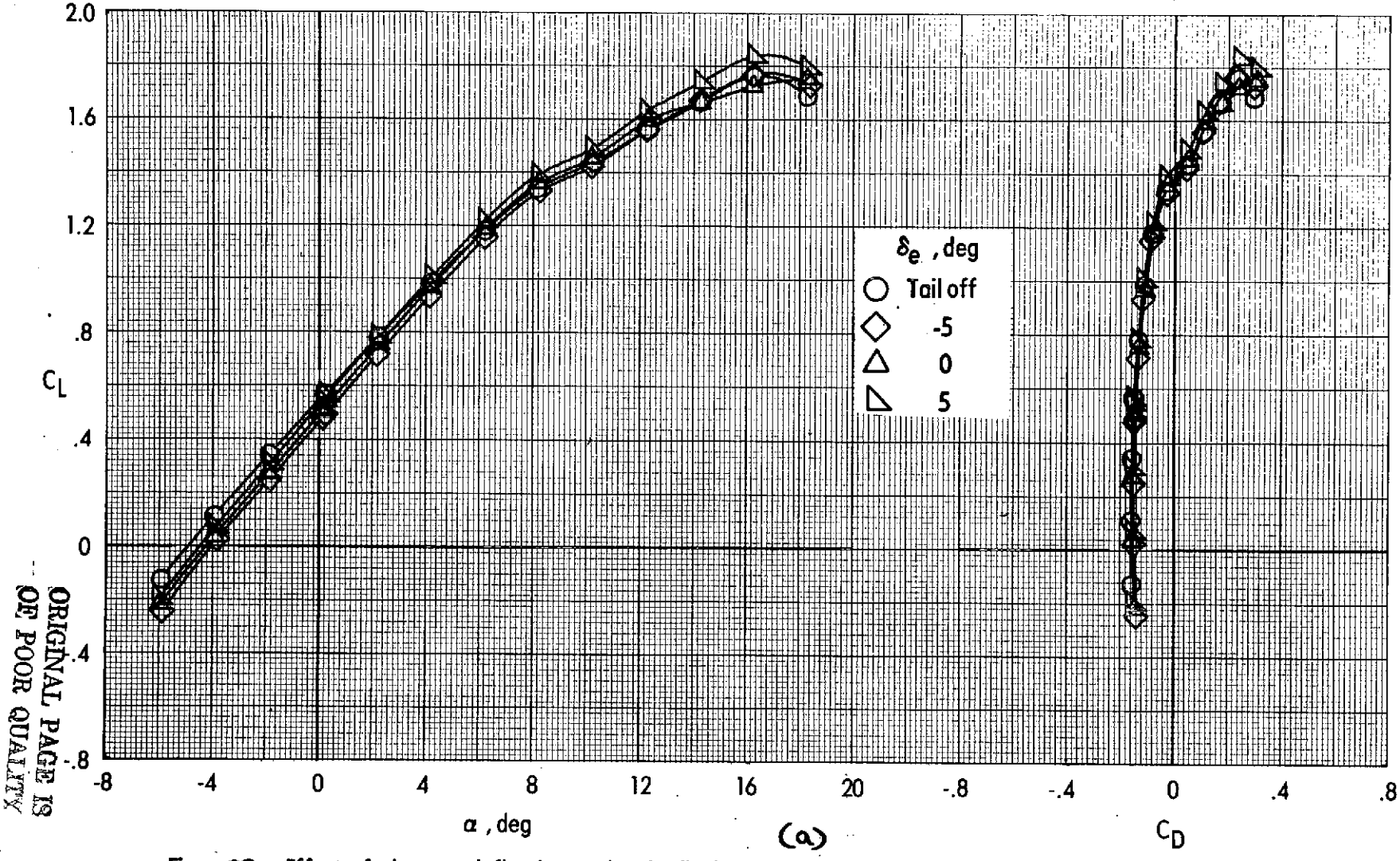

Figure 83. - Effect of elevator deflection on longitudinal aerodynamic characteristics of the cruise configuration.

δ_L = closed δ_{LC} = 0° δ_f = 40° i_t = 0° C_μ = 0.37 q_∞ = 2672 N/m^2 (55.8 lb/ft^2)

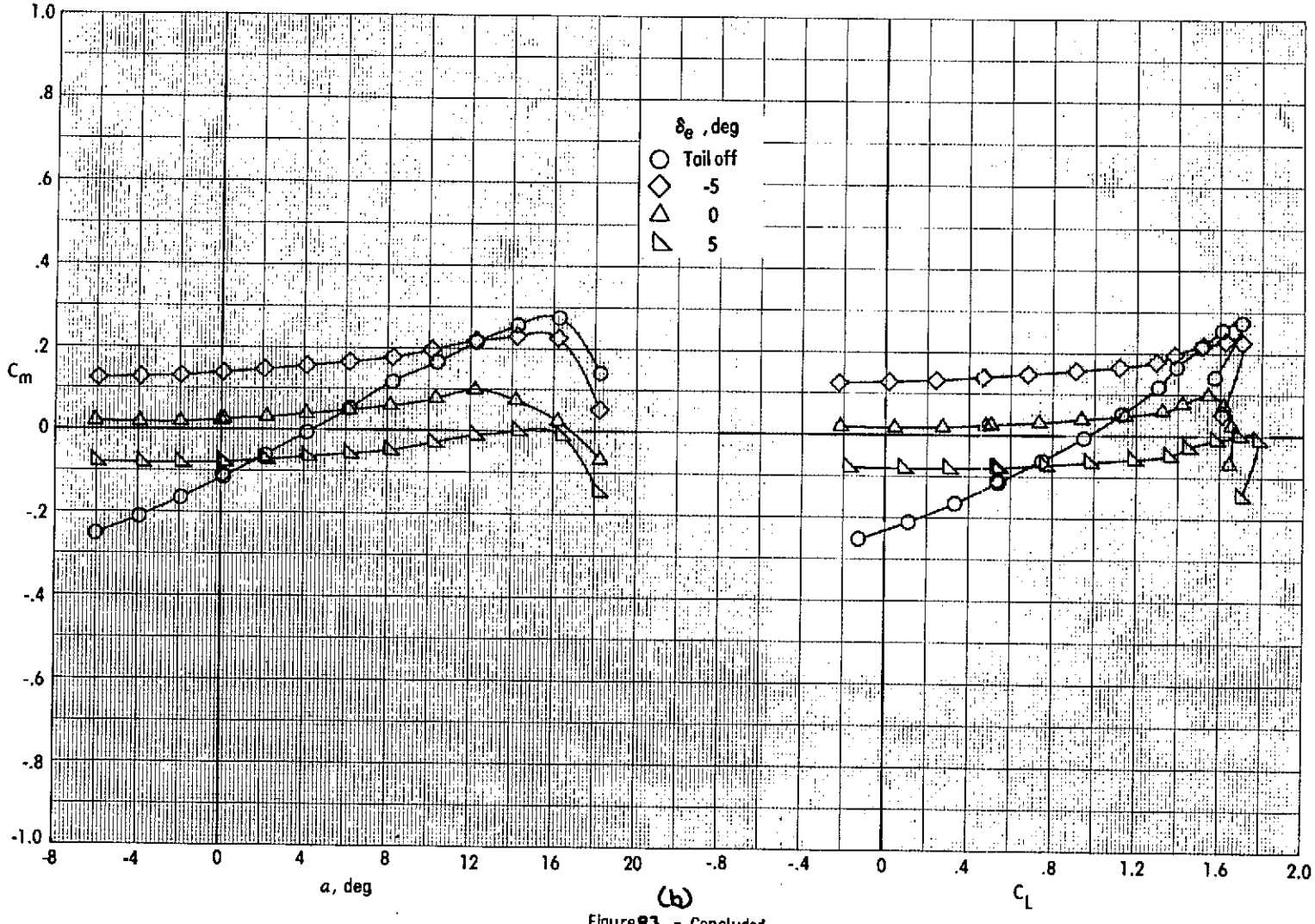

(b)

Figure 31 - Concluded.

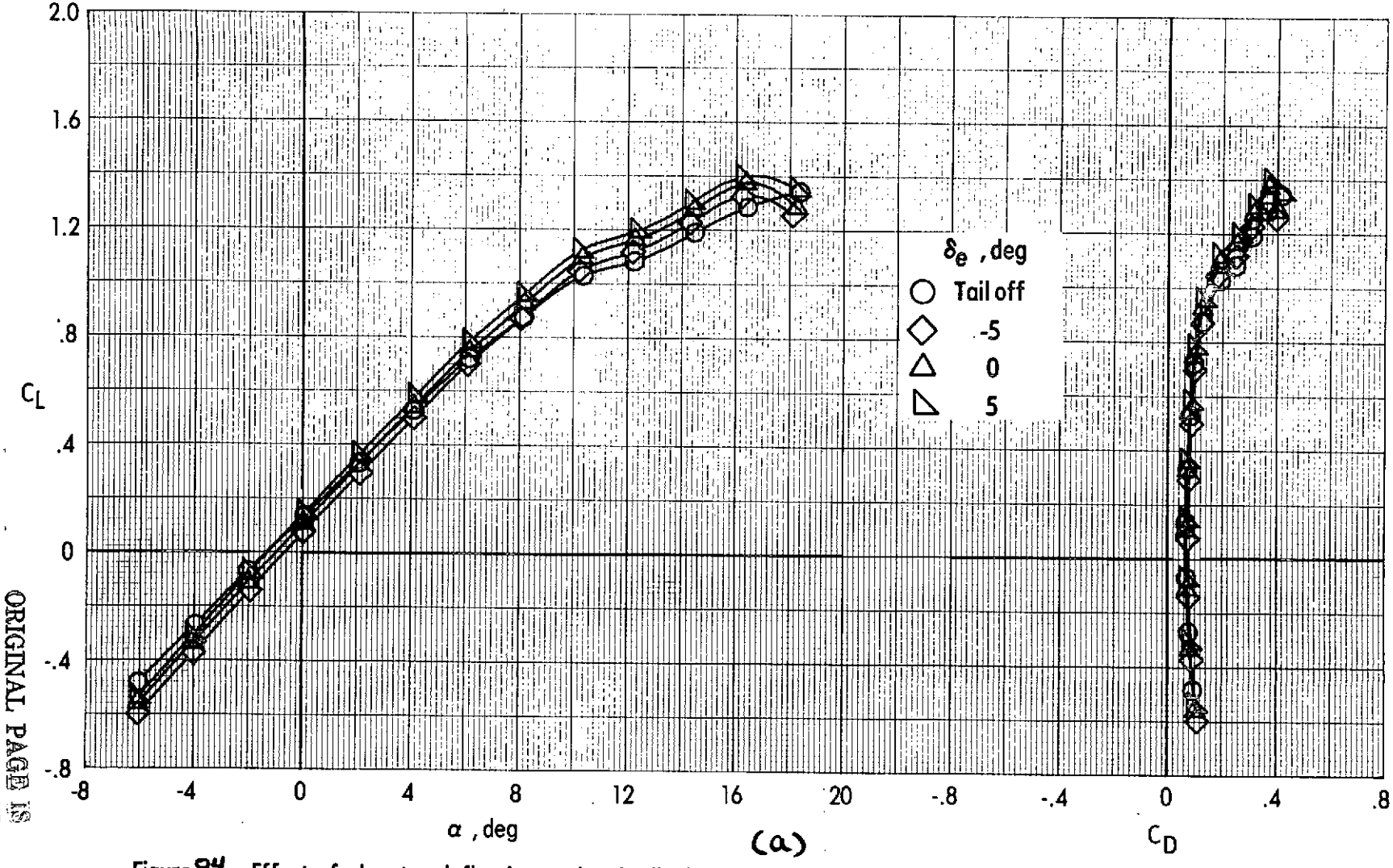

Figure 84 - Effect of elevator deflection on longitudinal aerodynamic characteristics of the cruise configuration.

δ_L = closed δ_{LC}= 0° δ_f= 0° i_t = 0° C_μ=0 q_∞= 2672 N/m^2 (55.8 lb/ft^2)

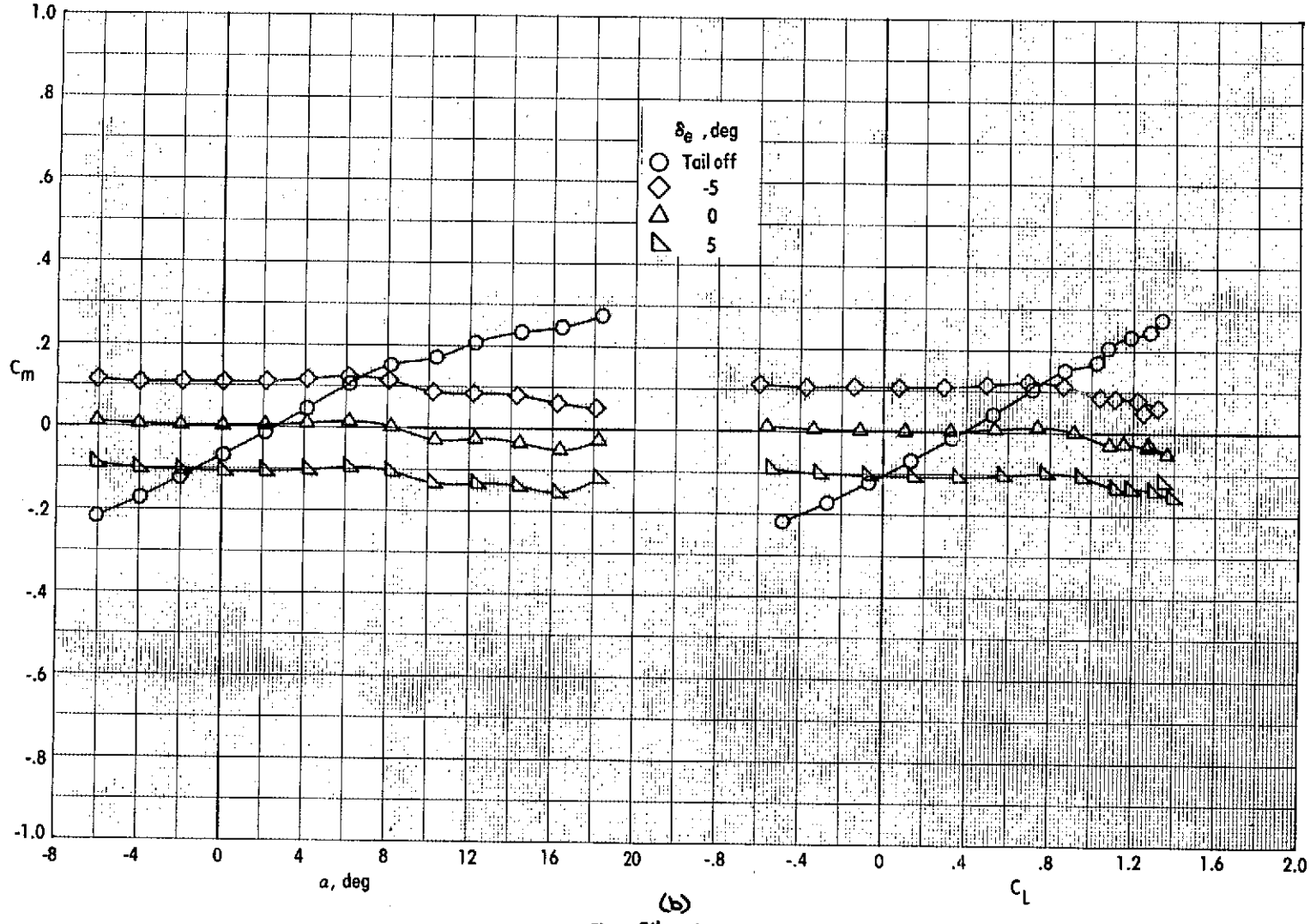

(b)

Figure 84. - Concluded.

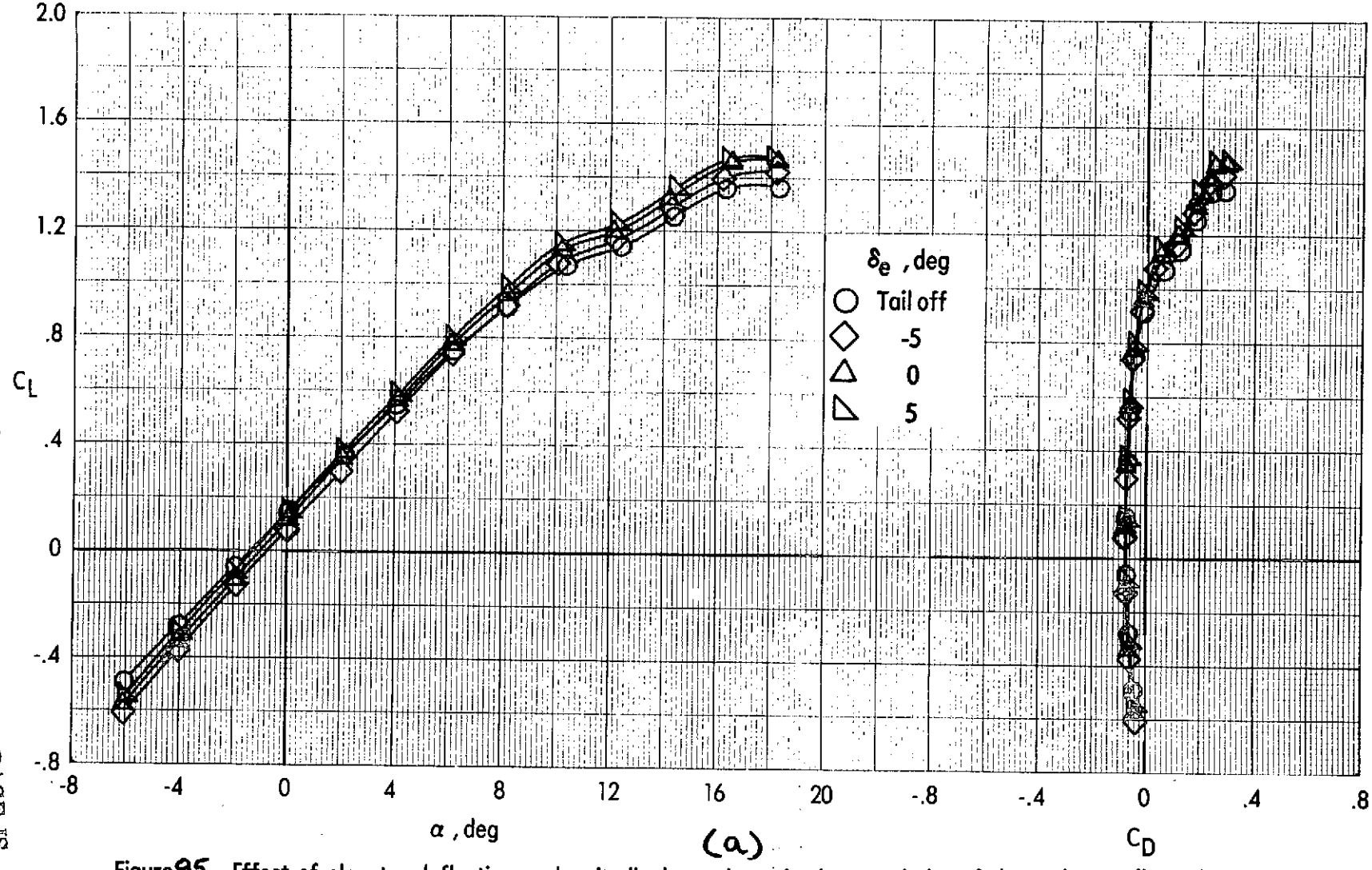

Figure 85 - Effect of elevator deflection on longitudinal aerodynamic characteristics of the cruise configuration.

δ_L = closed δ_{LC} = 0° δ_f = 0° i_t = 0° C_μ = 0.19 q_∞ = 2672 N/m^2 (55.8 lb/ft^2)

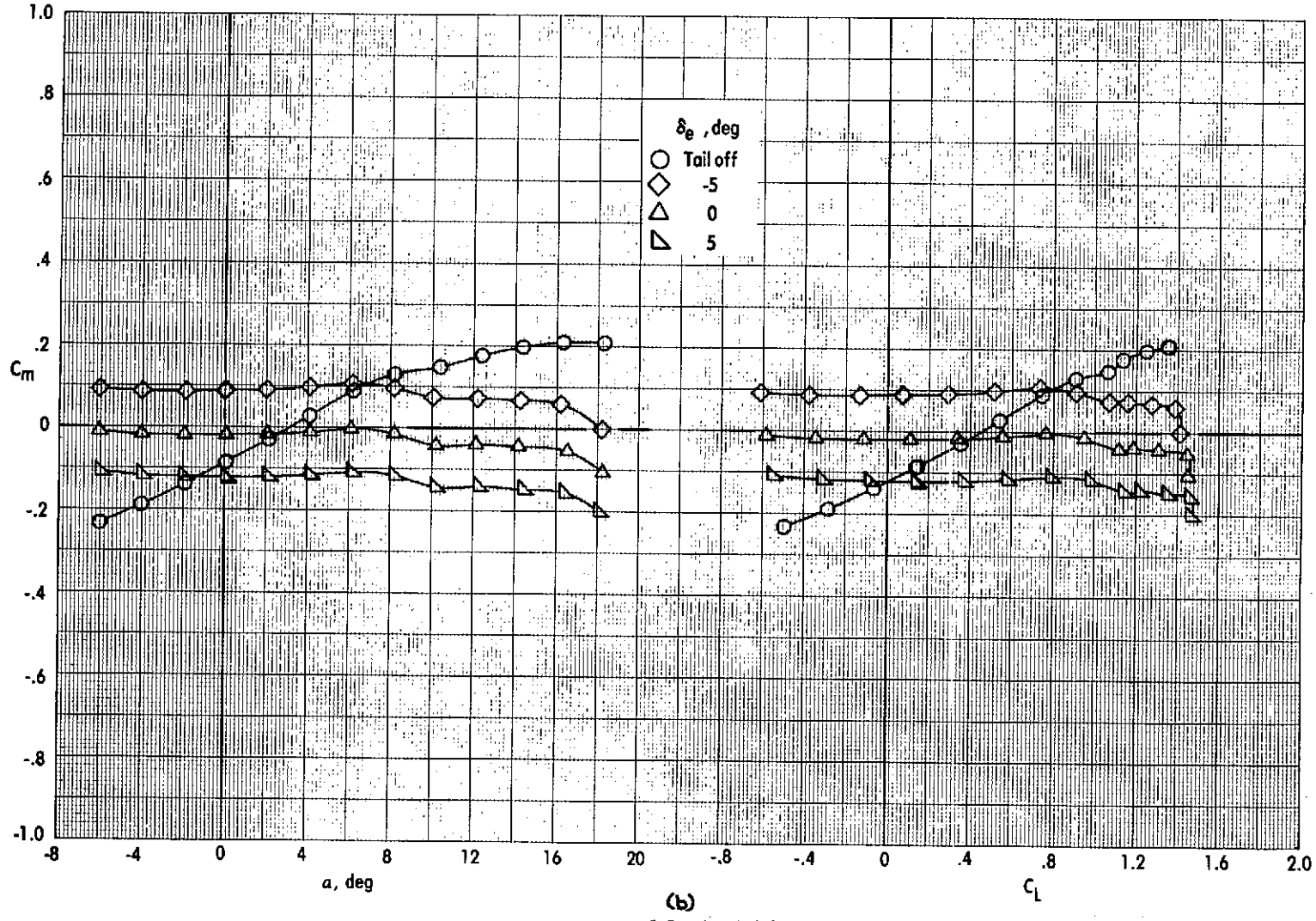

(b)

Figure 85. - Concluded.

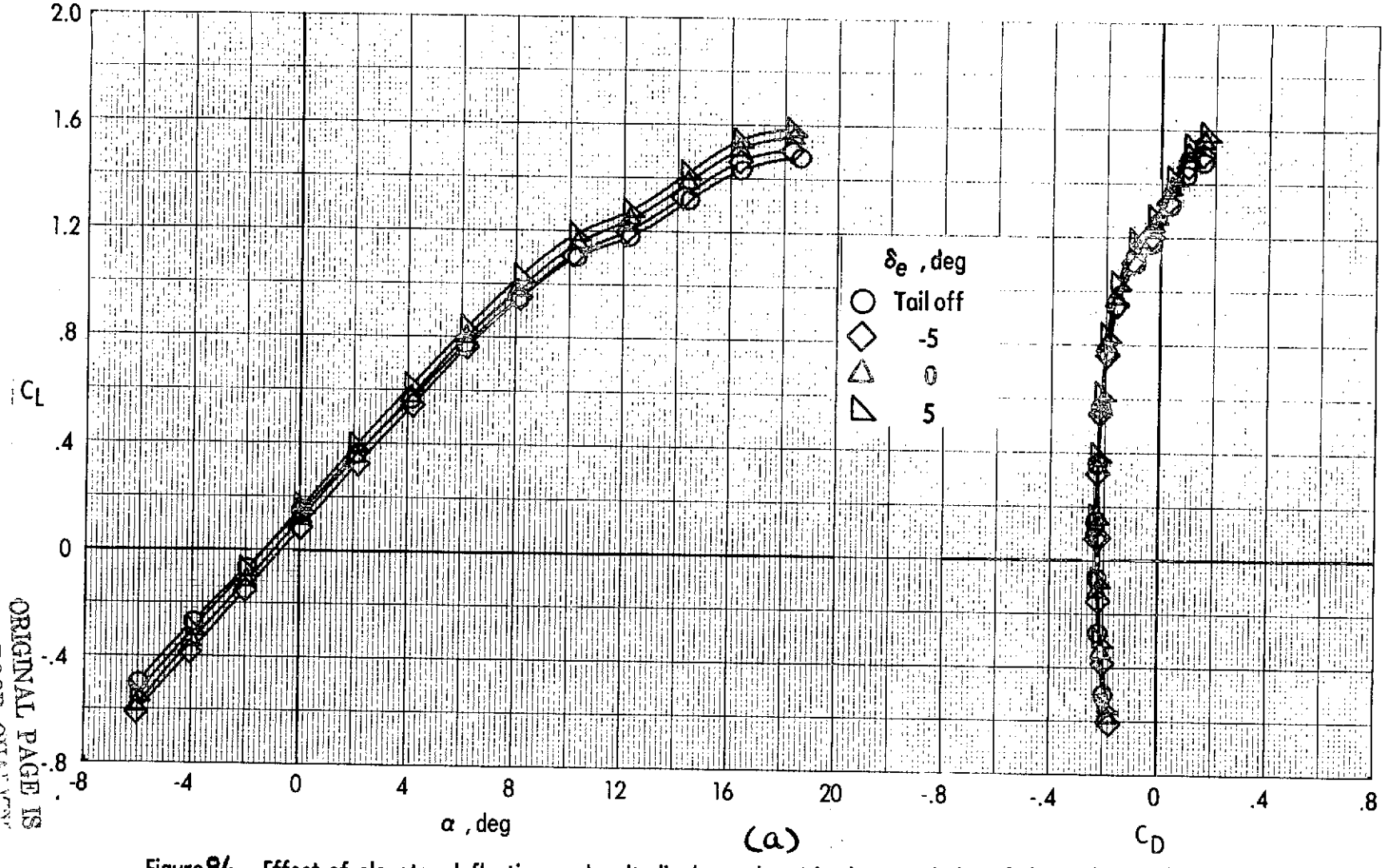

Figure 86 - Effect of elevator deflection on longitudinal aerodynamic characteristics of the cruise configuration.

δ_L = closed δ_{LC} = 0° δ_f = 0° i_t = 0° $C_{\mu} = 0.37$ $q_\infty = 2672\ N/m^2$ (55.8 lb/ft^2)

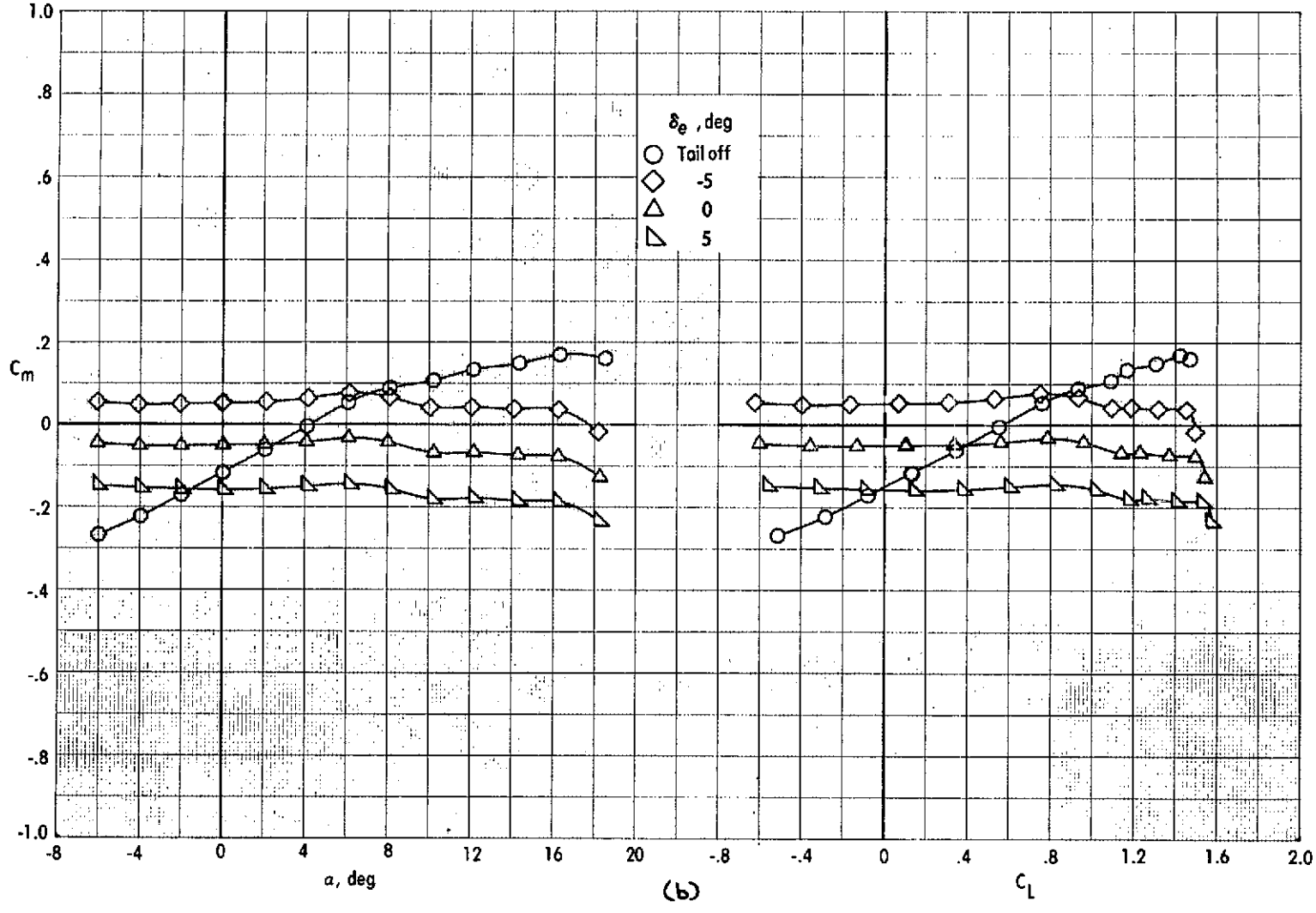

Figure 8b. - Concluded.

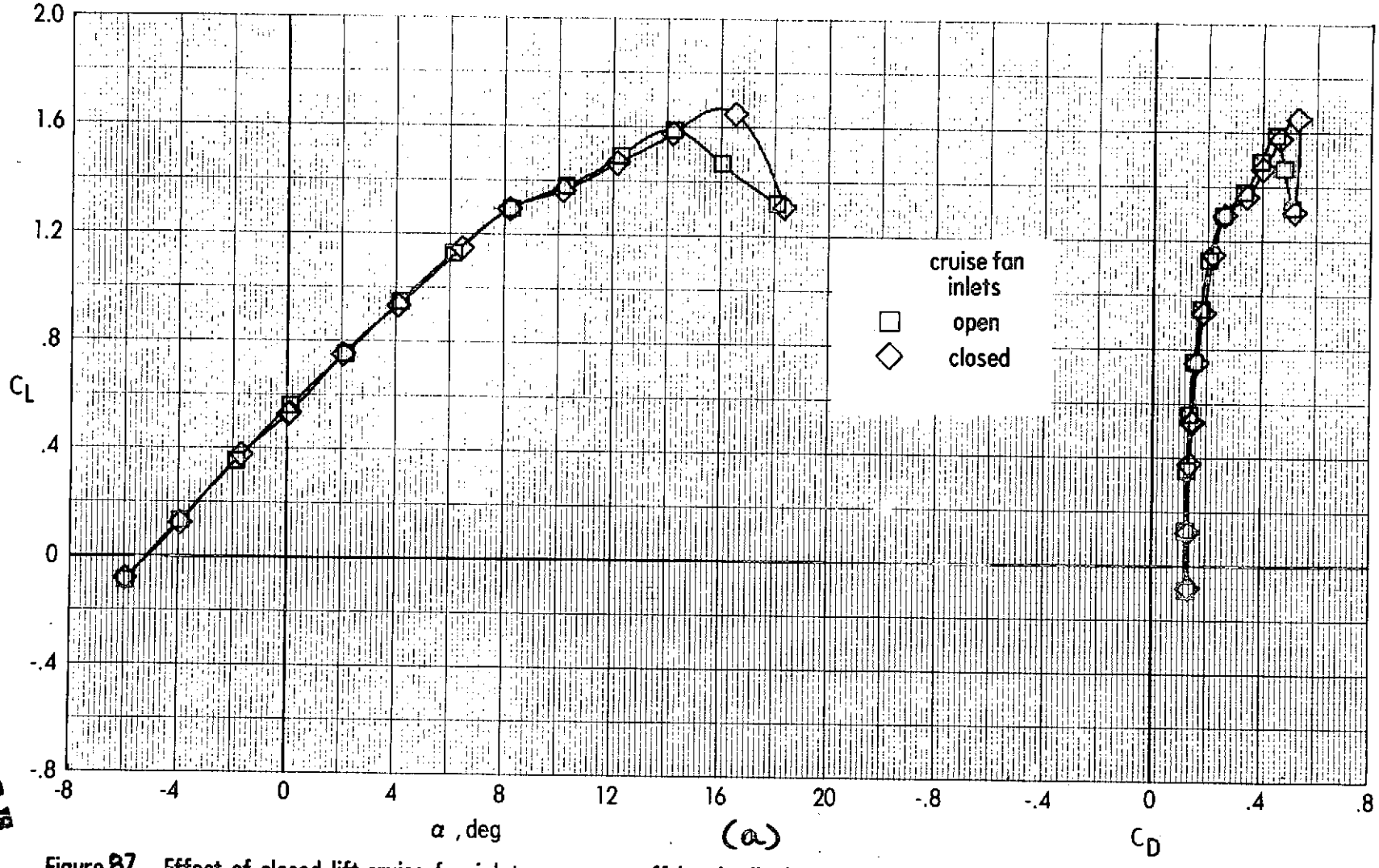

Figure 87. - Effect of closed lift-cruise fan inlets on power-off longitudinal aerodynamic characteristics of the cruise configurtion.

δ_L = closed δ_{LC} = 0° δ_f = 40° tail off $C_\mu = 0$ $q_\infty = 2672$ N/m² (55.8 lb/ft²)

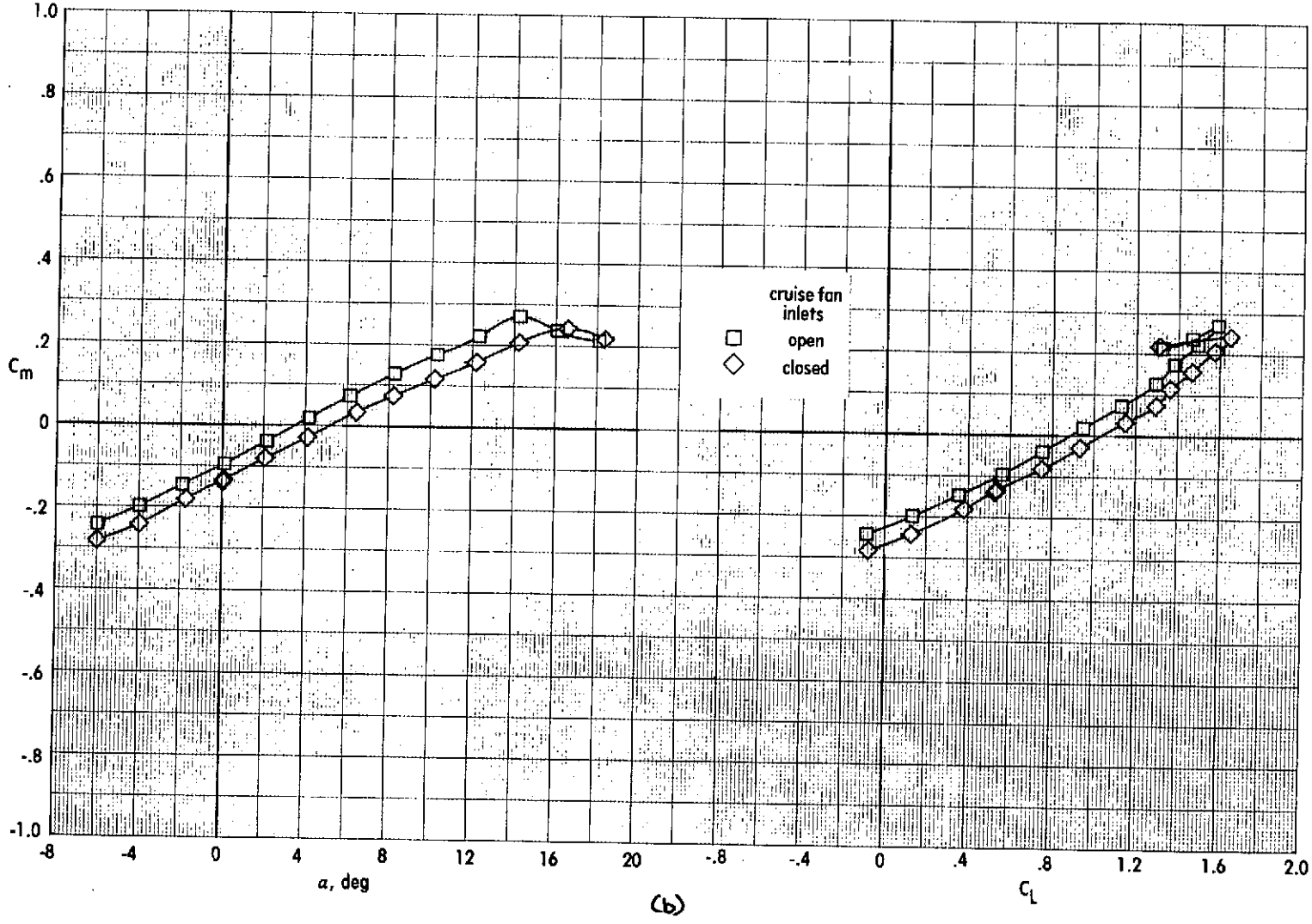

(b)

Figure 87. - Concluded.

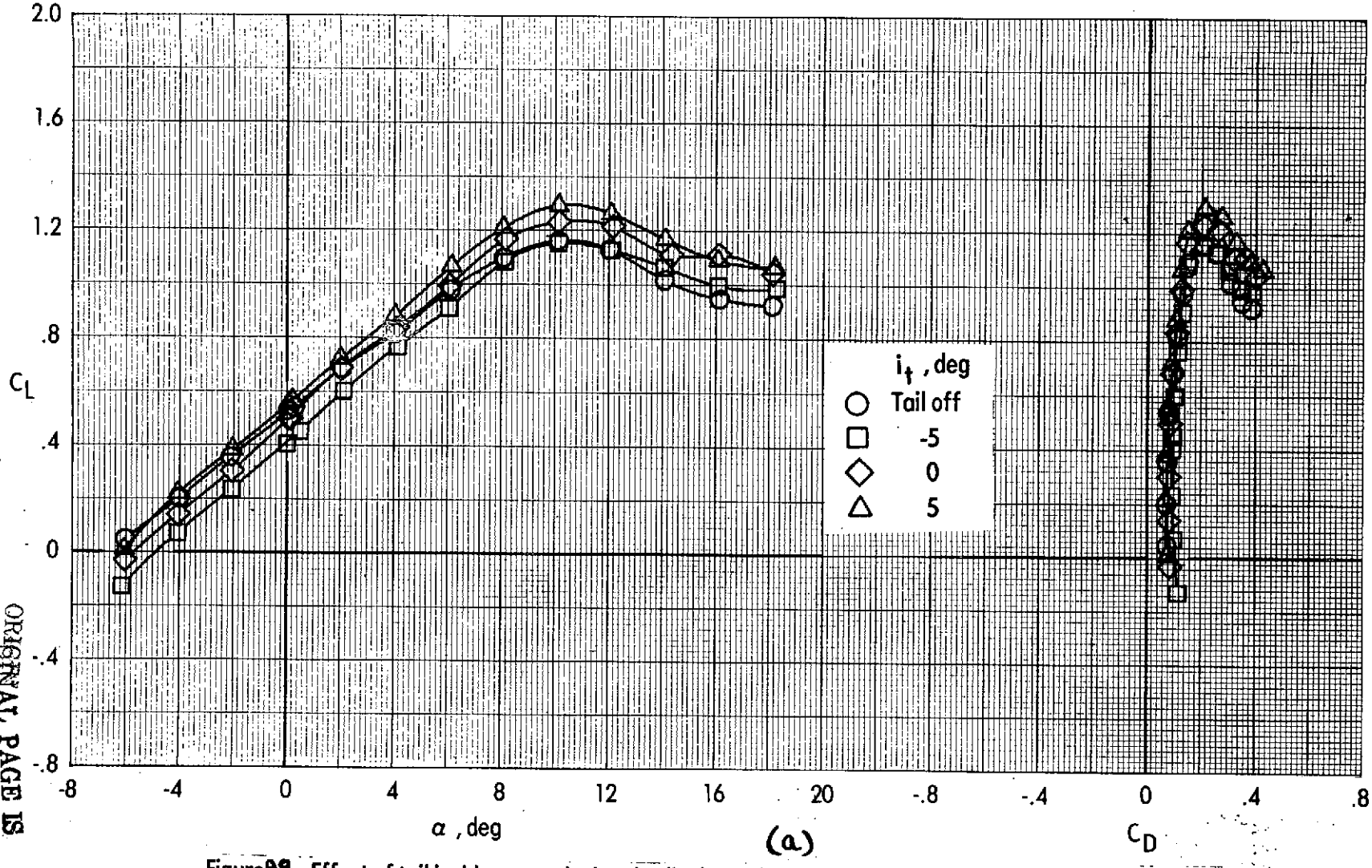

Figure 28. -Effect of tail incidence on the longitudinal aerodynamics and stability of the cruise configuration with the lift-fan pods and lift-cruise fans removed.

$\delta_f = 40°$ $\delta_e = 0°$ $C_\mu = 0$ $q_\infty = 2672$ N/m² (55.8 lb/ft²)

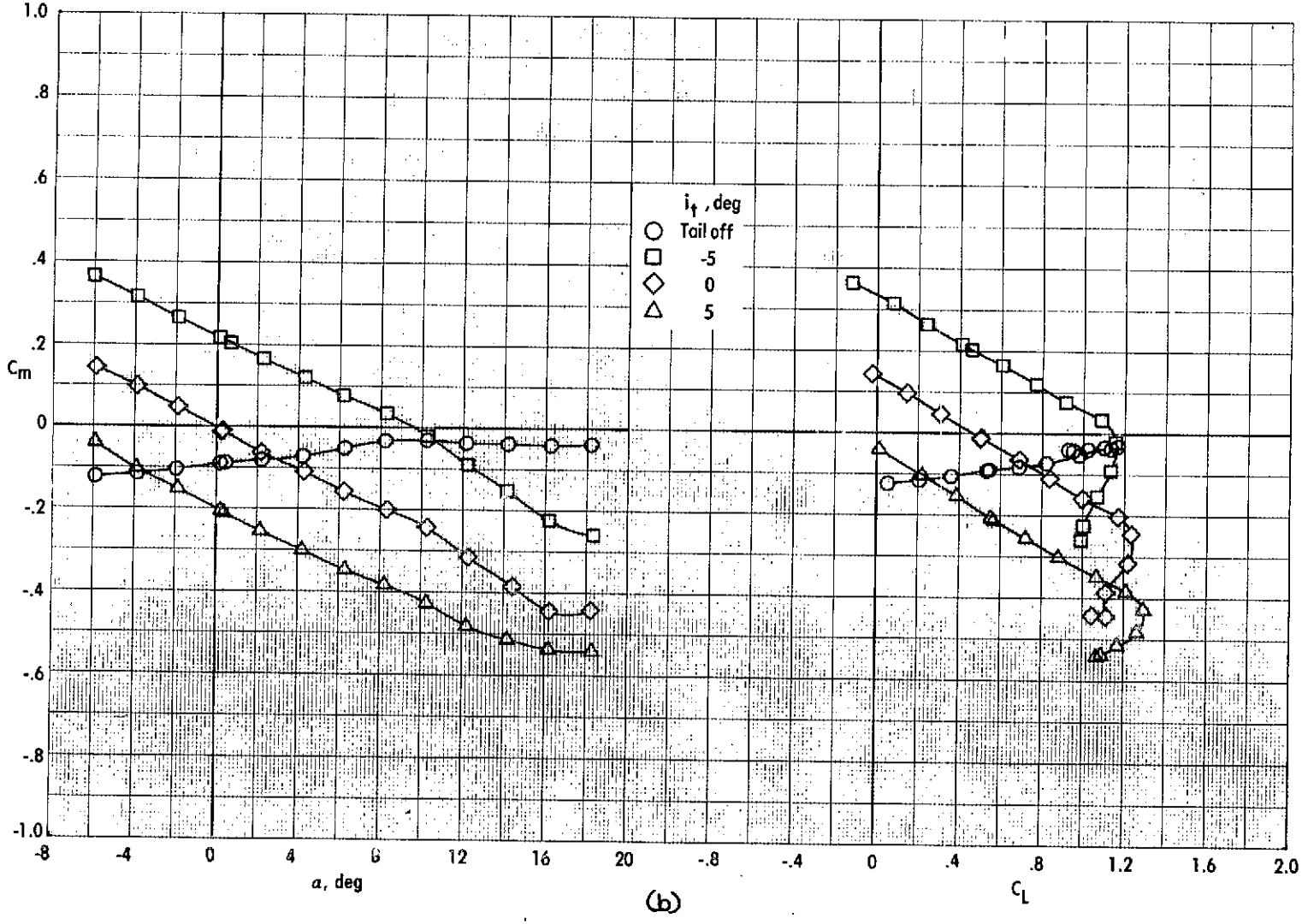

(b)

Figure 8. - Concluded.

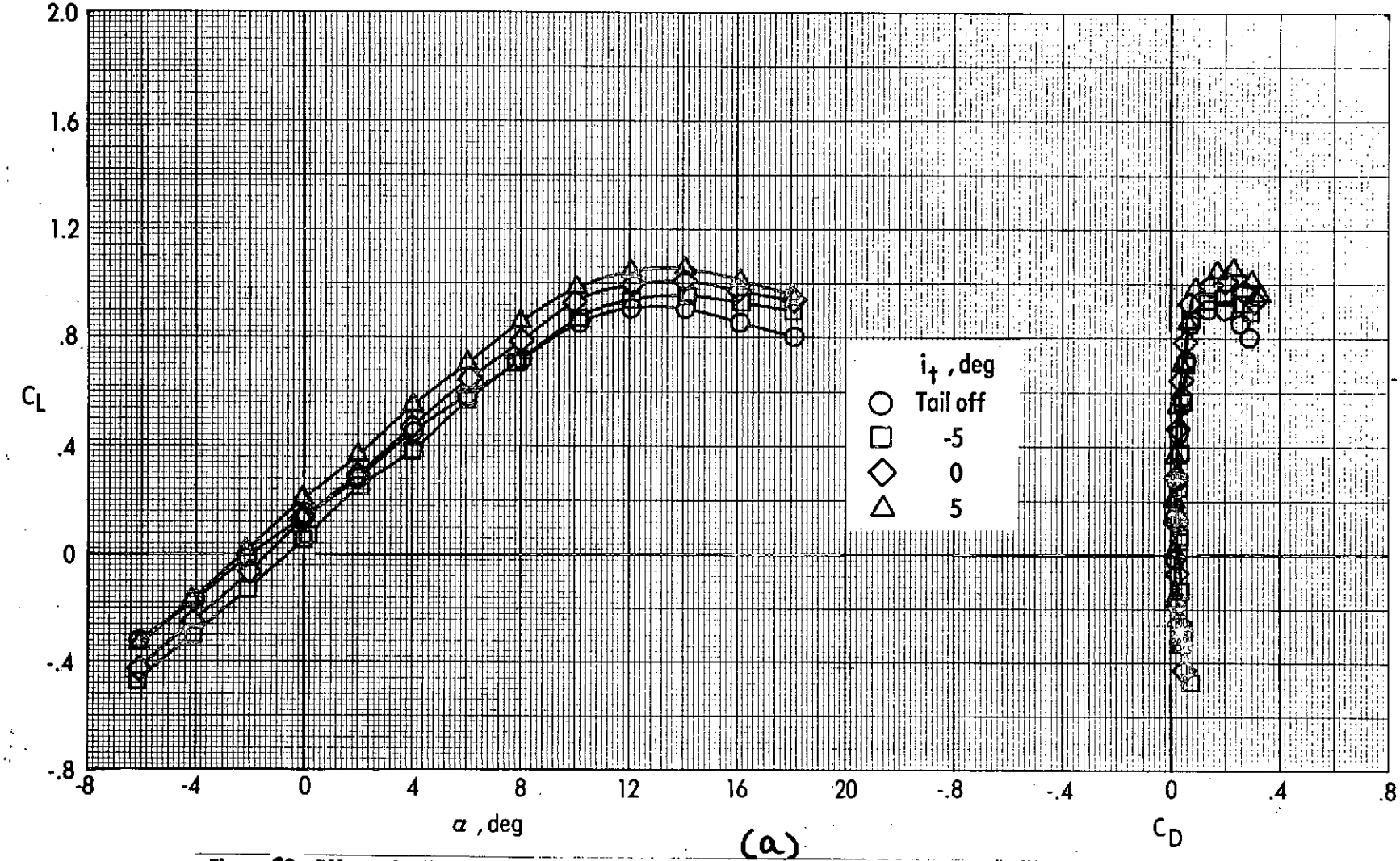

(a)

Figure 89. -Effect of tail incidence on the longitudinal aerodynamics and stability of the cruise configuration with the lift-fan pods and lift-cruise fans removed.

$\delta_f = 0°$ $\delta_e = 0°$ $C_\mu = 0$ $q_\infty = 2672$ N/m² (55.8 lb/ft²)

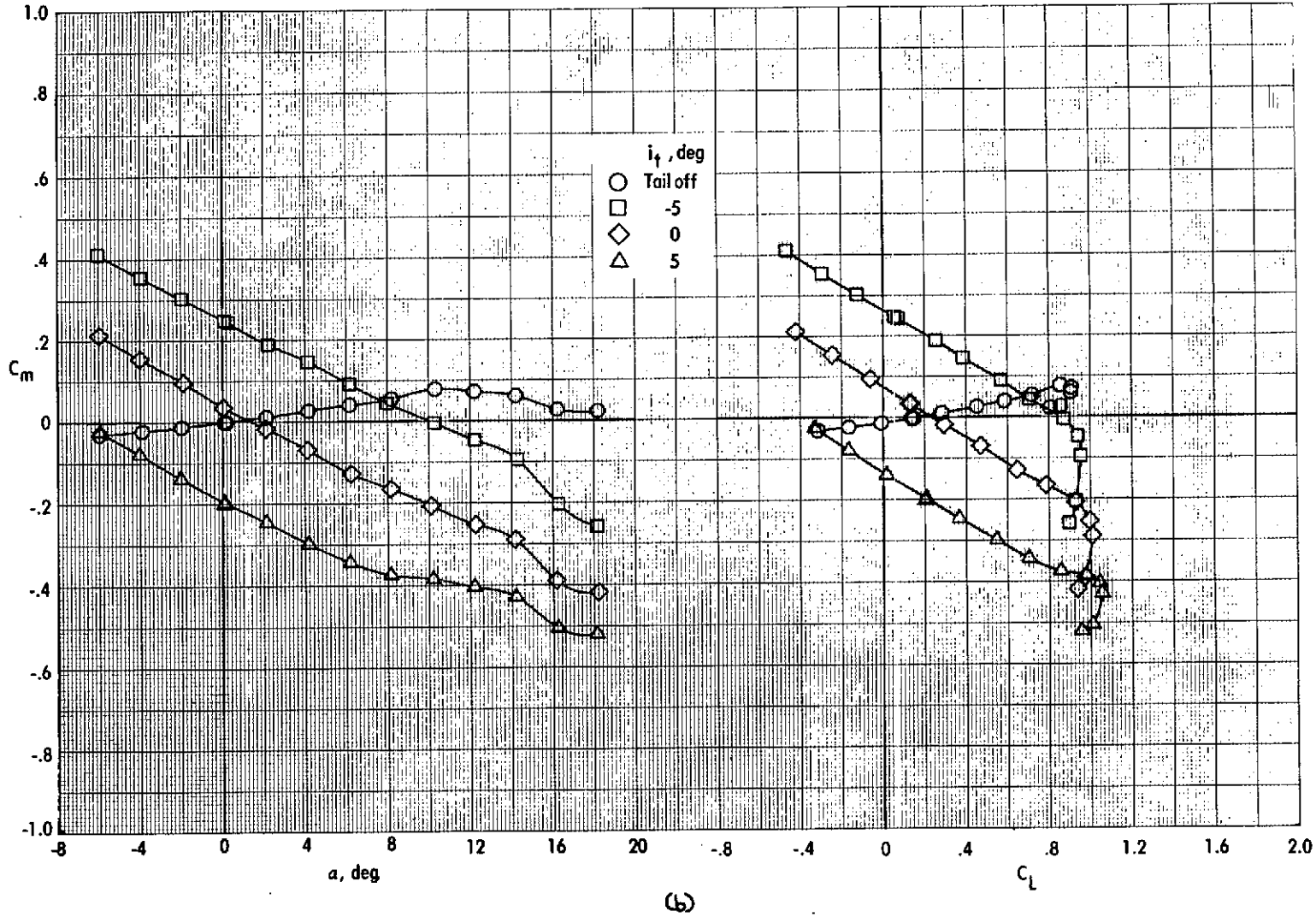

(b)

Figure 89. - Concluded.

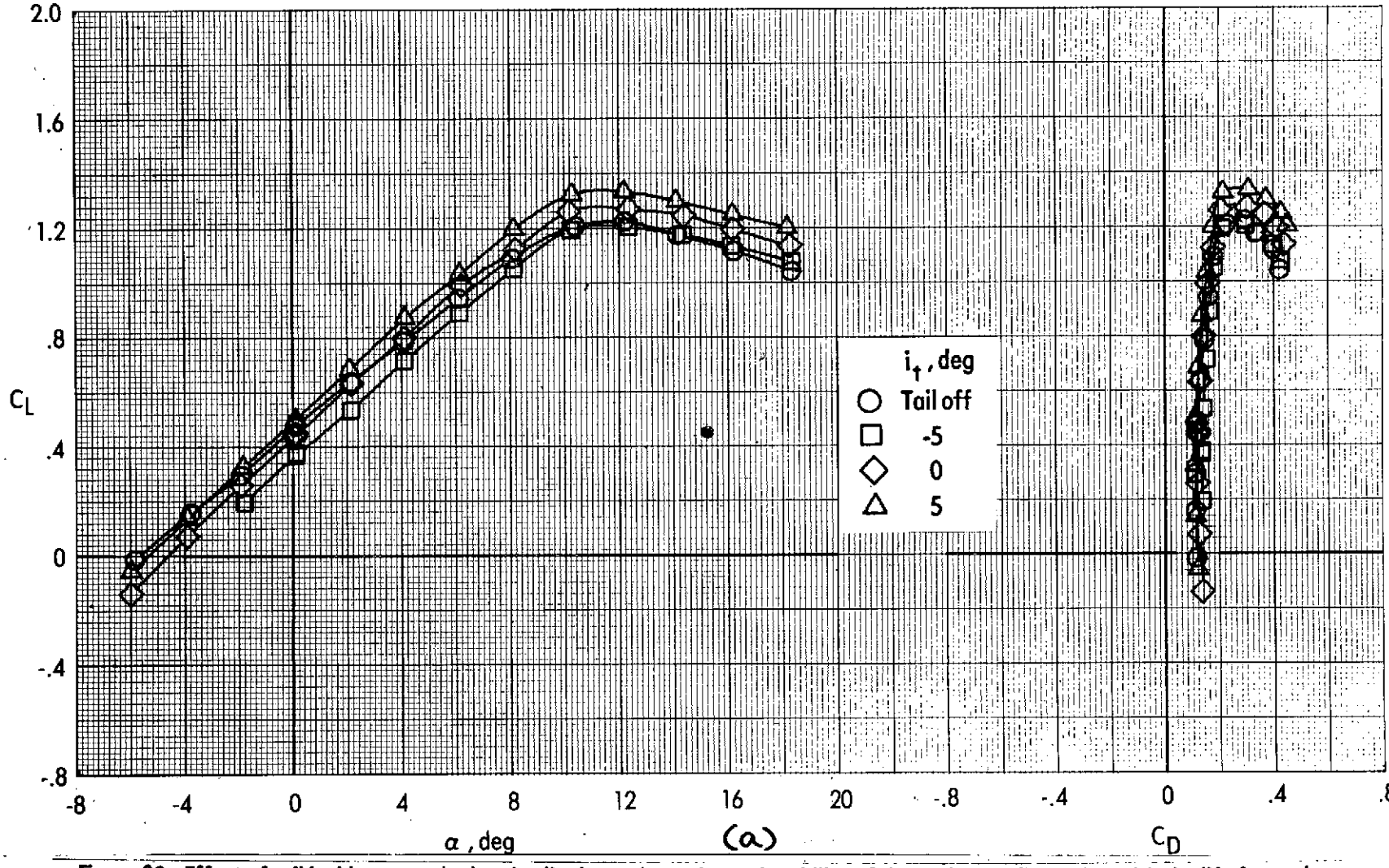

Figure 90. -Effect of tail incidence on the longitudinal aerodynamics and stability of the cruise configuration with the lift-fan pods removed.

$\delta_{LC} = 0°$ $\delta_f = 40°$ $\delta_e = 0°$ $C_\mu = 0$ $q_\infty = 2672$ N/m² (55.8 lb/ft²)

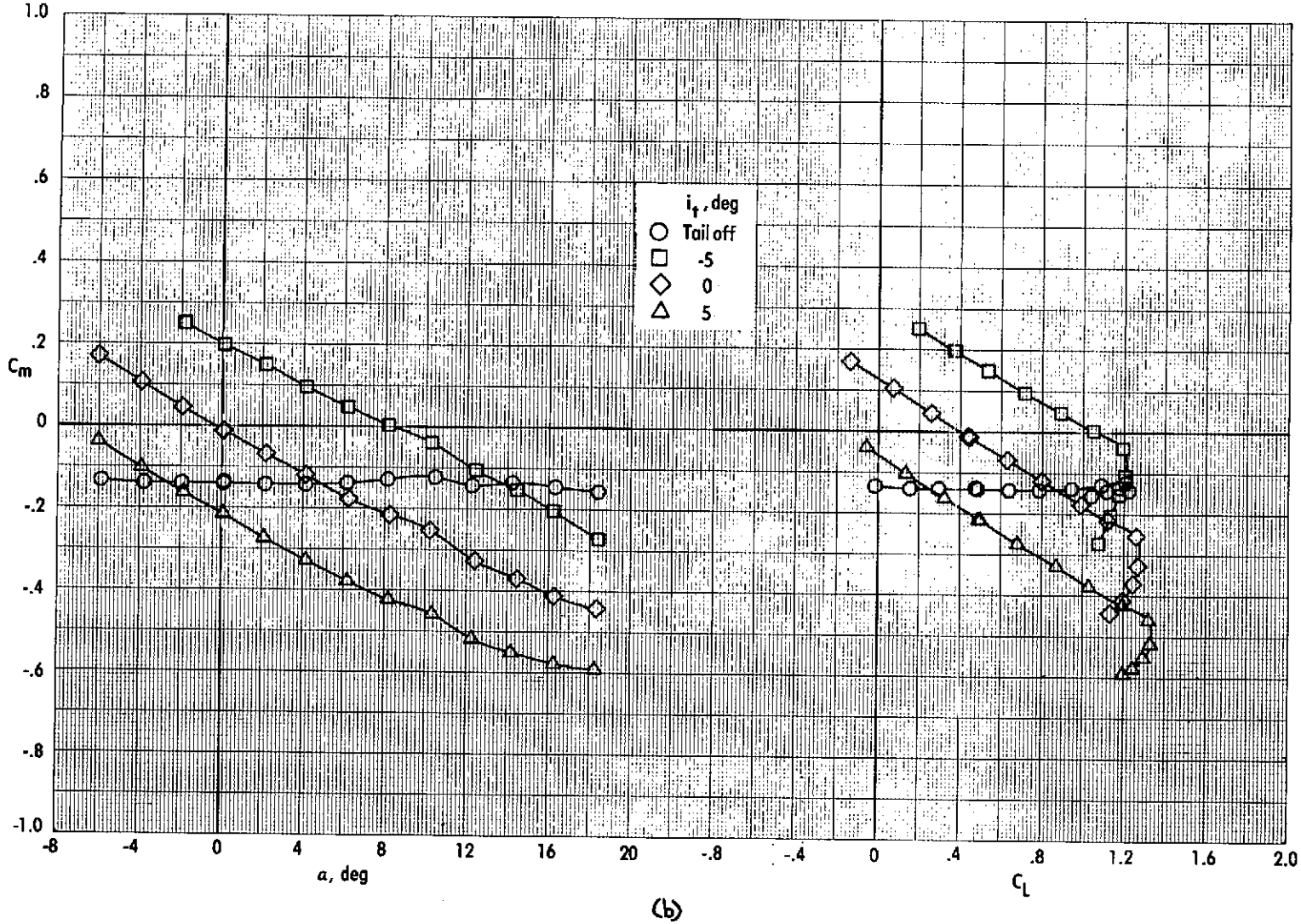

(b)

Figure 90. - Concluded.

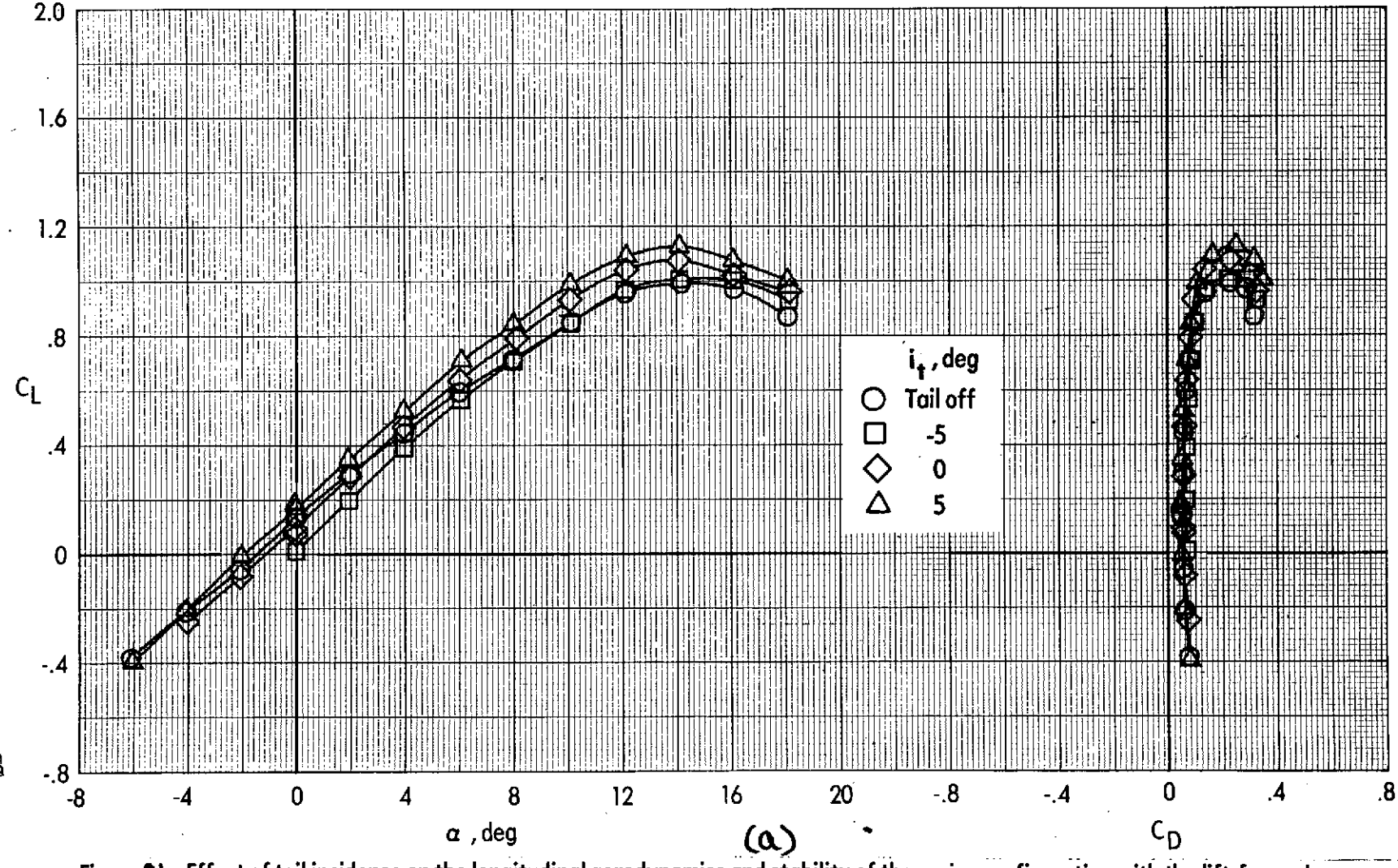

Figure 91. -Effect of tail incidence on the longitudinal aerodynamics and stability of the cruise configuration with the lift-fan pods removed.

δ_{LC}= 0° δ_f= 0° δ_e = 0° C_μ=0 q_∞= 2672 N/m² (55.8 lb/ft²)

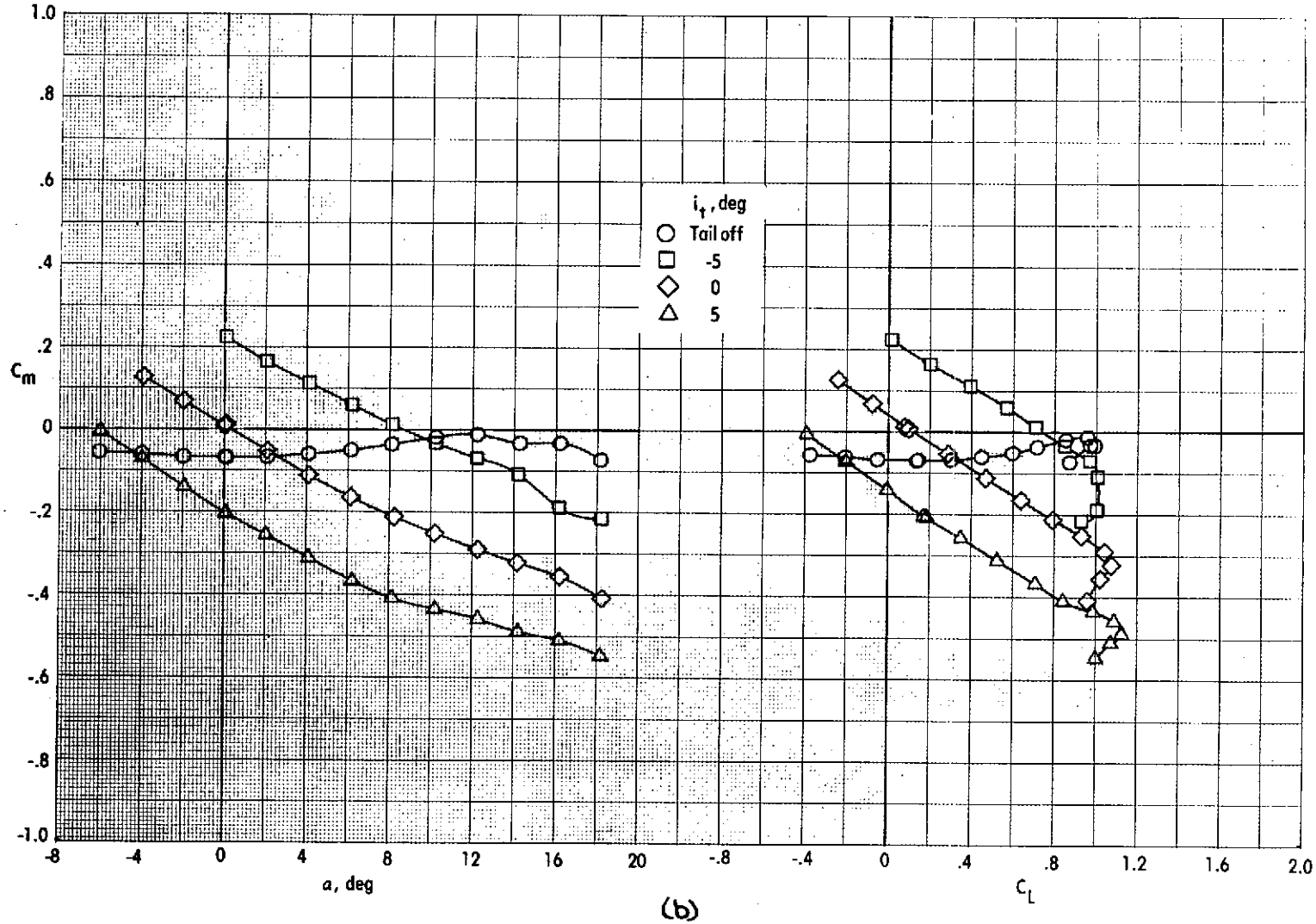

(b)

Figure 91. - Concluded.